Cellular and molecular heterogeneity in the synovial tissue of osteoarthritis patients

Thesis for the degree of Doctor of Philosophy

Matthew John Wood, BSc (Hons)
Musculoskeletal Research Group
Institute of Cellular Medicine
Newcastle University
Newcastle upon Tyne, UK

Supervisors
Dr Catharien Hilkens[1,2]
Professor Simon Milling[1,3]
Professor Muzlifah Haniffa[2]
Professor John Isaacs[1,2]

[1]Rheumatoid Arthritis Pathogenesis Centre for Excellence (RACE – Arthritis Research UK)
[2]Institute of Cellular Medicine, Newcastle University, Newcastle upon Tyne, UK
[3]Institute of Infection, Immunity and Inflammation, College of Veterinary, Medical and Life Science, University of Glasgow,
Glasgow, Scotland, UK

October 2017

Abstract

Osteoarthritis (OA) is the most common form of arthritis and one of the leading causes of disability globally. There are no disease modifying treatments, and for end stage disease, total joint replacement is the only therapeutic option. There is a major unmet clinical need for OA patients. Compared to peripheral blood and inflammatory arthritis (IA), there has been less research into the cellular mechanisms and inflammatory processes involved in the synovial tissue of OA. A barrier to this research has been difficulty in isolating cells from tissues at the site of disease activity. I aimed to identify and compare the cellular phenotype, functional capacity and gene expression of synovial tissue mononuclear cell subsets in OA and IA.

After assessing an array of published tissue digestion protocols, I developed a standardised synovial tissue digestion protocol allowing the isolation of multiple cell subsets with high yields, preserved cellular antigens and high cell viability. A multi-colour flow cytometry panel was established to allow the accurate identification and fluorescence-activated cell sorting of cDC2 dendritic cells, $CD14^+$ monocytes, HLA-DR^+CD14^+ macrophages and $CD4^+$ T cells.

Computational analysis of flow cytometry data sets demonstrated greater cellular infiltrate in IA, but an increased proportion of macrophages in OA. However, this proportion was not seen in all OA patients. Owing to their increased but varied proportion, and previously described role in OA pathogenesis, I conducted an in-depth analyses of these cells. OA macrophages had higher expression of surface proteins associated with activation such as CD206, FOLR2 and CD86. Functionality of isolated macrophages was retained, demonstrated by their high phagocytic activity. Next generation RNA-sequencing was performed to better understand their function and heterogeneity in OA synovial tissue. Two distinctive OA endotypes were proposed based on functional gene signatures. One gene signature comprised of cell cycle and proliferation mechanisms, whilst the other consisted of cartilage and tissue development.

Despite its central role in arthritic processes, the role of the synovium has remained obscure. This optimised digestion protocol now allows the interrogation of individual cell subsets. Analysis of synovial macrophages using this protocol has demonstrated distinct endotypes within OA patients. Improved investigation into the pathogenesis of OA, especially in the context of OA subtypes, can now be conducted. This could ultimately lead to the modification of treatment strategies for OA patients.

Acknowledgements

I would firstly like to thank my supervisors - Dr Catharien Hilkens for her invaluable support and enthusiasm throughout this project; Prof Simon Milling for his guidance and wise words; and Prof Muzlifah Haniffa and Prof John Isaacs for their insights and encouragement. I would also like to extend my thanks to Dr Gary Reynolds for his technical and scientific help at the start of my PhD.

I would like to thank the Rheumatoid Arthritis pathogenesis Centre for Excellence (RACE - Arthritis Research UK) and JGW Patterson foundation (JGWP) for funding this project. Many thanks to Dr Arthur Pratt and Dr Kenneth Rankin for sample collection and interest in this project. Thank you to everyone at the flow cytometry core facility for their support, and to Adam Leckenby for his assistance in bioinformatic analyses.

Finally, I would like to express my thanks to everyone in the Musculoskeletal Research Group for their friendship and support throughout my PhD.

Publications

Wood MJ, Leckenby A, Reynolds G, Spiering R, Pratt AG, Rankin K, Haniffa MA, Isaacs JD, Milling S, Hilkens CMU (2017). "Cellular and molecular heterogeneity in the synovial tissue of Osteoarthritis patients" *Manuscript in preparation.*

Clifford T, **Wood MJ**, Stocks P, Howatson G, Stevenson EJ, Hilkens CMU (2017). "T-regulatory cells exhibit a biphasic response to prolonged endurance exercise in humans." Eur J Appl Physiol. doi: 10.1007/s00421-017-3667-0.

Reynolds G, Gibbon JR, Pratt AG, **Wood MJ**, Coady D, Raftery G, Lorenzi AR, Gray A, Filer A, Buckley CD, Haniffa MA, Isaacs JD, Hilkens CMU (2015). "Synovial CD4+ T-cell-derived GM-CSF supports the differentiation of an inflammatory dendritic cell population in rheumatoid arthritis." Ann Rheum Dis. doi:10.1136/annrheumdis-2014-206578.

Scientific Communication

Effective communication and dissemination of scientific research has been demonstrated throughout my PhD through oral, poster and journal club presentations listed. I have also regularly presented at lab, group and departmental meetings (not listed).

Those denoted with '*' indicate awards won.

Wood MJ, (2017, October 26th). **Poster Presentation**. "Cellular and Molecular Heterogeneity in the synovial tissue of Osteoarthritis patients". **'Macrophage biology in the single cell era'**, Ghent, Belgium.

Wood MJ, (2017, October 23rd). **Poster Presentation**. "Cellular and Molecular Heterogeneity in the synovial tissue of Osteoarthritis patients". Cell Symposia **'Human Immunity'**, Banff, Canada.

***** *Wood MJ,* (2017, June 28th). **Poster Presentation**. "Investigation of antigen presenting cells in inflammatory and non-inflammatory arthritis". **Fourth International Therapeutic Tolerance Workshop**, Newcastle University.

Wood MJ, (2017, June 27th). **Chairing** 'Cells and Mechanisms' Session. **Fourth International Therapeutic Tolerance Workshop**, Newcastle University.

***** *Wood MJ,* (2017, June 16th). **Oral Presentation**. "Investigation of antigen presenting cells in inflammatory and non-inflammatory arthritis". **Immunology North East Symposium**, Newcastle University.

Wood MJ, (2017, March 30th). **Journal Club Presentation**. "Unsupervised High dimensional Analysis Aligns Dendritic Cells across Tissues and Species." **Immunology North East Journal Club**, Newcastle University.

Wood MJ, (2017, February 6th). **Oral Presentation**. "Do Synovial Dendritic Cells Contribute to the Pathogenesis of Rheumatoid Arthritis?" Rheumatoid Arthritis Pathogenesis Centre for Excellence **(RACE) scientific meeting**, University of Birmingham.

Wood MJ, (2016, December 8th). **Poster Presentation**. "Investigation antigen presenting cells in inflammatory and non-inflammatory arthritis". **British Society for Immunology Annual Congress,** ACC Liverpool.

Wood MJ, (2016, March 2nd). **Oral Presentation**. "Do Synovial Dendritic Cells Contribute to the Pathogenesis of Rheumatoid Arthritis?" **Institute of Cellular Medicine Research Seminar**, Newcastle University.

Wood MJ, (2016, January 28th). **Oral Presentation**. "Do Synovial Dendritic Cells Contribute to the Pathogenesis of Rheumatoid Arthritis?" Rheumatoid Arthritis Pathogenesis Centre for Excellence **(RACE) scientific meeting**, University of Birmingham.

Wood MJ, (2015, September 30th). **Oral Presentation**. "Do Synovial Dendritic Cells Contribute to the Pathogenesis of Rheumatoid Arthritis?" **Northern and Yorkshire Rheumatology Meeting**, York National Railway Museum.

Wood MJ, (2015, January 20th). **Oral Presentation**. "Do Synovial Dendritic Cells Contribute to the Pathogenesis of Rheumatoid Arthritis?" Rheumatoid Arthritis Pathogenesis Centre for Excellence **(RACE) scientific meeting**, Newcastle University.

Table of Contents

Figures

Tables

List of Appendices

List of Abbreviations

Throughout this thesis, inflammatory arthritis (IA) is a term which will be used to describe classically inflammatory arthritic conditions being used as a control or comparator. Although this mainly encompasses rheumatoid arthritis (RA), it also includes other inflammatory conditions such as Psoriatic arthritis (PsA). When disease specific mechanisms or research is being discussed, IA will not be used and instead, the disease specific abbreviation.

ACPA	Anti-citrullinated protein antibody
ADAM	A disintegrin and melloprotease with thrombospondin
ADAMTS5	ADAM metallopeptidase with thrombospondin type 1 motif 5
ARUK	Arthritis Research UK
ASPM	Abnormal spindle microtubule assembly
BATF	Basic leucine transcription factor, ATF-like
BC	Bi-compartmental
BCR	B-cell receptor
BMI	Body mass index
CCL '#'	Chemokine ligand
CCP	Cyclic citrullinated protein
CCR '#'	Chemokine receptor
CD '#'	Cluster of differentiation
cDC	Conventional dendritic cell
CDT1	Chromatin licensing and DNA replication factor 1
COX	Cyclooxygenase
CPM	Counts per million
CRP	C-reactive protein
CSF1	Colony stimulating factor 1
CSF1R	Colony stimulating factor receptor
CTLA-4	Cytotoxic T-lymphocyte associated protein
CTRL	Chymotrypsin like
DAMP	Damage-associated molecular pattern
DAPI	4'6-diamidino-2-phenylindole
DAS28	Disease activity score in 28 joints
DEG	Differentially expressed gene
DC	Dendritic cell
DC-SIGN	Dendritic cell-specific intracellular adhesion molecule-3-grabbing non-integrin
DIC	Differential interference contrast
DMARDs	Disease modifying anti-rheumatic drugs
DMSO	Dimethyl sulfoxide
DPX	Distyrene plasticizer xylene
EA	Early arthritis
EDTA	Ethylenediaminetetraacetic acid
EFEMP1	EGF containing fibulin like extracellular matrix protein 1
ESR	Erythrocyte sedimentation rate
FACS	Fluorescence activated cell sorting
FBS	Fetal bovine serum
FC	Fold change
FCCF	Flow cytometry core facility
FCS	Flow cytometry standard
FMO	Fluorescence minus one

FOLR2	Folate receptor 2
FSC	Forward scatter
FCS-A	Forward scatter area
GCF	Genomics core facility
GM-CSF	Granulocyte macrophage colony stimulating factor
GO	Gene ontology database
GPRC5A	G protein coupled receptor class C group 5 member A
GvHD	Graft-versus- host disease
HBSS	Hanks balanced salt solution
HLA-DR	Human leucocyte antigen - D related
HTRA1	High temperature requirement seine protease A1
IA	Inflammatory Arthritis
ICAM	Intracellular adhesion molecule
ID2	DNA-binding protein inhibitor ID-2
IFN	Interferon regulatory factor 8
Ig '#'	Immunoglobulin
IGFBP	Insulin like growth factor binding protein
IL '#'	Interleukin
IRF8	Interferon regulatory factor 8
KEGG	Koto encyclopaedia of genes and genomes
KL	Kellgren and Lawrence
KLF4	Kruppel-like factor 4
KMT5A	Lysine Methyltransferase 5A
LFA	Lymphocyte function associated antigen
LogFC	Log fold change
LPS	Lipopolysaccharide
LRS	Leucocyte reduction system
LRRN4CL	LRRN4 C-terminal like
MACS	Magnetic assisted cell sorting
MAPK	Mitogen-activate protein kinases
MARCO	Macrophage structure with collagenous structure
MCP-1	Monocyte chemoattractant protein-1
MDS	Multi-dimensional scale
MFI	Mean fluorescence intensity
MHC	Major histocompatibility complex
M-CSF	Macrophage colony stimulating factor
Mins	Minutes
MØ	Macrophage
MMP	Metalloproteinases
moDC	Monocyte derived dendritic cell
moMac	Monocyte derived macrophage
MPS	Mononuclear phagocyte system
MRI	Magnetic Resonance Imaging
MST	Minimal spanning tree
MYB	Myeloblastosis proto-oncogene protein
NBJS	Newcastle bone and joint study
NCAM1	Nuclear adhesion molecule
NEAC	Newcastle early arthritis clinic
NFATc1	Nuclear factor of activated T-cells, cytoplasmic 1
NICE	National institute for health and care excellence
NIDDM	Non-insulin dependent diabetes mellitus
NK	Natural killer

NO	Nitric Oxide
NSAIDs	Non-steroidal anti-inflammatory drugs
OA	Osteoarthritis
PAMP	Pathogen-associated molecular pattern
PBMC	Peripheral blood mononuclear cell
PBS	Phosphate buffered saline
PCA	Principle component analysis
PCR	Polymerase chain reaction
pDC	Plasmacytoid dendritic cell
PLK1	Polo like kinase 1
PRR	Pattern recognition receptor
PsA	Psoriatic arthritis
RANK	Receptor activator of nuclear factor kappa-B
REC	Research ethics committee
RF	Rheumatoid factor
RF10	RPMI + 10% FBS
RA	Rheumatoid Arthritis
RNA	Ribonucleic acid
RUNX	Runt related transcription factor
SAM	Significance Analysis of Microarrays
Secs	Seconds
SSC	Side scatter
SSC-A	Side scatter area
Tfh	T follicular helper
TGF-β	Transforming growth factor beta
Th	T helper cell
TIM	T cell immunoglobulin mucin protein
TKR	Total knee replacement
TLR	Toll-like receptor
TNF	Tumor necrosis factor
TRAC	T-cell receptor alpha constant
Treg	Regulatory T cell
TSKU	Tsukushi
tSNE	t-distributed stochastic neighbour embedding
UC	Uni-compartmental
ULK	Unc-51 like autophagy activating kinase
XRCC3	X-Ray repair cross complementing 3
7AAD	7-aminoactinomycin D

Chapter 1. Introduction

1.1 Overview

Osteoarthritis (OA) is the most common form of arthritis and one of the leading causes of disability with knee OA affecting ~18.2% of adults over the age of 45 in England (Arthritis Research UK, 2017). Progressive destruction of cartilage and bone is multifactorial, resulting in pain and loss of joint function. As OA risk factors include age, obesity and metabolic syndrome, OA is particularly becoming a major health burden for the western world. There is no treatment for OA. Clinically, pain is managed, and for patients at end stage disease, total joint replacement is the only therapeutic option. In 2015, >90,000 patients received a total knee replacement in the U.K; this figure is expected to double over the next decade (Guerra, Singh et al. 2015) (National Joint Registry, 2016). Disease modifying anti-rheumatic drugs (DMARDs) often used for treatment in IA, have been trialled in patients with OA with limited success (Hunter 2008, Philp, Davis et al. 2017).

Synovial inflammation present in OA patients is usually low grade and does not lead to overt systemic inflammation (Sokolove and Lepus 2013). However, this local synovial inflammation is present in 50%-70% of OA patients throughout disease progression, and it is becoming recognised that inflammation within the joint of OA patients contributes to disease pathogenesis (Haywood, McWilliams et al. 2003, Baker, Grainger et al. 2010, Roemer, Crema et al. 2011).

Macrophages are a diverse population of tissue resident cells. They are relatively large cells which specialise in phagocytosis, but have great multifunctional capacity and heterogeneity. These functional roles encompass phagocytosis, antigen presentation, inflammation, tissue homeostasis and tissue repair. Synovial macrophages have been previously described in the pathogenesis of OA. It has been found that the number of macrophages in synovium correlates with the degree of synovial angiogenesis (Haywood, McWilliams et al. 2003, Kraus, McDaniel et al. 2016). However, compared to the research of blood in OA and the study of the synovium in rheumatoid arthritis (RA), there has been relatively little research into macrophages and cellular mechanisms in the synovial tissue of OA.

1.2 The mononuclear phagocyte system

Furth, Hirsch and Cohn described the mononuclear phagocyte system (MPS) in the late 1960s, comprising of dendritic cells (DCs), monocytes and macrophages. The MPS contributes to the immune system through the initiation of innate and adaptive immune responses, pathogen clearance, tissue maintenance and healing.

Guilliams *et al.,* (2014) proposed a unified nomenclature system in mice, consisting of a two tiered approach based on ontogeny, location, function and phenotype (Guilliams, Ginhoux et al. 2014). From this, and existing information, a model of mononuclear phagocyte differentiation can be compiled (Fig. 1.1). However, much knowledge of the MPS in humans has been derived from studying its components in blood. Research on tissue has been difficult due to limited sample availability, methods to derive single cell suspensions and identification of unique markers for cell subsets. It is these tissue environments that may heavily manipulate cells of the MPS in steady state as well as in disease. For example, macrophages can functionally differ between tissues; Kupffler cells of the liver specialise in the degradation of red blood cells whereas muscularis macrophages contribute to gut peristalsis. Additionally, during inflammation monocytes can infiltrate inflamed tissue and acquire macrophage-like properties, similar to that of *in vitro* monocyte-derived macrophage (moMac) differentiation. There is a need to advance knowledge of the MPS in human tissues and in the context of inflammation and disease.

1.3 Macrophages

In 1882 Elie Metchnikoff, regarded the father of natural immunity, described antimicrobial defence and the requirement of the immune system to kill and eat pathogens as part of this defence (Gordon 2008). Specialised cells termed phagocytes were observed to uptake and intracellularly digested foreign bodies and microorganisms. *'big-eater'* is the English translation of the Greek word macro-phage, describing this cells large size and high ability to phagocytose pathogens and apoptotic cells. In addition to phagocytosis, macrophages can also, present antigen and produce large quantities of secretory molecules including chemokines, cytokines and proteinases. Macrophages are functionally variable throughout different tissues. In mice, macrophages from different tissue sites were shown to have great transcriptomic diversity (Gautier, Shay et al. 2012). In addition to tissue-specific environments, macrophages are additionally influenced by exposure to activation signals and their ontogeny, be that monocyte or embryonically derived.

Macrophages can be identified by the expression of CD11b, CD14, CD68 and colony stimulating factor 1 (CSF1R) in both mice and humans. F4/80 is an additional marker exclusive to mice. However, in humans none of these markers are exclusive to macrophages, and can be co-expressed on monocytes and dendritic cells. Macrophages additionally express a range of membrane proteins for specific cellular functions. These include macrophage receptor with collagenous structure (MARCO) for the clearance of microbes, T cell immunoglobulin mucin protein 4 (TIM-4) for the clearance of apoptotic cells, toll-like receptor 4 (TLR4) and CD14 for recognition of bacterial membrane components such as lipopolysaccharide (LPS) and chemokine receptor 2 (CCR2) for the recognition of chemokine monocyte chemoattractant protein-1 (MCP-1) (Gordon and Pluddemann 2017).

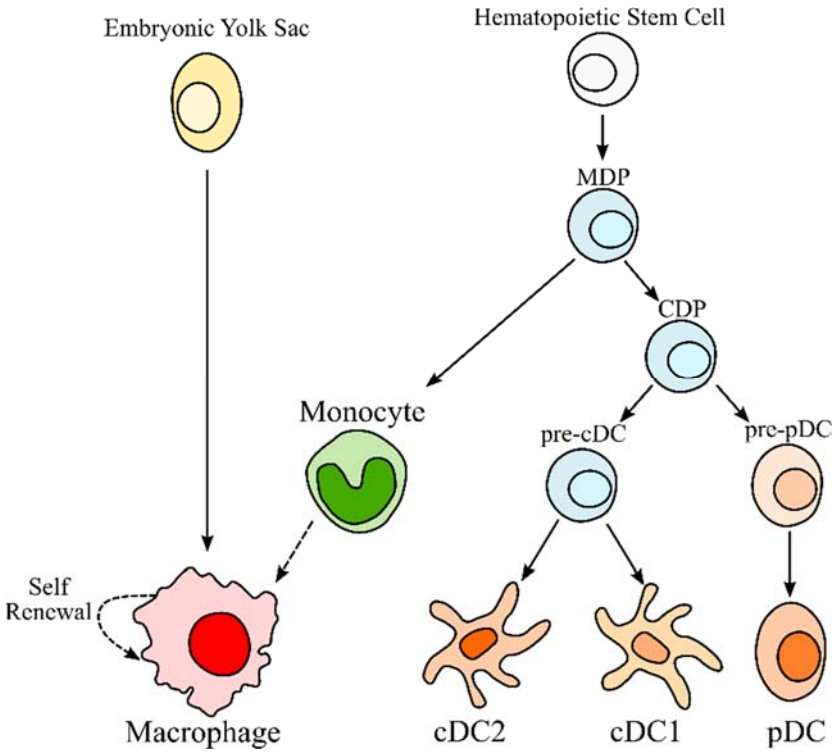

Figure 1.1: The mononuclear phagocyte system differentiation
Depiction of differentiation in the mononuclear phagocyte system based on Guilliams *et al.,* (2014). Macrophages are derived from embryonic yolk sac precursors and are maintained by self renewal in addition to monocyte replacement. Hematopoietic stem cells give rise to the macrophage and dendritic cell progenitor (MDP), and subsequent monocytes can further differentiate into monocyte-derived macrophages. The common dendritic cell precursor (CDP) differentiates into pre-pDC and pre-cDC precursor cells, differentiating into pDCs and cDC1/cDC2 respectively.

1.3.1 *Macrophage development*

Although macrophages were historically considered to be exclusively derived and replenished by circulating monocytes, it is now known that many types of macrophages are self-renewing and embryonically derived (van Furth and Cohn 1968). During development, macrophages are seeded throughout the tissues of the body by embryonic yolk sac and foetal liver precursors. These tissue resident populations are mostly self-replenishing. After development, bone marrow-derived blood monocytes contribute to the replenishment of these macrophages to various extents. However, this renewal process is variable by tissue site and in the presence of inflammation. For example, in the gut there is a large proportion of monocyte-derived macrophages during steady state. Additionally, during inflammation, infection or after tissue injury, there can be an increase in the proportion of these monocyte-derived macrophages.

Control of macrophage regulation, differentiation, proliferation and survival is contributed to by macrophage-colony stimulating factor 1 (CSF1) (Yu, Chen et al. 2012, Zhang, Wang et al. 2014). However, the transcriptional requirements of embryonically derived macrophages differ considerably from that of haematopoetic stem cell-derived macrophages. For example embryonic microglial macrophages require the transcription factors Pu.1 and interferon regulatory factor 8 (IRF8), and develop independently of myeloblastosis proto-oncogene protein (MYB), DNA-binding protein inhibitor ID-2 (ID2), basic leucine transcription factor, ATF–like (BATF) and kruppel-like factor 4 (KLF4) (Kierdorf, Erny et al. 2013). It is also thought that specialised tissue macrophages express independent transcription factors. For example, osteoclasts require the transcription factor nuclear factor of activated T-cells, cytoplasmic 1 (NFATc1) for development whereas splenic macrophages require Spi-C (Kohyama, Ise et al. 2009, Kim and Kim 2014).

1.3.2 *Macrophage activation*

Pathogen-associated molecular patterns (PAMPs) and damage-associated molecular patterns (DAMPs) are molecules that initiate and perpetuate infectious and non-infectious inflammatory responses, respectively. Macrophages express pattern recognition receptors (PRRs) such as TLRs, which allow them to recognise PAMPs and DAMPs. In addition to recognising pathogens and damage signals, macrophages can respond to cytokines. An *in vitro* model of macrophage activation has been studied for many years, the M1 and M2 paradigm. This has advanced our understanding of macrophage activation greatly. M1 macrophages are considered to be the classically activated subset and have enhanced antimicrobial, inflammatory and antigen-presenting properties. These cells have been observed in intracellular infections and tissue injury such as seen in tuberculosis (Mosser and Edwards 2008). M2 macrophages have

anti-inflammatory properties and have been observed in allergy, parasitic infection, repair and fibrosis (Murray and Wynn 2011, Wynn and Ramalingam 2012). Interferon gamma (IFN-γ) largely produced by T-helper (Th)1 cells can induce an M1 phenotype, whereas the Th2 signature cytokines interleukin 4 (IL-4) and IL-13 promote an M2 phenotype (Mantovani, Sica et al. 2004, Wallet, Wallet et al. 2010). IRF3, IRF4 and NF-kappa B p50 are transcription factors shown to influence M2 polarisation whereas IRF5 is thought to influence M1 (Biswas, Gangi et al. 2006, Porta, Rimoldi et al. 2009, Satoh, Takeuchi et al. 2010, Krausgruber, Blazek et al. 2011).

However, the M1/M2 model of macrophage activation is becoming recognised as polar representations of activation states and may not be representative of *in vivo* macrophages (Barros, Hauck et al. 2013, Martinez and Gordon 2014, Xue, Schmidt et al. 2014). Additionally, Xue *et al.* showed stimulated macrophage transcriptome data demonstrating a range of additional macrophage activation states extending past the current M1/M2 models (Xue, Schmidt et al. 2014). The differences between macrophages at different polarisation states is clear, however these states are not easily identifiable in the tissue, and may not be completely representative of *in vivo* macrophage activation.

1.3.3 *Macrophage tissue residency*

It has been shown in mice that monocytes can differentiate into macrophages at interfaces with specific environments such as gut, lung and skin (Varol, Landsman et al. 2007, Bain, Bravo-Blas et al. 2014, Cerovic, Bain et al. 2014). The mechanisms that induce macrophage differentiation and tissue specific functions are yet to be fully understood. For example, it is known that osteoclast differentiation mechanisms involve the receptor activator of NF kappa-B (RANK) signalling cascade (Boyle, Simonet et al. 2003). In addition, Okabe *et al.* explored the tissue-specific controls of peritoneal macrophages in mice, finding that GATA6 and retinoic acid are responsible for their localisation (Okabe and Medzhitov 2014). This demonstrates the ability of macrophages to acquire tissue-specific functions dependent on their location.

Influences of specific tissue environments can be exemplified by a number of macrophage populations (Fig. 1.2). Kupffer cells specialise in the degradation of red blood cells, muscularis macrophages in gut peristalsis, osteoclasts in bone resorbtion and microglia in neural network development and maintenance (Willekens, Werre et al. 2005, Kettenmann, Kirchhoff et al. 2013, Muller, Koscso et al. 2014). This demonstrates how tissue-specific environments can influence these cells.

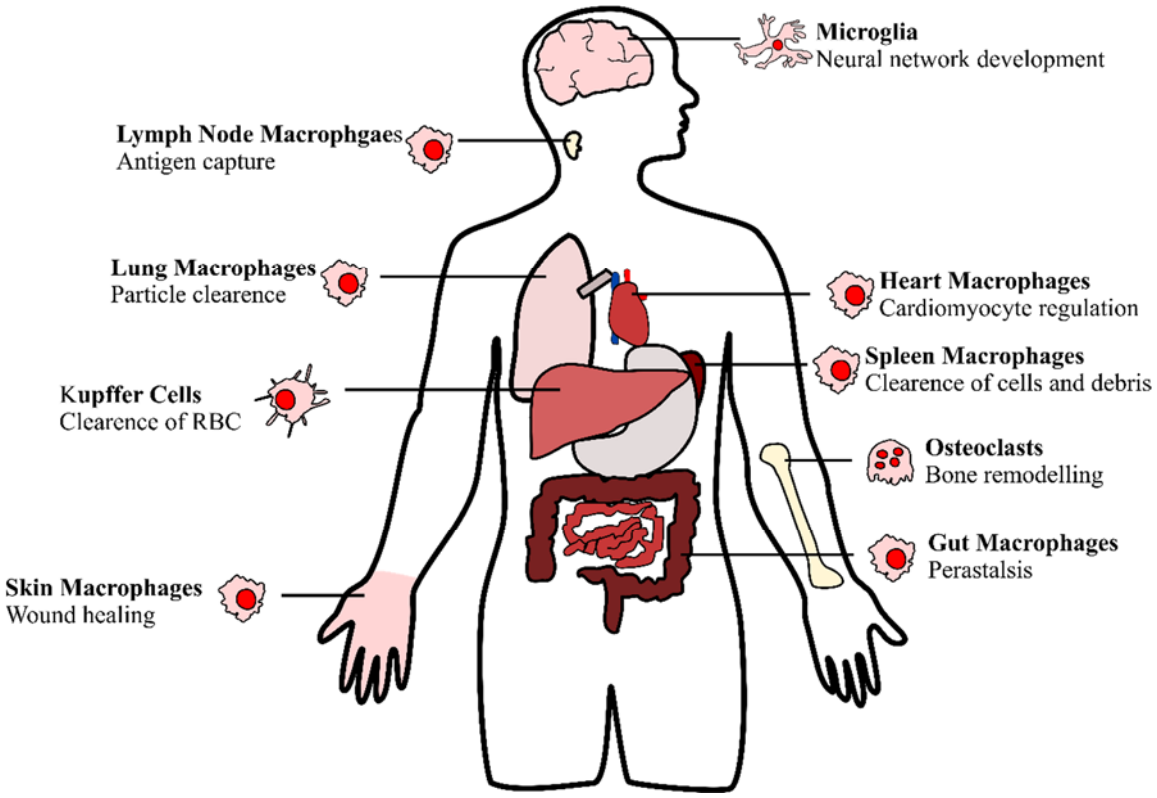

Figure 1.2: Specialised tissue macrophages
In addition to wide ranging macrophage functions, macrophages from different tissue environments can perform specialised functions. These include microglia of the brain and neural network development, lymph node macrophages and antigen capture, lung macrophages and particle clearance, heart macrophages and cardiomyocyte regulation, spleen macrophages and clearance of cells and debris, Kupffer cells of the liver and clearance of red blood cells (RBC), Osteoclasts of the bone and bone remodelling, Gut macrophages and peristalsis and skin macrophages and wound healing.

1.4 Dendritic Cells

DCs are professional antigen-presenting cells and specialise in initiating adaptive immune responses. Although found in the blood and throughout the body, they are concentrated in tissues with environmental exposure. These tissues include the skin, lungs and gut. Paul Langerhans first described Langerhans cells, a skin-resident cell population resembling DCs in 1868. However, characterisation of DCs as professional antigen presenting cells, did not occur until 1973 by Ralph Steinman (Steinman and Cohn 1973). Isolated from mouse spleen, Steinman reported that these cells were required for mixed lymphocyte reactions. These DCs were described as having dendrite-like branching projections, few lysosomes and limited phagocytic activity compared to other immune cells such as macrophages.

1.4.1 *DC activation*

Similarly to macrophages, DCs also recognise PAMPs and DAMPs through a similar range of PRRs. Key differences include the expression of Galectin 3 and TLR6 on macrophages, aiding

in phagocytosis and inflammation (Netea, Brown et al. 2008), and the expression of dendritic cell-specific intracellular adhesion molecule-3-grabbing non-integrin (DC-SIGN) on dendritic cells (Netea, Brown et al. 2008). DC-SIGN functions as an adhesion molecule and antigen receptor (Garcia-Vallejo and van Kooyk 2013). However, DC-SIGN expression has been reported on tissue macrophages (Soilleux, Morris et al. 2002, Conde, Rodriguez et al. 2015). Additionally, DCs express high levels of major histo-compatibility complex II (MHCII), allowing the efficient presentation of antigens (Steinman 1991, Steinman and Idoyaga 2010). Once activated through these mechanisms, DCs can migrate to T cell areas of draining lymph nodes where they present antigen on MHC stimulating cell proliferation and differentiation (Ganguly, Haak et al. 2013). DCs are efficient at activating naïve T cells, hence they are referred to as 'professional' antigen-presenting cells.

T cells are key effector cells in the adaptive immune response, contributing through the secretion of cytokines and activation of other immune cell types, including B cells and macrophages. They also play a crucial role in destroying tumour cells and infected cells in addition to preventing auto-reactive immune responses to self-antigens. To become fully activated, a T cell requires three types of activation signals (Corthay 2006). The first is binding of peptide:MHC to the T cell receptor complex. Secondly, co-stimulatory molecules on DCs, CD80 and CD86, bind to T cell CD28. This promotes expansion and survival of the T cell. The third signal involves a polarising signal such as cytokine production by the DC, and membrane molecules including OX40L and ICAM-1. This polarisation signal instructs the differentiation of T cells towards functionally distinct Th subsets.

During maturation, DCs lower their rate of antigen uptake and reduce Fc receptor expression, but upregulate co-stimulatory molecules such as CD80, CD86 and peptide:MHC complexes. These changes in expression allows DCs to become proficient in T cell stimulation (Liu, Gao et al. 2006). Expression of chemokine receptors is also altered during DC maturation, including the upregulation of CCR7. Chemokine ligand 19 (CCL19) and CCL21 are the ligands of CCR7, and are expressed by stromal cells in the T cell areas of lymph nodes. Adhesion molecules such as intercellular adhesion molecule 1 (ICAM-1) and CD58 are upregulated allowing initial binding to T cell integrin lymphocyte function associated antigen 1 (LFA-1) (Staunton, Dustin et al. 1989, Long 2011). These signalling pathways facilitate migration of DCs to the draining lymph nodes (Hansson, Lundgren et al. 2006). DCs that migrate in steady state without activation may 'patrol' for pathogenic stimuli (Banchereau and Steinman 1998).

1.4.3 *DC subsets*

Human DCs can be split into functionally distinct subsets, conventional DCs (cDC), including cDC1 and cDC2, and plasmacytoid DCs (pDCs). Identification of these subsets in blood is determined by their expression of surface markers BDCA1 (CD1c; cDC2), BDCA2 (CD303; pDC), BDCA3 (CD141; cDC1) and BDCA4 (CD304; pDC). DCs found in the blood are thought to be the likely immature precursor of DCs found in tissue and lymphoid organs (Collin, McGovern et al. 2013). The independence of these subsets from one another has been confirmed by their requirement for specific transcription factors. These include BATF3 (cDC1), IRF4 (cDC2) and E2-2 (pDC) (Guilliams, Dutertre et al. 2016).

Although the nomenclature proposed by Guilliams *et al* is now commonly recognised and used, a previous nomenclature system can still be found in use. This can cause confusion owing a relative similarity in naming of subsets. This alternative nomenclature classifies the conventional DC subsets (cDCs) as myeloid DCs (mDCs) and again splits them by their expression of BDCA1 (CD1c) and BDCA3 (CD141). Those $CD1c^{+}CD141^{-}$ are referred to as mDC1 (cDC2 equivalent). Those $CD1c^{-}CD141^{+}$ are referred to as mDC2 (cDC1 equivalent) (Nizzoli, Krietsch et al. 2013, Chen, Denniston et al. 2015). Since this alternative nomenclature can still be found in use in recently published journals, as well as by commercial brands, it is important to highlight this difference. The remainder of this thesis discusses the nomenclature outline by Guilliams *et al* (cDC1, cDC2 and pDC).

cDC1s are highly efficient at cross-presentation to $CD8^{+}$ T cells once activated with poly I:C, promoting cytotoxic Th1 responses, in addition to producing large amounts of IFN-α after stimulation through TLR3 (Jongbloed, Kassianos et al. 2010, Meixlsperger, Leung et al. 2013). The murine equivalent of human cDC1 DCs has been identified as $CD8^{+}$ DCs (Jongbloed, Kassianos et al. 2010). cDC2s are the dominant subset of DCs driving $CD4^{+}$ Th2 and Th17 responses and express TLR1-8, with TLR 2, 4 and 5 expressed at high levels (Schlitzer, McGovern et al. 2013, Segura, Touzot et al. 2013). Although cDC2s can cross-present to $CD8^{+}$ T cells, they are less efficient than cDC1s (Haniffa, Shin et al. 2012). CD11b DCs are the murine equivalent of human cDC2s (Collin, McGovern et al. 2013). As well as being inducers of Th2 and Th17 responses, cDC2s are capable of inducing Th1 responses (Nizzoli, Krietsch et al. 2013). pDCs largely respond to viral components through TLR7 and TLR9, and produce large quantities of type I IFNs, especially IFN-α (Reizis, Bunin et al. 2011). They are distinguished from cDCs by their expression of CD303 and CD304 (Dzionek, Fuchs et al. 2000).

Recently, a reclassification of DC subsets was proposed based on single cell RNA-sequencing and functional studies of human blood DCs and monocytes (Villani, Satija et al. 2017). In total, six DC populations were identified. In addition to the identification of cDC1 (DC1) and pDCs (DC6), an additional DC population was discovered within the traditional pDC gate, identified by its $AXL^{+}SIGLEC6^{+}$ expression (DC5; 'AS DCs'). A subdivision of cDC2s reveals DC3 and DC4, identified using CD1c in combination with CD32B, CD36 and CD163. Both subsets are potent inducers of T cell proliferation. DC4 was defined by a $CD1c^{-}CD141^{-}CD11c^{+}$ and $CD16^{+}$ surface marker expression and shares gene signatures with monocytes (Villani, Satija et al. 2017). This research highlights the importance in the accurate identification of DC subsets when assessing gene signature and function. However, due to the recent publication, the remainder of this thesis discusses the traditional cDC1, cDC2 and pDC classification.

Characterisations of human DCs, nomenclatures and lineages in tissue have been limited. This has been mainly owing to difficulties obtaining human tissue, low cell numbers and a lack of distinctive markers. Therefore, most characterisation work has been carried out on circulating blood DCs, although characterisation of DCs in a number of tissues are now being studied (MacDonald, Munster et al. 2002, Haniffa, Gunawan et al. 2015).

1.5 Monocytes

Monocytes are a heterogeneous population of multi-functional mononuclear leukocytes contributing to ~10% of circulating blood mononuclear cells (Ziegler-Heitbrock, Strobel et al. 1992, Geissmann, Jung et al. 2003). They have a high cytoplasm to nucleus ratio, irregular cell shape, cytoplasmic vesicles and kidney shaped nuclei (Qu, Brinck-Jensen et al. 2014). Monocytes contribute to the innate immune response by phagocytosis, antigen presentation and cytokine production. As previously discussed, circulating monocytes were originally thought to play a major role in replenishment of macrophages in tissue (van Furth & Cohn, 1968). However, other than some specific tissues, it has been shown that most tissue-resident macrophages are actually self-renewing populations originating from embryonic stem cells. (Hashimoto, Chow et al. 2013, Gomez Perdiguero, Klapproth et al. 2015). This opens up the debate for monocytes' additional functions. Jakubizick *et al.* suggest that monocytes share the tissue surveillance characteristics of DCs as well as supporting antigen presentation and adaptive immunity. They suggest that monocytes do this without becoming professional antigen presenting cells themselves, and instead act as a surveillance and effector cell in tissues, complementary to DCs (Jakubzick, Gautier et al. 2013). However, *in vitro,* monocytes can

acquire DC-like and macrophage-like characteristics, under the appropriate culture conditions. The conditions *in vivo* which contribute to circulating monocytes entering tissues and acquiring these DC- and macrophage-like characteristics are the subject of much discussion.

1.5.1 *Monocyte subsets*

In humans, three subsets of circulating monocytes have been identified by CD14 and CD16 expression, these are; $CD14^{++}CD16^{-}$ 'classical', $CD14^{++}CD16^{+}$ 'intermediate' and $CD14^{+}CD16^{+}$ 'non-classical' (Cros, Cagnard et al. 2010, Ziegler-Heitbrock, Ancuta et al. 2010, Wong, Yeap et al. 2012). The classical $CD14^{++}CD16^{-}$ subset is the major population of monocytes, contributing to ~85% of human circulating monocytes (Wong, Yeap et al. 2012). Wong *et al.* carried out microarray analysis of this classical ($CD14^{++}CD16^{-}$) subset, revealing that a gene signature involved in tissue repair and sensing receptors, in addition to expression of inflammatory S-100 proteins (Wong, Tai et al. 2011). This demonstrates a broad range of functions. Passlick *et al.* described the non-classical ($CD14^{+}CD16^{+}$) fraction of blood monocytes. With different functional capabilities to classical monocytes, they account for approximately 10% of circulating monocytes (Passlick, Flieger et al. 1989, Wong, Yeap et al. 2012). They can stimulate T cells and patrol endothelium of blood vessels producing an inflammatory response to viral nucleic acids through TLRs 7 & 8 (Cros, Cagnard et al. 2010). It was demonstrated that this $CD14^{+}CD16^{+}$ monocyte subset is a truly independent subset through genome wide expression profiling, rather than a DC subset expressing CD16, as previously reported (Ancuta, Liu et al. 2009, Cros, Cagnard et al. 2010). The intermediate ($CD14^{++}CD16^{+}$) fraction accounts for ~5% of circulating monocytes and has a role in reactive oxygen species (ROS) production as well as angiogenesis and T cell proliferation (Wong, Tai et al. 2011). Zawada *et al.* suggested these cells are predisposed for antigen presentation and subsequent T cell proliferation due to higher expression of MHCII (Zawada, Rogacev et al. 2011). Furthermore, this subset is thought to produce the largest amounts of tumor necrosis factor-alpha (TNF-α) and IL-1β after stimulation by LPS.

1.5.2 *Monocyte differentiation in tissue*

It has been demonstrated that the extent of monocyte differentiation in tissues is unclear. How the synovial tissue may mediate monocyte differentiation is also unknown. Kawanka *et al.* indicate that circulating monocytes are activated by excess cytokines into a $CD16^{+}$ phenotype, before entry into the synovial compartment. Cytokines involved in this process include TGFβ1, macrophage colony stimulating factor (M-CSF) and IL-10 (Kawanaka, Yamamura et al. 2002). This coincides with early findings by Burmester *et al.* that monocytes infiltrate synovial tissue, and that the cytokines produced by $CD16^{+}$ cells contribute to the pathogenesis of RA

(Feldmann, Brennan et al. 1996, Burmester, Stuhlmuller et al. 1997). This leaves the idea of a feedback loop, in which infiltrating monocytes are activated by cytokines including TNF-α and IL-1β. Once activated by these cytokines, monocytes then contribute to this TNF-α and IL-1β production.

In sequence with recent investigations of monocyte differentiation in tissues, McGovern *et al.* challenged the classification of a dermal $CD14^+$ 'DC' population in steady-state tissues, classified as DC on the basis of their MHCII expression and *ex vivo* migratory behaviour. They demonstrate that their gene-expression profile overlaps with that of circulating monocytes and tissue macrophages. Additionally their inability to stimulate naïve T cells suggests that they more closely resemble a monocyte-derived tissue resident macrophage population (McGovern, Schlitzer et al. 2014).

Monocytes may enter tissue, carrying out specialised functions and change their phenotype entirely. However, contrasting arguments suggest that monocytes do not differentiate in tissue and instead survey the environment and migrate back out. This level of conflict in literature highlights the importance of research into monocyte functions, with special regard to their role once migrated to tissue from blood. Overall, further investigation needs to be carried out to advance the understanding of monocyte activation and differentiation in tissues.

1.6 The Musculoskeletal System

The human musculoskeletal system provides support and stability, in addition to allowing controlled movement of the body. It is primarily composed of the skeletal and muscular systems, in addition to a range of connective tissues including cartilage, tendons, ligaments and other connective tissues within the joint space. Synovial joints are indirectly connected by ligaments. These ligaments are lined by a synovial membrane, which secretes synovial fluid to lubricate the joint.

Musculoskeletal disorders cause acute and chronic pain and are one of the largest burdens to global morbidity. Between 1990-2010, musculoskeletal disorders had one of the largest (88%) global increases in incidence out of non-communicable diseases (Global Burden of Disease, 2010). There are over 200 musculoskeletal disorders including fibromyalgia, ankylosing spondylitis, idiopathic lower back- and neck-pain and arthritis (Arthritis Research UK, 2017). The two most common forms of arthritis are OA and RA, both causing joint stiffness, pain and inflammation. However, the causal mechanisms of disease pathogenesis differ greatly between these two arthritides.

The normal synovial membrane is relatively acellular, only 1-2 cells thick across the intimal layer (Smith, 2011). The sublining consists of mainly fat cells and fibroblasts, although macrophages and lymphocytes can be identified in lesser quantities. Conversely, macrophages are the main cell type in the intimal layer.

1.7 Inflammatory Arthritis

Throughout this thesis, inflammatory arthritis (IA) is a term that will be used to describe classically inflammatory arthritic conditions, when being used as a control or comparator. Although this mainly encompasses RA, it also includes other inflammatory conditions such as Psoriatic arthritis (PsA). When disease-specific mechanisms or research are being discussed, IA will not be used and instead, the disease-specific abbreviation.

RA is thought to be a chronic autoimmune disease inducing synovial inflammation and joint destruction resulting in significant disability, morbidity as well as increased mortality compared to the general population (Chen, Wang et al. 2006, Lebre, Jongbloed et al. 2008, Pieringer and Pichler 2011, Koo, Kim et al. 2013). RA is a systemic disease and can lead to diffuse inflammation in the lungs, heart membrane, whites of the eyes and nodular lesions in the skin (McInnes and Schett 2011). Autoimmunity is an aberrant immune response to 'self' cells and tissues. Central and peripheral tolerance are immunological mechanisms developed to prevent autoimmunity. Central tolerance involves the deletion of self-reactive T- and B-cells during their development in primary lymphoid organs. However, not all auto-reactive cells are deleted by this process. Therefore, additional mechanisms of tolerance operate within peripheral tissues. These mechanisms include the induction of anergy through antigen presentation in the absence of co-stimulatory signals, or through active suppression by cells such as Tregs. It is thought that a break in central tolerance leads to the generation of auto-reactive T cells, whereas a break in peripheral tolerance may lead to the aberrant activation and expansion of pre-existing auto-reactive T cells. A failure of either of these mechanisms may contribute significantly to RA pathogenesis (Chen, Wang et al. 2006).

The antigen-specific reaction in RA remains unclear. In seropositive disease, post-translational modifications may result in citrullinated peptides (Burska, Hunt et al. 2014). Indeed, the clinical presentation of RA includes production of the autoantibodies rheumatoid factor (RF) and anti-citrullinated protein antibody (ACPA)), as well as synovial inflammation and hyperplasia, and joint destruction (McInnes and Schett 2011). Genetics factors have been shown to contribute ~60% variation in liability to RA, with environmental factors such as smoking

also playing a role (MacGregor, Snieder et al. 2000). As treating RA early results in a more beneficial outcome, there is much research being carried out into early biomarkers for RA as well as defining predictors for drug response (Isaacs and Ferraccioli 2011). Unlike OA, there are disease-modifying medications available for RA, including anti-inflammatory drugs, such as steroids, which may suppress symptoms and inflammation. Non-steroidal anti-inflammatory drugs (NSAIDs), are potent suppressors of disease activity, but may have many unwanted side effects over time. DMARDs, such as non-biologic methotrexate, used first line, and biologics such as anti-TNF, aim to stop the progression of disease activity and have proved effective in many patients. However, the pathogenesis of RA is yet to be fully understood.

RA is characterised by the inflammation of the synovial tissue. In RA, joint damage initiates within the synovial tissue, where vasculitis and immune cell infiltrate, predominantly T- and B-cells, result in synovitis. Antigen presentation and cytokine production within the synovial tissue further exacerbate this inflammation and angiogenesis. The formation of an invading synovial pannus may cause erosions of nearby bone. Subsequent production of pro-inflammatory cytokines and metalloproteinases (MMPs) by synoviocytes and chondrocytes causes cartilage degradation. Although many of the mechanisms of joint destruction in PsA are similar to RA, there are key differences. These include a T cell predominance in PsA synovium, absence of circulating autoantibodies in PsA and the early expression of vascular growth factors and distinct vascular pathology in PsA (Veale and Fearon 2015). PsA is associated with the development of psoriasis. Similarly, a number of other arthritic conditions can be associated with co-morbidities. These include enteropathic arthritis and inflammatory bowel disease, gout and the build up of sodium urate crystals in the joint, and reactive arthritis after infection.

1.8 Osteoarthritis

OA has historically been viewed as a wear and tear disease. However, it is becoming recognised that synovial inflammation may be a key mediator in disease pathogenesis. The understanding of synovial cellular mechanisms in OA pathogenesis is lagging behind the detailed understanding of how synovial cells perpetuate RA pathogenesis. This may be partly explained by the relatively recent recognition of these inflammatory processes in OA. Figure 1.3 demonstrates the recent increase in ‘Osteoarthritis’ research articles being published.

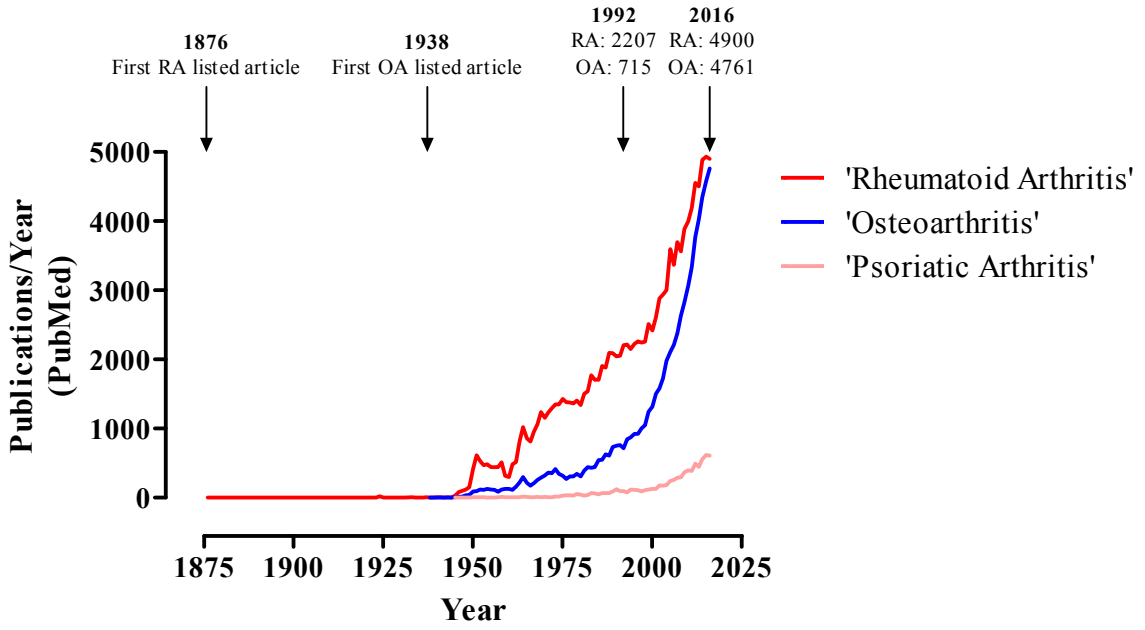

Figure 1.3: Published research relating to rheumatoid arthritis, osteoarthritis and psoriatic arthritis
PubMed was used to search for articles with the terms 'Rheumatoid arthritis', 'Osteoarthritis' or 'Psoriatic Arthritis' (18/09/2017). Lists of publications by year were downloaded and plotted in GraphPad Prism.1876 and 1938 are the first recorded publications for RA and OA listed on PubMed, respectively. In 1992, there was a difference of 1492 articles between RA and OA, whereas in 2016 this difference has reduced to 139 articles.

1.8.1 *National Institute for Health and Care Excellence (NICE) guidelines for diagnosis of OA*

OA is characterised by the progressive degradation of articular cartilage and subchondral bone (Fig. 1.4). This leads to the pain, stiffness and inflammation of the associated joint. The primary sites of OA are synovial joints, including knees, hips and hands.

A diagnosis of OA can be made without investigation if the patient is over 45, has activity-related joint pain, and has either no morning joint-related stiffness or morning joint-related stiffness that lasts no longer than 30 minutes. Signs of OA joint involvement include joint pain, stiffness, effusion, tenderness, crepitus and locking. A holistic approach assesses the disease effect on a patient's quality of life, summarised in Figure 1.5. Imaging can also be used to aid in the diagnosis of OA. X-rays, magnetic resonance imaging (MRI) and ultrasound are used to identify joint space narrowing and the presence of osteophytes (Braun and Gold 2012).

OA is a multifactorial disorder with risk factors including, age, ethnicity, sex, nutrition, obesity, genetics and local injury (Felson, Lawrence et al. 2000). OA can be further characterised into primary and secondary OA. Primary OA is used as a classification for patients where there is no clear cause for their disease development, including the aging population. Secondary OA is used for patients who have an associated risk factor which is the probable cause such as local injury, obesity, genetics and inflammation in the joint (Felson, Lawrence et al. 2000).

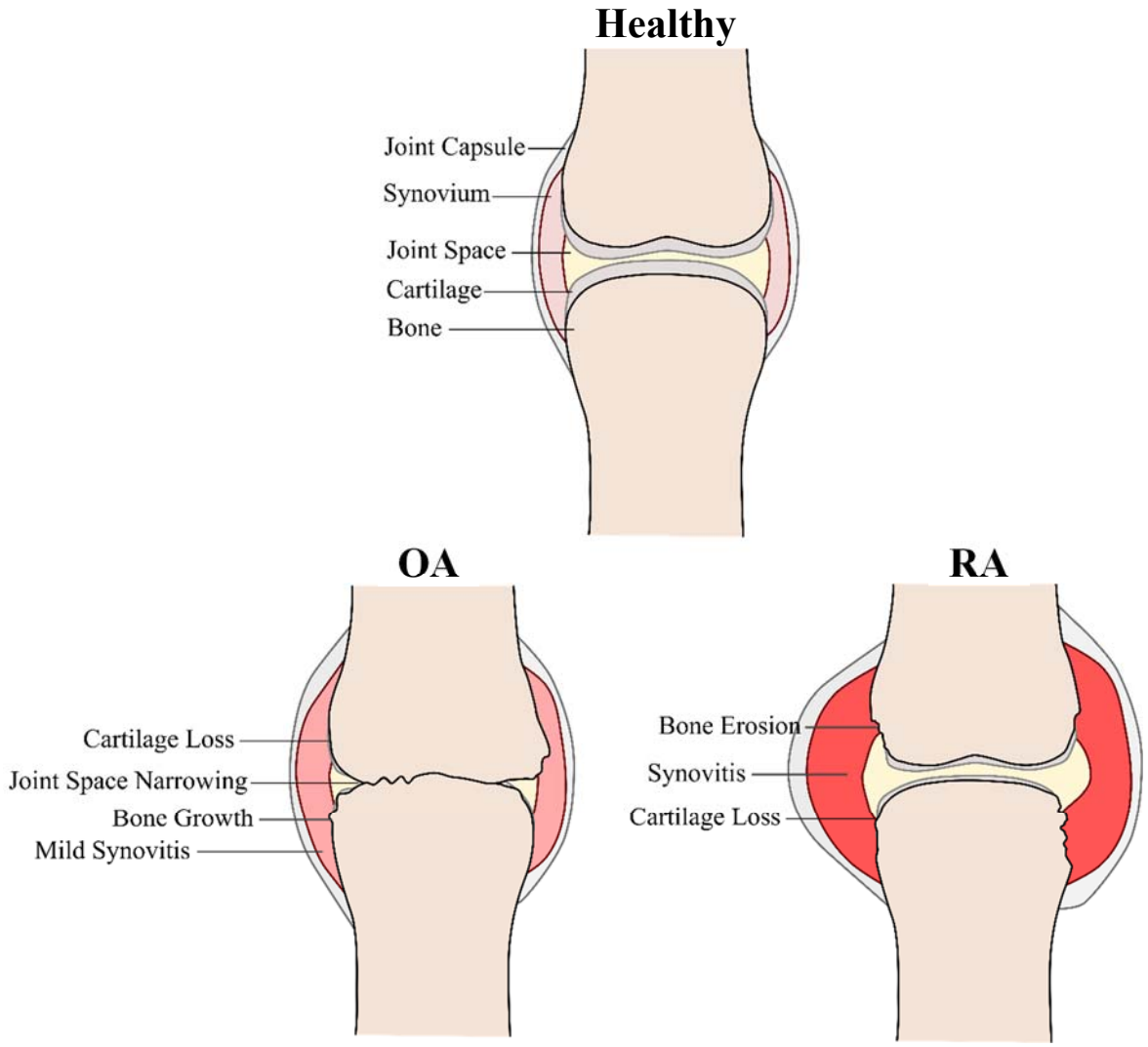

Figure 1.4: Key characteristics of healthy, osteoarthritis and rheumatoid arthritis joints
The healthy synovial joint is mainly composed of the bone ends lined with cartilage. These are connected by the synovial membrane and joint capsule. The joint space is filled with synovial fluid secreted by the synovial membrane. Osteoarthritis (OA) is characterised by narrowing of the joint space, degradation of cartilage and osteophyte formation. Rheumatoid arthritis (RA) is characterised by synovial inflammation and bone destruction.

Figure 1.5: Holistic approach to OA diagnosis and management
A holistic approach to the diagnosis and management of osteoarthritis (OA) is taken to assess the effect of disease on the patients overall quality of life. Key factors include health, social and occupational impacts in addition to range of other issues depicted above.

1.8.2 *Pathogenesis of Osteoarthritis*

Risk factors of OA can be distinguished by two mechanisms initiating the early stresses on the joint. These are the abnormal loading on a normal joint structure or the normal loading on an abnormal joint structure (Goldring and Goldring 2010). Alongside cartilage degradation, subchondral bone sclerosis occurs and subsequent biochemical and biomechanical changes disrupt joint homeostasis, affecting other local tissues. This joint damage is associated with the overproduction of cytokines and growth factors. It has been previously shown that synovial macrophages play a key role in the overt production of TNF-α and IL-1β in OA synovium (Bondeson, Wainwright et al. 2006). These can subsequently influence the production of aggrecanases and collagenases such as MMP1, MMP13, a disintegrin and metalloprotease with thrombospondin (ADAMTS4) and ADAMTS5, contributing to cartilage destruction. Proteoglycans and type II collagen fragments produced during cartilage breakdown enter the synovial fluid. This in turn elicits an immune response resulting in synovitis. Whether this synovitis is primary or secondary to disease remains unclear. The resultant expression of MMPs and cytokines from joint damage are catabolic, resulting in a positive feedback loop promoting the further production of these catabolic factors and cartilage destruction (Fig. 1.6). Although the extent of joint damage in OA is known, the underlying pathology, particularly at the cellular level, remains poorly understood.

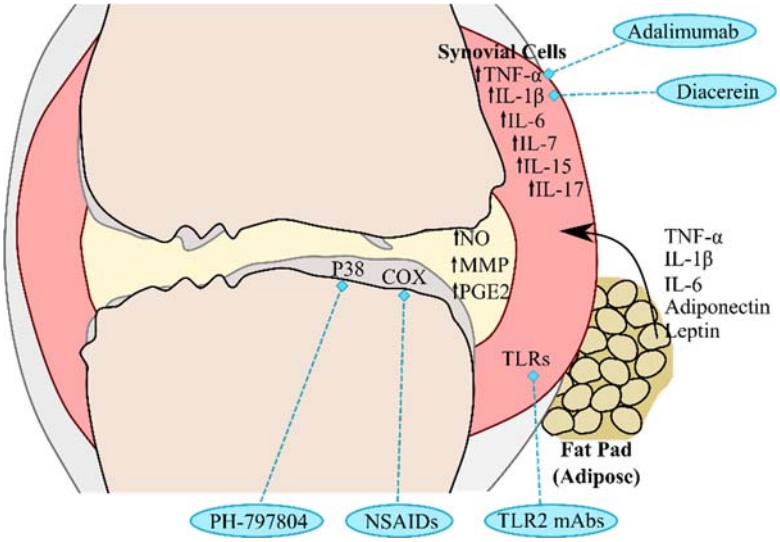

Figure 1.6: Pathogenesis of joint destruction and disease modifying strategies for OA
Joint destruction in OA is led by a number of mechanisms. These include the secretion of adipokines by the fat pad, and cytokines by cells in the synovial membrane. Cartilage degradation promotes the further upregulation of MMPs, PGE2 and NO further contributing to cartilage destruction. Proteoglycans and type II collagen fragments enter the synovial fluid. It remains unclear whether associated synovitis is primary or secondary to disease. A number of disease modifying treatments have targeted specific pathways in OA, but have had disappointing results (Philp, Davis et al. 2017).

1.8.3 *Management and treatment of OA*

Similar to diagnosis, a holistic approach is taken with the management and treatment of a patient with OA. Currently, there are no disease modifying treatments in use clinically, and instead, symptoms and pain are managed.

Non-pharmacological treatments include exercise, weight loss, diet improvement, thermotherapy, acupuncture and physical aids such as adaptive footwear, external braces and walking sticks. Pharmacological treatments encompass mainly NSAIDs in the form of oral analgesics and topical treatments. Selective cyclooxygenase 2 (COX-2) inhibitors can also be used. For severe pain, articular corticosteroid injections may be administered. Surgical intervention will be considered if previous management strategies fail, but before the patient has prolonged functional limitation and severe pain. Patients who are referred for surgery typically experience joint pain, stiffness, and reduced joint function, all having a substantial impact on their quality of life. Although total joint replacement can provide therapeutic relief, they are only suitable for end-stage disease, provide reduced function compared to a healthy joint, and can 'wear out' over time.

In a meniscal tear model of OA in rats, an autologous protein solution was shown to decrease collagen and cartilage degradation (King, Bendele et al. 2017). This solution contained white blood cells, platelets, concentrated plasma and anti-inflammatory IL-1Rα, sIL-1RII and sTNF-RII. Although this did not have a completely regenerative effect, it did demonstrate that this autologous treatment had a disease-modifying effect in this model of OA.

1.8.4 *Inflammation in Osteoarthritis*

It is now becoming clear that inflammatory processes may be a key mediator in the pathogenesis of OA (Sellam and Berenbaum 2010, Scanzello and Goldring 2012). Synovial inflammation in OA exhibits synovial hypertrophy and hyperplasia, a mixed leukocyte infiltrate and is present in 50-70% of OA patients (Sellam and Berenbaum 2010, Kapoor, Martel-Pelletier et al. 2011, Scanzello and Goldring 2012, Moradi, Rosshirt et al. 2015). Elevated levels of pro-inflammatory mediators including TNF-α, IL-1β, IL-6, IL-15, IL-17, IL-18 and nitric oxide (NO) have been reported in the serum and synovial fluid of OA patients compared to healthy controls (Benito, Veale et al. 2005, Kapoor, Martel-Pelletier et al. 2011). However, inflammation is usually local and low grade, not resulting in systemic inflammation as observed in RA patients. Correlations between OA synovial inflammation and clinical symptoms of OA, including pain, swelling, reduced joint mobility and cartilage damage, have been reported (Ayral, Pickering et al. 2005, Torres, Dunlop et al. 2006, Baker, Grainger et al. 2010, Conaghan,

D'Agostino et al. 2010, Roemer, Crema et al. 2011, Scanzello, McKeon et al. 2011). The presence of synovitis in early OA has been observed before radiographic joint damage can be detected, suggesting it plays an active role in subsequent damage. However, it remains unknown whether this inflammation is causal or consequential. Understanding these early mechanisms, and how they interlink, will be essential to fully understanding the underlying causes of joint damage in OA.

Although it has been shown in animal models that targeting synovitis slows OA progression and reduces symptoms, clinical trials for OA patients with anti-inflammatory drugs have shown limited success (Frisbie, Ghivizzani et al. 2002, Schelbergen, Geven et al. 2015, Philp, Davis et al. 2017). These have included TNF-α inhibition, IL-1β inhibition, arachidonic acid pathway inhibitors and NO inhibitors. However, there is a range of alternative strategies currently undergoing *in vitro* and *in vivo* pre-clinical validation. These target a range of cytokines (IL-7, IL-15, IL-17), p38 mitogen-activated protein kinases (MAPKs), TLR2 & 4, adipokines (leptin), TNF-α siRNA and pan cytokine siRNA (Fig. 1.6) (Philp, Davis et al. 2017).

When studying inflammation and synovitis in OA, it may also be important to consider disease pattern. For example, it has been demonstrated that the cellular infiltrate differs between uni-compartmental (UC) and bi-compartmental (BC) OA of the knee (Moradi, Rosshirt et al. 2015). BC OA had a high inflammatory profile driven by both $CD14^+$ macrophages and $CD4^+$ T cells, whereas in UC OA, $CD14^+$ macrophages were the predominant cell type. Another consideration will be the analysis of synovial tissue from different joint sites. Although differences have been observed phenotypically and through RNA-sequencing of gene expression, these differences were deemed acceptable, and the use of tissue from multiple joints suitable when necessary (Kraan, Reece et al. 2002, Frank-Bertoncelj, Trenkmann et al. 2017). This is discussed further in Chapter 4.

The disappointing early results in clinical trials testing disease modifying drugs for OA could be due to the known heterogeneity of OA patients, and a lack of appropriate patient stratification. Indeed, through assessment of historical clinical trial data, it was found that OA patients have not been previously stratified on the basis of synovitis or other inflammatory biomarkers (Philp, Davis et al. 2017). A more comprehensive understanding of the cellular and molecular mechanisms that govern low-grade synovial inflammation in OA will be instrumental in identifying patients that could be targeted for clinical benefit.

1.8.5 *Synovial macrophages in OA*

Although there is extensive research focussed on the pathogenesis of OA, there is limited information about the roles of immune cell subsets in the synovial tissue. Early studies showed that macrophages are a key contributor to the pathogenesis of RA within the inflamed synovial joint, where they are found in abundance and produce pro-inflammatory cytokines including IL-1β, TNF-α, IL-18 and GM-CSF (Gracie, Forsey et al. 1999, Kinne, Brauer et al. 2000, Liew, Wei et al. 2003). Much of this research has included histological analysis (Haywood, McWilliams et al. 2003, Kennedy, Fearon et al. 2011, Manferdini, Paolella et al. 2016). Additionally, a recent non-invasive imaging study with a folate receptor-β-based agent has shown that the quantity of activated macrophages in the knee of OA patients correlated with disease severity and progression (Kraus, McDaniel et al. 2016).

Macrophages in OA synovial tissue are thought to respond to DAMPs, and as a consequence, contribute to cartilage destruction and osteophyte formation through the production of MMPs and cytokines including IL-1β, TNF and TGFβ (Blom, van Lent et al. 2004, van Lent, Blom et al. 2004, Bondeson, Blom et al. 2010). Further evidence of the macrophages' role in pathogenesis is the histological observation of enhanced numbers in OA synovium correlating with the degree of synovial angiogenesis, in line with the previously mentioned findings from the folate receptor imaging study (Haywood, McWilliams et al. 2003, Benito, Veale et al. 2005, Manferdini, Paolella et al. 2016). Furthermore, it has been shown that depletion of macrophages from synovial tissue cultures *in vitro* eliminates IL-1β and TNF production, in addition to downregulation of fibroblast produced cytokines and MMPs (Bondeson, Wainwright et al. 2006). It was also shown that, unlike in RA, IL-1β production was independent of TNF-α in OA.

It has been shown that depletion of macrophages in animal models reduces osteophyte formation (Blom, van Lent et al. 2004, van Lent, Blom et al. 2004). This study used a collagen induced OA model and chlodronate depleted macrophages. The authors suggest that macrophages may be the pivotal cell in the synovium mediating OA pathology including fibrosis and osteophyte formation. In contrast, results from a meniscal-tear induced OA model demonstrated no mitigation of cartilage degeneration, and instead enhanced joint synovitis, characterised by an infiltration of $CD3^+$ T cells and neutrophils (Wu, McNeill et al. 2017). Although osteophyte formation was similarly reported to be reduced, this was only to the same level as the non-macrophage depleted control. This may be owing to the decreased levels of TGFβ1 measured in the serum. These decreased levels of TGFβ1 were mirrored by an increase of pro-inflammatory cytokines in both serum and synovial fluid. It was hypothesised that in the

setting of obesity, macrophages are vital for modulating homeostasis of immune cells, and that the targeted depletion of specific macrophage subsets may mitigate inflammation and OA in obesity. It has additionally been reported that a mix of both pro- and anti- inflammatory M1 and M2 macrophages are present in the synovium of OA patients (Manferdini, Paolella et al. 2016).

These studies demonstrate the possible heterogeneity of macrophage function in OA. Despite the evidence of macrophages contribution to OA pathogenesis, it is likely that their role is more complex than causing just inflammation through production of various pro-inflammatory factors, or just contributing to tissue regulation. Macrophages are heterogeneous cells with wide ranging anti-inflammatory functions relevant to OA, including tissue repair, phagocytosis and dampening down of inflammation. A traditional model for the study of macrophages is the discussed M1/M2 paradigm. This macrophage model has been useful for understanding the roles macrophages play in inflammation and repair, but it is becoming recognised that this paradigm does not accurately represent macrophage activation *in vivo,* and rather demonstrates extreme examples of macrophage activation (Xue, Schmidt et al. 2014). There is a need to further understand the role of macrophages in OA pathogenesis. This will aid in the design of therapies that potentially target only a subset of macrophages.

During tissue remodelling after injury, pro-inflammatory macrophages remove necrotic material, kill pathogens if present, and may promote proliferation of new tissue cells. Subsequently, anti-inflammatory macrophages dampen down inflammation, promote differentiation of newly recruited or expanded cells, and stimulate depositions of new extracellular matrix. The recognition of both pro- and anti-inflammatory macrophages playing roles in tissue remodelling has been previously observed (Novak and Koh 2013, Brown, Sicari et al. 2014). However, the specific processes involved in these roles will depend on the specific tissue environment, and will likely differ greatly between different tissues and types of tissue injury. Although both pro- and anti-inflammatory macrophages are thought to be crucial in tissue repair, the transition from these states is key to resolution and avoidance of associated complications (Sindrilaru, Peters et al. 2011).

There is a substantial body of evidence to suggest the presence of activated synovial macrophages in OA, and their correlation with disease progression. However, the specific mechanisms of action are yet to be fully understood. In the context of the synovium in OA, it is unknown whether macrophages are pro- or anti-inflammatory, or a mixture, fluctuating between different stages of disease. Despite this lack of knowledge, it is likely that an imbalance between pro- and anti-inflammatory macrophages contributes to low-grade chronic

inflammation, subsequently progressing OA disease activity. To fully understand these polarisation states, it is first necessary to establish the full phenotypes of macrophages present in OA synovium.

Previously conducted gene expression work in synovial macrophages has been mostly by candidate polymerase chain reaction (PCR) in RA. RNA-sequencing has been previously conducted on synovial fibroblasts, likely owing to their relative abundance, and ease of expansion *ex vivo*. Again, this has been mostly conducted in RA, but with some studies using OA as controls. The only evidence of RNA-sequencing on macrophages in the context of arthritis is $CD14^+$ cells isolated from peripheral blood of healthy donors. These cells were differentiated *ex vivo* into a macrophage phenotype (Heruth, Gibson et al. 2012, Donlin, Jayatilleke et al. 2014, Wang, Xia et al. 2014, Shepherd, Skelton et al. 2015, Mizoguchi, Slowikowski et al. 2017). Although previous studies on the synovium of arthritis patients have been mostly histology- and imaging-based, the use of tissue digestion, flow cytometry and gene expression has been shown to be achievable (Kraan, Reece et al. 2002, Van Landuyt, Jones et al. 2010, Frank-Bertoncelj, Trenkmann et al. 2017). An accurate and in-depth analysis of the cellular mechanisms in OA synovial tissue, particularly those involving macrophages, will be key to progress our understanding of the role that synovial inflammation plays in this disease.

1.9 Hypothesis and aims

It is has become recognised that synovial inflammation contributes to the pathogenesis of OA. However, it is unclear what the role of synovial immune cell subsets in driving and regulating this process is. This is partly due to technical barriers.

1.9.1 *Hypothesis*

I hypothesise that there is heterogeneity at the cellular and molecular level in the synovial tissue of osteoarthritis patients, particularly within synovial macrophages. Heterogeneity within these synovial macrophages will be important to address as this likely reflects heterogeneity in the specific tissue environment of these arthritic joints.

1.9.2 *Aims*

To investigate this hypothesis, a set of three overarching aims were outlined, summarised below. These aims are discussed in detail in the subsequent three results chapters.

(1) Develop technical protocols to allow the successful isolation, identification and purification of immune cell populations from synovial tissue. This will encompass the isolation of a single cell suspensions from synovial tissue with high cell viability, large yields, and minimal surface marker cleavage. The design of a flow cytometry panel will allow the purification of multiple cell subsets by fluorescence-activated cell sorting.

(2) Enumerate the immune cell subsets present in the synovial tissue of OA and IA patients. To achieve this, methods for the accurate quantification will be assessed and confirmed with computational analyses.

(3) Conduct an in-depth analysis of synovial macrophages in OA. Highly purified synovial macrophages from OA and IA patients will be extensively phenotyped and functionally assessed. The gene expression profiles of synovial macrophages will be determined by RNA-sequencing.

Chapter 2. Materials and Methods

2.1 Ethical Approval

Osteoarthritis synovial tissue and peripheral blood samples were obtained through the Newcastle Bone and Joint Study (NBJS) after suitable elective patients were identified by designated research nurses (Freeman Hospital). Informed consent was obtained and patients enrolled as study participants. In line with patient confidentiality, samples were allocated anonymised NBJS numbers. Ethical approval was granted by the Newcastle and North Tyneside Research Ethics Committee (REC reference number 09/H0906/72).

IA synovial tissue and peripheral blood samples were obtained from the Newcastle Early Arthritis Clinic (NEAC). Ultrasound-guided synovial tissue biopsies were collected by Dr. Arthur Pratt. Informed consent was obtained and patients enrolled as study participants. In line with patient confidentiality, all samples were allocated anonymised Early Arthritis (EA) numbers. Ethical approval was granted by the Newcastle and North Tyneside 2 Research Ethics committee (REC reference number 12/NE/0251).

Healthy peripheral blood samples were obtained from volunteers following informed consent from the Newcastle Academic Health Partners Bioresource. Ethical approval was granted by the Newcastle and North Tyneside Research Ethics Committee (REC reference 12/NE/0395). Leucocyte Reduction System (LRS) cones from platelet donations by healthy volunteers were purchased from the National Blood Service (Newcastle upon Tyne).

2.2 Tissue Culture

All cell cultures were carried out in RF10: (RPMI 1640; Sigma Aldrich) supplemented with 10% (v/v) Fetal Bovine Serum (FBS; Gibco), 100U/ml penicillin, 100µg/ml streptomycin, and 2mM glutamine (All Sigma-Aldrich) at 37ºC, 5% CO_2. Cell washes were carried out with Hanks Balanced Salt Solution (HBSS Ca^{2+} and Mg^{2+} free; Lonza) supplemented with 1% (v/v) FBS. All cell counts were carried out using trypan blue (Sigma Aldrich) exclusion on a Burker counting chamber (Mairenfel-Superior). The average of three counts over 25 squares in a grid was taken as the cell count. The cell count was multiplied by 10^4 to account for the chamber volume, and the dilution factor, to gain cells/ml.

2.3 Cell isolation

2.3.1 *Peripheral Blood Mononuclear Cell (PBMC) Isolation*

Fresh peripheral blood was collected in EDTA (Ethylenediaminetetraacetic acid; Fischer Scientific) vacutainers (Greiner Bio-One). Peripheral blood was diluted 1:1 (LRS Cones 1:2) with room temperature HBSS +2mM EDTA. PBMCs were isolated using density gradient centrifugation over Lymphoprep (Axis Shield). 20ml diluted blood was layered over 15ml Lymphoprep and centrifuged for 30 mins at room temperature (895g). PBMCs were recovered from the interface and washed for 7 mins at 4ºC (600g) to remove any contaminating Lymphoprep. PBMCs were then washed for 7 mins at 4ºC (250g), twice, to remove any platelets. Final cell suspension was filtered through a 70µm nylon filter to remove any debris, and counted as previously described.

2.3.2 *$CD14^+$ Monocyte Isolation*

$CD14^+$ monocytes were positively selected using magnetic assisted cell sorting (MACS®) with anti-CD14 magnetic microbeads (Miltenyi Biotec). PBMCs were washed and resuspended in ice-cold MACS buffer (Phosphate Buffered Saline (PBS; Lonza), + 2mM EDTA, + 0.5% FBS) at 80µl per $10x10^6$ PBMC. 10µl CD14 MicroBeads per $10x10^6$ PBMCs were added with gentle agitation. PBMCs were incubated on ice for 20 mins with gentle agitation every 5 minutes. PBMCs were washed with MACS buffer for 7 mins at 4ºC (400g) to remove any unbound microbeads. Cell pellet was resuspended in 3ml MACS buffer. PBMCs were added to an LS column mounted in a MACS® magnetic separator (Miltneyi Biotec), pre-rinsed with MACS buffer. Columns were washed through 3 times with 3ml ice-cold MACS buffer. $CD14^+$ labelled cells are retained by attraction to the magnetic beads in the column, and $CD14^-$ cells are washed through. LS column was removed from separator and $CD14^+$ cells flushed out with 5ml MACS buffer. Cells were washed in ice-cold MACS buffer and resuspended in cold culture media. An average yield of 15-20% $CD14^+$ monocytes was expected from the PBMC population.

2.3.3 *Synovial tissue mononuclear cell isolation*

Synovial tissue was stored overnight (<18 hours) in RF10 at 4ºC. Where possible, any visible fat was carefully removed from the synovial tissue. Synovial tissue was mechanically digested into 1mm fragments using scissors, scalpel and forceps. During mechanical digestion, tissue was always submerged in RF10 to avoid drying. Tissue and media was transferred to a 20ml universal tube and topped up to 10ml with warm RF10. Liberase TM (Roche) was added at a final concentration of 15µg/ml and DNase (Roche) at 30µg/ml. Tube was transferred to a shaking incubator and shaken for 45 mins at 37ºC (260rpm). Additional manual vigorous

shaking was applied every 15 mins during incubation. Solution was filtered through a 100µm filter and filtrate immediately placed on ice to inhibit enzymatic digestion. Any remaining tissue was subjected to a second repeated mechanical and enzymatic digestion with filtering. A third digestion on any remaining tissue was carried out. The three filtrates were pooled, washed and counted.

2.4 Generation of monocyte-derived macrophages (moMac)

$CD14^+$ monocytes were cultured at a concentration of $0.5x10^6$cells/ml RF10 in 24-well plates (Corning) for 6 days. Cells were cultured with 50ng/ml M-CSF (Peprotech). On day 3 media was refreshed by removal of 450µl media, and addition of 500µl warm RF10 supplemented with 100ng/ml M-CSF. After 6 days, cells were incubated on ice for 1 hour to loosen from the plate. Cells were then harvested, washed three times and resuspended in appropriate media.

2.5 Generation of monocyte-derived dendritic cells (moDC)

$CD14^+$ monocytes were cultured at a concentration of $0.5x10^6$cells/ml RF10 in 24-well plates for 6 days. Cells were cultured with 50ng/ml IL-4 (Immunotools) and 50ng/ml GM-CSF (Immunotools). On day 3, media was refreshed by removal of 450µl media, and addition of 500µl warm RF10 supplemented with 100ng/ml IL-4 and 100ng/ml GM-CSF. After 6 days, cells were incubated on ice for 1 hour to loosen from the plate. Cells were then harvested, washed three times and resuspended in appropriate media.

2.6 Flow Cytometry

2.6.1 *Cell surface staining*

For cell surface staining, single cell suspensions were resuspended at either $1x10^6$ cells or entire tissue digest ($\leq 5x10^6$ cells) per 100µl staining buffer (PBS + 3% FBS, + 2mM EDTA, + 0.1% sodium azide (Sigma-Aldrich)). Cells were incubated for 30 mins on ice with 2.5µl human IgG per $1x10^6$ cells, and selected flow cytometry antibodies (Table 2.1). Titration of antibodies for optimised flow cytometry panel (Chapter 3) were carried out on PBMCs (data not shown), and efficacy confirmed on synovial tissue cells. Additional antibody titrations were carried out by members of the Musculoskeletal Research Group, or antibodies used at manufacturers recommended dilution. Dilutions of all antibodies are listed in table 2.1. After incubation, cells

were washed twice in staining buffer for 7 mins at 4ºC (400g) and resuspended in a final volume of 200µl staining buffer. 7-Aminoactinomycin D (7-AAD) viability dye (BD Biosciences), was added at 20µl/1x10^6 cells, 10 mins prior to data acquisition on an LSR Fortessa X20 (BD Bioscience). Flow cytometry data were analysed using FlowJo (TreeStar) software and CytofKit bioconductor package for R. In addition, tSNE, SPADE and CITRUS analyses were performed in Cytobank on flow cytometry data sets.

2.6.2 *Fluorescence activated cell sorting (FACS)*

Cell suspensions were prepared following the same methods outlined in 2.6.1, and resuspended at ≤5x10^6 cells/ml staining buffer. Cell subsets were isolated on a BD FACSAria FUSION cell sorter (BD Biosciences) at 4ºC using the gating strategy discussed in Chapter 3. Gates were applied using fluorescence minus one (FMO), such as CD45 described in Chapter 3.5. Additional examples are demonstrated in Appendix 2.1. During FACS sorting, the stream of cells is separated into single cell droplets, to which electrical charges are applied according to their fluorescent parameters. These droplets then pass through oppositely charged plates, guiding them into assigned eppendorfs. For all sorts, the FACS sorter was operated on the highest purity configurations. For downstream applications involving cell culture, cells were sorted into 4ºC RF10. For genomic analysis, cells were sorted directly into RLT buffer (Qiagen) +1% Beta-Mercaptoethanol (Sigma Aldrich), vortexed and immediately frozen on dry ice.

Antibody	Dilution	Fluorophore	Clone	Company
CCR2	1:50	BV421	48607	BD Biosciences
CCR7	1:20	APC	150503	R&D Systems
CD1c	1:50	PE	L161	Biolegend
CD1c	1:50	PE-Cy7	L161	Biolegend
CD11b	1:50	BV785	ICRF44	Biolegend
CD11c	1:50	BV421	B-ly6	BD Biosciences
CD11c	1:50	V450	B-ly6	BD Biosciences
CD14	1:50	APC-Cy7	HCD14	Biolegend
CD16	1:20	BV711	3G8	Biolegend
CD16	1:50	BV605	3G8	Biolegend
CD172a/Sirp-α	1:50	PerCP-Cy5.5	SE5A5	Biolegend
CD19	1:100	PE-Cy5.5	SJ25cl	eBiosciences
CD19	1:50	AF700	HIB19	BD Biosciences
CD20	1:100	PE-Cy5.5	2H7	eBiosciences
CD20	1:50	AF700	2H7	BD Biosciences
CD206	1:50	BV786	19.2	BD Biosciences
CD206	1:50	APC	15-2	Biolegend
CD3	1:20	BV786	UCHT1	BD Biosciences
CD3	1:100	AF700	UCHT1	BD Biosciences
CD3	1:20	APC	UCHT1	Biolegend
CD4	1:200	PE-Cy7	RPA-T4	Biolegend
CD4	1:200	PE	SK3	Biolegend
CD45	1:10	V500	HI30	BD Biosciences
CD64	1:50	APC	10.1	Biolegend
CD64	1:50	PE	10.1	Biolegend
CD83	1:50	PE-Cy7	HB15E	Biolegend
CD86	1:50	PerCP-Cy5.5	IT2.2	Biolegend
CD90	1:50	APC	5E10	BD Biosciences
FOLR2	1:50	PE	EM-35	EXBIO
HLA-DR	1:50	APC	G-46-6	BD Biosciences
HLA-DR	1:20	PerCP	L203	R&D Systems
Viability Dyes	**Concentration**	**Detection**	**Clone**	**Company**
DAPI	3µm	355nm 379/28	-	Life Technologies
7-AAD	20µl/1x10^6 Cells	561nm 780/60	-	BD Biosciences

Table 2.1: Flow cytometry antibodies used for surface staining

2.7 Microscopy Slide Preparations

2.7.1 *Cytospins and Giemsa Stain*

After FACS sorting, cell populations were washed once and re-suspended in 50µl FBS. Glass Cytoslides were loaded into Cytoclips with filter cards and Cytofunnels (All ThermoFisher Scientific). Cell suspensions were transferred to Cytofunnels and centrifuged in a Cytospin^{TM} 4 Cytocentrifuge (ThermoFisher Scientific) for 8 mins at room temperature (600g). Slides were dried overnight. Cells were fixed by submersion in ice-cold methanol for 30seconds. Slides were then stained on a Siemens Advia S60 Autoslide system with Hematek® Wright-Giemsa Stain PAK. Glass coverslip was applied with DPX (Sigma-Aldrich). Slides were stored at 4ºC in the dark.

2.7.2 *CellTAK Fluorescent Preparations*

For fluorescent microscopy, cell suspensions were prepared using CellTAK (Corning) and Millicell EZ slides (Merck millipore – 8 well), both kindly gifted by Dr. Nicola Maney. A 1X HEPES neutral buffer solution was prepared. The amount of Cell-TAK solution required was calculated by multiplying 25µg/ml Cell-Tak solution by cm^2 surface area of slide. Required amount of Cell-Tak (12.5µl) was diluted with neutral buffer solution (1ml). 100µl of Cell-Tak solution was added to each well within 10 mins. Slides were incubated for 3 hours at 37ºC. Cell-Tak solution was aspirated and wells washed with sterile water to remove bicarbonate. 50,000 cells were added per well in 200µl of media and incubated for 30 mins at 37ºC. Media was aspirated and wells washed with PBS. Chambers were removed from the slides, and glass cover slip (Corning) mounted with 2 drops of DAPI-containing Vectorshield (Vector Laboratories). Slides were stored at 4ºC in the dark.

2.8 Phagocytosis

To measure the phagocytic activity of macrophages, 1µm fluorescent (λ_{ex} ~470 nm; λ_{em} ~505 nm) latex beads (Sigma Aldrich – L4655) were added to either moMac or moDC on day 6 of culture, synovial tissue mononuclear cells at $0.5x10^6$cells/ml RF10 in 24-well plates or FACS sorted synovial macrophages at $0.5x10^4$cells/ml RF10 in 96 well round bottom plates. An optimal bead dilution of 1/4000 was determined by Jane Langford (MRes), and used for all experiments. Cells were incubated for 3 hours at 37ºC. After incubation cells were harvested and washed 3 times with PBS to ensure removal of unbound beads or beads on the cell surface. Viability dye 7-AAD was added at 20µl/$1x10^6$ cells and bead uptake measured by flow cytometry. Slide preparations were carried out as described in section 2.7.2. Confocal

microscopy (Section 2.9) was used to confirm the beads had been engulfed by the phagocytic cells as opposed to attaching to the cell surface.

2.9 Microscopy

Cytospin preparations were imaged using an Olympus CKX41 inverted phase contrast microscope with Olympus CAMEDIA C-7070 digital camera. Fluorescent microscopy was carried out using an EVOS FL Cell Imaging System (Life Technologies). Prepared slides were imaged in bright field, phase contrast and merged with green and blue channels in ImageJ 1.8.0 (ImageJ). Microscopy was carried out at 4X, 10X and 100X magnification, with scale bars generated. Confocal microscopy was performed using a Leica TCS SP8 confocal microscope and LAS X Software with the assistance of Dr. Rolando Berlinguer-Palmini at the Newcastle University Bio-imaging Facility. Fluorescent latex beads were detected at ~505nm. For analysis of bead internalisation, 'Z stacks' were generated. As the thickness of a single focal plane is less than that of a cell within the sample, multiple focal planes can be imaged with sensitive microscopes. Z stacks were generated by recording multiple images taken at incremental focal planes throughout the sample. Projections of these Z stacks were then created using LAS X software and ImageJ. This allowed the visualisation of latex bead internalisation by phagocytic cells (Section 2.8).

2.10 Genomic Analyses

2.10.1 *Isolation of RNA*

RNA was isolated from purified peripheral blood and synovial tissue cells using QIAGEN Micro RNeasy kit according to the manufacturers protocol. Cell lysates were stored in RLT buffer at -80^{o}C. After defrosting, lysates were homogenised by centrifugation for 2 min (full speed) in a QIAshredder spin column. One volume of 70% ethanol was added, transferred to a MinElute spin column and centrifuged for 15 secs (8000g), discarding flow-through. 350µl Buffer RW1 was added to the MinElute spin column and centrifuged for 15 secs (8000g), discarding flow-through. DNase I incubation mix (DNase I & buffer RDD) was added to the MinElute spin column membrane and incubated at room temperature for 15 mins. 350µl buffer RW1 was added to the MinElute spin column and centrifuged for 15 secs (8000g), discarding flow-through. 500µl Buffer RPE was added to the MinElute spin column and centrifuged for 15 secs (8000g), discarding flow-through. 500µl 80% ethanol was added to the MinElute spin column and centrifuged for 2 mins (8000g), discarding flow-through. MinElute spin column

was centrifuged for 5 min (full speed), discarding flow through. 14µl RNase-free water was added to the MinElute spin column and centrifuged for 1 min (full speed) to elute RNA. RNA was stored at -80ºC until RNA-sequencing was performed.

2.10.2 *RNA sequencing*

Next generation RNA-sequencing was carried out at the Newcastle University Genomics Core Facility (GCF) led by Dr. Jonathan Coxhead. Using RNA isolated following procedures in section 2.10.1, quantification and quality control was carried out using High Sensitivity RNA Screentape (Agilent Technologies) on an Agilent 2200 Tapestation. Samples were diluted accordingly to normalise quantities of RNA. Smart-seq v4 (Clonetech) amplification was performed on samples due to low RNA quantities and Nextera XT DNA library prep kit for sequence library. Sequencing was performed on an Illumina NextSeq 500 at a 10 million, 75 base pair read depth.

2.11 Statistical analyses

2.11.1 *Basic Statistics*

Statistical analyses were carried out in Prism 5.03 (Graphpad Software), Minitab 17 Statistical Software (Minitab Inc) and R Studio (R Studio Inc).

2.11.2 *Bioinformatic analyses*

Quality control of sequencing was carried out with FastQC. Read trimming was performed with trimmomatic, mapping and alignment with STAR and quantification with HTSEQ. SeqMONK was ran to account for any DNA contamination. Counts were filtered to remove those of low number (<0.5 Counts Per Million) followed by assessment of batch effect and library sizes. All high level analysis of RNA-sequencing data was performed in R studio. After Limma-Voom normalisation of data, differential gene expression was performed using Limma, with an adjusted p-value threshold of <0.05 based upon Benjamini-Hochberg correction, and Log fold change (LogFC) of >1.5. Exploratory Kyoto Encyclopaedia of Genes and Genomes (KEGG) pathway analysis was performed on differentially expressed genes.

Chapter 3. Isolation of immune cell populations from synovial tissue

3.1 Introduction

In inflammatory forms of arthritic diseases, the synovial membrane is a site for disease activity. As previously discussed, in inflammatory arthritides there is a well-described cellular infiltrate (Tak, Smeets et al. 1997). However, the extent to which this occurs in OA is less clear. To date, a large amount of research carried out in arthritis is on peripheral blood samples, owing to their non-invasive collection and availability, in addition to research on mouse models. This has yielded a wide range of knowledge, advancing our understanding of the pathogenesis of these diseases, and giving rise to therapeutic strategies and biomarkers.

The extent of research conducted on human synovial tissue is demonstrated in current published literature. There are 294,297 '*arthritis*' termed research articles listed on Pubmed, with 135,815 matching the query '*patient*'. Out of these 135,815, only 15.34% match the query '*synovial tissue*' or '*synovium*'. In contrast, 44.19% of these articles match the query '*blood*'. Furthermore, research which has been carried out on synovial tissue is largely histology based. 52.50% of research articles listed under '*arthritis*' AND '*synovial tissue*' return the query '*histology*' (all Pubmed queries conducted on 17/08/17). There is an increased interest in studying disease at the relevant tissue site, because that is the place disease process takes place. In order to investigate the disease site in arthritis, the synovium, appropriate methods of tissue digestion need to be applied.

There is a range of published and established digestion protocols, encompassing varying different methodologies (Loewi, Lance et al. 1975, Kohem, Brezinschek et al. 1996, Fearon, Mullan et al. 2006, Nagai, Miyamoto et al. 2006, Miller, Manning et al. 2009, Connolly, Marrelli et al. 2010, Ng, Biniecka et al. 2010, Sakuraba, Fujimura et al. 2015). However these can result in poor cell viability, low cell yields, biased isolation of different cell subsets and cleavage of extracellular proteins. 'Walk out' assays are an example of cell isolation, whereby the tissue explants are left in appropriate media at 37^{o}C, and cells migrate from the tissue into the media (Loewi, Lance et al. 1975, Fearon, Mullan et al. 2006, Nagai, Miyamoto et al. 2006, Connolly, Marrelli et al. 2010, Sakuraba, Fujimura et al. 2015). However, with this approach only migratory cells will leave the tissue, and the subsequent single cell suspension would not be representative of the entire tissue cell population.

Most digestion protocols involve mechanical digestion, and some include additional enzymatic digestion. These protocols typically involve the mechanical mincing of tissue into small fragments, allowing more efficient enzymatic activity. Conversely, the use of a homogeniser is

an example of a purely mechanical digestion method often used for the isolation of murine cells. Enzymatic digestion protocols have a range of different approaches, but there is little justification for the specific choice or concentration of enzymes. Many of these described protocols are not truly optimised for human, or synovial tissue, and are adopted from digestion protocols of other tissues or species.

There is a need for a protocol that is specifically optimised for the digestion of human synovial tissue. A common protocol would also be extremely useful to the field of arthritis research, specifically in the interest of understanding the cellular mechanisms within synovial tissue. This would reduce technical 'noise' between experiments. The careful and accurate identification of cell subsets would be an additional aspect to this process.

3.2 Aims

The successful isolation and identification of immune cell populations from synovial tissue is a crucial step in understanding the pathogenesis of joint disease in inflammatory and non-inflammatory arthritis. I therefore aimed to:

- Develop a digestion protocol specific for human synovial tissue which results in sufficient cell yields for downstream analyses, high cell viability and does not cleave extracellular antigens
- Design a multi-colour flow cytometry panel for the accurate identification of multiple immune cell subsets within the synovial tissue
- Apply the digestion protocol and flow cytometry panel to FACS to purify immune cell subsets for downstream analyses

3.3 Assessment of established protocols for tissue digestion

To assess the suitability of different synovial tissue digestion protocols, $CD14^+$ myeloid cells and cDC2s were initially identified (Fig. 3.1). My initial interest of synovial tissue cell populations was cDC2s, owing to their antigen presenting capacity in disease pathogenesis. In addition, I was interested in $CD14^+$ monocytes and how they may contribute to the synovial myeloid compartment.

Firstly, cell debris was gated out using the FSC-A and SSC-A properties of the synovial tissue cell suspension. Non-viable cells were gated out by their expression of DAPI, and synovial leukocytes identified by expression of common leukocyte antigen CD45. T- & B-cells and natural killer (NK) cells were excluded by gating on cells lacking CD3 (T cells), CD19, CD20 (B-cells) and CD56 (NK cells), and gating on the remaining cells expressing MHC-II (HLA-DR; human leukocyte antigen – D related). $CD16^+$ monocytes were excluded by gating on the $CD16^-$ negative cells, followed by exclusion of pDCs and cDC1s by gating on the $CD11c^{hi}$ expressing cells. Finally, cDC2s were identified by their expression of CD1c, and $CD14^+$ myeloid cells were identified by their expression of CD14 (Fig. 3.1).

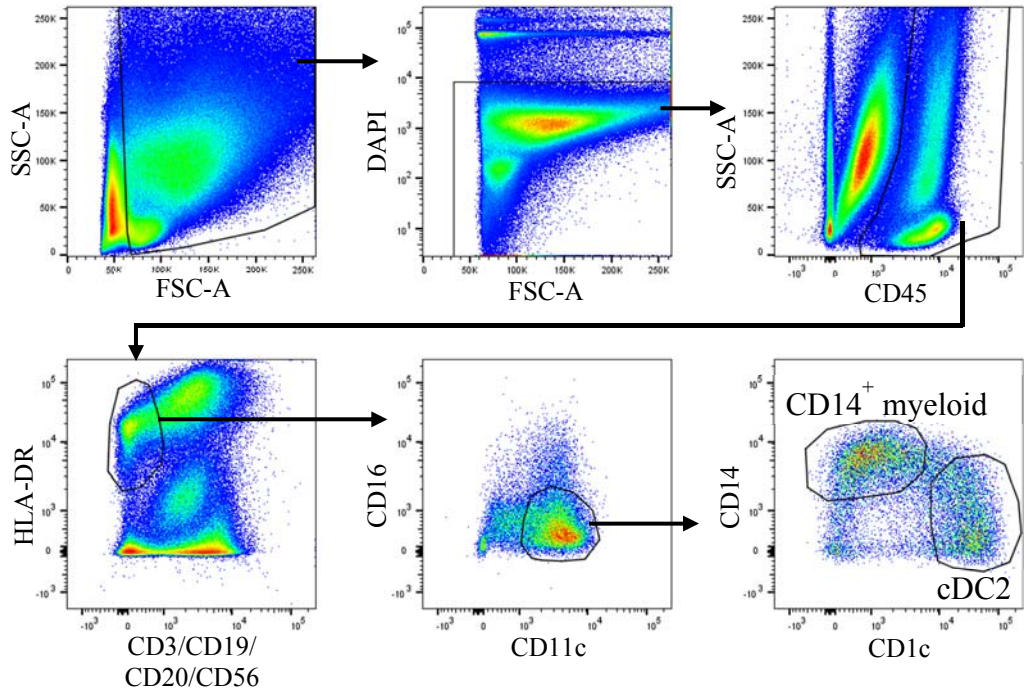

Figure 3.1: Preliminary gating strategy for identification of synovial $CD14^+$ myeloid cells and cDC2s
Synovial tissue from OA total knee replacement was digested using a sub-optimal digestion protocol (Collagenase P; 10µg/ml – 2 hours) to obtain single cell suspension. Cell surface expression for markers indicated in the figure were identified by flow cytometry. Viability was determined by staining with DAPI. The gating strategy applied to identify $CD14^+$ myeloid cells and cDC2s is depicted. Data is representative of two independent experiments.

I initially assessed an in-house digestion protocol for synovial tissue, which involved the mechanical digestion of tissue, and then incubation with Collegenase IV (1mg/ml, Thermo Fisher) at 37ºC for either 2 hours (Fig. 3.2 A) or 24 hours (data not shown). Both of these protocols resulted in loss of CD16, CD14 and CD11c expression (Fig. 3.2 A), in addition to poor cell yields and viability (data not shown). To improve cell yield and viability, the 2-hour digestion with Collagenase IV (1mg/ml) was repeated but after digestion the cells were rested overnight at 37ºC, a common step in published protocols (Fig. 3.2 B). This was successful in improving the yield of $CD45^+$ cells and cDC2s, however there was still cleavage of CD16,

CD14 and CD11c (Fig. 3.2 B). It was concluded that the enzymatic aspect of this protocol resulted in the cleavage of these surface proteins. I therefore tested a synovial tissue digestion protocol from the Institute of Infection, Immunity and Inflammation at Glasgow University (Fig. 3.2 C). This protocol involved reducing synovial tissue to 1-2mm^3 fragments followed by incubation with Liberase (150µg/ml) (Roche) at 37^{o}C for 1.5-2hours while rotating on a Miltenyi MACSmix tube rotator. Although this protocol resulted in greater cell yield and viability, cleavage of CD16 and CD11c was still apparent (Fig. 3.2 C).

Collagenase P (Sigma Aldrich) was trialled as an alternative enzyme. After mechanical digestion, Collagenase P was added at either 1mg/ml (Fig. 3.2 D) or 10µg/ml (Fig. 3.2 E), both for 2h at 37^{o}C. Both concentrations showed reduced cleavage of surface proteins, most prominently in the 10µg/ml concentration, in contrast to previous attempts with alternative enzymes (Fig. 3.2 D&E). The final enzymes trialled were based on a protocol for digestion of mouse small intestine and colon, with the enzymes kindly gifted by Prof Simon Milling, Glasgow University. The mix incorporated Collagenase VIII (1mg/ml, Sigma-Aldrich), Collagenase D (1.25mg/ml, Roche), Dispase (1mg/ml, Gibco) and DNase (30ug/ml, Roche) (Fig. 3.2 F). This protocol also involved mechanical digestion, but was followed by enzymatic digestion carried out in a shaking incubator at 37^{o}C for 40-60mins (260RPM), with additional shaking every 15 minutes. This protocol resulted in high viability assessed by DAPI staining, and moderate cell yield, however cleavage of extracellular CD14 and CD16 was still present. In addition to these protocols, a number of others were also tested, but due to a lack of reproducibility in creating a single cell suspension, were not taken forward (data not shown). In contrast to enzymatic methods, a protocol involving a homogeniser and no enzymes was also trialled (Fig. 3.2 G). Although no cleavage of extracellular proteins was observed, there was poor cell yield. Synovial tissue digestion results are summarised in Table 3.1.

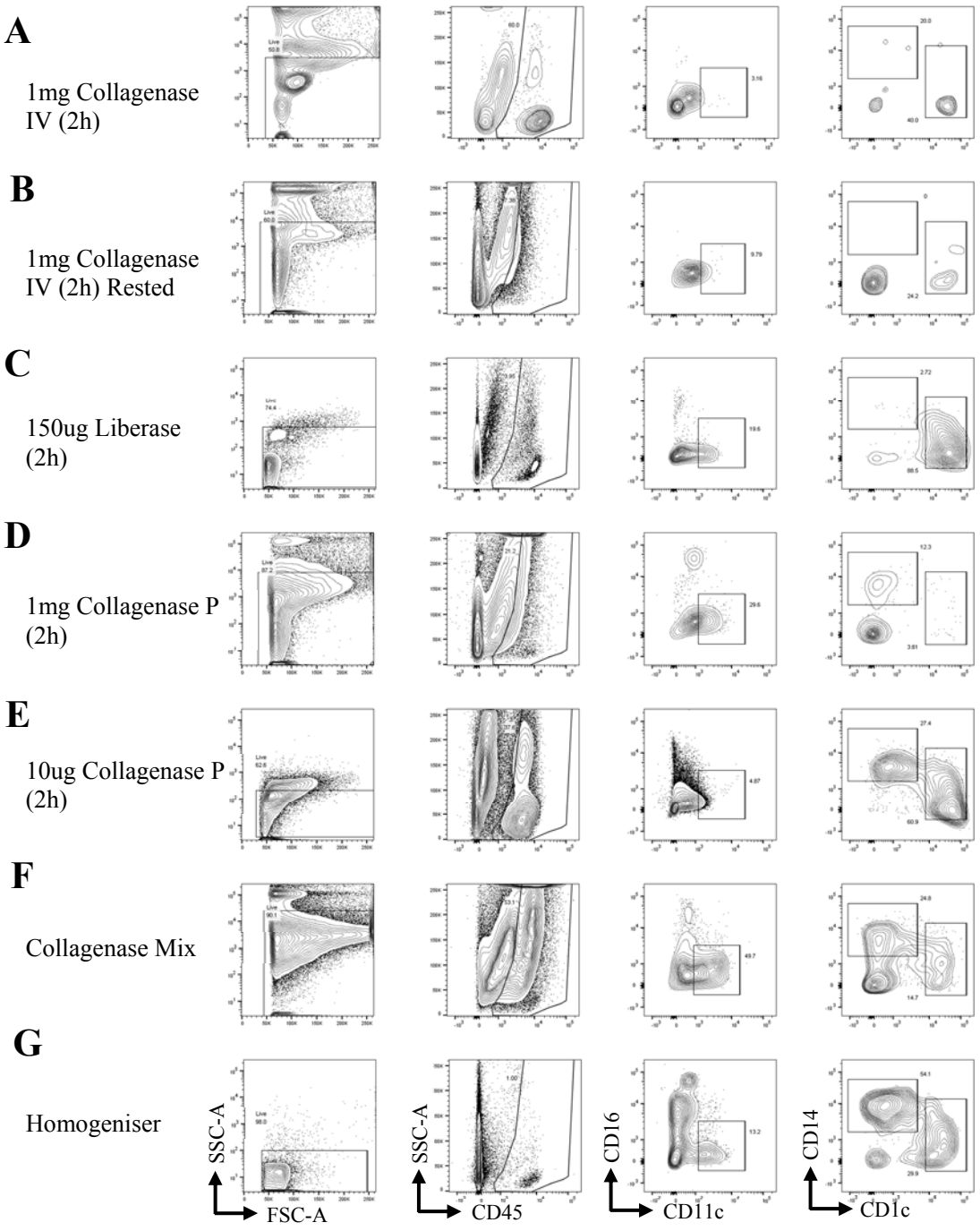

Figure 3.2: Comparison of different digestion methods on synovial tissue
The following digestion protocols were tested on synovial tissue from OA total knee replacements. **A:** 1mg/ml Collagenase IV added to mechanically digested tissue and incubated for 2 hours. **B:** 1mg/ml collagenase IV added to mechanically digested tissue, incubated for 2 hours, washed and rested in incubator overnight. **C:** 150µg/ml Liberase added to mechanically digested tissue and incubated for 2 hours. **D:** 1mg/ml Collagenase P added to mechanically digested tissue and incubated for 2 hours. **E:** 10µg/ml Collagenase P added to mechanically digested tissue and incubated for 2 hours. **F:** 1mg/ml Collagenase VIII, 1.25mg/ml Collagenase D, 1mg/ml Dispase and 20µg/ml DNase added to mechanically digested tissue and transferred to a shaking incubator for 45 mins. **G:** Tissue mechanically digested using a homogeniser. All incubations took place at 37^{o}C. CD14^{+} myeloid cells and cDC2s were identified for each digestion method by flow cytometry; gating strategy shown in Figure 3.1 was applied. Data are representative of two independent experiments.

To conclusively determine whether these enzymatic digestion protocols were cleaving surface markers, three of the protocols were tested on a peripheral blood sample, and compared to the same blood sample not subjected to any digestion (Fig. 3.3). Both methods using Collagenase showed reduced expression of CD16, CD14 and CD1c (Fig. 3.3 C&D and Fig. 3.4 A). The protocol using Liberase showed a similar level of viability to the other protocols, but reduced expression of HLA-DR (Fig. 3.3 B and Fig. 3.4 B).

Enzyme	Method	Yield	Surface Markers	Viability
Collagenase IV	Overnight 1mg/ml	✗	✗	✗
	2h – 1mg/ml	✗	✗	✗
	2h – 1mg/ml then Rested	✗	✗	✗
No Enzyme	Homogeniser	✗	✓	✓
Collagenase VIII, Collagenase D, Dispase, DNase	1mg/ml 1.25mg/ml 1mg/ml 30µg/ml	✗	✗	✓
Collagenase P & DNase	1mg/ml	✗	✗	✗
	10µg/ml	✓	✗	✗
Liberase & DNase	2h – 150µg/ml	✗	✗	✓
	45min - 15µg/ml - filter and re digest x3	✓	✓	✓

Table 3.1: Summary of tissue digestion protocols. Thresholds: A yield of over 3000 cDC2s quantified by flow cytometry, was considered a positive result. The visible cleavage of surface markers assessed by flow cytometry was considered a negative result. A viability of over 70%, assessed by DAPI staining and flow cytometry was considered a positive result. Positive results are indicated by a green tick '✓'. Negative results are indicated by a red cross '✗'.

The assessment of these established tissue digestion protocols showed mixed results (Table 3.1), most notably, low cell yield and viability, cleavage of surface markers, or both. Despite these limitations, some aspects of these protocols worked well. These aspects could potentially allow for the development of an optimal protocol for synovial tissue digestion.

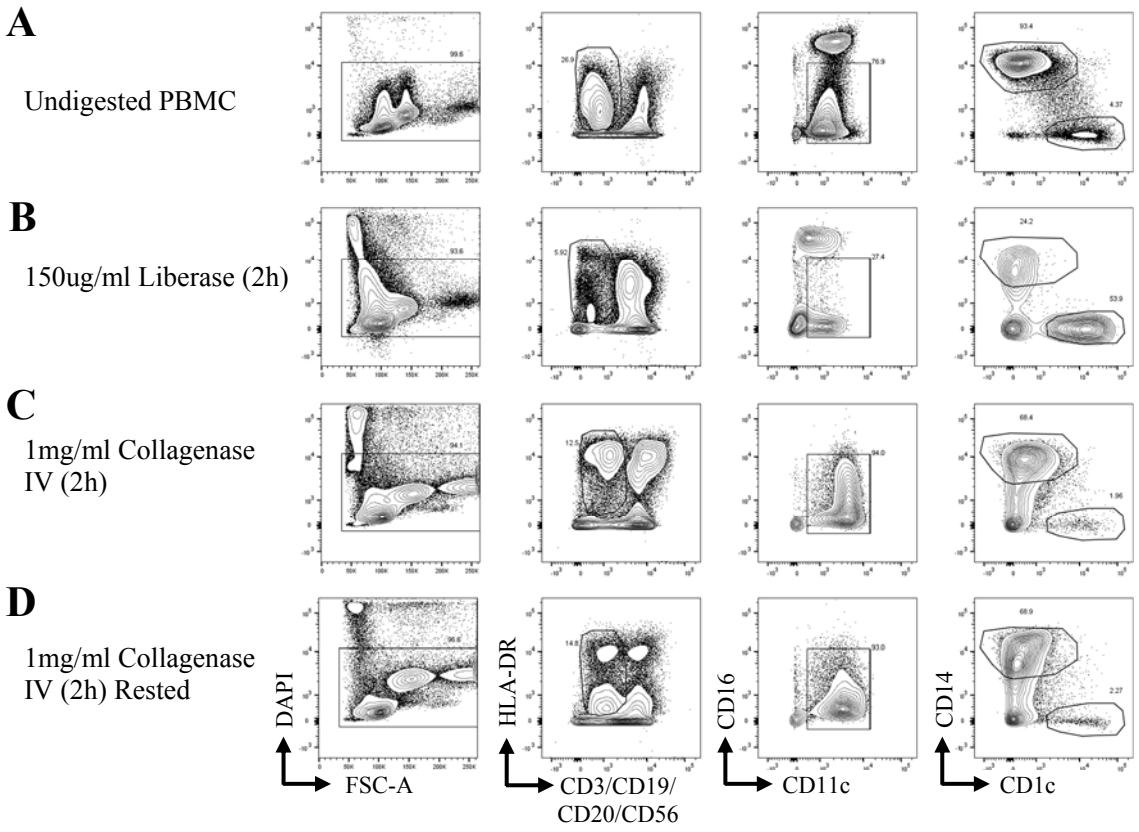

Figure 3.3: Effect of tissue digestion methods on identification of CD14$^+$ myeloid cells and cDC2 in PBMC

Three tissue digestion methods from Figure 3.2 were applied to PBMC obtained from a healthy donor. **A:** PBMC not subjected to digestion. **B:** 150ug/ml Liberase added to PBMC and incubated for 2 hours. **C:** 1mg/ml Collagenase IV added to PBMC and incubated for 2 hours. **D:** 1mg/ml Collagenase IV added to PBMC, incubated for 2 hours, washed and rested in an incubator overnight. All incubations took place at 37^{o}C. CD14$^+$ myeloid cells and cDC2s were identified for each digestion method by flow cytometry; gating strategy shown in Figure 3.1 was applied. Data are representative of two independent experiments.

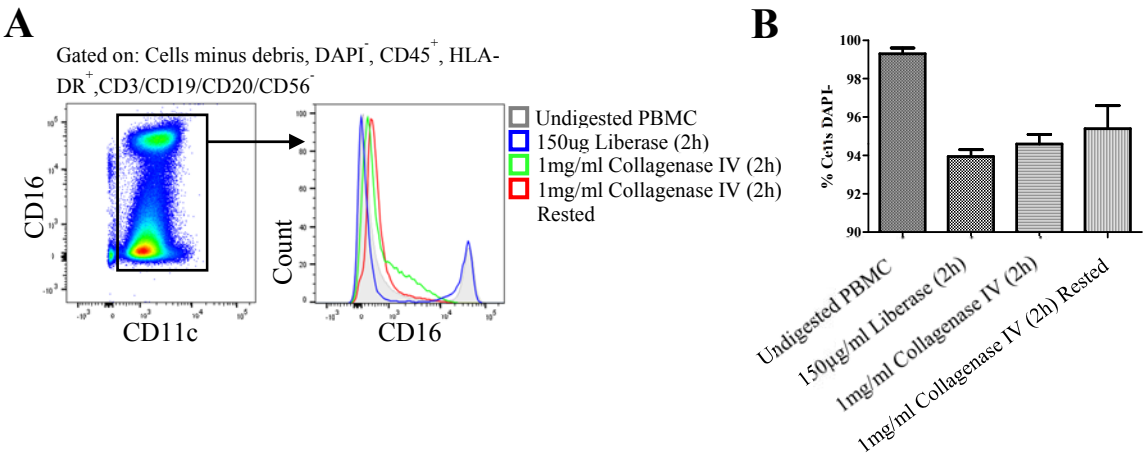

Figure 3.4: Viability and CD16 surface marker preservation of PBMC undergoing different tissue digestion methods

Three tissue digestion methods from Figure 3.2 were applied to PBMC obtained from a healthy donor. The following digestion methods were used: 150ug/ml Liberase added to PBMC and incubated for 2 hours; 1mg/ml Collagenase IV added to PBMC and incubated for 2 hours; 1mg/ml Collagenase IV added to PBMC, incubated for 2 hours, washed and rested in an incubator overnight. All incubations took place at 37^{o}C. **A:** CD16 expression was determined by flow cytometry. Left plot summarises the gating strategy. Right plot depicts expression of CD16 within the CD11c$^+$ population. **B:** Viability is depicted as % DAPI$^-$ cells. Data are representative of two independent experiments.

3.4 Development of an optimal digestion protocol for synovial tissue

After assessment of established protocols, I decided that an optimised synovial tissue digestion protocol needed to be developed, to allow greater cell yield, minimal cleavage of surface markers, and acceptable cell viability.

From the established protocols tested, a new protocol was developed using a low concentration of Liberase (15ug/ml) and multiple mechanical digestions (Fig. 3.5). Although Liberase previously showed low cell yields and surface marker cleavage, the extent of this was lesser than that of the other digestion protocols. By lowering the concentration of Liberase, it was hypothesised that surface marker expression would be preserved and viability would be increased. However as a result it was likely that cell yield would be affected owing to a lower efficiency of enzymatic digestion. To overcome this, I decided to attempt multiple mechanical digestions with the lower concentration of Liberase. The adapted Liberase protocol involved reducing synovial tissue to 1-2mm^3 fragments with sterile scissors and scalpel followed by incubation with Liberase (15ug/ml) and DNase (30ug/ml) in a shaking incubator at 37^oC for 45mins (260RPM), with additional shaking every 15 minutes. After incubation, the cell suspension was filtered and filtrate immediately placed on ice to inhibit enzymatic digestion. Any remaining tissue was subjected to a second digestion following the same steps. On any still remaining tissue, a third and final digestion was carried out (Fig. 3.6).

The optimised digestion approach resulted in high cell yields (Fig. 3.5 & 3.7 A), and when tested on PBMC (Fig. 3.5 & 3.7 B), viability and surface marker preservation were comparable to undigested PBMC. When compared with all previous digestion protocols, this protocol achieved one of the highest cell viabilities, in addition to the highest yield of $CD14^+$ myeloid cells and cDC2s (Fig. 3.7 A&B). Figure 3.5 & 3.7 C demonstrates lack of surface marker cleavage using this optimised protocol.

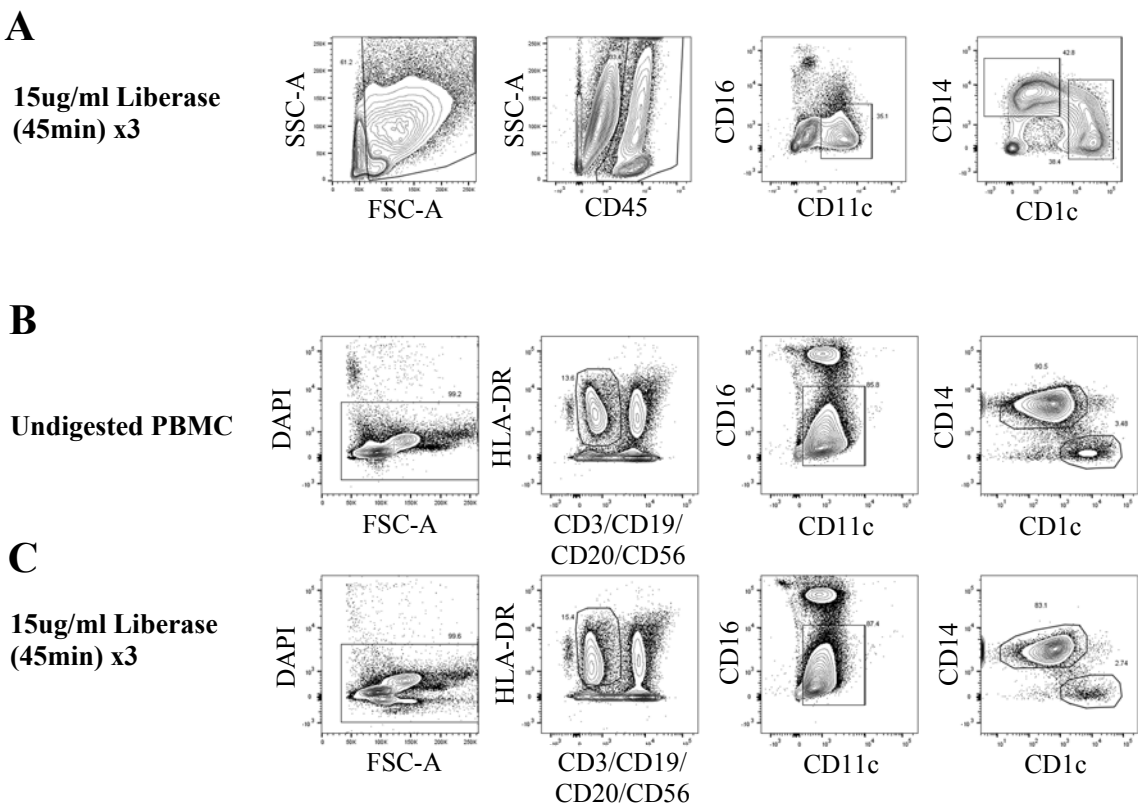

Figure 3.5: Effect of optimised digestion protocol on synovial tissue and PBMC
The optimised digestion protocol was applied to synovial tissue from OA total knee replacement and PBMC obtained from healthy donor. **A:** Optimised digestion protocol applied to synovial tissue: 15ug/ml Liberase and 30ug/ml DNase added to mechanically digested synovial tissue and transferred to a shaking incubator for 45 minutes. After filtering, any remaining tissue was subjected to one or two more cycles of digestion. **B:** PBMC not subjected to digestion. **C**: Optimised digestion protocol applied to PBMC. All incubations took place at 37°C. $CD14^{+}$ myeloid cells and cDC2s were identified by flow cytometry; gating strategy shown in Figure 3.1 was applied. Data are representative of two independent experiments.

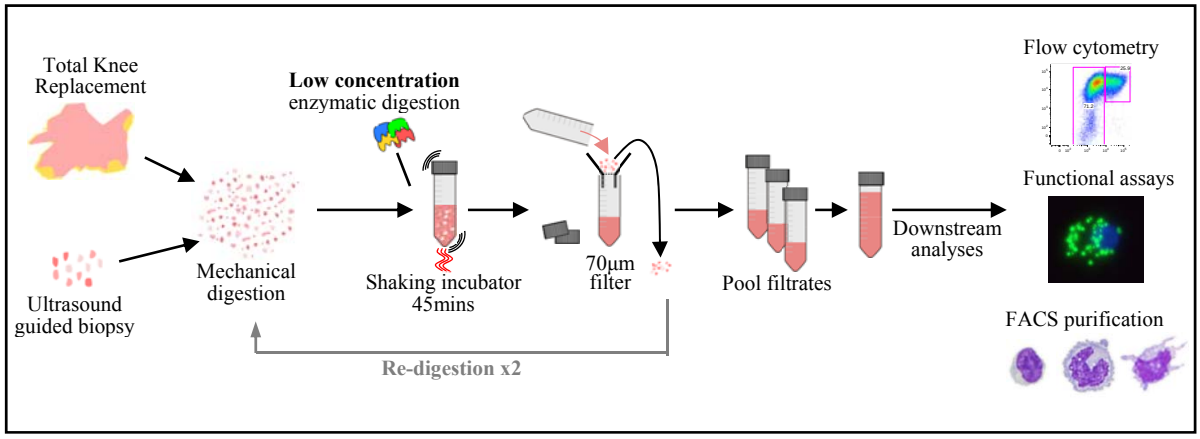

Figure 3.6: Optimised synovial tissue digestion protocol
Illustration of optimised synovial tissue digestion protocol. Synovial tissue from either total knee replacement or ultrasound guided biopsy is subjected to mechanical digestion and subsequent low concentration enzymatic digestion (150µg/ml; Liberase) in a shaking 37°C incubator for 45 mins (260RPM). After filtering, any remaining tissue is subjected to one or two more digestion cycles. Filtrates were pooled, washed and single cell suspension used for downstream analysis.

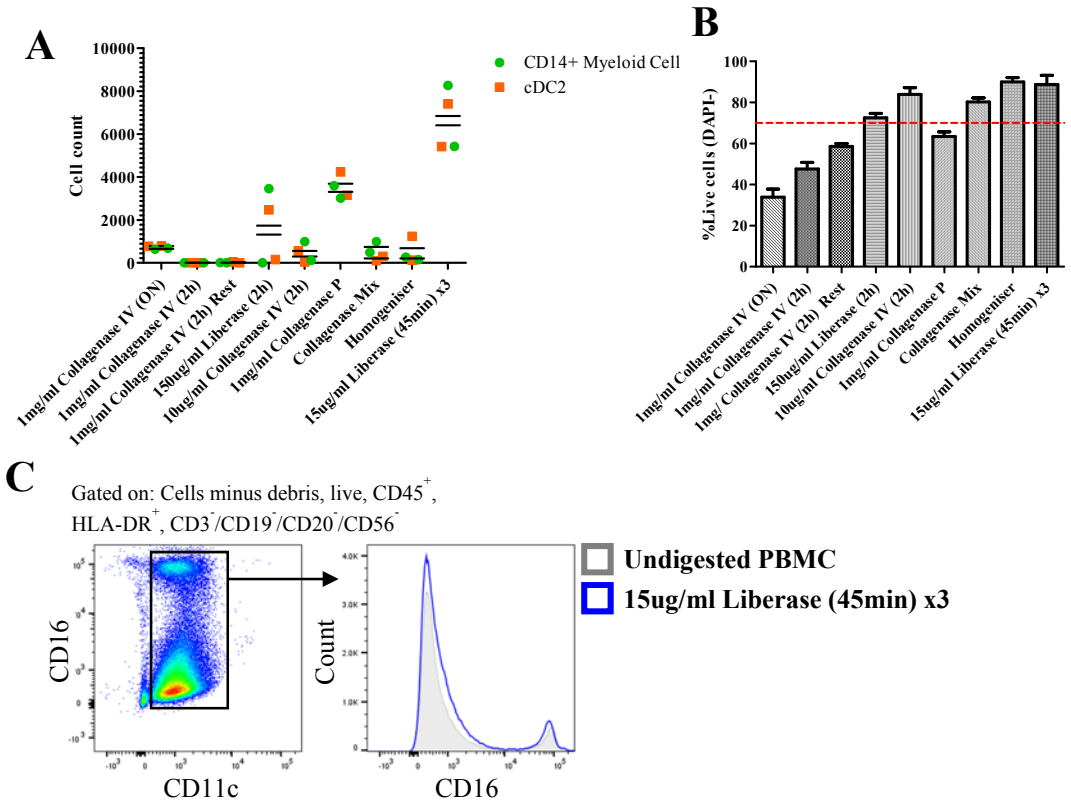

Figure 3.7: Verification of optimised digestion protocol
Optimised digestion protocol was tested on synovial tissue from OA total knee replacement and PBMC obtained from a healthy donor. This was compared to previous digestion methods. **A:** Cell numbers of $CD14^+$ myeloid cells and cDC2s achieved from synovial tissue by each digestion method. Gating strategy used to identify is shown in Figure 3.1. **B:** Viability of cells isolated from synovial tissue is depicted as % $DAPI^-$ cells. **C:** CD16 expression on PBMC sample as determined by flow cytometry. Left plot summarises the gating strategy. Right plot depicts expression of CD16 within the $CD11c^+$ population. Data are representative of two independent experiments.

3.4.1 *Storage of synovial tissue*

Total knee arthroplasty surgeries take place throughout the day, and samples are often not available until late in the day. Owing to this, it was assessed whether storing samples overnight with isolation carried out the following day would have an adverse effect on the sample quality. A synovial tissue sample was divided in half, with one half digested fresh and analysed by flow cytometry. The other half was placed in RF10, stored overnight at 4ºC, and subsequently digested and analysed the following day (Fig. 3.8). Although viability was lower, this was only marginal (2%), and the identification of cell subsets and surface marker proteins was not affected (Fig. 3.8). Therefore, it was deemed feasible to leave samples overnight (stored at 4ºC in RF10) for digestion and analysis the following day.

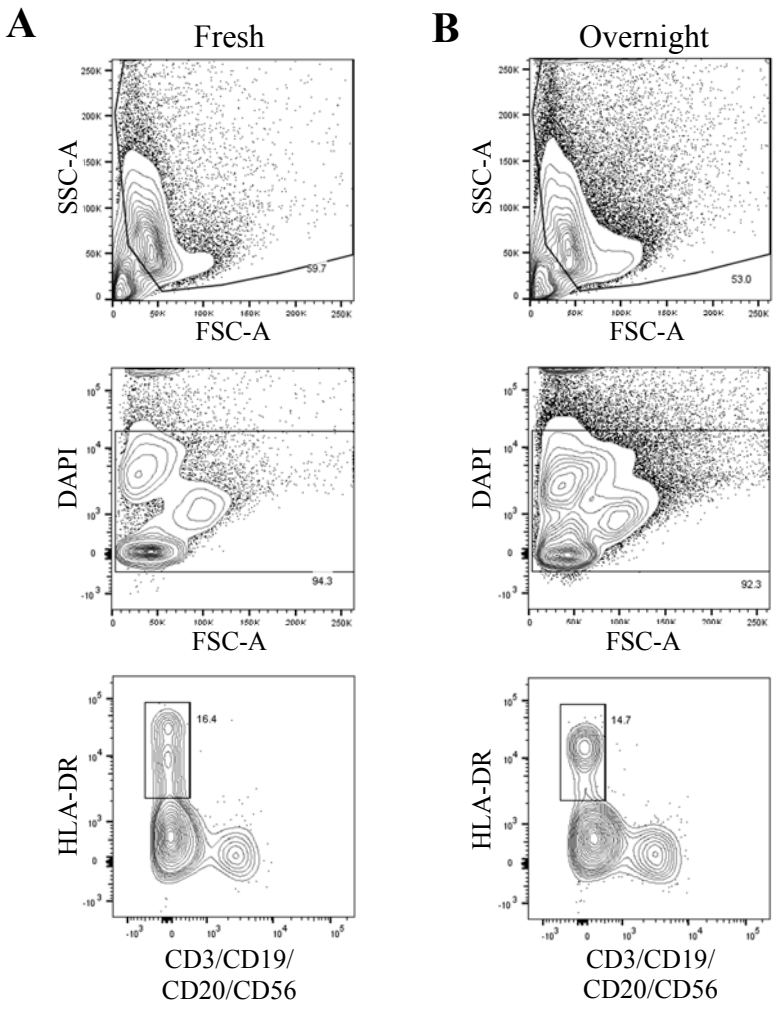

Figure 3.8: Storage of synovial tissue
Synovial tissue from OA total knee replacement was digested using the optimised protocol shown in Figure 3.6. **A:** Synovial tissue was digested immediately. **B:** Synovial tissue was left in RF10 at 4^{o}C overnight. Tissue was digested the following day. Gating strategy shown in Figure 3.1 was applied. Viability was determined by staining with DAPI. Data are representative of one experiment.

3.4.2 *Composition and yield of cell isolates*

As the optimised digestion protocol involved multiple stages of digestion, I assessed whether cell subsets were preferentially isolated in different stages of digestion. For this, media was taken from tissue storage as well as from the three separate digestion filtrates. All four samples were analysed by flow cytometry (Fig. 3.9). This experiment demonstrated that it is necessary to carry out three stages of digestion in order to generate cell yields sufficient for carrying out functional analyses (Fig. 3.9 A). Once this protocol had been repeated it was expected that after three digestions stages, no or very little tissue would remain to undergo a fourth digestion. When comparing the cell yields as a percentage of their sum, it was observed that the CD4^{+} T cell compartment had a much higher yield during the 'walk-out' stage of digestion, when the tissue is stored in media (Fig. 3.9 B). This higher yield of CD4^{+} T cells suggests that out of the cells analysed, they have the highest capacity to non-specifically migrate out of tissue. During

the subsequent three digestion stages, the percentages of different cell subsets did not alter greatly, suggesting that the relative yields would not be affected or cell subsets preferentially isolated. (Fig. 3.9 B). An expected decrease of viability was observed between the digested filtrates and the storage media (Fig. 3.9 C). However this was not a major difference, and was consistent across all three isolates.

By analysing the composition and yield from each of the cell isolates, I have demonstrated that it is necessary to carry out three digestion stages in addition to retaining media from tissue storage, in order to achieve sufficient cell yields for carrying out functional analyses. In addition, this experiment has shown that throughout the three digestion stages, there is no preferential isolation of the cell subsets.

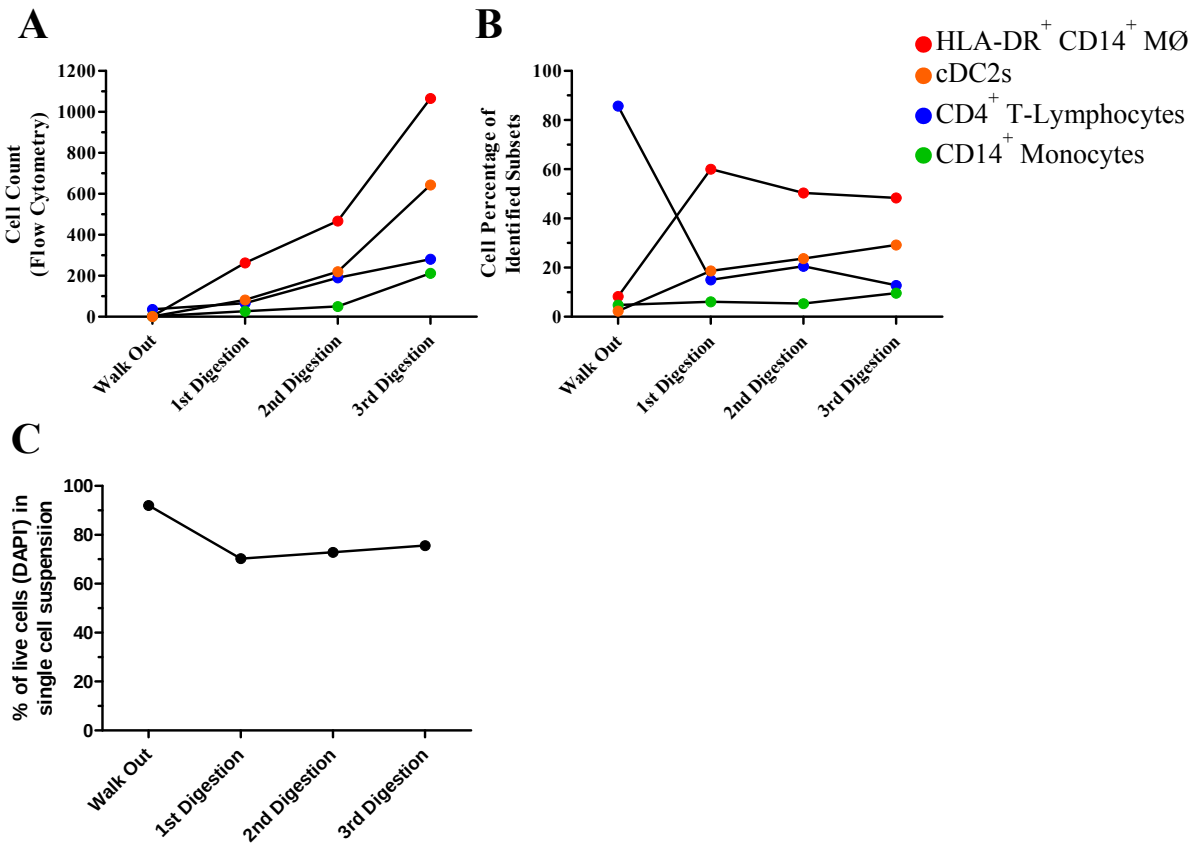

Figure 3.9: Composition and yield of cell isolates

Synovial tissue from OA total knee replacement was stored overnight in RF10 at 4°C and media removed the following day. Tissue was digested using the optimised protocol shown in Figure 3.6, but filtrates not pooled and analysed separately. **A:** Cell subset count analysed by flow cytometry. **B:** Cell subset counts from **A** as a percentage of their sum. Gating strategy shown in Figure 3.17 was applied. Data are representative of one experiment. **C:** Proportion of live ($DAPI^-$) cells in each filtrate.

3.5 Identification of peripheral blood and synovial tissue immune cell subsets

As previously discussed, my initial interest of synovial tissue cell populations was cDC2s, owing to their antigen presenting capacity in disease pathogenesis. In addition, I was interested in $CD14^+$ monocytes and HLA-DR^+CD14^+ macrophages and how they may contribute to the synovial myeloid compartment. However, since there was potential to sort five populations from one tissue sample, I decided to also identify stromal cells as well as $CD4^+$ T cells, to understand their corresponding role to the myeloid cells. To identify these cell subsets within the same sample, a multi-colour flow cytometry panel was optimised.

3.5.1 *FACS*

For FACS, an Aria Fusion (BD Biosciences) cell sorter was available. This allows the sorting of four cells populations simultaneously using electrical charges applied to the cell droplets. During the period of setting up this flow cytometry panel, the flow cytometry core facility announced the purchase of an additional cell sorter, a MoFlo Astrios EQ (Beckman Coulter). The advantages of this system over the Aria Fusion are increased speed of sorting, increased cell viability due to the sorting mechanics ('jet-in-air' system rather than electrical charges), and the ability to sort six cell populations from a single sample. One limitation of this system was that it did not have a UV laser, and therefore the flow cytometry panel had to be modified as cell viability was measured by DAPI at 355nm. Instead, 7AAD was used as an alternative viability dye, which could be measured on the same wavelength as the lineage cocktail, PE Cy5.5. Figure 3.10 shows original flow cytometry panel, and modified panel to accommodate additional cell subset markers, and compatibility with MoFlo Astrios cell sorter.

When comparing a synovial tissue sample on both the Aria Fusion and on the MoFlo Astrios, the cells have different FSC-A properties, but similar levels of viability (Fig. 3.11 A&B). It is difficult to distinguish $CD45^+$ and $CD45^-$ populations on the MoFlo Astrios. In addition, auto-fluorescence, used for the identification of tissue macrophages, was also difficult to identify on the MoFlo Astrios (Fig. 3.11 A&B). $CD3^+$ T cells were well resolved, but HLA-DR^+ cells, and subsequent $CD14^+$ monocytes and cDC2s were not possible to identify (Fig. 3.11 A&B).

Cytospins were performed on cell populations sorted from the MoFlo Astrios to check purity and cell morphology (data not shown). Although some cells could be found matching expected morphology for macrophages, T cells and monocytes, there was a large amount of debris and cell death present (data not shown). This flow cytometry panel was attempted with full set-up and compensation three additional times on synovial tissue and peripheral blood samples (data not shown). Although the identification and resolution of some cell subsets was improved, it

was not possible to identify auto-fluorescence. For these and the above reasons, I decided to discontinue the optimisation of a panel for the MoFlo Astrios, and to carry out all future cell sorting on the Aria Fusion.

A

Flurochrome	Antibody
PerCP	HLA-DR
PE	Spare
PE-Cy7	CD1c
V450	CD11c
V500	CD45
BV605	CD16
APC	Spare
AF700	CD3, CD19, CD20, CD56
APC-Cy7	CD14
DAPI	DAPI

B

Flurochrome	Antibody
FITC	AF
PerCP	HLA-DR
PE	CD4
PE-Cy5.5	7AAD
PE-Cy7	CD1c
V450	CD11c
V500	CD45
BV605	CD16
APC	CD3, CD90
AF700	CD19, CD20, CD56
APC-Cy7	CD14

Figure 3.10: Preliminary and modified flow cytometry panels
Flow cytometry panels for the identification of cell subsets from synovial tissue and PBMC. Panels were set up on BD Fortessa X20. **A:** Preliminary flow cytometry panel for identification of $CD14^+$ myeloid cells and cDC2s. **B:** Modified flow cytometry panel for the identification of $CD14^+$ monocytes, cDC2s, $CD4^+$ T-lymphocytes, $CD90^+$ stromal cells and $HLA\text{-}DR^+CD14^+$ MØ.

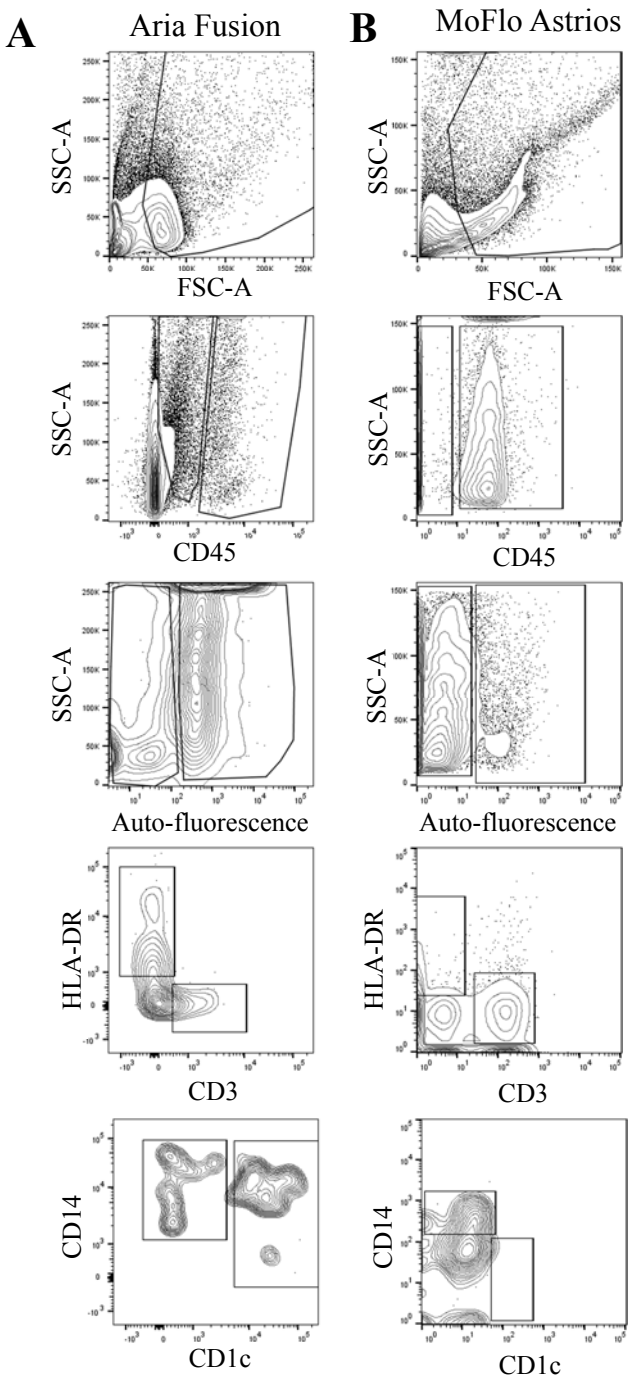

Figure 3.11: Comparison of synovial tissue acquisition on Aria Fusion and MoFlo Astrios cell sorters
Synovial tissue from OA total knee replacement was digested using the optimised protocol shown in Figure 3.6. Single cell suspension was divided into two before acquisition. **A:** Synovial tissue single cell suspension acquired on Aria Fusion cell sorter. **B:** Synovial tissue single cell suspension acquired on MoFlo Astrios cell sorter. Gating strategy shown in Figure 3.17 was applied. Data are representative of four independent experiments.

3.5.3 *CD3 & CD90*

As there was not an extra channel in the current flow cytometry panel to put a stromal marker in, CD3 and CD90 were initially used with the same conjugated fluorophore, APC (Fig. 3.12). As these two cell types should be split by their CD45 expression, it was hypothesised there should not be an issue with their identification. An experimental control was carried out to ensure there was no cross-contamination of either the T cell or stromal cell populations (Fig. 3.12). Figure 3.12 A is the view of $CD45^-$ stromal and $CD3^+$ T cell populations when both CD3 and CD90 antibodies are used. Figure 3.12 B demonstrates that there is no contamination of $CD3^+$ cells within the $CD45^-$ fraction, where $CD90^+$ stromal cells would be identified. However, in the HLA-DR^- $CD3^+$ cell fraction, there was contamination by $CD90^+$ cells (Fig. 3.12. C). Owing to this, CD3 and CD90 were measured on separate fluorophores.

3.5.4 *pDC and cDC1 contamination check*

Although the optimised digestion protocol yields high enough cell numbers of cDC2s for functional and genomic analyses, I was unable to isolate sufficient numbers of cDC1s or pDCs. I therefore decided not to include any markers of these DC subsets in the flow cytometry panel. To confirm they would not contaminate the cDC2 or monocyte populations, CD123, a marker of pDCs, and CD141, a marker of cDC1, were added to a synovial tissue sample to identify where these two DC subsets fall in my gating strategy (Fig. 3.13). Furthermore, when assessing the expression of CD123 on cDC2s and pDCs there is distinguishable expression suggesting no contamination (Appendix 3.1). Although the expression of CD141 between cDC1 and cDC2 was not as clear, there was distinguishable expression of CD11c (Appendix 3.1). This demonstrates that these DC subsets fall in the cDC2 and $CD14^+$ monocyte gating strategy up until the CD11c and CD16 gate. At this point, they both fall within the $CD11c^{lo}$ population, which is excluded when identifying cDC2s and $CD14^+$ monocytes.

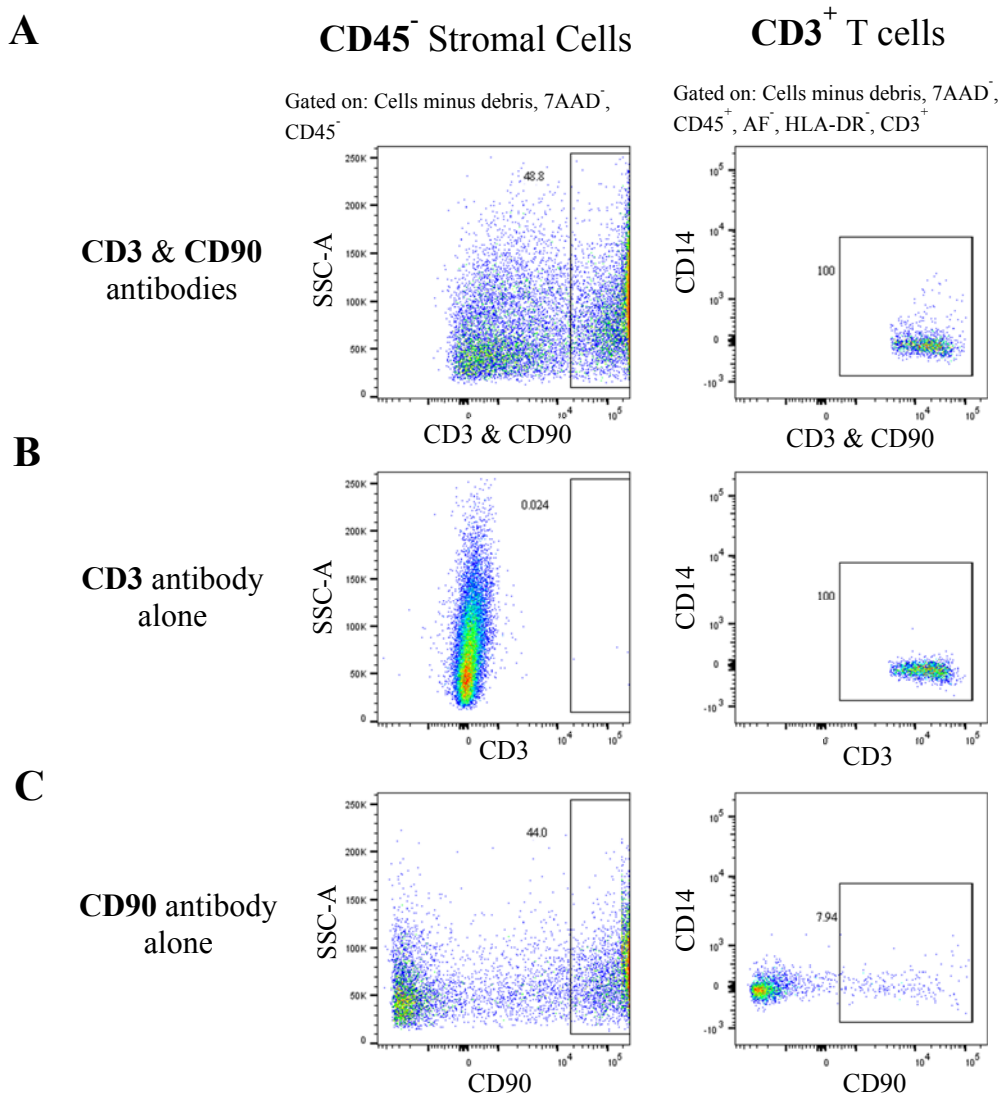

Figure 3.12: Combination of CD3 & CD90 on APC
Synovial tissue from OA total knee replacement was digested using the optimised protocol shown in Figure 3.6. Single cell suspension was divided into three before flow cytometry antibody staining. **A:** Single cell suspension was stained with both CD3 and CD90 (both APC). **B:** Single cell suspension was stained with CD3 (APC). **C:** Single cell suspension was stained with CD90 (APC). Left hand panels depict $CD45^-$ population. Right hand panels depict $CD3^+$ population. Gating strategy shown in Figure 3.17 was applied. Data are representative of one experiment.

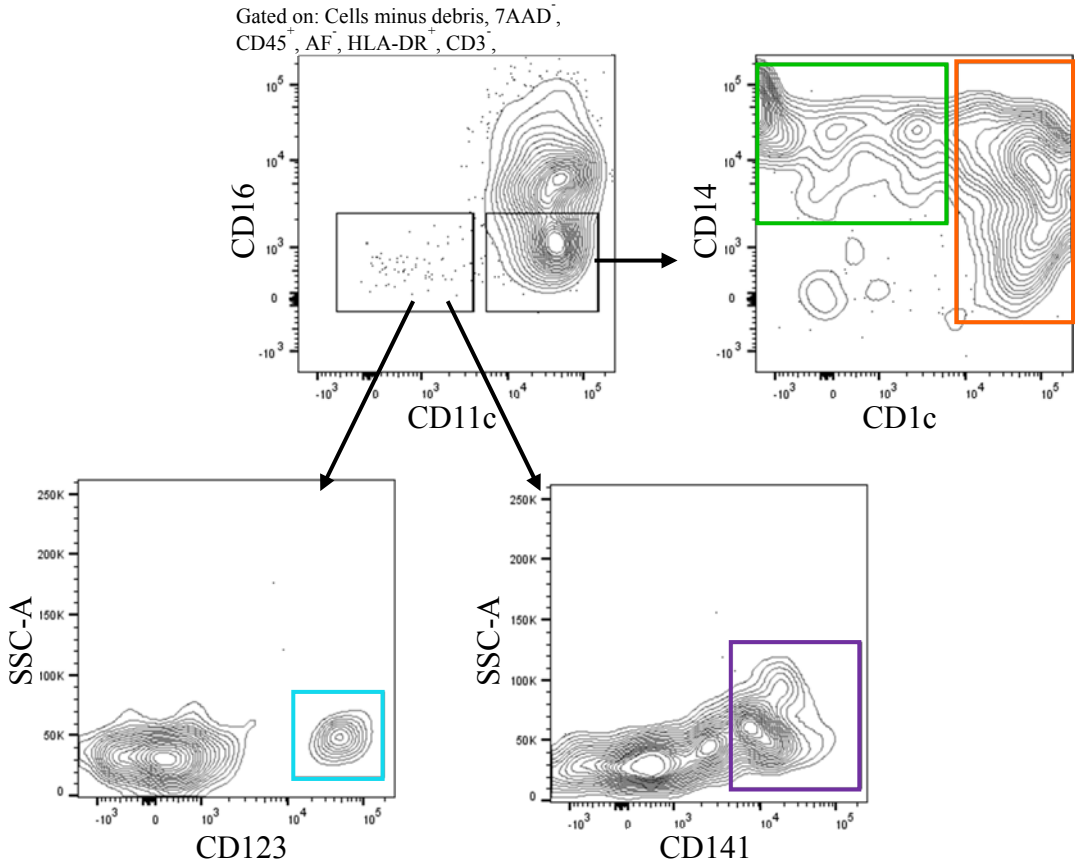

Figure 3.13: Identification of pDC, cDC1, cDC2 and CD14^{+} monocyte
Synovial tissue from OA total knee replacement was digested using the optimised protocol shown in Figure 3.6. Flow cytometry panel shown in Figure 3.16 was used with the addition of CD123 (PerCP-Cy5.5) and CD141 (PE-Cy7) in place of CD4 (PE-Cy7). Gating strategy shown in Figure 3.17 was applied. Data are representative of one experiment.

3.5.5 *CD45 FMO*

As the distinction of CD45^{+}, CD45^{-} and debris was not completely clear, an FMO was carried out to identify the true CD45^{-} population, debris, and where gating should be applied for the CD45^{+} population (Fig. 3.14 A&B). Although the FMO assisted in the identification of the CD45^{+} cell population, an alternative antibody was tested on APC-Cy7 to see if this yielded a clearer distinction (Fig. 3.14 C). The resolution of cell populations using APC-Cy7 (Fig. 3.14 C) was not as clear as the original V500 antibody (Fig. 3.14 B), therefore CD45 on V500 was used for the final panel.

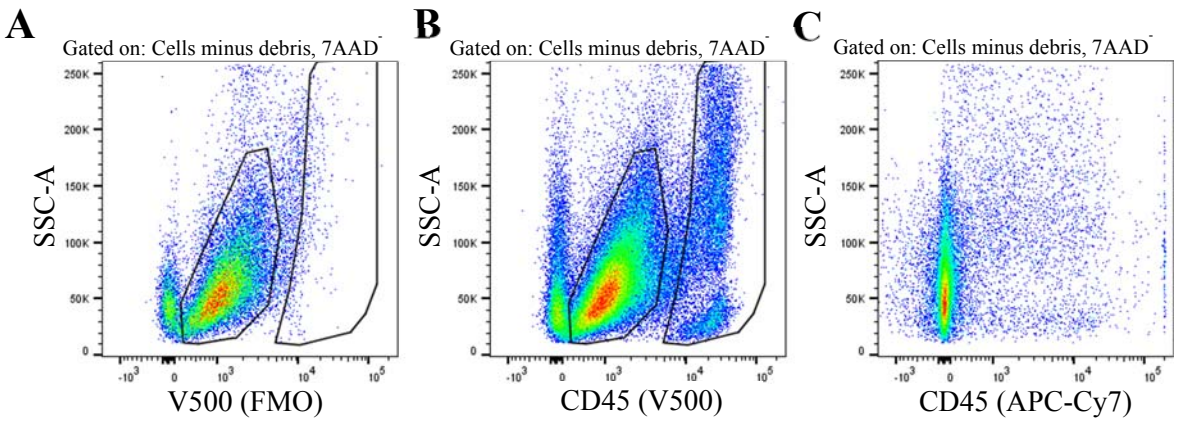

Figure 3.14: CD45 flow cytometry antibody validation
Synovial tissue from OA total knee replacement was digested using the optimised protocol shown in Figure 3.6. Single cell suspension was divided into three before flow cytometry antibody staining. **A:** Flow cytometry panel shown in Figure 3.16 was used with the exception of CD45. **B:** Flow cytometry panel shown in Figure 3.16 was used. **C:** Flow cytometry panel shown in Figure 3.16 was used with the exception of CD45 (V500) and addition of CD45 (APC-Cy7). Gating strategy shown in Figure 3.17 was applied. Data are representative of one experiment.

3.5.6 *Auto-fluorescence for the identification of synovial macrophages*

When considering the approach for the identification of macrophages, there are many different methods in the literature. One strategy is the use of $CD64^{hi}$, $CD11b^{+}$, HLA-DR^{+} cells taken as synovial macrophages. However when I tested this, a small (2.31%) amount of cDC2 contamination was found (Fig. 3.15 A). Although this is a relatively small amount, it equated to >50% of the total cDC2 population within synovial tissue. As I was interested in sorting synovial cDC2s in addition to macrophages from the same sample, this gating strategy would not yield the number of DCs required, or the purity of macrophages desired. When analysing synovial tissue single cell suspensions by flow cytometry, auto-fluorescence occurs in the FITC channel, which is not present with peripheral blood single cell suspensions (Fig. 3.15 B). This allowed me to assume that the cells auto-fluorescing were larger and with more structure, and most likely tissue specific cells. With this, and the addition of HLA-DR^{+} and $CD14^{+}$ gating, I could achieve highly pure synovial tissue macrophages. It was shown that cDC2s express CD64 in addition to macrophages, resulting in the cDC2 contamination of the macrophage population (data not shown).

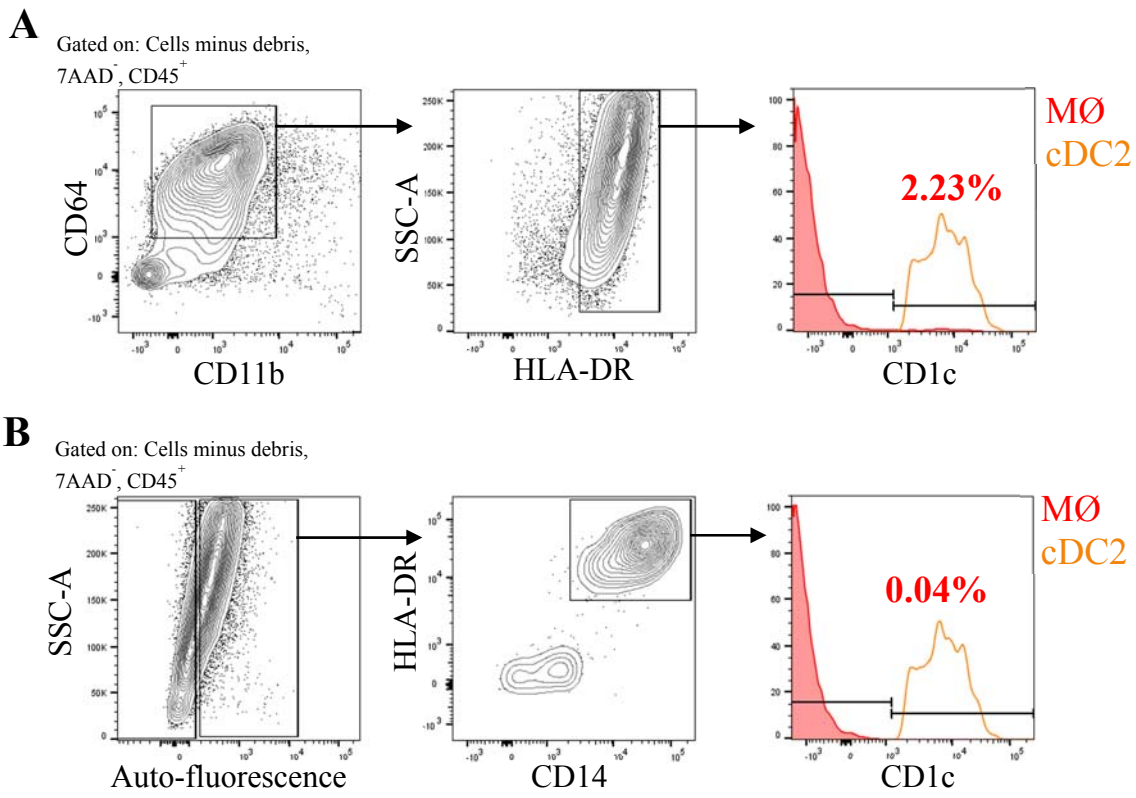

Figure 3.15: Auto-fluorescence for the identification of MØ
Synovial tissue from OA total knee replacement was digested using the optimised protocol shown in Figure 3.6. Single cell suspension was divided into two before flow cytometry antibody staining. **A:** Gating strategy shown in Figure 3.17 was applied with the exception of macrophage identification. Alternatively CD64, CD11b and HLA-DR were used as positive identification markers. **B:** Gating strategy shown in Figure 3.17 was applied. Right hand panels depict CD1c expression on macrohages. Data are representative of two independent experiments.

3.5.7 *Full gating strategy*

In brief, the full identification of all cell subsets was achieved using the panel in Figure 3.16 and gating strategy in Figure 3.17. Firstly, debris was excluded using the FSC-A and SSC-A profile and dead cells and B cells excluded using 7AAD, CD19 and CD20 (Fig. 3.17 A&B). $CD45^+$ cells were gated on to exclude stromal cells in tissue, in addition to debris. In synovial tissue, auto-fluorescent cells were gated on, and cells expressing HLA-DR and CD14 identified as synovial macrophages (T4). The auto-fluorescent negative population was split by expression of HLA-DR and CD3, with identification of $CD4^+$ ($CD14^-$) T cells within the $CD3^+$ fraction (B1 & T1). $CD11c^+$, $CD16^-$ cells were gated on in the $HLA\text{-}DR^+$ cell fraction, and $CD14^+$ monocytes (B2 & T2) and cDC2s (B3 & T3) identified by the respective expression of CD14 and CD1c. An additional FMO of CD1c was performed to ensure there were no auto-fluorescencent monocytes contaminating this gate (Appendix 3.2). Full surface marker phenotypes of synovial cell subsets are listed in Table 3.2.

Flurochrome	Antibody
FITC	AF
PerCP-Cy5.5	Blank
PE	CD1c
PE-Cy5.5	CD19/CD20/ CD56 /7AAD
PE-Cy7	CD4
BV421	CD11c
V500	CD45
BV711	CD16
BV786	CD3
APC	HLA-DR
APC-Cy7	CD14

Figure 3.16: Optimised flow cytometry panel
Flow cytometry panel for the identification of $CD14^+$ monocytes, cDC2s, $CD4^+$ T cells and HLA-DR^+CD14^+ MØ from synovial tissue and PBMC. Panel was set up on BD Fortessa X20 and BD Aria Fusion cell sorter.

Cell Population	Surface Marker Phenotype
Macrophage **($HLA\text{-}DR^+CD14^+$)**	Live, $CD19^-$, $CD20^-$, $CD45^+$, AF^+, $CD14^+$, $HLA\text{-}DR^+$
T Cell **($CD4^+$)**	Live, $CD19^-$, $CD20^-$, $CD45^+$, AF^-, $HLADR^-$, $CD3^+$, $CD14^-$, $CD4^+$
Monocyte **($CD14^+$)**	Live, $CD19^-$, $CD20^-$, $CD45^+$, AF^-, $HLADR^+$, $CD3^-$, $CD16^-$, $CD11c^+$, $CD14^+$
Dendritic Cell **(cDC2)**	Live, $CD19^-$, $CD20^-$, $CD45^+$, AF^-, $HLADR^+$, $CD3^-$, $CD16^-$, $CD11c^+$, $CD1c^+$

Table 3.2: Full surface marker phenotype of cell subsets isolated from synovial tissue and peripheral blood

Owing to the problems experienced with the MoFlo Astrios cell sorter, it was decided that $CD90^+$ stromal cells would not be sorted in future samples to maximise the yields from the other subsets, when sorting four ways on the Aria Fusion cell sorter.

Here, a multi-colour flow cytometry panel has been carefully developed to allow the simultaneous and accurate identification of HLA-DR^+CD14^+ macrophages, $CD4^+$ T cells, $CD14^+$ monocytes and cDC2s. Although the set up of this panel was attempted on the MoFlo Astrios cell sorter, this was not successful. Therefore all future sorts were carried out on the Aria Fusion.

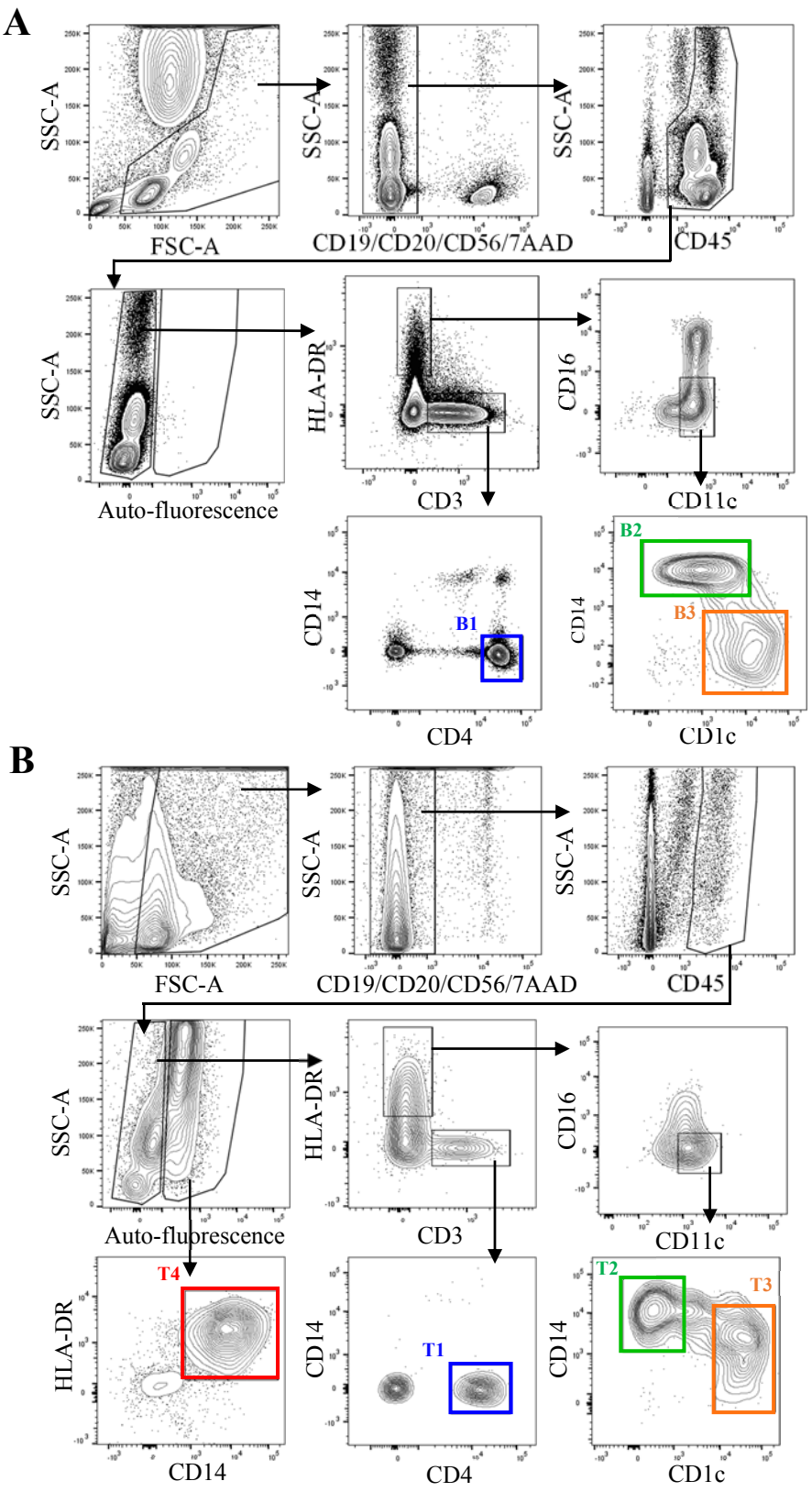

Figure 3.17: Gating strategy for identification of cell subsets from synovial tissue and peripheral blood
Synovial tissue from OA total knee replacement was digested using the optimised protocol shown in Figure 3.6. Matched PBMC was obtained from corresponding OA total knee replacement patient. **A:** PBMCs isolated from peripheral blood stained with flow cytometry panel shown in Figure 3.16. **B:** Single cell suspension from synovial tissue (digested following optimised protocol shown in Figure 3.6). Stained with flow cytometry panel shown in Figure 3.16.

3.6 Immune cell subset morphology

After successful FACS sorting of cell subsets from peripheral blood and synovial tissue, cytospins were carried out to assess the morphology of these subsets, in addition to ensuring the populations were pure. Both blood and synovial tissue T cells shared similar expected morphology of a relative small size, with small amounts of cytoplasm (Fig. 3.18 B1 & T1). They could further be distinguished from any potential contaminating NK cells by their lack of cytoplasmic granules.

$CD14^+$ monocytes isolated from blood were spherical with the presence of small membrane ruffles (Fig. 3.18 B2). Those isolated from tissue had a more irregular cell shape compared to their blood counterparts (Fig. 3.18 T2). Both exhibited 'indented' shaped nuclei and lack of cytoplasmic granules, discriminating them from both neutrophils and NK cells.

cDC2s isolated from peripheral blood had irregular cell shapes, ruffled cell membranes and the appearance of small dendrite structures (Fig. 3.18 B3). cDC2s isolated from synovial tissue had similar irregular cell shapes, but with larger and more prominent dendrite structures (Fig. 3.18 T3). Both blood and tissue cDC2s could be discriminated from macrophages due to their absence of any prominent phagocytic vacuoles, in addition to their shape and cell structure as previously discussed. Macrophages isolated from synovial tissue were large with membrane ruffles and increased cytoplasmic vacuoles compared to monocytes (Fig. 3.18 T4). There were no potential contaminating cells detected in all cell populations.

Confirmation of microscopic morphology assessment was carried out by comparing the SSC-A and FSC-A profiles of blood- and tissue-derived cDC2s and $CD14^+$ monocytes (Fig. 3.19 A&B). The SSC-A mean fluorescence intensity (MFI) of both cell types is significantly increased in tissue-derived cells compared to those from blood, suggesting that the tissue cells have more structural complexes (Fig. 3.19 A&B). This difference was not observed in the $CD4^+$ T cells (Fig. 3.19 A). This corresponds with our microscopic observations of larger dendrite structures on the synovial DCs, and more irregular cell shapes of synovial tissue isolated $CD14^+$ monocytes. The FSC-A MFI of both cell types suggests similar cell size from either blood or tissue (Fig. 3.19 B).

The morphological assessment of these FACS sorted cell populations confirms their identity and purity. The higher SSC-A observed in tissue cells could be a result of liberase treatment. However matched tissue and blood cells which had both undergone liberase treatment had comparable SSC-A MFI (data not shown). Therefore these data suggest that tissue-derived

CD14^{+} monocytes and cDC2s contain more structural complexes than their peripheral blood counterparts.

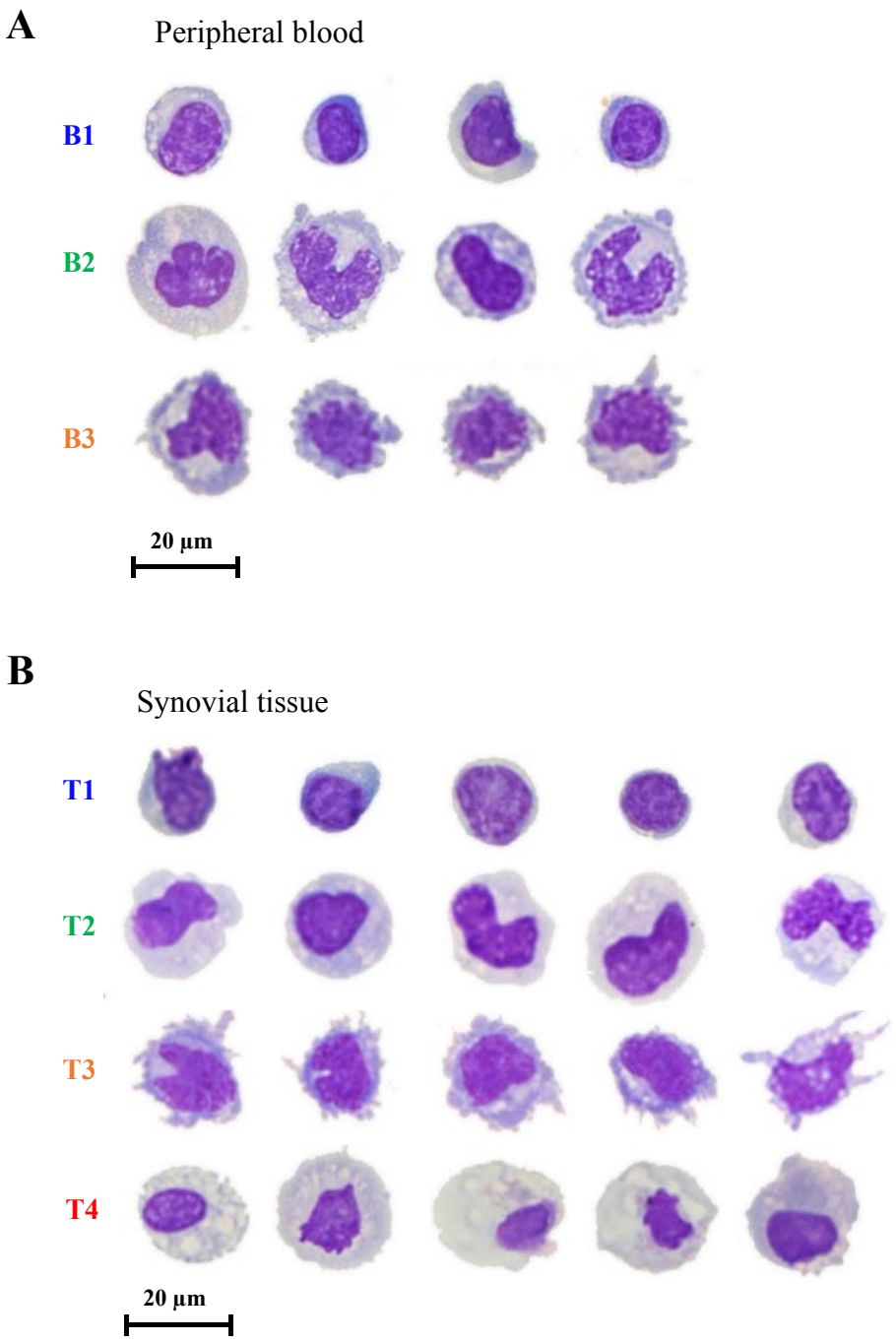

Figure 3.18: Morphology of cell subsets isolated from synovial tissue and peripheral blood
Synovial tissue from OA total knee replacement was digested using the optimised protocol shown in Figure 3.6. Matched PBMC was obtained from corresponding OA total knee replacement patient. Single cell suspensions were FACS sorted following gating strategy shown in Figure 3.17. Cytospin slides were prepared with FACS purified cells. **A:** Cytospin images of CD4^{+} T cells (**B1**), CD14^{+} monocytes (**B2**) and cDC2s (**B3**) from PBMC. **B:** Images of CD4^{+} T cells (**T1**), CD14^{+} monocytes (**T2**), cDC2s (**T3**) and HLA-DR^{+}CD14^{+} MØ (**T4**) from synovial tissue. Data are representative of three independent experiments.

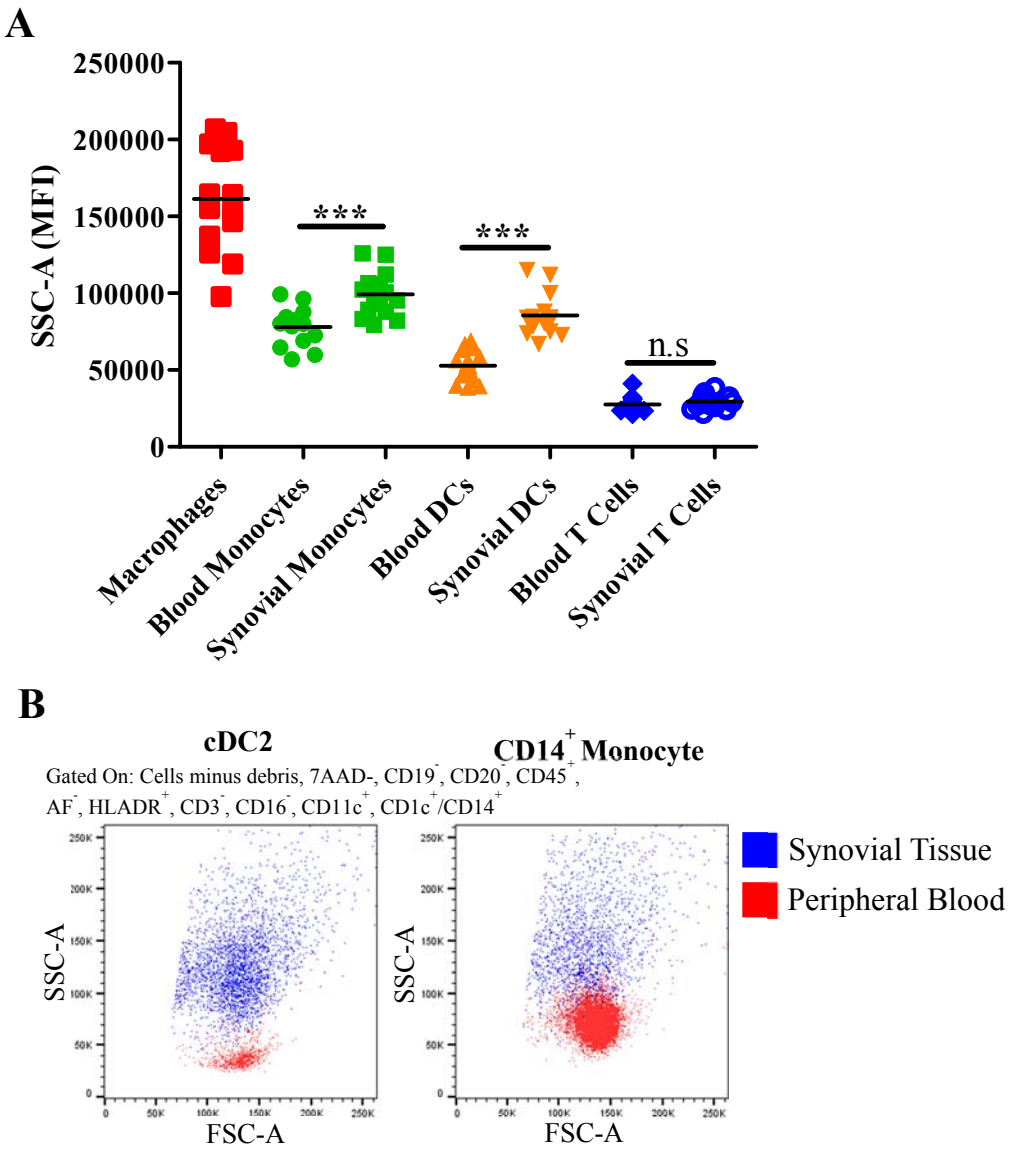

Figure 3.19: SSC-A profile of CD14$^+$ monocytes, cDC2s and CD4$^+$ T-lymphocytes from synovial tissue and PBMC

Synovial tissue from OA total knee replacement was digested using the optimised protocol shown in Figure 3.6. Matched PBMC was obtained from corresponding OA total knee replacement patient. **A:** SSC-A of HLA-DR$^+$CD14$^+$ macrophages, CD14$^+$ monocytes, cDC2s and T-Lymphocytes from matched synovial tissue and PBMC. **B:** SSC-A and FSC-A profiles OF CD14$^+$ monocytes and cDC2s from matched synovial tissue and PBMC. Cell subsets were identified by flow cytometry; gating strategy shown in Figure 3.17 was applied. Data are representative of fourteen independent experiments. ****P≤0.001, ****P ≤0.0001*.

3.7 Discussion

Here I have outlined a method for the isolation, identification and purification of immune cell subsets from synovial tissue, summarised in Figure 3.20. A lack of clarity or clear development of these experimental aspects has limited research into the pathogenesis and cellular mechanisms at the disease site of arthritis, the synovial membrane. Owing to this and the invasive nature and limited availability of tissue samples, much current published research has been carried out on peripheral blood samples or mouse models. In IA such as RA, symmetrical swelling of joints is persistent and characteristic (van der Helm-van Mil, Verpoort et al. 2005, Aletaha, Neogi et al. 2010). Commonly affected joints include wrists, elbows, knees and metatarsophalangeal (MTP) joints (van der Helm-van Mil, Verpoort et al. 2005, Aletaha, Neogi et al. 2010). Similarly, OA can affect multiple joints including those of the hand, however hips and knees are most commonly affected (Peat, Thomas et al. 2006, Haugen and Boyesen 2011, Fernandes, Hagen et al. 2013). Using tissue from these disease sites can aid in understanding the full cellular mechanisms and pathogenesis of these diseases.

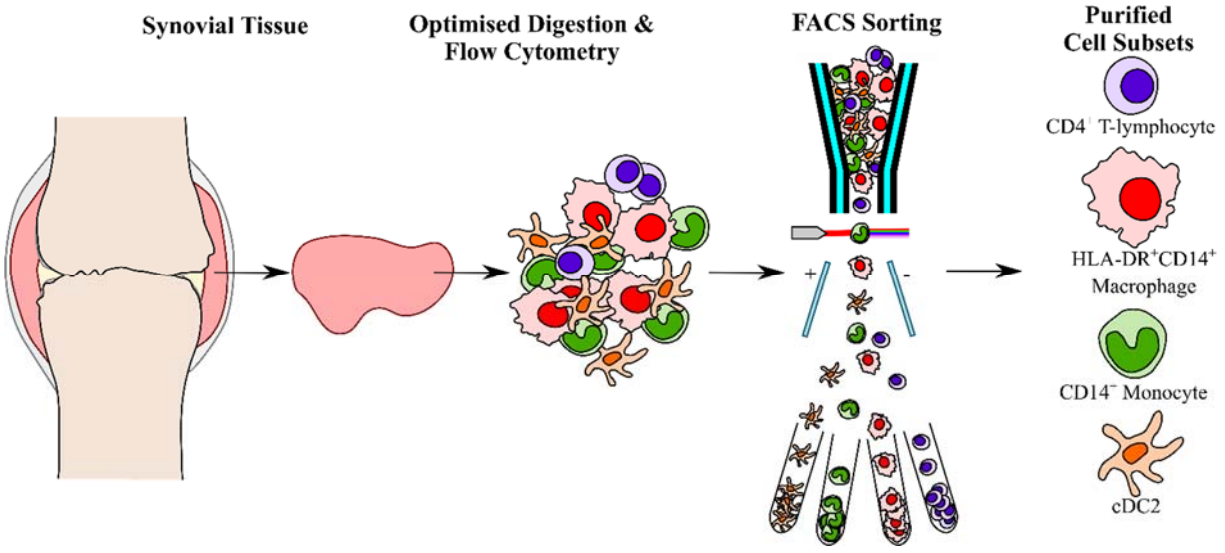

Figure 3.20: Illustrative summary of Chapter 3 results
Depiction of the methods optimised in Chapter 3 for the isolation, identification and purification of mononuclear cells from synovial tissue. This involves the use of an optimised synovial tissue digestion protocol for isolation, multi-colour flow cytometry for identification and optimised FACs for purification. Purity and morphology of cell subsets were confirmed using cytospin preparations.

I have demonstrated that many published and established protocols for achieving single cell suspensions from synovial tissue have a number of limitations. Most notably, poor cell viability, low cell yields and cleavage of extracellular proteins. Owing to this, I have developed an optimal synovial tissue digestion protocol, which results in high cell yields, viability and little cleavage of extracellular antigens. This allows me to be confident in my cell identification by flow cytometry using these extracellular proteins, in addition to minimally manipulated isolated cells. When assessing the individual digestion stages of this protocol, no cell subsets were preferentially enriched, allowing for unbiased characterisation of cell subsets within the tissue.

Although this optimised digestion protocol is improved on previous protocols, there remain limitations. Despite this protocol showing higher viability of cells, it is still likely that cells will be altered during this mechanical digestion process, especially with regard to gene expression. Because there is currently no clear alternative to studying these purified cell subsets, this limitation will be taken into consideration for future analyses. Furthermore, the involvement of enzymes will likely alter isolated cells, especially their surface marker phenotype. However, it is essential to include enzymes to achieve sufficient cell yields. I have further shown that there is minimal to no cleavage of surface markers (of those tested) with this protocol.

Developing a well-tested, multi-colour flow cytometry panel for the identification of multiple cell subsets is an important, and often overlooked step in cellular analyses. When considering flow cytometry-based cell sorting and the cell subset downstream applications, it is vital that the accuracy and purification of these subsets is of the highest quality possible. Contaminating cell subsets in both functional assays and genomic analysis can mask the true function and phenotype of a cell population. Using structural properties of the cells, in addition to a comprehensive yet conserved panel of fluorescently labelled antibodies, I am able to identify and phenotype cDC2s, $CD14^+$ monocytes, $CD4^+$ T cells and HLA-DR^+ $CD14^+$ macrophages. This has been applied to FACS sorting and has resulted in high cell yields and successful use in functional and genomic analysis. Purity of FACS sorted cell subsets was confirmed by carrying out cytospins of these populations and manually checking for contaminating cells. Additionally, this also allowed the assessment of cell morphology, confirming their correct identification.

Finally, I compared the morphology and structure of blood cell subsets with their tissue counterparts. From cytospin preparations, it was observed that although the blood monocytes had minor cell surface ruffles, the tissue monocytes had more irregular cell shapes. Tissue cDC2s appeared to have more pronounced dendrite structures compared to their blood counterparts. T cells between both blood and tissue showed no distinct differences. These

observations were mirrored when comparing the SSC-A profiles of the matched blood and tissue cells by flow cytometry, demonstrating no difference between T cells, but significantly higher SSC-A MFI measurements of tissue monocytes and cDC2s as compared to blood. This could suggest that unlike T cells, monocytes and cDC2s are more susceptible to influential changes from the tissue environment. Additionally, since both monocytes and dendritic cells are phagocytic, this could represent higher rates of engulfment within the tissue environment and therefore increased granularity. Indeed, macrophages are highly efficient at phagocytosis and were observed to have the highest levels of SSC-A.

Taken together, this series of optimisation steps is essential to the accurate study of immune cell populations within the disease site of arthritis patients. Although there are established and published protocols being used, limitations could ultimately result in poor application in downstream studies. To allow comparable cellular data from synovial tissue between research laboratories, a common digestion protocol should be utilised to reduce technical differences between experiments. In our application, the pairing of this protocol with a carefully constructed flow cytometry panel has allowed the isolation of highly pure cell subsets. These techniques will now be used for the characterisation of immune cell subsets in synovial tissue, in addition to their purification for functional and transcriptomic analyses.

Chapter 4. Characterisation of immune cell populations in peripheral blood and synovial tissue of OA and IA patients

4.1 Introduction

There is an extensive body of research surrounding synovial inflammation in RA. During inflammation, there is cellular infiltration into the synovial sublining by T and B cells, macrophages, NK cells, and DCs (Tak, Smeets et al. 1997). Resultant angiogenesis exacerbates this infiltration allowing increased leucocyte migration, and the forming of a synovial 'pannus' (Reece, Canete et al. 1999). This pannus is thought to cause cartilage and bone destruction through expansion and invasion. Production of pro-inflammatory cytokines and MMPs can exacerbate this.

Published literature has described OA synovium as limited to areas of fibrosis, hyper-vascularization and cartilage fragments, with considerably less inflammation than seen in RA synovium (Petersson, Sandqvist et al. 1997, Struglics, Larsson et al. 2006, Remst, Blaney Davidson et al. 2015). OA has therefore often been used in research as a non-inflammatory comparator for RA. However, synovitis in OA is becoming more recognised. Synovial inflammation has been reported in over 50% of OA patients (Haywood, McWilliams et al. 2003, Attur, Samuels et al. 2010, Baker, Grainger et al. 2010).

Cellular infiltration in the synovium of OA patients has been previously identified by histological methods. Angiogenesis and synovitic lesions have been reported, with infiltration of mononuclear cells, particularly CD68 macrophages (Ene, Sinescu et al. 2015). This synovitis was seen throughout OA patients with varying stages of radiographic joint damage. T cells in addition to macrophages have also been reported in OA synovium (Saito, Koshino et al. 2002, Rollin, Marco et al. 2008). The presence of pro-inflammatory mediators may also suggest a role for cellular synovitis in OA disease progression (Sellam and Berenbaum 2010, Scanzello and Goldring 2012). However, it is still not clear whether synovitis initiates, or is a consequence of OA joint damage.

The cellular composition of the synovium can additionally act as a therapeutic biomarker. In 1989, (Rooney, Whelan et al. 1989) showed that treatment with gold therapy resulted in a decrease of T and B cell numbers. Since then, macrophages have been the focus of many of these therapeutic biomarker studies. Numbers of macrophages have been shown to be decreased in the synovium after treatment with gold therapy, prednisolone, methotrexate and leflunomide (Yanni, Nabil et al. 1994, Kraan, Reece et al. 2000, Smith, Kraan et al. 2001, Gerlag, Haringman et al. 2004). Reports of lymphocyte numbers in patients have described mixed results. Other

studies have shown reductions in synovial CD3 T cells in addition to CD68 macrophages after treatment with infliximab, and B cells after treatment with rituximab (Tak, Taylor et al. 1996, Smeets, Kraan et al. 2003, Thurlings, Vos et al. 2008). In addition, there are a number of studies that suggest direct links between macrophages and RA disease progression, and the potential use of macrophages as a direct biomarker of disease activity (Haringman, Gerlag et al. 2005). Although histological methods are extremely useful, they also have limitations. One example is a lack of specificity owing to a restricted number of possible parameters. For example, most research identifying macrophages use the marker CD68. However, it has been well reported that this is not a specific macrophage marker and can be expressed by monocytes, monocyte-derived DCs, fibroblasts and adipocytes (Kunz-Schughart, Weber et al. 2003, Khazen, M'Bika J et al. 2005, Gottfried, Kunz-Schughart et al. 2008, Pilling, Fan et al. 2009). Due to CD68 expression on multiple cell types previous enumerations of synovial macrophages in disease using CD68 as a sole marker could be inaccurate. Additionally, it has been reported that the cellular composition of 'healthy' synovium is often not well represented (Smith, Barg et al. 2003). This was attributed to variable architecture of the synovial membrane, including thickness and sub intimal cellular infiltrate. By using the whole synovium from OA total knee replacement (TKR), and unbiased IA synovial biopsies, the cellular content will be more representative.

Recent advances in tissue digestion, flow cytometry and omics technologies have allowed new methods of studying the synovium in arthritic diseases. Studies using these approaches have characterised fibroblasts, macrophages, T and B cells (Komatsu, Okamoto et al. 2014, Leipe, Schramm et al. 2014, Yeo, Lom et al. 2015, Yeo, Adlard et al. 2016, Mizoguchi, Slowikowski et al. 2017). However published research that use these techniques mostly focus on a single cell type within RA.

The cellular composition of synovial tissue has proven to be extremely important. However, this research has been predominantly carried out in RA, and there has been a lack of similar research in OA. Furthermore, studies of cellular composition in OA have been limited to histological and imaging methods. Understanding the cellular compartment in both IA and OA, and identifying multiple subsets within the same tissue could lead to a better understanding of these disease mechanisms.

4.2 Aims

The characterisation of immune cell subsets in the synovial tissue has been limited, especially in OA patients. Furthermore, most characterisation to date has been carried out by histological methods. This has been owing to difficulty in isolating cells from tissues at sites of disease activity, as discussed in Chapter 3. Now that a protocol has been optimised allowing the isolation and accurate identification of these cells, extensive analyses of the cellular content in arthritic synovial tissue can be conducted. I therefore aimed to:

- Assess and select the most relevant method for the quantification of the immune cell subsets in synovial tissue
- Identify the cellular compartments using flow cytometry data from the peripheral blood and synovial tissue of both OA and IA patients
- Compare and contrast identified cellular compartments between OA and IA patients
- Explore computational analysis techniques on flow cytometry data with a view to validating results of manual quantification

4.3 Patient characteristics

Peripheral blood and synovial tissue samples from OA and IA patients were used throughout the analyses described in Chapter 4. All OA samples were collected from elective TKR surgery. IA samples were collected from either elective TKR surgery, or ultrasound guided needle biopsy of the wrist. Patient information regarding basic clinical information, disease severity and treatment is summarised in Table 4.1.

Between the two disease cohorts, patients were of similar age and sex. However, the Body Mass Index (BMI) of OA patients was significantly higher than that of IA patients. In OA patients a mean BMI of 32.7 (SD 5.6) was recorded. In adults, this is classed as obese by NICE guidelines (NICE, 2017). As Obesity is a known risk factor of OA, an obese patient cohort is not unusual (Davis, Ettinger et al. 1988, Cooper, Snow et al. 2000, Field, Coakley et al. 2001). The mean BMI of IA patients was 27.2 (SD 3.9), and whilst this is classed as overweight (NICE, 2017), it does not constitute obesity. As obesity may potentially play a causal role in the underlying cellular mechanisms, this significant difference was deemed acceptable when considering the comparative analyses performed throughout this chapter.

C-reactive protein (CRP) and erythrocyte sedimentation rate (ESR) are both routine clinical tests that non-specifically measure inflammation. CRP is an acute phase reactant produced in the liver. ESR is the sedimentation of erythrocytes, which during inflammation can become

denser owing to excess proteins, including fibrinogen, in blood. Additionally the can clump further increasing density. A higher sedimentation rate, measured in millimetres travelled in one hour (mm/hr), is an indicator of inflammation. Both CRP and ESR were significantly higher in the IA patients. This was expected as the clinical criteria for RA diagnosis includes abnormal ESR or CRP measurements (Aletaha, Neogi et al. 2010). Although it has been indicated that in OA, CRP and ESR levels are associated with local joint inflammation, this link is less clear (Pearle, Scanzello et al. 2007, Keenan, Swearingen et al. 2008, Hanada, Takahashi et al. 2016). These differences were therefore also deemed acceptable. This is justified, as the higher CRP and ESR levels are likely due to differences in disease mechanisms, of which I am aiming to compare in the cellular composition of the synovial tissue.

OA specific data collected included Kellgren and Lawrence (KL) X-ray score, previous menisectomy or TKR, and disease patterns. The Kellgren and Lawrence system for classification of OA using radiographic images from X-rays is graded from 0-4. A score of 0 suggests no radiographic features of OA present. Conversely, the most severe score is 4. The median score recorded in our OA patients was 3. This suggests active OA disease in our cohort, showing multiple, moderately sized osteophytes, definite joint space narrowing, some sclerotic areas and possible bony end deformity (NICE, 2017). 15% and 20% of OA patients had previously undergone a menisectomy or TKR, respectively.

Of note, 32.95% of OA patients recruited were currently taking statins (Atorvastatin or Simvastatin). It has been suggested that statins can have modulatory roles in the context of immune cell subsets (Yilmaz, Reiss et al. 2006, Tuomisto, Lumivuori et al. 2008, Jameel, Ooi et al. 2013). In addition, 12.5% and 2.5% of OA patients also had clinical diagnosis of non-insulin-dependent diabetes mellitus (NIDDM) and gout respectively. These data were taken into consideration when conducting comparative analyses.

IA specific data collected included Disease Activity Score in 28 Joints (DAS28), Rheumatoid Factor (RF) and Cyclic Citrullinated Protein (CCP). Patients recruited showed a median DAS28 of 3.42. A DAS28 score of 3.2-5.1 indicates moderate disease activity (Fransen and van Riel 2005).

	OA (n=64)	IA (n=19)	Variation
Age (years; mean, SD)	65.8 (10.5)	65.2 (13.3)	n.s.
% Females	56.5	43.8	n.s.
BMI (mean, SD)	32.7 (5.6)	27.2 (3.9)	**
Disease Duration (years; median, SD)	3.5 (1.8)	N/A	N/A
Symptom Duration (weeks; median, SD)	N/A	12 (15.4)	N/A
CRP (mg/l; median, SD)	0 (9.55)	22.5 (34.4)	****
ESR (mm/hr; median, SD)	12 (13.1)	40.0 (30.7)	****
DAS28 (median, SD)	N/A	3.42 (1.2)	N/A
RF$^+$ (%)	N/A	37.5	N/A
CCP$^+$ (%)	N/A	31.3	N/A
KL X-ray Score (median, SD)	3 (0.9)	N/A	N/A
Joint (%R TKR)	67.7	N/A	N/A
% NIDDM	12.5	N/A	N/A
% Gout	2.5	N/A	N/A
% Previous Menisectomy	15	N/A	N/A
% Previous TKR +/- DTOS	20	N/A	N/A
OA Pattern (% bilateral, % unilateral)	55, 45	N/A	N/A
% No Medication (% medication)	57.5 (5.9 Alendronate, 5.9 Allopurinol, 29.4 Atorvastatin, 58.8 Simvastatin)	N/A	N/A
Joint Specific Pattern (% Pattern)	59 Medial, 19.6 Patellofemoral, 10.9 Lateral, 10.9 Tricomp	N/A	N/A
Disease (% RA, % PsA, % Undifferentiated)	N/A	62.5, 6.25, 31.25	N/A

Table 4.1: Patient characteristics for synovial tissue cellular characterisation analyses
For cellular characterisation, 64 OA patients and 19 IA patients were used. Patient data were collated and tabulated. As these patients were recruited from separate clinics, a number of clinical parameters were not available for each group. Some patient records were incomplete or unavailable, values therefore represent proportion of all disease specific patients used. N/A – not applicable, n.s. – no significance, ***P ≤0.01, ****P ≤0.0001*.

4.4 Characterisation of immune cell subsets in synovial tissue

4.4.1 *Immune cell infiltration in IA*

When quantifying immune cell infiltration in tissues, there are a number of different approaches that can be taken. One method often used in published literature is the number of cells isolated per gram of tissue. Using a calculation of cells per gram of tissue allows the normalisation for differing amounts of synovial tissue acquired from TKRs and wrist biopsies. When applied to my data set, there is a significantly higher proportion of live cells per gram of synovial tissue in IA compared to OA (Fig. 4.1 A).

CD45, the leukocyte common antigen is expressed ubiquitously on all haematopoietic cells. As this encompasses human immune cells, and owing to the lack of expression on stromal cells, a greater quantity of $CD45^+$ cells found within a tissue could be indicative of immune cell infiltration during inflammation. To calculate this in the flow cytometry data, dead cells and debris were gated out and the number of $CD45^+$ and $CD45^-$ cells were determined (Fig. 4.1 B). Percentages of these two cell numbers were then calculated from their sum. In the synovial tissue samples of these two patient cohorts, a significantly higher proportion of $CD45^+$ cells was observed in the IA patients and accordingly a significantly higher proportion of $CD45^-$ cells was observed in OA patients (Fig. 4.1 C). This difference was also observed when measuring

absolute CD45$^+$ cell numbers per gram of synovial tissue (Fig. 4.1 D). This supports the observation of increased immune cellular infiltrate into the synovial tissue of IA patients.

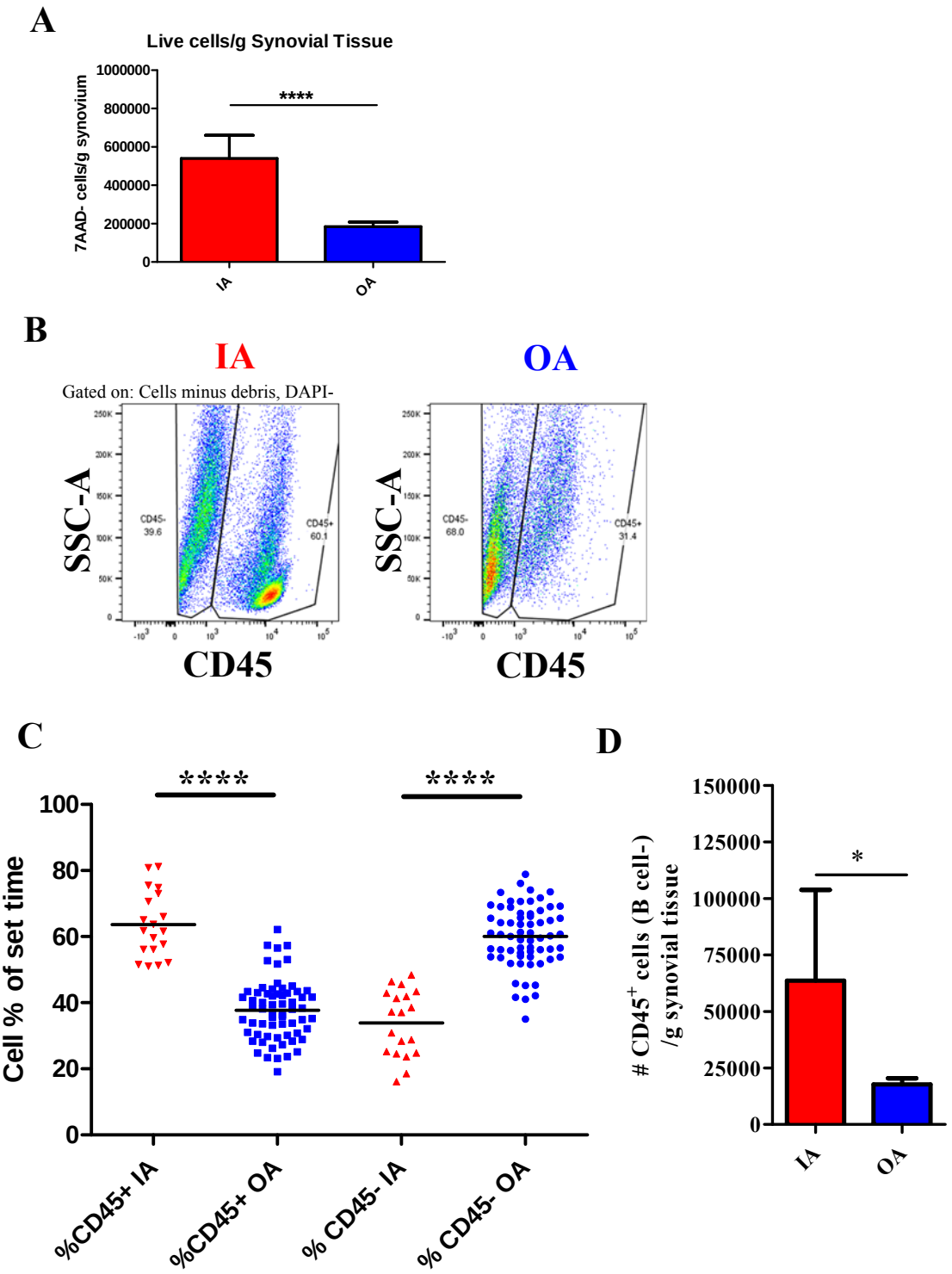

Figure 4.1: Analyses of cellular infiltration in IA and OA synovial tissue
Synovial tissue from OA total knee replacement and IA ultrasound guided biopsy was digested and analysed by flow cytometry using techniques described in Chapter 3. **A:** Quantification of live cells (DAPI-) per gram of synovial tissue. **B:** Gating strategy for identification of CD45$^+$ and CD45$^-$ cells. Left plot is representative of an IA sample, right plot is representative of an OA sample. **C:** Percentage of CD45$^+$ and CD45$^-$ cells in IA and OA. **D:** CD45+ cells per gram of synovial tissue in IA and OA. Data are representative of >20 independent experiments. *****P ≤0.0001*.

Using CD90, stromal cells can be identified within the $CD45^-$ population (Fig. 4.2 A). Morphology of these cells was assessed by cytospin (Fig. 4.2 B). Stromal cells are known to contribute to the pathogenesis of both OA and IA. However, as discussed in Chapter 3 the detailed investigation and isolation of this stromal cell population was not taken further.

These initial comparisons have demonstrated a larger proportion of cells, particularly $CD45^+$ immune cells, in IA synovial tissue. I next aimed to characterise the cell subsets within this $CD45^+$ cell population.

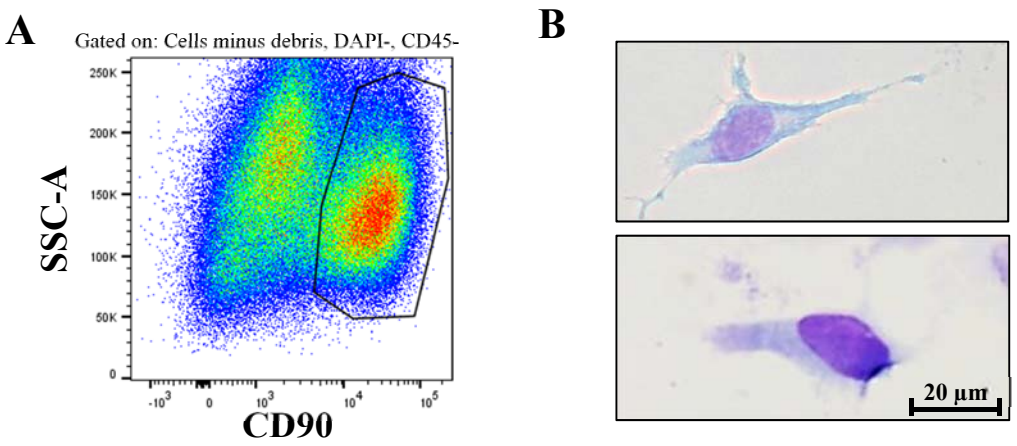

Figure 4.2: Identification of CD90+ stromal cells
Synovial tissue from OA total knee replacement and IA ultrasound guided biopsy was digested and analysed by flow cytometry using techniques described in Chapter 3. Cytospin slides were prepared with FACS purified cells. **A:** Gating strategy for identification of $CD90^+$ Stromal cells. **B:** Cytospin images of $CD90^+$ stromal cells. Data are representative of three independent experiments.

4.4.2 Identification and quantification method of additional cell subsets

For the analyses carried out in this chapter, the gating strategy for the identification of $HLA\text{-}DR^+$ macrophages, $CD14^+$ Monocytes, cDC2s and $CD4^+$ T cells discussed in Chapter 3 was used. In addition, for some analyses, additional cell subsets were taken into account. These include all $CD3^+$ T cells and $CD3^+CD4^-$ T cells, $CD16^+$ monocytes and the $CD11c^{lo}$ fraction of cells which cDC1s and pDCs are likely to contribute (Fig. 4.3).

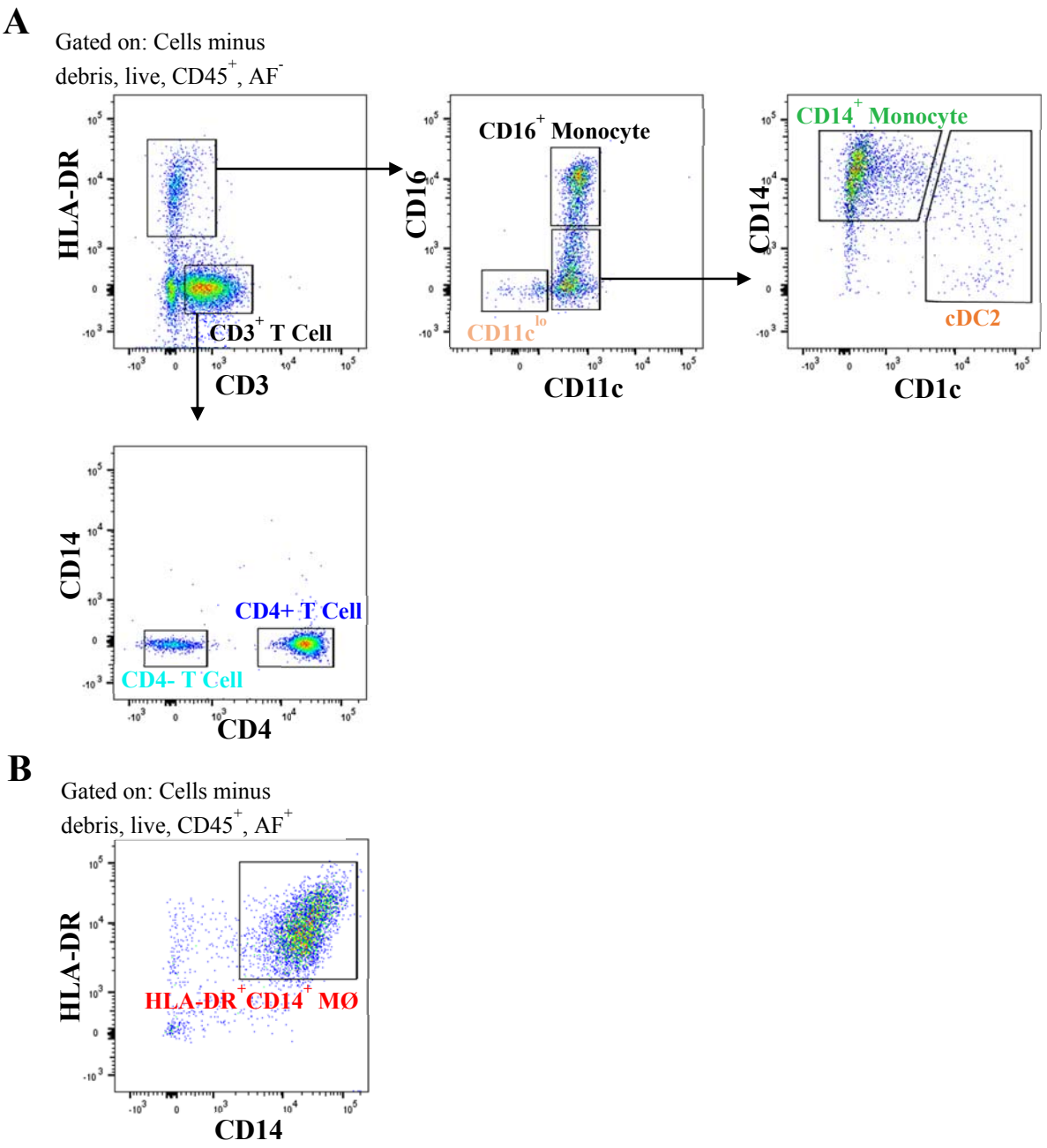

Figure 4.3: Identification of immune cell subsets for quantitative analyses
Synovial tissue from OA total knee replacement and IA ultrasound guided biopsy was digested and analysed by flow cytometry using techniques described in Chapter 3. **A:** Identification of $CD3^+$, $CD4^+$ & $CD4^-$ T cell populations, $CD11c^{lo}$ cells, $CD16^+$ & $CD14^+$ monocytes and cDC2s. **B:** Identification of $HLA\text{-}DR^+CD14^+$ MØ. Data are representative of both OA and IA samples from 22 independent experiments.

4.4.3 *Quantification method immune of cell subsets*

When quantifying these multiple subsets, there are again a number of methods that could be used. As previously discussed, looking at the total event or cell number would not amount for biases in amount of tissue analysed. Therefore calculating cell number/g of tissue could be employed to these analyses (Fig. 4.4). Although this was a useful method, this did not control for anatomical source of tissue. For example, as it is difficult to control for the exact location from which tissue is taken, there may be large variations in the proportion of stromal cells to immune cells. An alternative is to calculate cell subset percentages from a total population of cells. I carried this out, calculating cell subsets as a percentage of either total events, cells minus debris, live cells or $CD45^+$ cells (Fig. 4.4). All four of these methods of calculating percentages yield the same result in terms of relative cell subset quantification (Fig. 4.4). However, due to the high number of events, in some of these, differences between the less abundant cells subsets can be less clear as smaller percentages are produced. I therefore decided to use cell subset numbers as a percentage of the $CD45^+$ cell population. This method will yield the same result as the other methods, but allow me to better compare differences at the subset level. Furthermore, as the flow cytometry panel was designed for identifying cells within the $CD45^+$ cell fraction, this could also be seen as the most relevant calculation to make.

4.4.4 *Manual quantification of immune cell subsets in peripheral blood*

The initial analyses conducted between OA and IA was on peripheral blood samples obtained from these patients (Fig. 4.5). First, the T cell compartment was compared. Although there were higher levels of $CD3^+$ T cells and $CD4^+$ T cells in IA patients, this difference was not significant (Fig. 4.5 A). There was no clear difference in the CD4- proportion of the T cell compartment between OA and IA (Fig. 4.5 A), or when comparing CD4 T cells as a percentage of $CD3^+$ T cells (Appendix 4.1). There was no difference in the percentages of monocytic populations between OA and IA (Fig. 4.5 B & C), or when analysed as total monocytes (Appendix 4.1). However, there were significantly higher levels of cDC2s in the OA group (Fig. 4.5 C). Conversely, there were significantly higher levels of $CD11c^{lo}$ cells in the IA group (Fig. 4.5 C). Although, it is likely the $CD11c^{lo}$ population represents cDC1s and pDCs, it is important to note that these are not specifically identified.

A

	Total event	Cells -debris	Live	CD45+	AF+	MØ	AF-	CD3+	CD4+	CD4-	HLA-DR+	CD11c+	CD11clo	CD14+	CD1c+
Total events	1645057.6	832474	759037	56574.8	27977.4	13244	23594	6243.67	4175.92	1888	4938.83	2707.33	1432.33	1328.92	1159.92
Total events/g tissue	826628.31	429800.48	396732	23425.3	9794.43	4805.79	11600.7	4322.65	2994.93	1258.42	2692.98	1329.59	774.28	693.62	527.33
% Total events	n/a	63.5	58.42	3.65	1.76	0.84	1.56	0.51	0.33	0.16	0.35	0.18	0.11	0.09	0.08
% Cells -debris	n/a	n/a	91.1	6.78	3.24	1.34	2.87	0.79	0.52	0.25	0.55	0.29	0.17	0.14	0.12
% Live cells	n/a	n/a	n/a	7.67	3.67	1.5	3.23	0.86	0.56	0.28	0.61	0.32	0.19	0.16	0.13
% CD45+ cells	n/a	n/a	n/a	n/a	45.89	19.69	45.62	17.06	10.96	5.71	9.9	4.14	3.47	2.16	1.49
Colour Scale	Highest Value			Lowest Value											

B

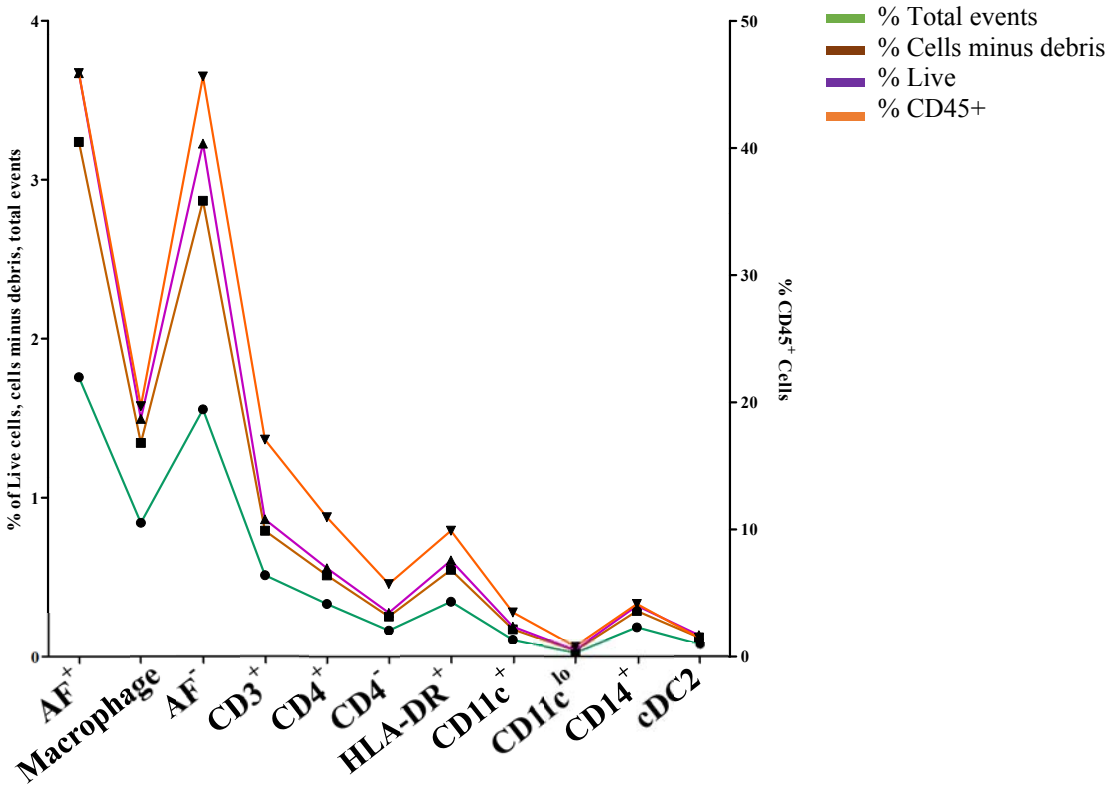

Figure 4.4: Quantification methods of immune cell subsets in synovial tissue
Synovial tissue from OA total knee replacement and IA ultrasound guided biopsy was digested and analysed by flow cytometry using techniques described in Chapter 3. **A:** Results from six different quantification methods. Orange cells indicate lowest value for that analyses. Blue cells indicate highest value for that analyses. **B:** Data of percentage quantifications from **A** plotted. %Total events, %Cells minus debris and %Live cells plotted on left Y-axis. %CD45^{+} cells plotted on right Y-axis. In addition to cell subsets described in Figure 4.5, Total AF^{+}, AF^{-}, HLA-DR^{+} and CD11c^{+} populations are plotted. Data are representative of 22 individual experiments.

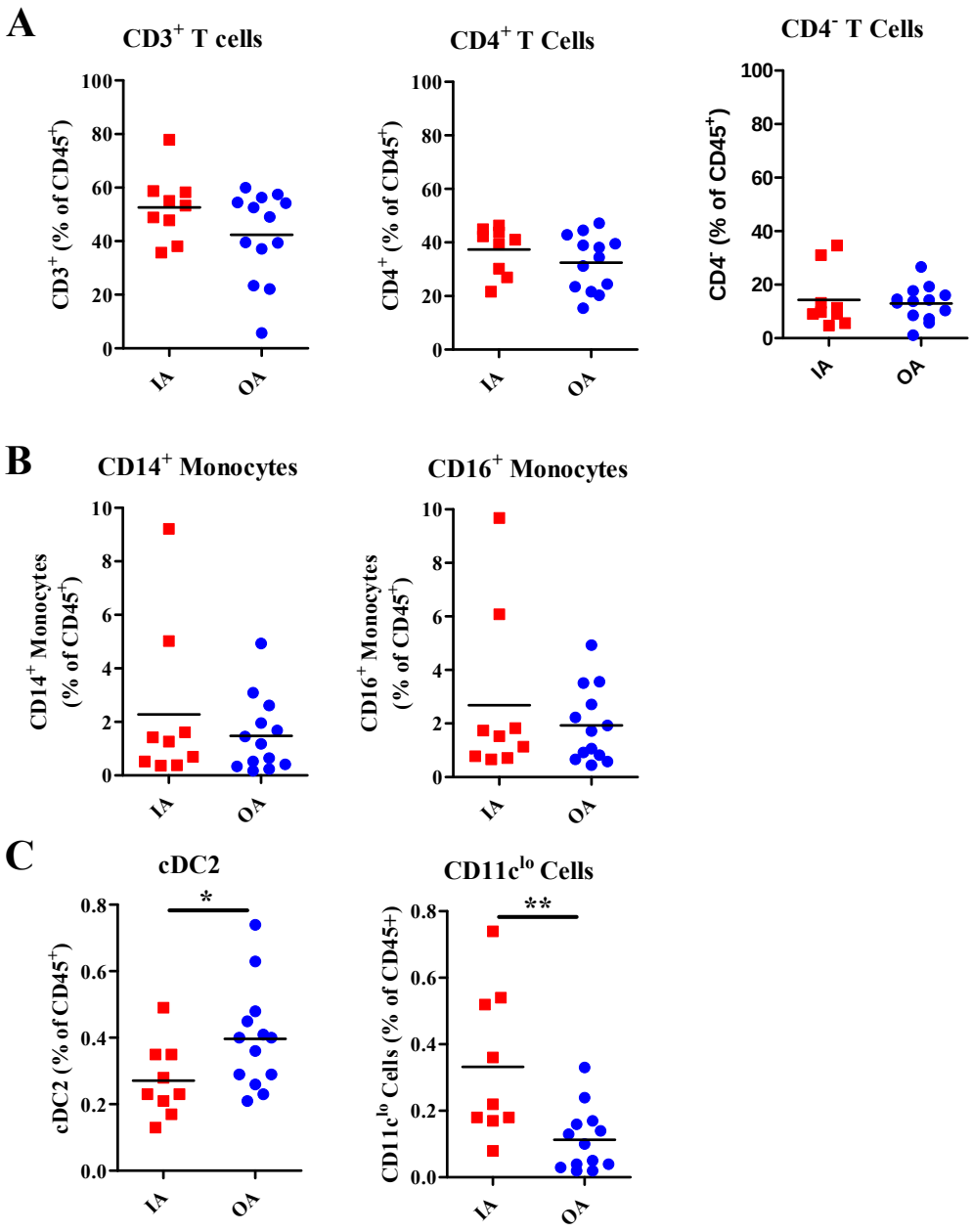

Figure 4.5: Quantification of immune cell subsets in peripheral blood
PBMCs were isolated from peripheral blood of OA total knee replacement and IA ultrasound guided biopsy patients. PBMCs were analysed by flow cytometry using techniques described in Chapter 3. **A:** Proportion of $CD3^+$, $CD4^+$ and $CD4^-$ T-cells in IA and OA peripheral blood. **B:** Proportion of $CD14^+$ and $CD16^+$ monocytes in IA and OA peripheral blood. **C:** Proportion of cDC2 and $CD11c^{lo}$ cells in IA and OA peripheral blood. All data presented as % of $CD45^+$ cells. *n=23. *P≤0.05, **P ≤0.01.*

4.4.5 *Manual quantification of immune cell subsets in synovial tissue*

The same set of comparisons conducted in Section 4.4.4 was conducted on the flow cytometry data from synovial tissue (Fig. 4.6, 4.7, 4.8). Within the T cell compartment, there were significantly higher levels of $CD3^+$ T cells in the synovial tissue of IA patients compared to OA (Fig. 4.6 A). In the IA group there appeared to be four tissue samples that contained lower levels of $CD3^+$ cells, akin to that of the OA group (Fig. 4.6 A). Conversely, there was a small number of OA tissue samples that had slightly higher levels of $CD3^+$ T cells (Fig. 4.6 A). The lower levels of $CD3^+$ T cells in the synovium of a number of IA samples was not mirrored by the level of $CD3^+$ T cells in the matched peripheral blood samples (Fig. 4.6 B). Although there was no clear difference in the levels of $CD3^+$ T cells between the matched blood and tissue of IA patients, there appeared to be significantly lower levels of these cells in the synovial tissue of OA patients, compared to matched blood samples (Fig. 4.6 B). When applied to the $CD4^+$ and $CD4^-$ populations, higher levels were again seen in the synovial tissue of IA patients compared to OA patients (Fig. 4.6 C & E). Likewise, there was no clear difference between the tissue and blood of IA patients, but lower levels of these T cell populations were seen in the tissue of OA patients compared to matched blood (Fig. 4.6 D & F). A group of patients with levels of $CD4^+$ T cells similar to OA was seen again in the IA patients, which too did not have distinct levels in the blood (Fig. 4.6 C).

Next, these analyses were applied to the monocytic populations (Fig. 4.7). There were no clear differences in quantities of either $CD14^+$ classical monocytes or $CD16^+$ non-classical monocytes in the synovial tissue of the IA and OA groups (Fig. 4.7 A & B). There appeared to be an increase in $CD14^+$ monocytes in the synovial tissue of OA patients compared to matched peripheral blood, not observed in the IA patient cohort (Fig. 4.7 B). A reduced quantity of $CD16^+$ monocytes was seen in the tissue of IA patients compared to peripheral blood (Fig. 4.7 D). This difference was not seen in the OA patients.

Similarly, to the observation in blood, there were significantly higher levels of cDC2 in the synovial tissue of OA patients compared to IA (Fig. 4.8 A). However compared to matched blood, an increase in cDC2s was observed in the synovial tissue of both IA and OA patients (Fig. 4.8 B). A greater proportion of the $CD11c^{lo}$ population was observed in the synovial tissue of IA compared to OA (Fig. 4.8 C). Although an increase was seen in the tissue compared to matched blood in both IA and OA, this difference was only significant in the OA group (Fig. 4.8 D).

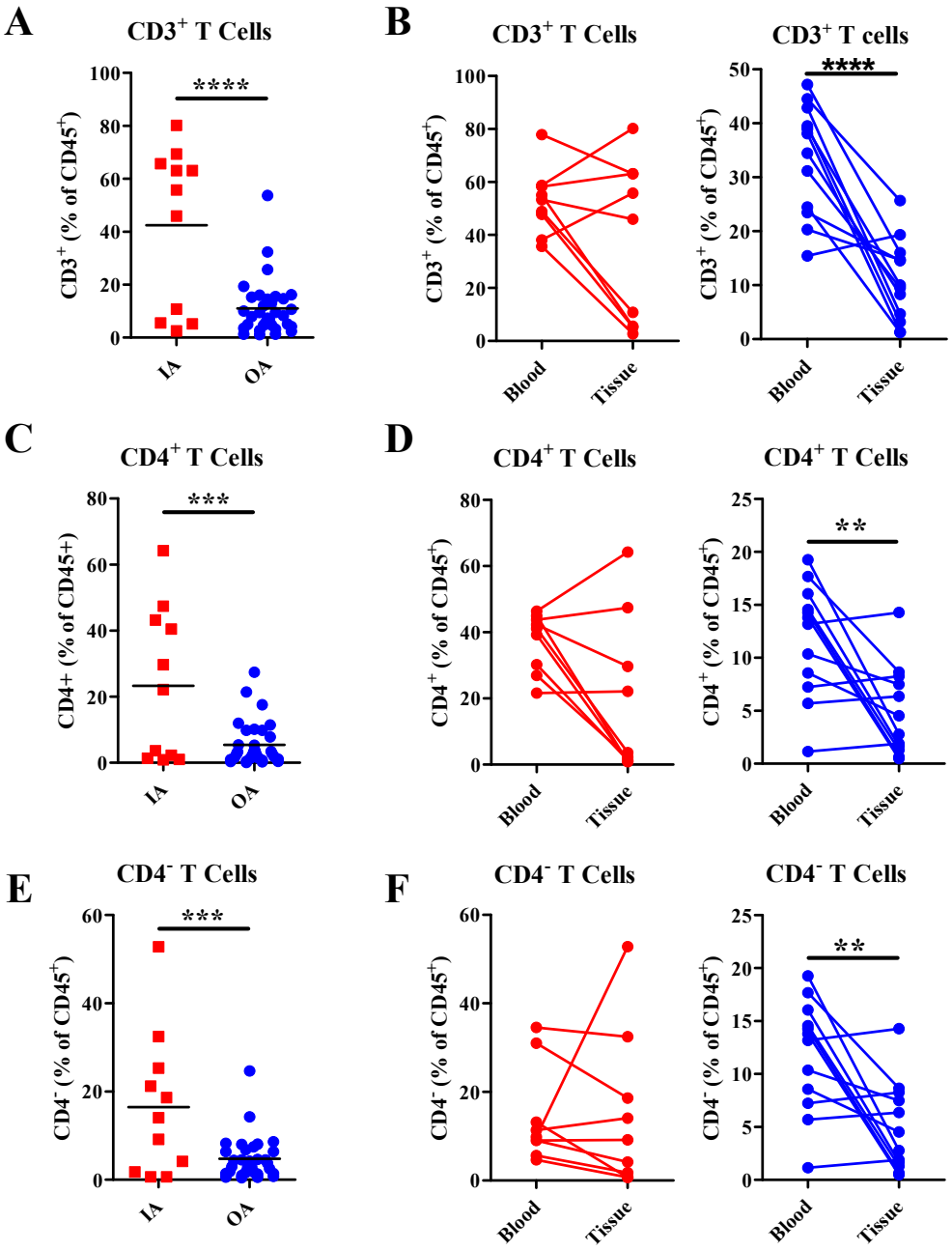

Figure 4.6: Quantification of T cells in synovial tissue
Synovial tissue from OA total knee replacement and IA ultrasound guided biopsy was digested and analysed using techniques described in Chapter 3. PBMCs were isolated from matched peripheral blood. Single cell suspensions were analysed by flow cytometry using techniques described in Chapter 3. **A:** Proportion of $CD3^+$ T cells in IA and OA synovial tissue. **B:** Proportion of $CD3^+$ T cells in matched synovial tissue and peripheral blood. Left hand panel depicts IA. Right hand panel depicts OA. **C:** Proportion of $CD4^+$ T cells in IA and OA synovial tissue. **D:** Proportion of $CD4^+$ T cells in matched synovial tissue and peripheral blood. Left hand panel depicts IA. Right hand panel depicts OA. **E:** Proportion of $CD4^-$ T cells in IA and OA synovial tissue. **F:** Proportion of $CD4^-$ T cells in matched synovial tissue and peripheral blood. Left hand panel depicts IA. Right hand panel depicts OA. All data presented as % of $CD45^+$ cells. *n=23. *P≤0.05, **P ≤0.01, *** P ≤0.001.*

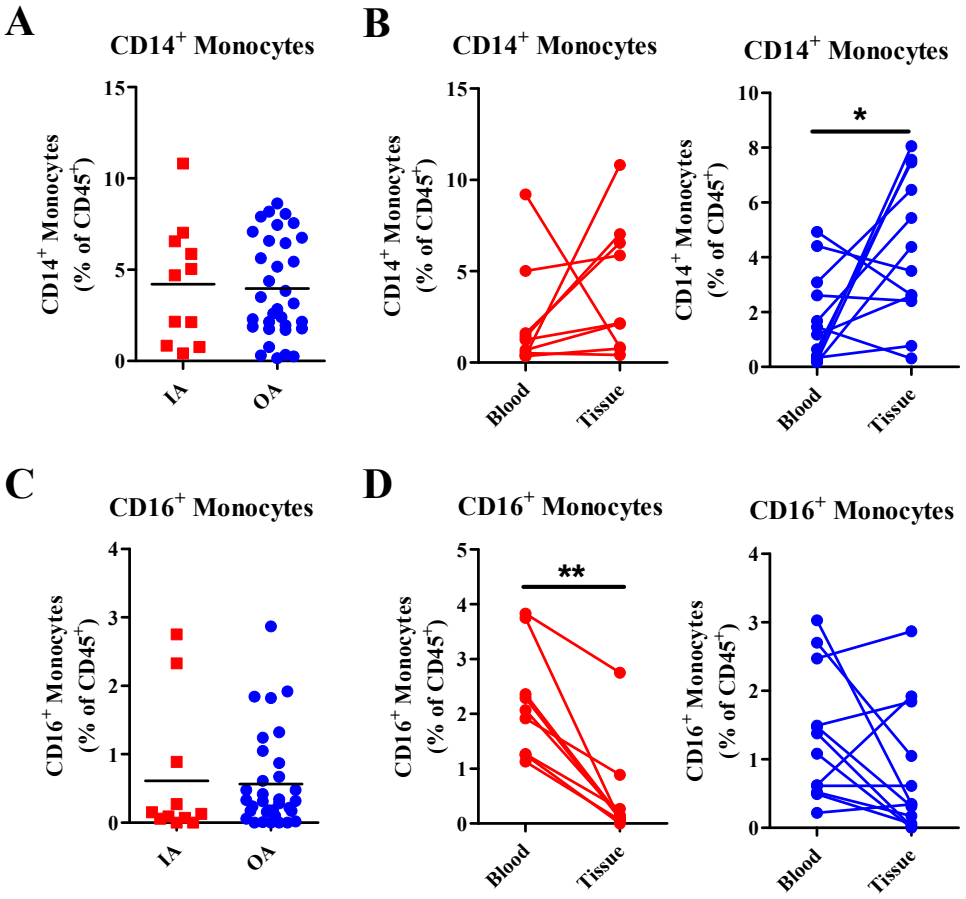

Figure 4.7: Quantification of monocytes in synovial tissue
Synovial tissue from OA total knee replacement and IA ultrasound guided biopsy was digested and analysed using techniques described in Chapter 3. PBMCs were isolated from matched peripheral blood. Single cell suspensions were analysed by flow cytometry using techniques described in Chapter 3. **A:** Proportion of $CD14^+$ monocytes in IA and OA synovial tissue. **B:** Proportion of $CD14^+$ monocytes in matched synovial tissue and peripheral blood. Left hand panel depicts IA. Right hand panel depicts OA. **C:** Proportion of $CD16^+$ monocytes in IA and OA synovial tissue. **D:** Proportion of $CD16^+$ monocytes in matched synovial tissue and peripheral blood. Left hand panel depicts IA. Right hand panel depicts OA. All data presented as % of $CD45^+$ cells. *n=23. *P≤0.05, **P ≤0.01.*

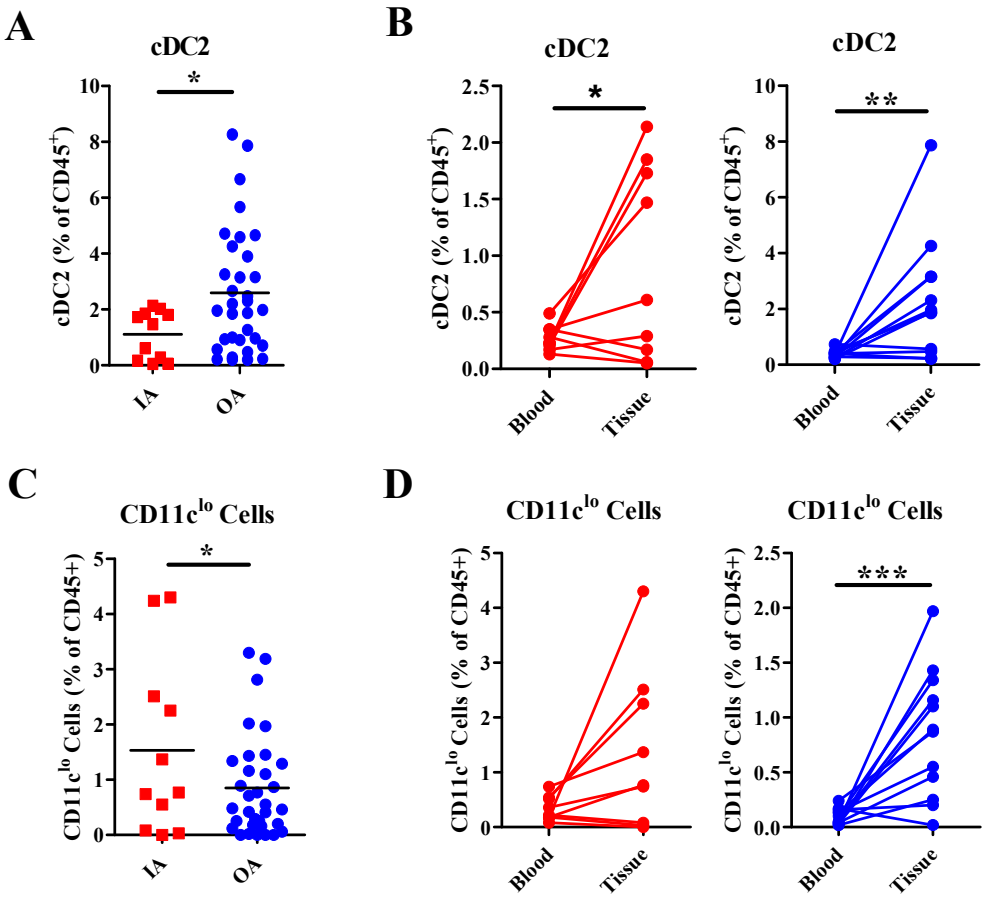

Figure 4.8: Quantification of dendritic cells in synovial tissue
Synovial tissue from OA total knee replacement and IA ultrasound guided biopsy was digested and analysed using techniques described in Chapter 3. PBMCs were isolated from matched peripheral blood. Single cell suspensions were analysed by flow cytometry using techniques described in Chapter 3. **A:** Proportion of cDC2 in IA and OA synovial tissue. **B:** Proportion of cDC2 in matched synovial tissue and peripheral blood. Left hand panel depicts IA. Right hand panel depicts OA. **C:** Proportion of $CD11c^{lo}$ cells in IA and OA synovial tissue. **D:** Proportion of $CD11c^{lo}$ cells in matched synovial tissue and peripheral blood. Left hand panel depicts IA. Right hand panel depicts OA. All data presented as % of $CD45^{+}$ cells. *n=24. *P≤0.05, **P ≤0.01, *** P ≤0.001.*

The final analyses carried out was that of HLA-DR^{+}CD14^{+} macrophages (Fig. 4.9). As these cells are primarily found in the tissue, and are extremely scarce and difficult to identify in the blood, the only comparison carried out was quantities in the synovial tissue between OA and IA. The quantity of these cells was significantly higher in OA compared with IA (Fig. 4.9).

A number of interesting differences between IA and OA have been uncovered through these manual analyses. In particular, this has shown the need for investigating individual cell populations, and the benefits of using tissues at disease site. However, as these analyses have been carried out manually, in terms of flow cytometry gating, there are inherent biases and limitations. To validate these findings, unbiased computational methods were employed.

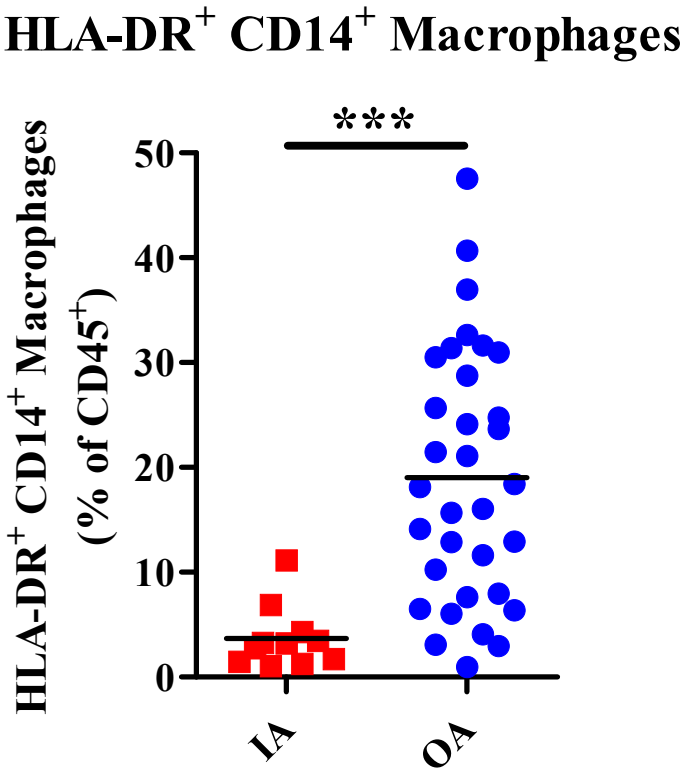

Figure 4.9: Quantification of macrophages in synovial tissue
Synovial tissue from OA total knee replacement and IA ultrasound guided biopsy was digested and analysed by flow cytometry using techniques described in Chapter 3. Proportion of HLA-DR^{+}CD14^{+} macrophages in IA and OA synovial tissue. *n=50.* Data presented as % of CD45^{+} cells. *** *P ≤0.0001.*

4.5 Computational analysis of flow cytometry data sets

There are a number of computational analysis tools available which can be applied to this type of data. Although many have been designed for application with mass cytometry and single cell data, they can also be applied to flow cytometry data sets. Here I have applied three of these computational techniques to my data set, with two aims. The first was to explore these techniques and fully understand their potential benefits in the analyses of this type of data, in addition to uncovering any limitations. The second aim was to validate the results from the manual gating analyses (Section 4.4), in an un-biased and un-supervised manner.

4.5.1 *SPADE*

The first tool employed was the spanning tree progression of density normalized events algorithm, commonly referred to as SPADE. SPADE applies a density dependent down sampling taking into account regions of density in the sample, and removing events to normalise the full dataset, resulting in a consistent distribution of data, but with representation of abundance lowered. This technique is particularly useful for the identification of rare cell types. Hierarchical clustering of phenotypically similar cells was then performed, without the abundance of a dominant cell type affecting the analyses. (Saeys, Gassen et al. 2016). A minimal spanning tree (MST) algorithm then visualises these clusters. Although this tool aids in visualising similarities between these clusters, developmental relationships cannot be directly interpreted, as cells that are similar may not be close within the tree, and vice versa.

SPADE was applied to the $CD45^+$ cell population of an OA and an IA synovial tissue sample (Fig. 4.10). The MST produced shows a series of nodes representing cell clusters, all interconnected. The size of these nodes represents the abundance of that cluster in the sample. The colour of the nodes represents the relative expression of the chosen cell property or marker for each grid. From assessing abundance and phenotype, nodes can be manually grouped into cell types. Comparing the OA and IA samples, these analyses agree with a number of my manual analyses. There appears to be an increased quantity of macrophages and cDC2s in the OA sample (Fig. 4.10). Additionally, there appears to be a higher proportion of monocytes in the OA sample, which was not observed through manual analyses (Fig. 4.10). Furthermore, in agreement with my manual analysis, there was no clear difference in the T cell compartment between OA and IA (Fig. 4.10).

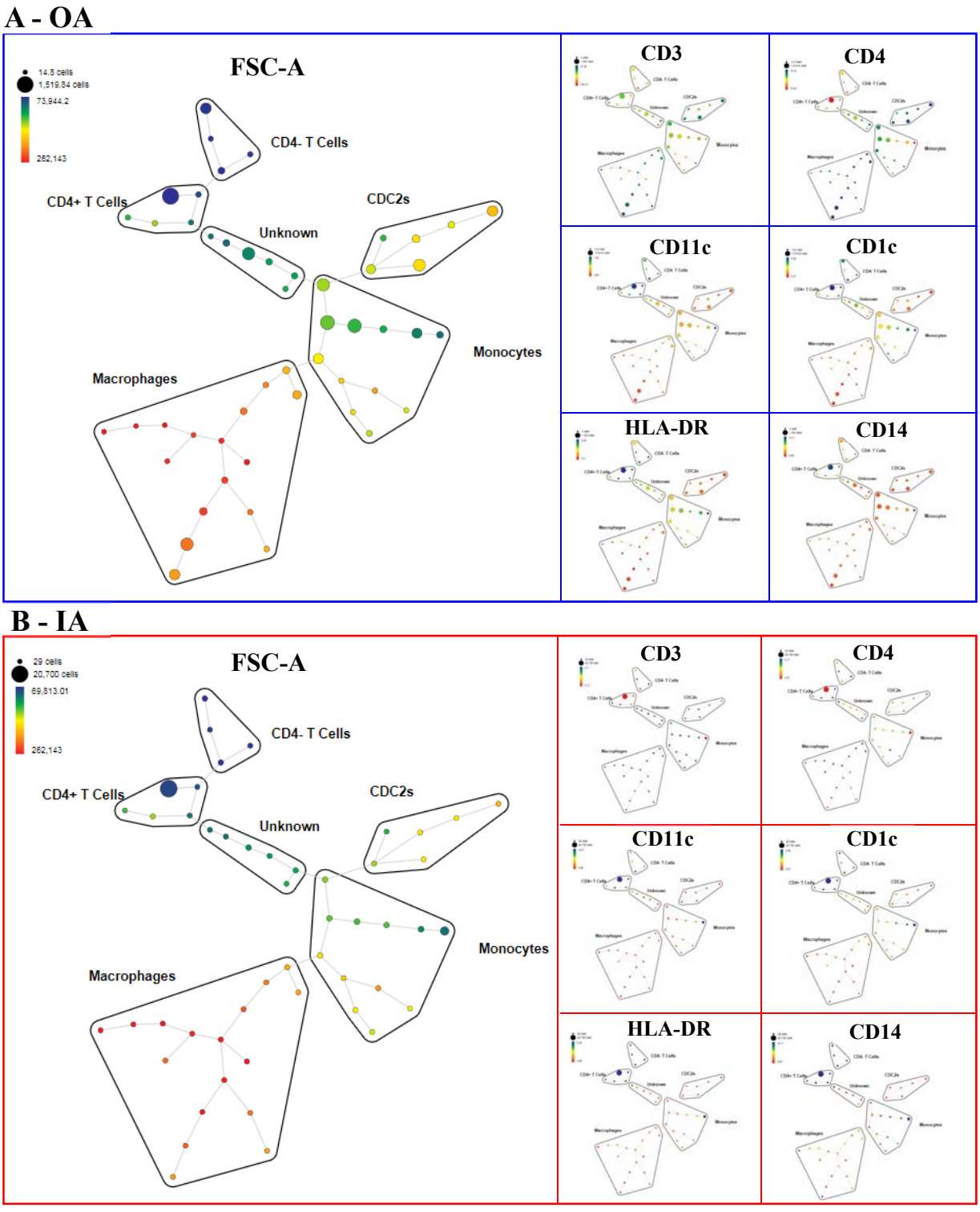

Figure 4.10: SPADE analyses of synovial tissue flow cytometry data set
Synovial tissue from OA total knee replacement and IA ultrasound guided biopsy was digested and analysed by flow cytometry using SPADE. **A:** OA synovial tissue sample. **B:** IA synovial tissue sample. Data are representative of 5 independent analyses.

4.5.2 *viSNE*

viSNE is based on the t-distributed stochastic neighbour embedding (tSNE) algorithm. This allows the mapping of high-dimensional cytometry data by reducing the data into two dimensions, whilst conserving high-dimensional structure (Amir el, Davis et al. 2013). The position of cells on the viSNE map reflects their proximity in high-dimensional space, and is therefore a powerful tool for the identification of cell subtypes. I applied viSNE analysis to the same OA and IA samples as the SPADE analyses (Fig. 4.11). Similarly to SPADE, viSNE maps use colour as a third dimension to display expression of cell property or marker (data not shown). Furthermore, using the cytofkit Bioconductor package in R, once analysis is completed, an analysed version of the original flow cytometry standard (FCS) file is created. This can then be used in traditional flow cytometry analysis software, such as FlowJo. Individual cells or clusters can be gated on and cell marker expression analysed to aid identification (data not shown). Using these data, clusters on the viSNE map can be assigned to cell types.

The subsets identified in the OA viSNE analysis are demonstrated with conventional flow cytometry gating (Fig. 4.11 A). The viSNE map produced demonstrates a large proportion of macrophages, as observed in all previous analyses (Fig. 4.11 B). The progression of these subsets can be interpreted by producing progression maps. The number of cells are down-sampled to remove potential influence from more abundant, dominant cell subsets. Diffusion maps plot the cells by marker expression patterns. This allows us to better examine the relationship between the cell subsets. The diffusion map plotted for this sample shows macrophages, cDC2s and monocytes clustered closely together (Fig. 4.11 C). $CD4^+$ and $CD4^-$ T cells are separate from both each other, and myeloid cells (Fig. 4. 11 C).

Within IA, a number of additional subsets were identified by the viSNE analyses. These are demonstrated with conventional flow cytometry gating (Fig. 4.11 D). From the viSNE map, it is clear that the $CD4^+$ and $CD4^-$ T cells are the most abundant in this sample (Fig. 4.11 E). Furthermore, activated $CD4^+$ and $CD4^-$ T cells ($HLA\text{-}DR^+$) are identified separately, but closely related to their non-activated counterparts (Fig. 4.11 E). Macrophages and monocytes are the next dominant cell type. $CD11c^{lo}$ cells are identified in addition to cDC2s (Fig. 4.11 E). When analysing the diffusion map, macrophages, cDC2s and monocytes are clustered closely together (Fig. 4.11 F). $CD11c^{lo}$ are contiguous, but split into two different clusters, potentially reflecting the presence of both cDC1s and pDCs (Fig. 4.11 F). The $CD4^+$ and $CD4^-$ T cells are separate from both each other, and the myeloid cells (Fig. 4.11 F). The activated $CD4^+$ and $CD4^-$ T cells ($HLA\text{-}DR^+$) are closely related to their non-activated counterpart (Fig. 4.11 F).

viSNE analyses was performed on these two samples separately. Comparisons can be made from this, such as the abundance of macrophages in the OA synovium, compared to T cells in the IA synovium (Fig. 4.11). However, to draw more robust conclusions, these two samples were subsequently analysed together (Fig. 4.12). This analysis of the combined samples confirms the previous suggestion of the relative abundance of macrophages and T cells in OA and IA synovium (Fig. 4.12 A). Again, the myeloid cells are clustered together on a diffusion map, and the $CD4^+$ and $CD4^-$ T cells clustered separately, regardless of disease type (Fig. 4.12 B).

These analyses provide a useful overview of cell populations within the synovial tissue data, and allows for a more detailed exploration of the cell subsets and their relationships.

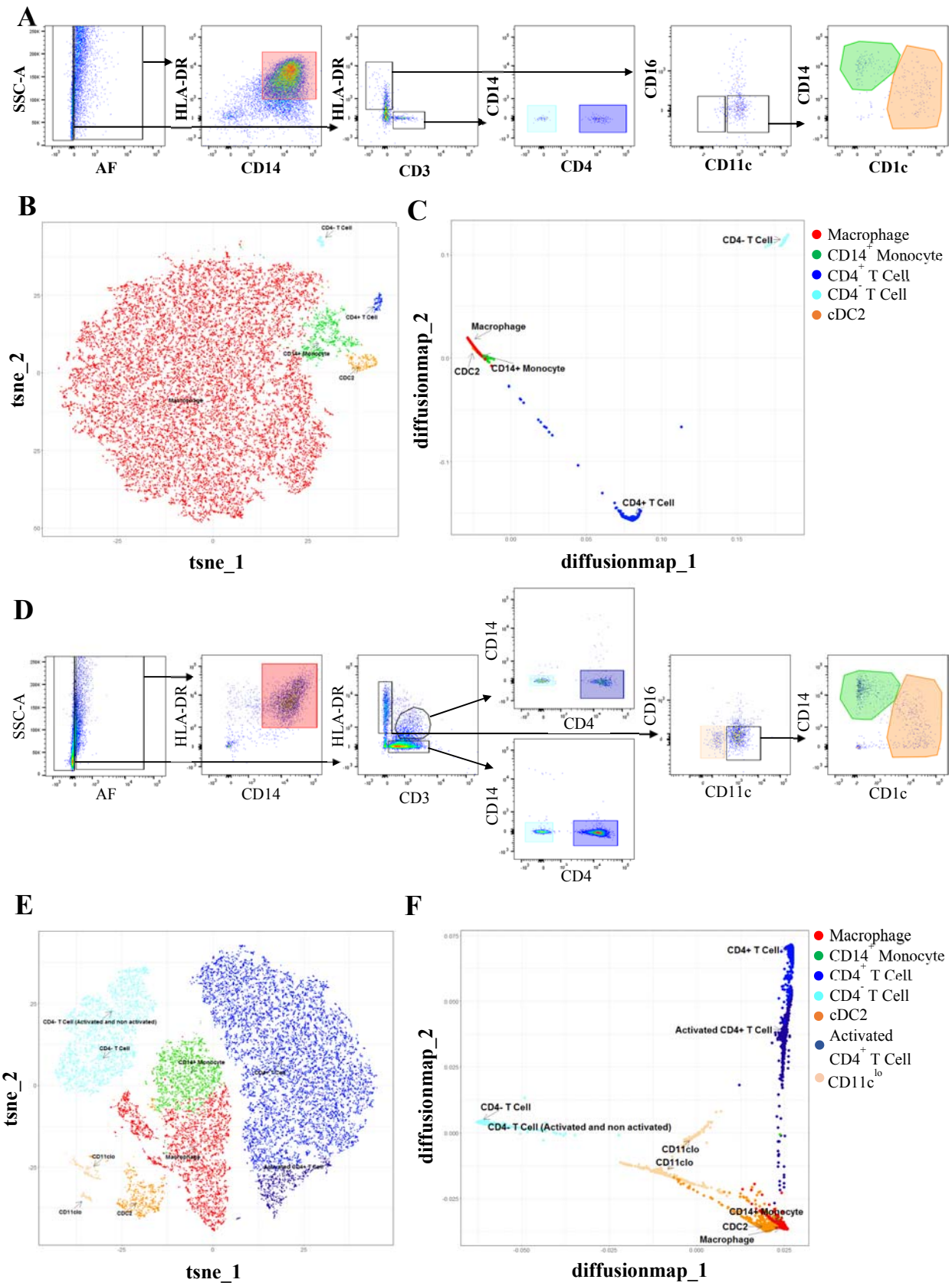

Figure 4.11: viSNE analyses of synovial tissue flow cytometry data set
Synovial tissue from OA total knee replacement and IA ultrasound guided biopsy was digested and analysed by flow cytometry using techniques described in Chapter 3. **A:** Manual gating of cell subsets in OA synovial tissue. **B:** viSNE map of OA synovial tissue. **C:** Diffusion map of IA synovial tissue. **D:** Manual gating of cell subsets in IA synovial tissue. **E:** viSNE map of IA synovial tissue. **F:** Diffusion map of IA synovial tissue. Data are representative of 5 independent analyses.

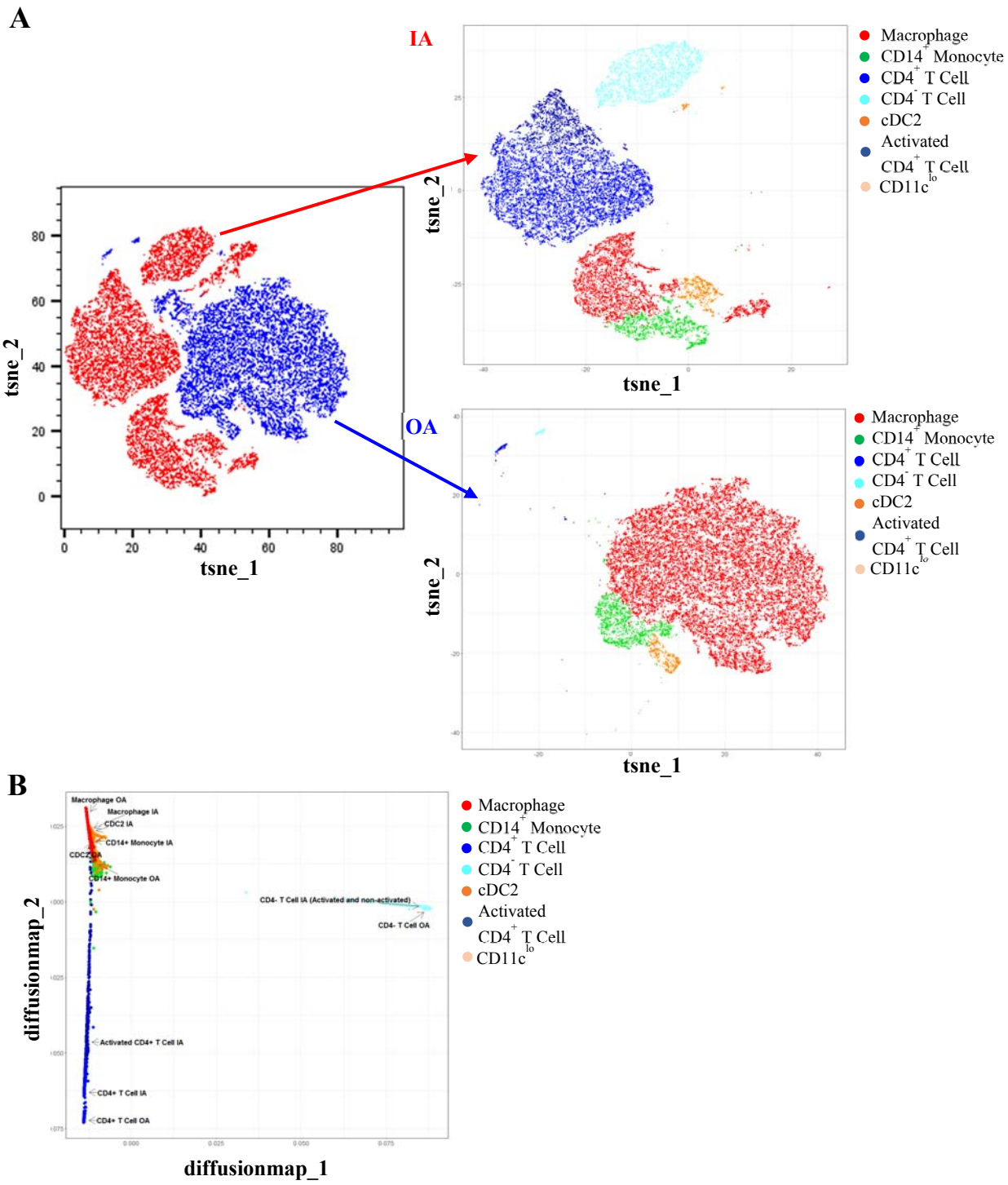

Figure 4.12: visNE analyses of IA and OA synovial tissue
Synovial tissue from OA total knee replacement and IA ultrasound guided biopsy was digested and analysed by flow cytometry using techniques described in Chapter 3. **A:** viSNE map of IA and OA synovial tissue. Left hand panel depicts both samples. Right hand panels depict separated IA and OA samples. **B:** Diffusion map of IA and OA synovial tissue. Data are representative of 5 independent analyses.

4.5.3 *CITRUS*

The previous analyses were carried out on one sample from each OA and IA group providing useful overviews of cellular content. However, to draw strong conclusions of differing cell quantitates between the two disease types, more comprehensive analyses needed to be undertaken. The CITRUS algorithm encompasses cluster identification, characterization and regression allowing a fully automated, unsupervised hierarchical clustering of cell populations in the entire dataset.

The Significance Analysis of Microarrays (SAM) correlative association model was applied to a fluorescent dynamic range normalised dataset of 24 OA and 9 IA synovial tissue samples (Fig. 4.13). Using the strictest false discovery rate of 0.01, an abundance featurePlots visualisation is created, highlighting significant cell clusters in the tree (Fig. 4.13 A). Similarly to SPADE and viSNE, expression values can be visualised in a third dimension using colour, allowing the identification of each of these cell clusters (Fig. 4.13 B). From this, and the histograms generated for each cluster (data not shown), it can be concluded that each cluster represents the following:

- Cluster 1 – Monocyte like cluster
- Cluster 2 – Macrophage like cluster
- Cluster 3 – T cell like cluster
- Cluster 4 – DC like cluster
- Cluster 5 – Unknown

From this, abundance plots of cell clusters can be analysed (Fig. 4.13 C). The clusters representing monocytes are slightly higher in abundance in the OA samples than IA. Both the macrophage and DC clusters have significantly higher abundance in the OA than IA. The T cell like clusters were significantly higher in abundance in the IA samples than the OA samples. Finally, the fifth unknown cluster has higher abundance in OA than IA. These results agree with all results found in the manual analyses.

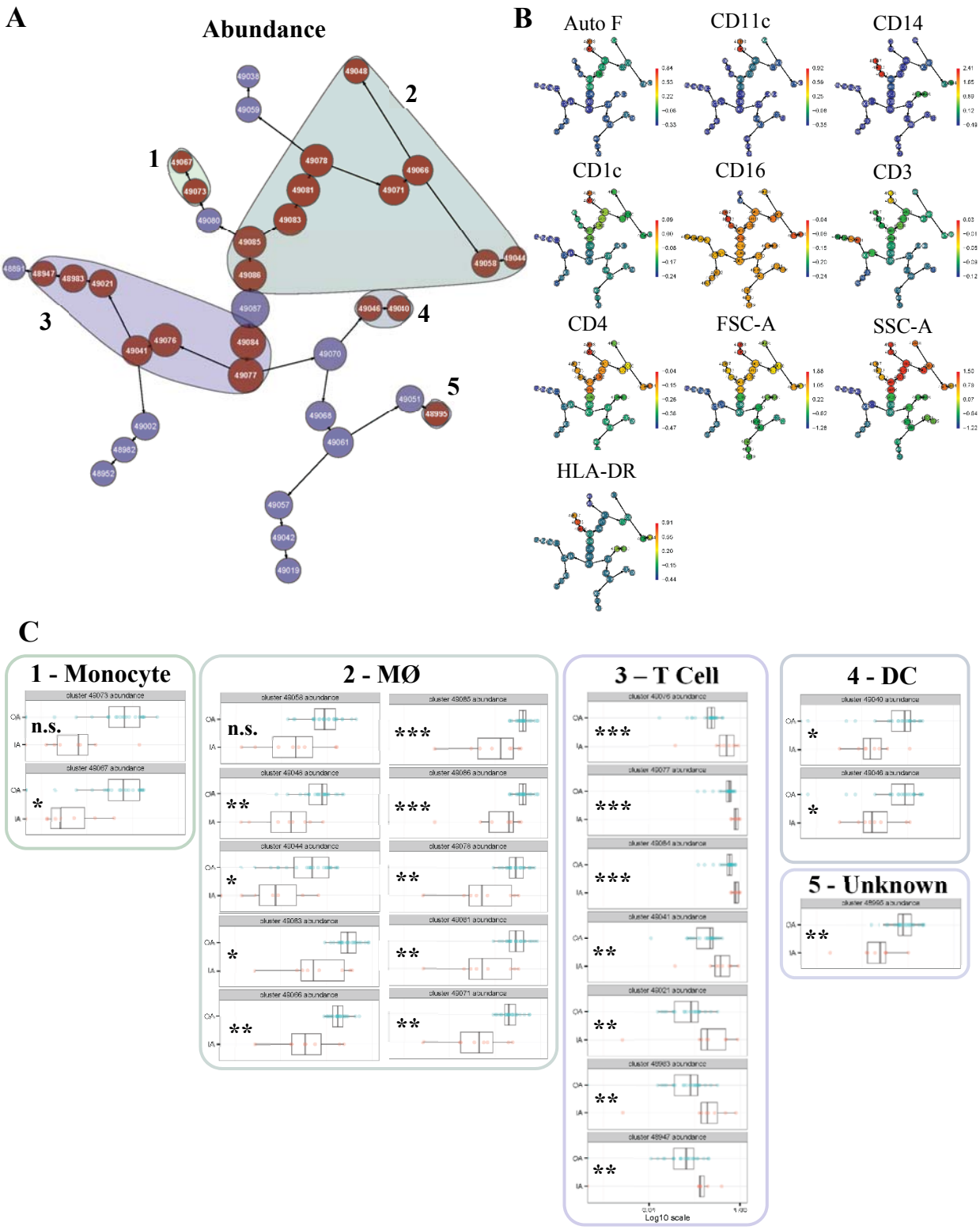

Figure 4.13: CITRUS analyses of synovial tissue flow cytometry data set
Synovial tissue from OA total knee replacement and IA ultrasound guided biopsy was digested and analysed by flow cytometry using techniques described in Chapter 3. 24 OA and 9 IA synovial tissue samples were analysed. **A:** featurePlots visualisation of all samples analysed. Significant cell clusters identified are numbered 1-5. **B:** Visualisation of marker expression on featurePlots. **C:** Abundance plots of all nodes within significant cell clusters numbered 1-5. $^{n.s.}$*P>0.05, *P≤0.05, **P ≤0.01, ***P ≤0.001.*

4.6 Histology and comparison with additional tissues

It is difficult to obtain healthy synovial tissue samples. Sources for healthy synovial tissue include trauma patients, such as motor accidents or falls. However, the latter are unlikely to be healthy as individuals susceptible to falls can often be of old age or obese, both risk factors for OA. Another source is from limb salvage surgery of patients with osteosarcoma, a rare type of bone cancer. However, throughout the duration of the final experimental stages of this PhD, I was unable to recruit any healthy synovial tissue samples. Alternatively, I digested and analysed an adipose sample from a TKR, in addition to a healthy dermis sample kindly provided by Prof. Matthew Collin (Newcastle University). The aim was to have a representation of cell types identified in a healthy tissue using my flow cytometry panel.

Although the OA adipose tissue is not representative of a healthy tissue, it is interesting to notice that the predominant cell type is also macrophages with very few of the other cell types measured (Fig. 4.14). There was a lot of debris in this sample, which may have skewed the proportion of the final cell percentages. However, through calculating cell percentages of $CD45^+$ cells this effectively excludes the debris. The healthy dermis sample showed a large number of T cells, similar to that seen in the IA patients (Fig. 4.14 A). In addition, there was a larger number of cDC2s in dermis than both OA and IA (Fig. 4.14 A & B).

One of my IA samples was sectioned and stained with haemotoxylin and eosin (Fig. 4.15 C). This was compared to a relevant OA TKR example from published literature (Ene, Sinescu et al. 2015) (Fig. 4.14 D). From these sections, there appeared to be increased cellular infiltration in the IA synovium. In addition, many of these were small in appearance. This could mirror my flow cytometry finding of increased proportion of T cells in IA synovium. However, no strong conclusions can be drawn from this until my samples have been analysed by histology, and compared with matched flow cytometry data.

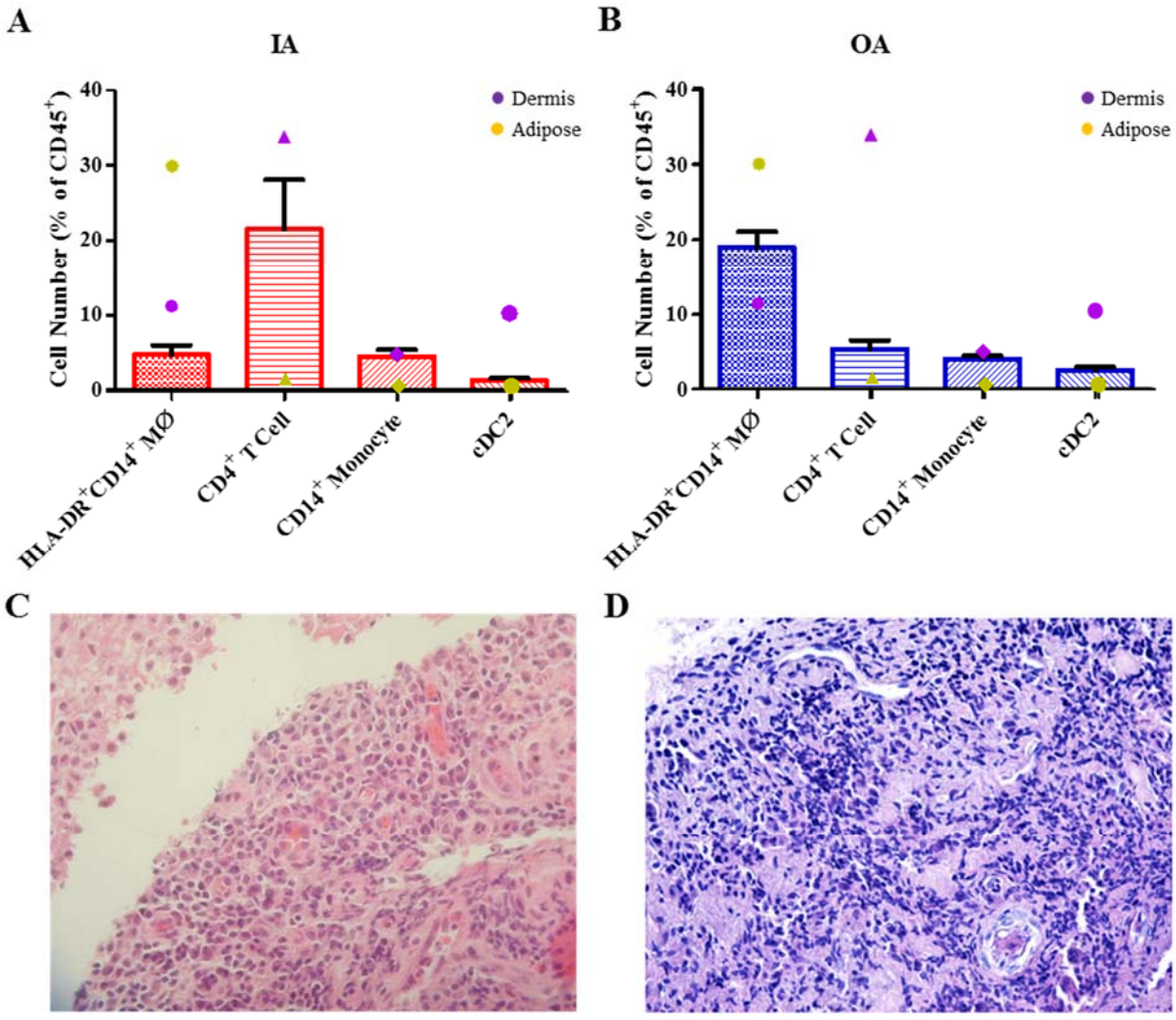

Figure 4.14: Analyses of dermis, adipose and synovial tissue
Synovial tissue and adipose tissue from OA total knee replacement and IA ultrasound guided synovial biopsy was digested and analysed by flow cytometry using techniques described in Chapter 3. **A:** Proportion of HLA-DR$^+$CD14$^+$ MØ, CD4$^+$ T cell, CD14$^+$ monocyte and cDC2 in synovial tissue (Red bars), dermis (Purple dots) and adipose tissue (Yellow dots). Data presented as % of CD45$^+$ cells. **B:** Proportion of HLA-DR$^+$CD14$^+$ MØ, CD4$^+$ T cell, CD14$^+$ monocyte and cDC2 in synovial tissue (Red bars), dermis (Purple dots) and adipose tissue (Yellow dots). Data presented as % of CD45$^+$ cells. **C:** IA synovial tissue. H&E staining. x20 magnification. **D:** OA synovial tissue. H&E staining. x200 magnification *Taken from Ene, Sinescu et al. 2015.*

4.7 Correlation of immunological and clinical data

Although clinical data was not specifically recorded for this project, routine clinical information for both OA and IA cohorts was collected. When comparing two inflammatory markers with each other (CRP & ESR), a significant correlation was found within the IA cohort ($p = 0.003$; $R^2 = 0.50$) (Fig. 4.15 A). This correlation was weaker in the OA cohort ($p = 0.021$; $R^2 = 0.13$) (Fig. 4.15 A). When assessing CRP with measures of disease activity in each group (IA – DAS28; OA – KL X-ray Score), a correlation was only found in IA ($p = 0.016$; $R^2 = 0.42$) (Fig. 4.15 B).

To investigate these clinical data in relation to my immunological data, I examined both of these datasets, and their relative importance to HLA-DR$^+$CD14$^+$ macrophages (% of CD45$^+$). The variability of the top two factors for OA (Tissue weight and ESR) is clear when assessing individual linear correlation plots (Fig. 4.16 A). However, there is less variability in the IA linear regression of CD14$^+$ monocytes and ESR, despite the smaller sample size (Fig. 4.16 A). When applying the bootstrapping method to this question, tissue weight and ESR are the two largest contributors in the OA cohort, explaining ~33% and ~22% of R^2, respectively (Fig. 4.16 B). In IA, CD14$^+$ monocytes are the most important factor, contributing ~70% to R^2 (Fig. 4.16 B). The Bootstrapping technique involves the random sampling and replacement of values within the data range. In this instance 5000 iterations where employed.

When assessing multiple regression models as predictors for HLA-DR$^+$CD14$^+$ macrophages (% of CD45$^+$), the highest R^2 value that can be achieved in OA is 0.55 (Fig. 4.17). In IA, this is improved with an R^2 of 0.85 (Fig. 4.18). However, a multiple regression model should aim for an R^2 value of >0.90 to be considered statistically acceptable, alongside a significant p-value.

In OA, the best model involved age, BMI, disease duration, ESR, CD4$^+$ T cells, CD14$^+$ monocytes, cDC2s and tissue weight ($R^2 = 0.55$) (Fig. 4.17). When reducing the factors of this model, the R^2 is not proportionately effected. A model of age, BMI, ESR, CD14$^+$ monocytes and tissue weight presents an R^2 of ~0.53 (Fig. 4.17 A). As with the previous linear regression, tissue weight and ESR were the most contributory to the model, in addition to CD14$^+$ monocyte levels. However, since all three of these factors had high variability of data, the regression is less reproducible. It is therefore possible that these are coincidental factors. When the best model and data are applied to a series of quality control plots, a non-linear relationship is observed (Fig. 4.17 B). This is demonstrated through the non-conformity in residuals v fitted values plot, and a curvature in the qqnorm plot, assessing data distribution (Fig. 4.17 B).

In IA, the best multiple regression incorporated age, gender, CRP, ESR, $CD4^+$ T cells, $CD14^+$ monocytes and tissue weight ($R^2 = 0.85$) (Fig. 4.18). When removing age from this model, the R^2 is reduced to ~0.73 (Fig. 4.18 A). When reducing this model further to disease duration, ESR and CD14, the R^2 value is only reduced to ~0.65, suggesting that these additional factors do not contribute greatly and that $CD14^+$ monocyte levels, ESR and disease duration are the most contributory factors. In the IA cohort, a non-linear relationship is again observed, but this is perhaps stronger after assessment of the scale-location plot and standardised residuals. However, it is possible that a small number of samples are skewing these data (Fig. 4.18 B). These analyses are ultimately limited by the sample size.

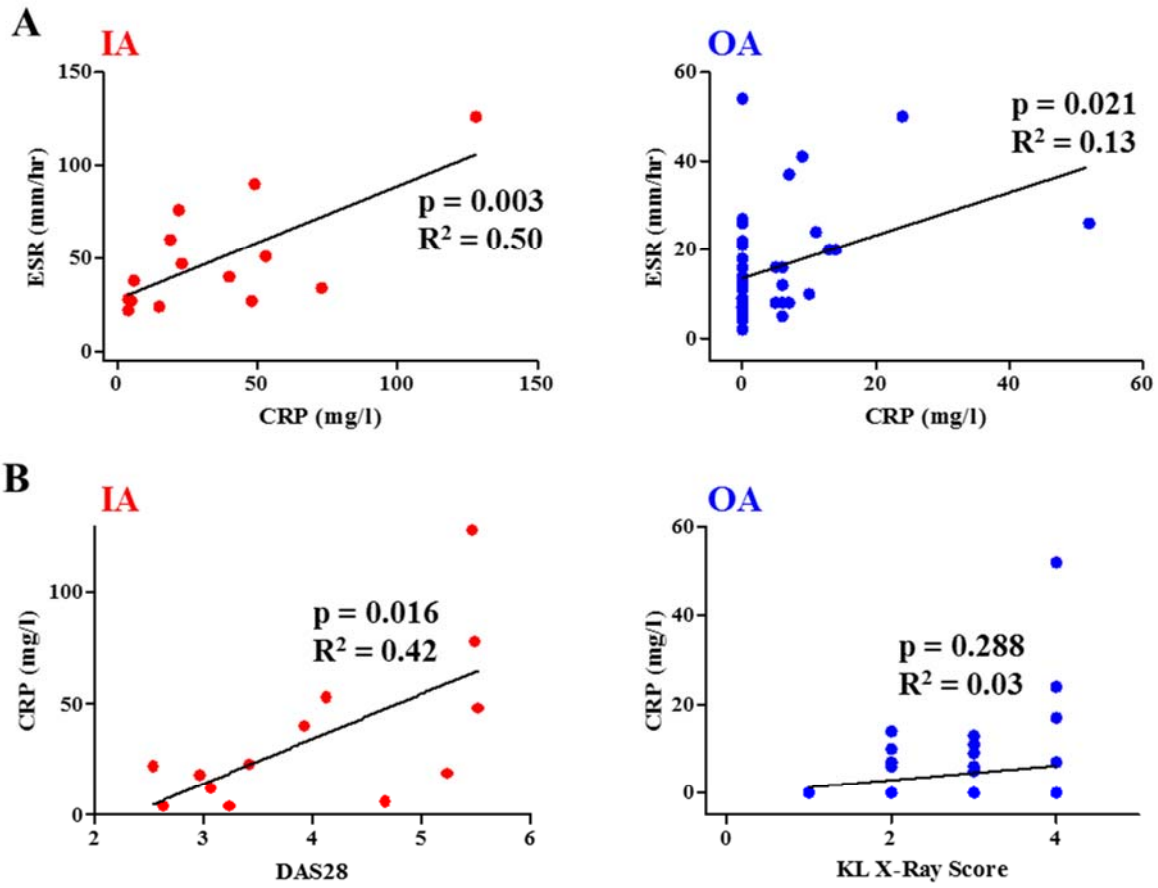

Figure 4.15: Correlation of clinical factors
Clinical data was collected for both IA and OA cohorts. **A:** Linear regression of ESR and CRP. Left plot depicts IA cohort. Right plot depicts OA cohort. **B:** Linear regression of CRP and DAS28 (IA; left plot) or KL X-ray score (OA; right plot).

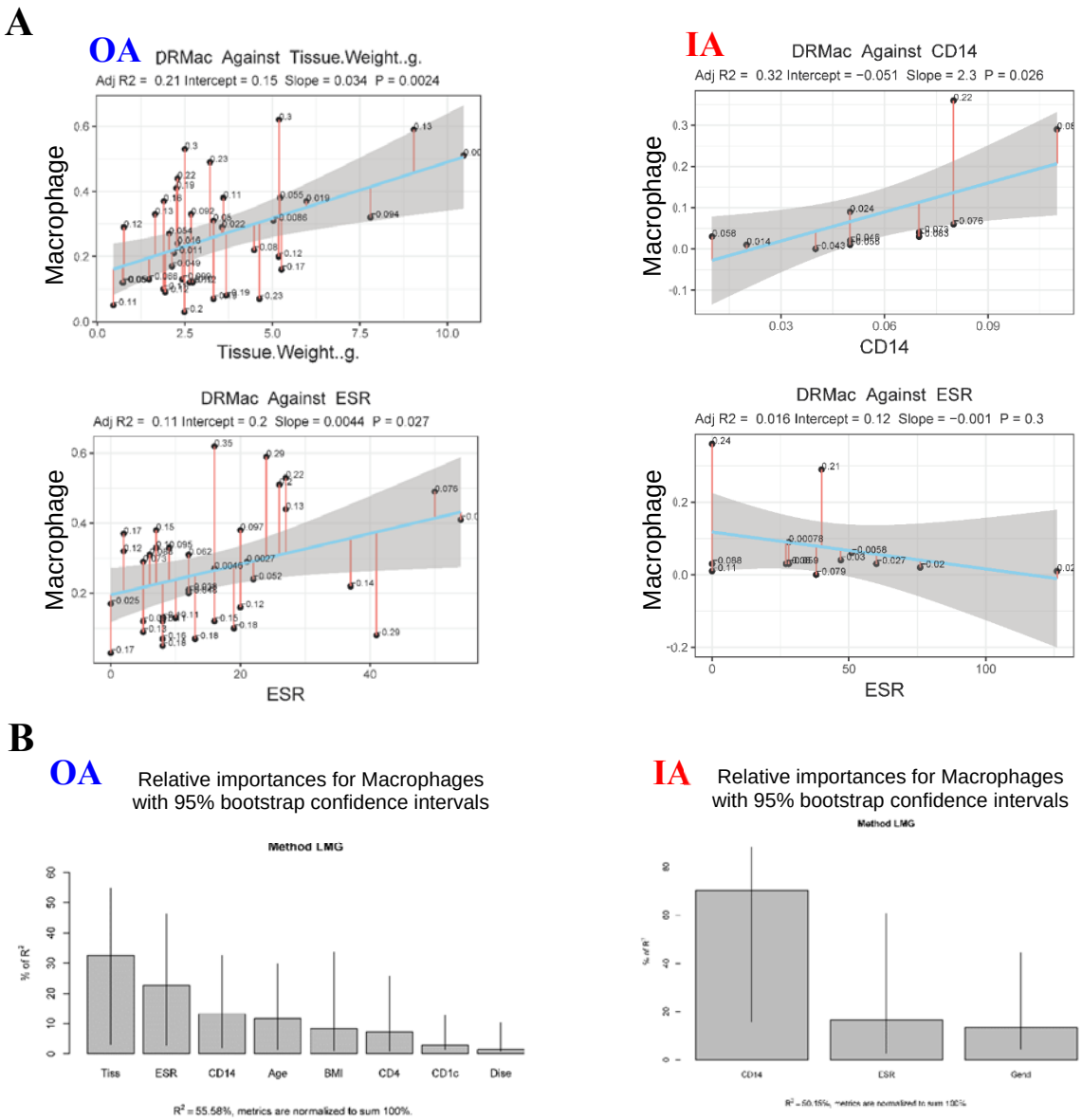

Figure 4.16: Correlation of clinical factors and immunological data
Clinical data was collected for both IA and OA cohorts. **A:** Linear regression of contributing factors to HLA-DR^{+}CD14^{+} macrophages. Left panels represent OA cohort, right panels represent IA cohort. **B:** Bootstrapping method assessing relative importance of variables to HLA-DR^{+}CD14^{+} macrophages. 5000 iterations were employed. Left panel represents OA cohort, right panel represents IA cohort.

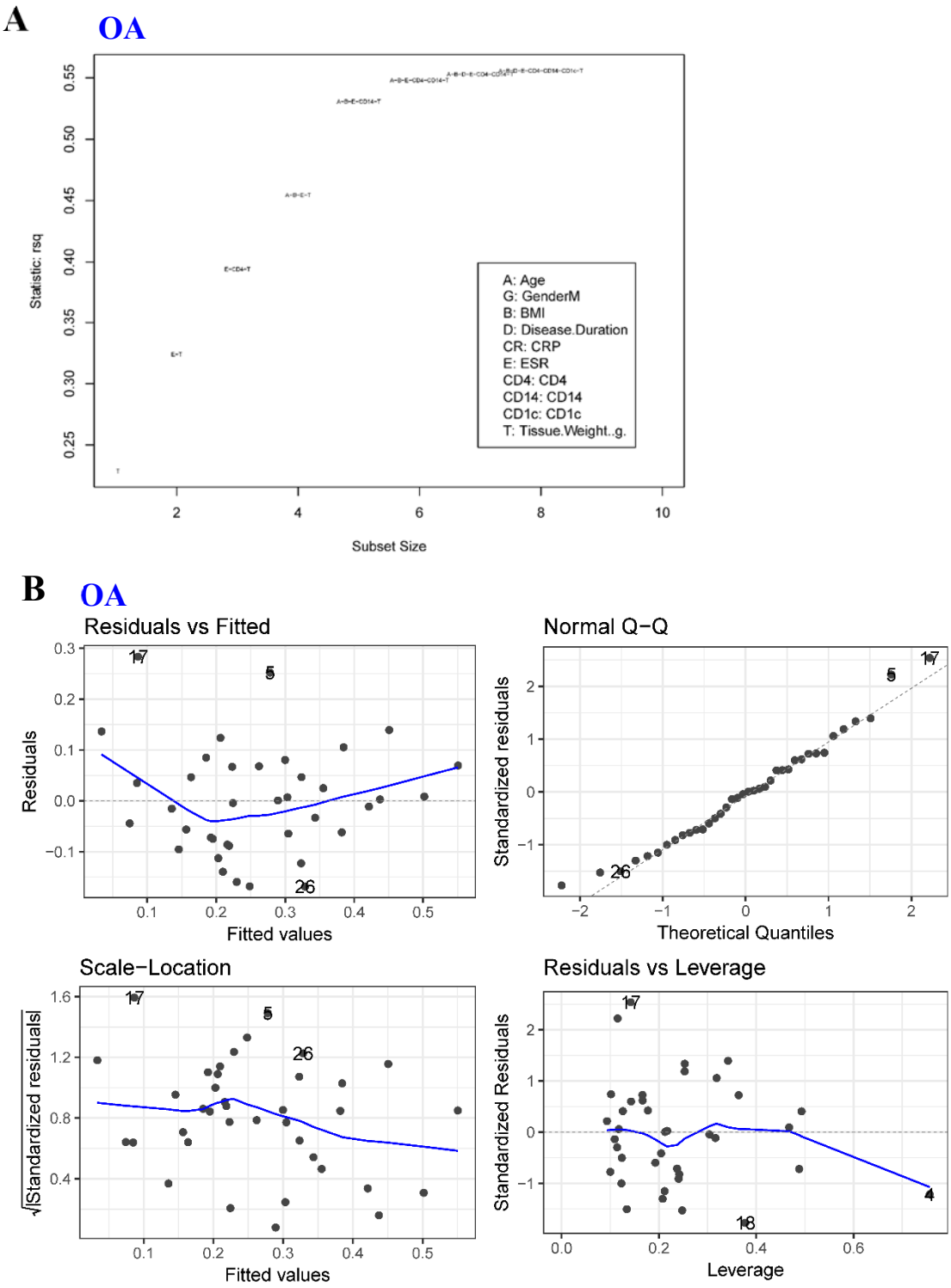

Figure 4.17: Fitted model of Osteoarthritis clinical and immunological data
Clinical data was collected for OA patient cohort. **A:** Fitted multiple regression models encompassing clinical and immunological variables. **B:** Fitted model with most relative importance for HLA-DR^{+}CD14^{+} macrophages applied to residuals vs fitted values plot (top left), qqnorm plot assessing data distribution assumptions (top right), standardised residuals vs fitted values plots (bottom left), and standardised residuals against leverage plot (bottom right).

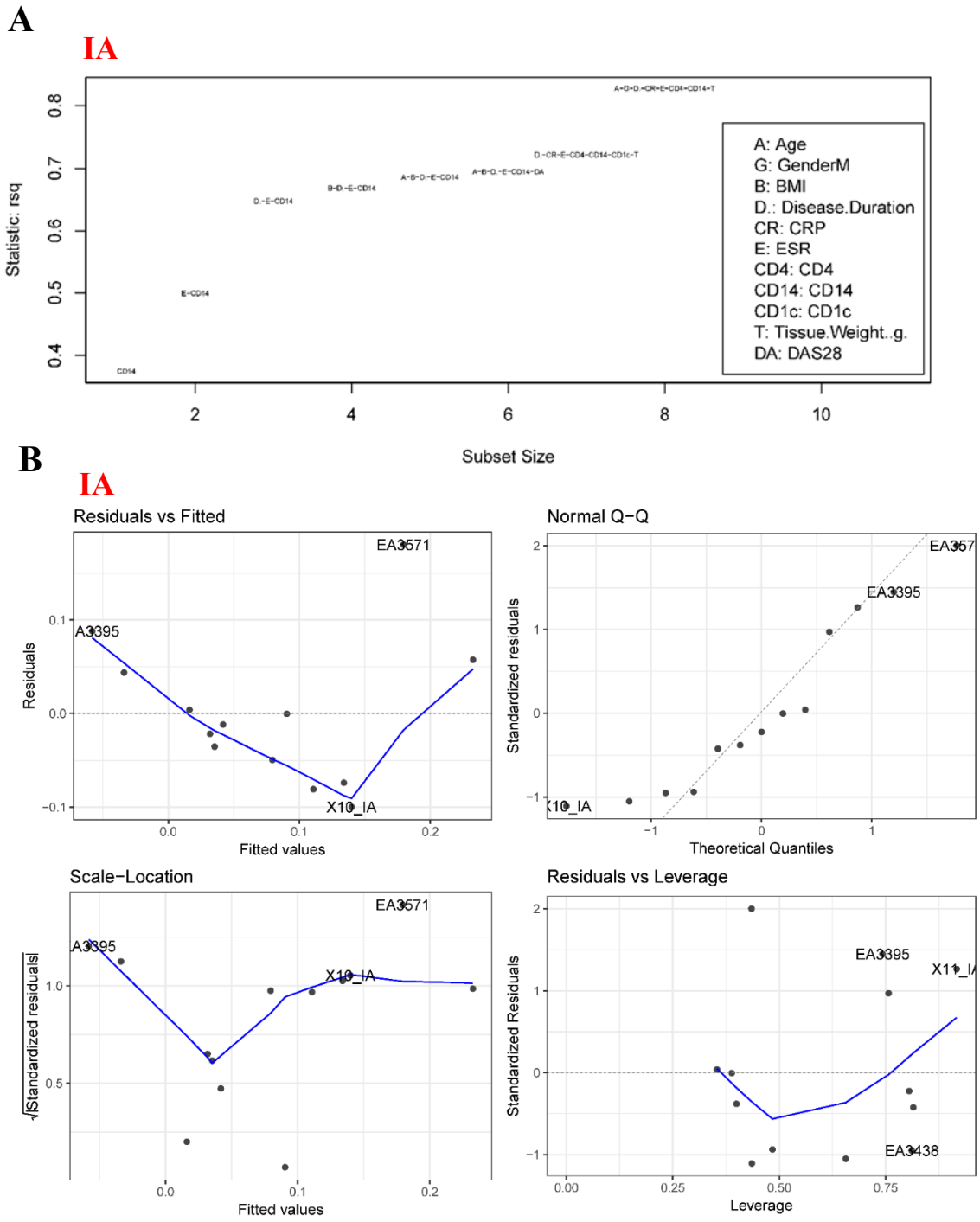

Figure 4.18: Fitted model of Inflammatory arthritis clinical and immunological data
Clinical data was collected for IA patient cohort. **A:** Fitted multiple regression models encompassing clinical and immunological variables. **B:** Fitted model with most relative importance for HLA-DR^{+}CD14^{+} macrophages applied to residuals vs fitted values plot (top left), qqnorm plot assessing data distribution assumptions (top right), standardised residuals vs fitted values plots (bottom left), and standardised residuals against leverage plot (bottom right).

4.8 Discussion

In this Chapter, I aimed to characterise the cellular compartment of synovial tissue in both OA and IA. In addition, I aimed to explore computational approaches for the analyses of flow cytometry data.

The patient cohorts used within these analyses were well matched between disease type with similar age and sex. Differences in BMI, CRP and ESR were deemed acceptable as these have all been identified as known risk factors, or disease-specific consequences. The OA group had active OA disease, assessed by Kellgren and Lawrence scoring of radiographic images. Likewise, the IA group had moderate disease activity measured by DAS28 score. 32.95% of the OA cohort were currently taking statins, known to affect immune cell subsets. Separate comparative analyses were conducted on this group and the remaining OA patients. No clear differences were found (data not shown).

First, the cellular content of the synovial tissue was quantified. When calculating the number of live cells per gram of tissue, significantly more cells where observed in IA. Additionally, when calculating the quantity of $CD45^+$ and $CD45^-$ negative cells, a significantly higher number of $CD45^+$ cells were also observed in IA synovium. The $CD45^-$ cell population contains $CD90^+$ stromal cells, in addition to other stromal cells including fibroblasts. As this was calculated as a percentage, it can be postulated that OA patients have a higher ratio of stromal cells than IA patients. Interestingly, a range of $CD45^+$ cells was observed in OA. Although the extent of cellular infiltration is clear in IA, this does not consequently mean that there is no cellular infiltration in OA. Alternatively, there appears to be similar levels of cellular infiltration in some of these OA patients, and a lower level within the remaining patients.

I next aimed to quantify multiple, individual cell subsets within these synovial tissue samples. Owing to a lack of similar published research, I first assessed the best method for this quantification. The most suitable method was to calculate each cell subset as a percentage of total $CD45^+$ cells within that sample. It was shown that calculating the cell subset as a percentage of $CD45^+$ or total events, cells –debris and live cells, yielded the same relative result. Furthermore, since the cell populations quantified were all $CD45^+$, this would be the most relevant value to calculate from.

When I conducted comparative analysis of peripheral blood from OA and IA, a limited number of differences were observed. The indication of increased quantity of $CD3^+$ and $CD4^+$ T cells in IA blood compared to OA again agrees with previously reported findings (Zhang, Li et al. 2012, Leipe, Schramm et al. 2014, Lurati, Laria et al. 2015). Although no clear differences were

observed in the monocytic populations, contrasting quantities of cDC2s and CD11c^{lo} populations were observed. Work previously carried out in our group has identified an increase in the quantity of pDCs in early RA patient blood (Cooles et al, JACI, 2017, in press). There is little information on the quantity of cDC2s in OA patient blood. Here, I observed a significant increase of cDC2s in the peripheral blood of OA patients compared to IA. Similarly, a significant decrease of cDC2s in the blood of RA patients compared to healthy controls has been previously reported (Jongbloed, Lebre et al. 2006). OA patients were also reported to have higher levels of cDC2s in peripheral blood than RA patients in this study. I found both OA and IA to have significantly lower percentages of cDC2s compared to healthy controls (Appendix 4.2). The authors later proposed a model whereby DCs migrate from the blood and traffic between the synovial fluid and tissue, accounting for this decrease in peripheral blood in RA patients (Lebre, Jongbloed et al. 2008).

Studies using peripheral blood of arthritis patients have yielded much beneficial knowledge previously. However, when quantifying cell subsets within a small cohort size, peripheral blood does not prove an overly useful tissue when used alone. I have identified potential differences in the quantities of DC subsets in the peripheral blood of these two arthritis patient groups. However, conducting these analyses alongside synovial tissue data is likely to yield more informative results.

The same set of comparisons were conducted in synovial tissue, in addition to comparing the relative cell quantities between matched blood and synovium samples. An increase of all T cell populations was observed in the synovial tissue of IA compared to OA. Two groups of IA are noticeable with high and low levels of T cells. Evidence for lymphoid, myeloid, fibroid and low inflammatory phenotypes of RA synovium have previously been described (Dennis, Holweg et al. 2014). Retrospective analyses of my data showed those samples with a lower percentage of T cells had higher percentages of myeloid cells than the samples with higher T cell percentages (data not shown). Additionally, a number of these samples had percentages of macrophages akin to that seen in OA.

The percentages of T cells measured in OA synovium were significantly lower than those measured in matched peripheral blood, suggesting that these patients are not systemically deficient in T cells. Interestingly there is a range of OA patients with varying levels of T cells, suggesting that this group is heterogeneous. It is likely that there is an infiltration of T cells present within the synovium of IA patients, absent in OA. This has been previously reported, and there is substantial evidence for the role of T cells in RA (McInnes and O'Dell 2010, Pratt, Swan et al. 2012, Anderson, Pratt et al. 2016). Conversely, the levels measured in OA could

either be decreased, or due to the increase of another cell type. As no healthy synovium samples were collected, this cannot be conclusively stated.

Similarly to blood, an increase of $CD11c^{lo}$ cells was seen in the synovium of IA patients compared to OA. This has only been previously shown by histological methods (Lebre, Jongbloed et al. 2008). Interestingly, there was an increased proportion of cDC2 in the tissue of OA compared to IA. Additionally, an increase of cDC2s and $CD11c^{lo}$ cells in OA synovial tissue compared to blood was not expected. Both cDC2s and $CD11c^{lo}$ DCs have been described in OA synovium previously, but in low numbers compared to IA (Lebre, Jongbloed et al. 2008). As an increase of DCs has been previously associated with obesity, this could explain the heightened levels in my obese OA cohort (Wu, Perrard et al. 2010, Bertola, Ciucci et al. 2012, Stefanovic-Racic, Yang et al. 2012). However, these data are primarily from diabetes literature. I found no correlation between the quantity of cDC2s with BMI (Appendix 4.3).

Finally, there was greater proportion of synovial macrophages observed in OA synovium compared with IA. In addition to a higher percentage of macrophages within the $CD45^{+}$ cell population, the number of macrophages was higher per gram of synovial tissue (Appendix 4.4). As previously discussed, macrophages have been implicated in the pathogenesis, and identified in the synovium of both of these disease types. However, the increased proportion of macrophages in OA is notable. Furthermore, the OA patients are variable; some have high levels of macrophages whilst others have levels similar to IA. It has been suggested that adipokines and DCs promote monocyte recruitment into tissues, which can differentiate into macrophages (Nakamura, Fuster et al. 2014, Bai and Sun 2015). If this mechanism were present in OA, it would suggest obesity may not just add mechanical stress to the joint. However, I similarly found no correlation of macrophages and monocyte quantities with BMI (Appendix 4.5).

After these initial findings, I investigated computational approaches to analyse the same data. I first carried out SPADE analysis. This was a helpful first step for visualising these data in a different manner. Although this was used as an initial step, it did provide confidence in the observation of a relative increase in cDC2 and macrophage populations within OA, compared to IA. Similarly, viSNE was used to reduce high parameter biological data into two dimensions generating easy to interpret visual data. With this, I again confirmed a greater quantity of macrophages in OA, in addition to increased T cells in IA. There was a more even ratio of monocytes and macrophages in IA, not seen in OA. Diffusion maps demonstrated close relationships between myeloid cells, but clear differences between $CD4^{+}$ and $CD4^{-}$ T cells. This suggests that the myeloid cells are relatively similar to one another, whereas $CD4^{+}$ and $CD4^{-}$ T

cells are distinct from each another. As a method for visualising these types of data, I found viSNE easy to use, interpret and yielded additional information.

After these visualisation steps, CITRUS was used to assess a broader range of both OA and IA samples. Unbiased cell cluster abundances were generated and compared between the two disease groups. Four cell clusters were identified pertaining to a monocyte, macrophage, T cell and DC-like clusters. Furthermore, macrophages and cDC2s were confirmed to be of greater abundance in OA synovium and T cells of greater quantity in IA synovium.

The use of computational tools with these data proved useful for validation of my manual analyses. In addition, they present ways of visualising high dimensional data, in a more simple and easier to interpret format.

One of the major limitations of these analyses was the lack of a healthy control tissue. Instead, a healthy dermis sample was analysed. Although this cannot be used as a direct comparator for healthy synovium, it was useful in understanding the cells identified in a healthy tissue by my flow cytometry panel. The large proportion of T cells identified in the dermis was initially unexpected. However, this finding agrees with current published literature (Wang, McGovern et al. 2014). In addition, a similar proportion of macrophages and DCs was also reported. The large proportion of macrophages observed in the adipose sample is similar to published research (Surmi and Hasty 2008). Additionally, increased infiltration of macrophages has been previously been reported in both obesity and OA (Weisberg, McCann et al. 2003, Clockaerts, Bastiaansen-Jenniskens et al. 2010). Although clinical data are not available for this patient, it was previously shown that our OA cohort is clinically classed as obese. This could be a contributing factor to the quantity of macrophages identified in this adipose tissue sample.

From a number of these samples characterised by flow cytometry, tissue has been fixed and wax embedded for histological analyses. This would be a final step for the validation of our flow cytometry panel. The aim was to identify and quantify macrophage, $CD3^+/CD4^+$ T cells, $CD14^+$ monocytes and cDC2s by both flow cytometry and histological methods. However due to time constraints this was not possible before the completion of my PhD. Although this experiment will be conducted in the near future, an alternative was to examine haematoxylin and eosin stained sections. The IA synovium used was one of my samples, compared with a relevant OA TKR synovium section found in published literature (Ene, Sinescu et al. 2015). This was a useful first step in validating our flow cytometry findings. Although quantities of specific immune cell types were not possible to enumerate, it was possible to suggest that there is a higher proportion of immune cell infiltrate in the IA synovium. Additionally, there appeared

to be a higher proportion of lymphocyte-like cells in the IA sample compared with the OA section.

With the clinical information available for these patients, correlative analyses were conducted using both these clinical, and immunological data generated. Clinical data is extremely useful in monitoring disease progression and identifying mechanisms in a number of diseases. However, I demonstrated that in OA, systemic inflammatory markers may not be too useful as they do not correlate well with each other. Additionally, these markers did not correlate with measures of disease activity. This was not observed in IA. This could be because synovitis and inflammation in OA may be limited to the joint space, unlike systemic inflammatory diseases such as RA.

Through multiple co-variate and linear regression analyses, it was found that the most important variables for the prediction of HLA-DR$^+$CD14$^+$ macrophages in OA were tissue weight, ESR and CD14$^+$ monocytes. Although none of the variables reached great statistical acceptability, they could potentially have interesting biological meaning. As tissue weight was not seen as a contributing factor in IA analyses, this could suggest that it is not a technical co-founder. Since IA samples were mainly sourced from biopsies, and for OA samples, the whole synovial membrane was removed from the joint, a greater tissue weight in OA samples could be indicative of greater inflammation. Although it was shown systemic inflammatory markers may not be extremely useful in the analyses of OA data, tissue weight taken together with ESR could suggest that an increased proportion of macrophages is associated with increased inflammation in these patients.

In the analysis of the IA cohort, CD14$^+$ monocytes and ESR were the greatest contributory factors, and although had a better statistical certainty than the OA analyses, this was still not statistically acceptable. However, the importance of CD14$^+$ monocytes in the synovium to macrophages, may agree with findings of a greater ratio of inflammatory, monocyte derived macrophages in IA, discussed in Chapter 5.

In addition to the lack of healthy synovial tissue samples, another confounding factor in these analyses is the dissimilarity in the source of synovial tissue from these two disease groups. As mentioned, OA synovium was sourced from TKR surgeries, whereas IA synovium was largely acquired from ultrasound-guided biopsies of the wrist. A thorough search of the relevant literature yielded only one related article which attempted to examine differences in synovial tissue from multiple joints (Kraan, Reece et al. 2002). The authors suggested that factors including differences in mechanical stress, innervation and vascularity could influence features

of synovial inflammation between joint sites. This was conducted in RA patients and compared arthroscopic synovial tissue biopsies taken on the same day from the knee and either wrist or MCP joints. Comparing fibroblasts, macrophages, T cells and IL-6, good correlation was found between the large and small joints suggesting that biopsies from small and large joints can be used in a similar way.

An additional limitation is that synovium from TKR is generally the whole synovial tissue, whereas tissue acquired from a biopsy is only a small sample and therefore may not be representative of the whole synovial tissue within the joint. To this end, it has been previously suggested that six tissue 'pieces' obtained by biopsy is representative of cell infiltration and whole tissue gene expression (Dolhain, Ter Haar et al. 1998, Smith, Kraan et al. 2001, Boyle, Rosengren et al. 2003). This concern was raised with Dr. Arthur Pratt who advised me that although these procedures were ultrasound-guided, they were just guided and that it was difficult to selectively sample inflamed areas only. Furthermore, during biopsy the aim was to acquire a representative range of tissue from the joint. Therefore the tissue recruited should have been done so in a fair, un-biased way. For all samples, 2-3 'pieces' were fixed and wax embedded for histological study, and on post-examination of photographs, each sample analysed contained 7-15 biopsy 'pieces'.

Although it has been demonstrated that synovium from different joint sites is comparable there will inevitably be variances beyond disease mechanisms between these two groups. However, because the collection of synovial tissue from IA patients was a relatively new technique for our group, and due to the time-scale of this project, it would not have been possible to standardise these samples any further.

Within this Chapter, I have been able to apply the optimised tissue digestion protocol and flow cytometry panel (Chapter 3) to a cohort of synovial tissue and peripheral blood samples from OA and IA patients. Through manual enumeration of the synovial tissue cellular compartment, in addition to exploration and validation with computational analyses, a number of thought-provoking results have been generated, illustrated in Figure 4.19. Firstly, I observed increased immune cellular infiltration in the IA samples, a very well regarded feature of IA like diseases. Using the most appropriate quantification method for these analyses, quantification of individual cell subsets was conducted. Many of these findings agree with published literature, giving confidence in these methods for isolation and characterisation of synovial tissue cell subsets. However, some novel findings were generated, notably, the increased proportion of macrophages and cDC2s in OA synovial tissue compared with IA. Although disease and

cellular mechanisms were not explored here, this is an important initial step in refining which component of the synovium to explore further.

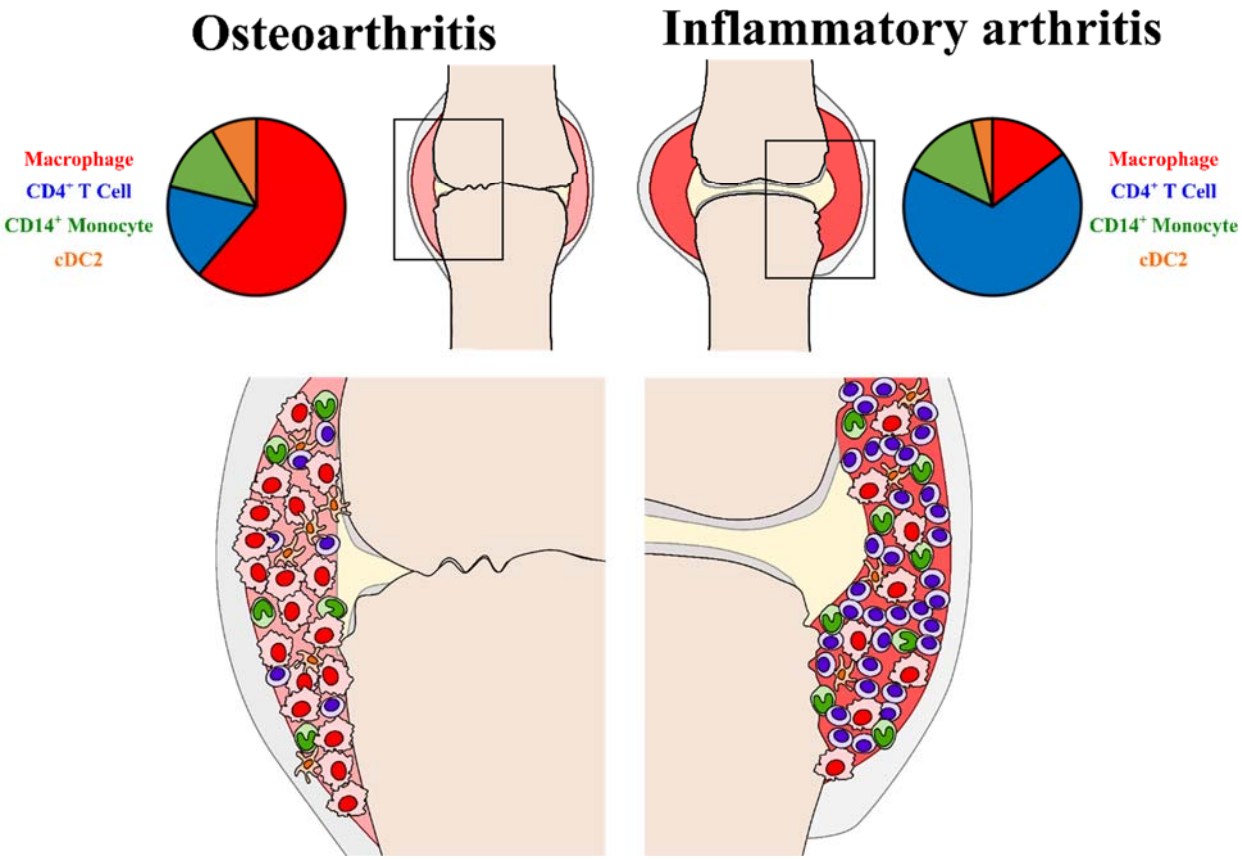

Figure 4.19: Illustrative summary of Chapter 4 results
Depiction of the main findings from Chapter 4. Pie charts display data from Figure 4.14 (cell subsets as a percentage of $CD45^+$ cell population). Visual representation of these results (bottom).

Chapter 5. Synovial macrophage phenotype, function and gene expression

5.1 Introduction

Macrophages are present alongside fibroblasts in normal synovium and are likely to be the front line cell 'sensing' joint damage (Smith 2011). In OA, macrophages contribute to cartilage destruction and osteophyte formation. This is through mechanisms such as cytokine production including but not limited to IL-1β, TNFα, TGFβ, and pro-matrix MMPs (Blom, van Lent et al. 2004, van Lent, Blom et al. 2004, Bondeson, Blom et al. 2010). Depletion of macrophages from synovial tissue cultures *in vitro* showed the elimination of IL-1β and TNF production (Bondeson, Wainwright et al. 2006). In animal models, macrophage depletion reduces osteophyte formation (Blom, van Lent et al. 2004, van Lent, Blom et al. 2004). In line with my previous findings (Chapter 4, Figures 4.9-4.14), histological studies have demonstrated enhanced numbers of macrophages in the synovium of OA patients (Haywood, McWilliams et al. 2003, Benito, Veale et al. 2005). Increased numbers of activated macrophages have further been shown to correlate with the severity and progression of disease in OA patients (Kraus, McDaniel et al. 2016).

Although macrophages have been implicated in the pathogenesis of OA, their role remains unclear. It is unlikely that macrophages are the single and direct cause of joint inflammation and destruction. Macrophages are heterogeneous cells with diverse functions including tissue repair, promotion and dampening of inflammation. A well-described paradigm in macrophage literature is that of the pro-inflammatory M1 and anti-inflammatory M2 macrophages. These were described based on *in vitro* responses to stimuli and have yielded a vast knowledge of macrophage activation. However, this paradigm reflects the polar extremes of macrophage activation, and may not truly represent tissue macrophages (Xue, Schmidt et al. 2014). Despite these macrophage states representing extremes of activation, they are both required for tissue remodelling after injury (Novak and Koh 2013, Brown, Sicari et al. 2014). Pro-inflammatory macrophages remove necrotic cellular material, kill pathogens and promote proliferation of new tissue cells. Anti-inflammatory macrophages subsequently dampen down inflammation, promote differentiation of newly recruited or expanded cells, and stimulate deposition of new extracellular matrix. It is thought that the timely and regulated transition from a pro- to anti-inflammatory macrophage phenotype is essential for tissue regeneration (Sindrilaru, Peters et al. 2011, Novak and Koh 2013). It is unknown if synovial macrophages in OA have a pro- or anti-inflammatory phenotype and whether an imbalance between these types of macrophages is a protagonist of OA synovial inflammation.

High-resolution gene expression analyses such as RNA-sequencing have been previously conducted on whole synovial tissue, other synovial immune cell types, and monocyte-derived macrophages. However, to my knowledge this has not been previously been conducted on purified human OA synovial macrophages. The role of macrophages in the synovium of IA and OA has been previously discussed (Chapter 1 & 4). To summarise, despite their well-researched role in IA, macrophages have also been implicated in the pathogenesis of OA. Additionally, I have demonstrated their abundance in the synovium of OA patients compared with IA patients (Chapter 4). Much of the previously published research has been histology-based, and has lacked the specificity and advanced techniques which I have now developed. An in-depth analysis of these cells in the synovium of OA patients is required to gain a better understanding of how these cells contribute to OA pathogenesis.

5.2 *Aims*

Macrophages have been implicated in the pathogenesis of both IA and OA. I have further demonstrated an increased quantity of synovial macrophages in OA compared to IA. I therefore aimed to carry out an in-depth analysis on highly pure synovial macrophages from OA and IA patients. The main aims of this chapter were:

- Phenotype the surface markers of synovial macrophages
- Evaluate the functionality of synovial macrophages after digestion and FACs
- Assess the gene expression profiles of synovial macrophages in OA

5.3 Phenotyping of synovial macrophages

I first carried out further phenotyping of synovial macrophages by flow cytometry. This involved exploring different gating strategies, and measuring specific surface marker expression on synovial macrophages from OA and IA.

5.3.1 *Resident and recruited macrophages*

After meeting with Professor Matthew Collin (Newcastle University), I tested a gating strategy developed for the identification of inflammatory and non-inflammatory monocytes and macrophages. Within his group, this gating strategy is applied to healthy dermis, and inflammatory samples from patients with graft versus host disease (Collin group, manuscript in preparation; Jahnsen *et al.,* 2017).

After gating on CD45$^+$ cells using the gating strategy described in Chapter 3, the first strategy involves gating on HLA-DR$^+$ and CD14$^+$ cells and then splitting this population based on CD14 and CD11c expression (Fig. 5.1 A). From this, DCs could be identified as CD14$^-$CD11c$^+$ and macrophages as CD14$^+$ CD11c^{lo}. The intermediate population could then be split by HLA-DR expression into two monocyte subtypes: 'monocyte 1' and 'monocyte 2'. It is thought that the quantity of monocyte 2 within inflammatory conditions is increased. The second gating strategy is for the identification of resident and infiltrating monocytes/macrophages. HLA-DR$^+$ (CD45$^+$) cells were gated on and split by expression of CD14 and CD11c (Fig. 5.1 B). CD11c^{lo}CD14$^-$ cells are identified as pDCs and cDC1 and CD11c^{lo}CD14$^+$ cells as 'resident' macrophages. CD11c$^+$ cells were then identified as CD14$^+$CD1c$^-$ 'inflammatory' macrophages, CD14$^+$CD1c$^+$ monocytes and CD14$^-$CD1c$^+$ cDC2.

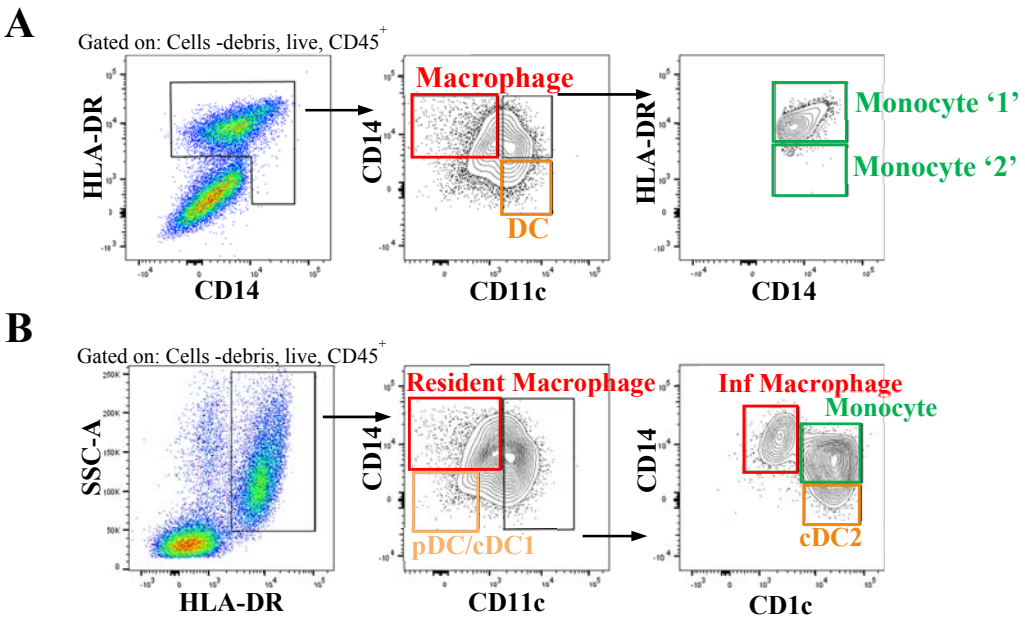

Figure 5.1: Identification of monocyte and macrophage subsets in dermis
Dermal mononuclear cells were analysed by flow cytometry using techniques described in Chapter 3. **A:** Identification of Monocytes '1' and '2'. **B:** Identification of resident and inflammatory macrophages. Data are representative of one experiment.

The first strategy was applied to OA and IA samples (Fig. 5.2 A) and monocytes 1 & 2 quantified (Fig. 5.2 B). The second strategy was also applied to OA and IA samples (Fig. 5.2 C) and the ratio of resident and inflammatory macrophages quantified (Fig. 5.2 D). When back-gating the 'resident' and 'inflammatory' macrophage populations to assess their auto-fluorescence, it was noticed that contamination with non auto-fluorescent cells was present, most likely monocytes (Fig. 5.3 A). I therefore incorporated auto-fluorescence into the gating strategy to achieve purer 'inflammatory' and 'resident' macrophages populations (Fig. 5.3 B). As CD11c was not previously incorporated into macrophage phenotyping panels, the only activation marker of interest I had for these populations was CD86. Higher levels of CD86 expression were measured on the inflammatory macrophages (Fig. 5.3 C).

Although interesting preliminary data were generated from testing this gating strategy, this was conducted towards the end of my project and was therefore left for future work. The remainder of this chapter focusses on the previously defined HLA-DR^{+}CD14^{+} synovial macrophages.

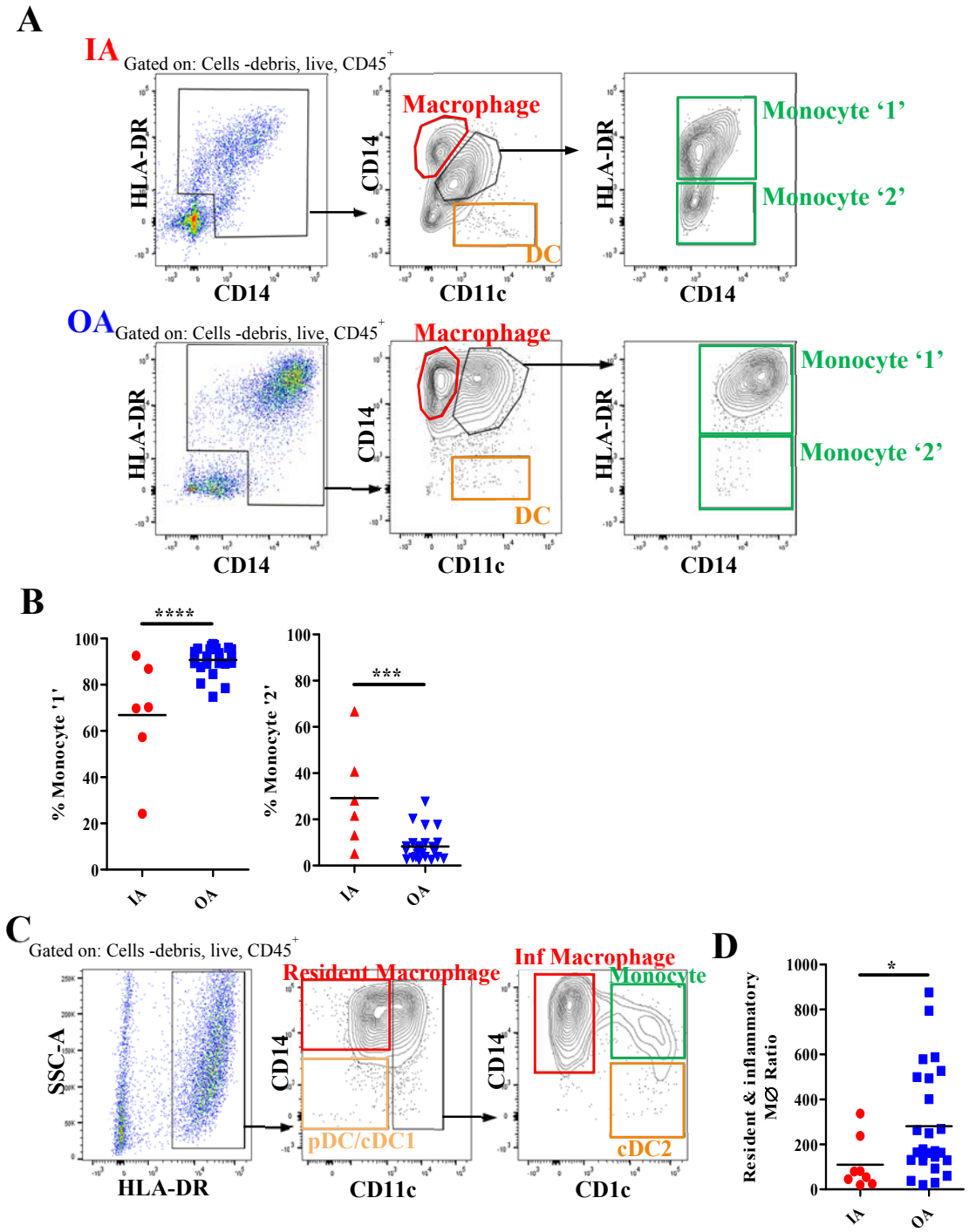

Figure 5.2: Identification and quantification of monocyte and macrophage subsets in synovial tissue

Synovial tissue from OA total knee replacement and IA ultrasound guided biopsy was digested and analysed by flow cytometry using techniques described in Chapter 3. **A:** Identification of monocytes '1' and '2' in synovial tissue. Top panels depict IA samples. Bottom panels depict OA samples. **B:** Quantification of monocytes '1' and '2' in synovial tissue. Left panel depicts % monocyte '1'. Right panel depicts % monocyte '2'. **C:** Identification of resident and inflammatory macrophages. Data are representative of 33 independent experiments. *$P \leq 0.05$, ***$P \leq 0.001$, ****$P \leq 0.0001$.

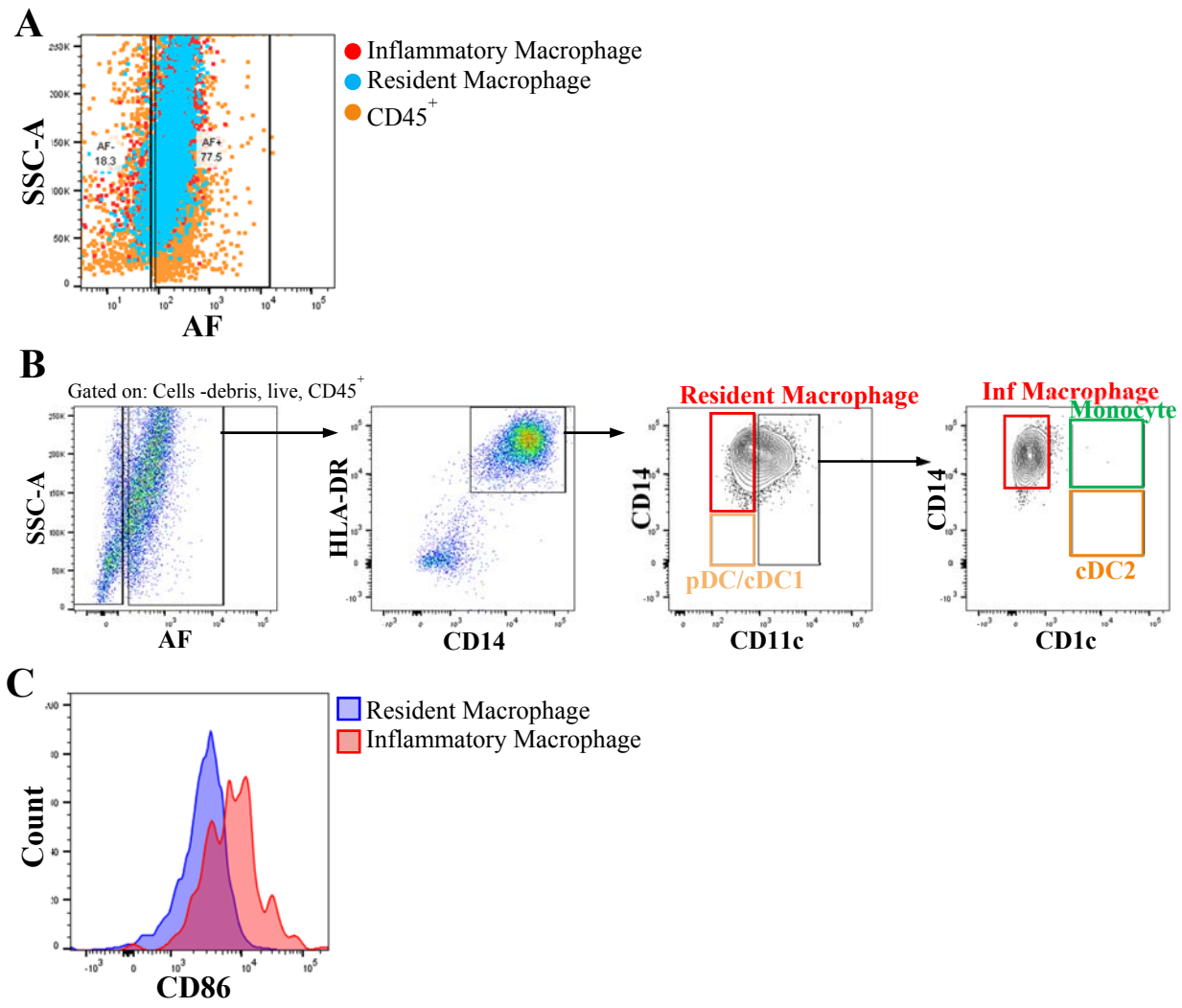

Figure 5.3: Identification of macrophage subsets in synovial tissue utilising auto-fluorescence
Synovial tissue from OA total knee replacement and IA ultrasound guided biopsy was digested and analysed by flow cytometry using techniques described in Chapter 3. **A:** Auto-fluorescence of macrophage subsets. **B:** Identification of macrophage subsets utilising auto-fluorescence. **C:** CD86 expression of macrophage subsets. Data are representative of 3 independent experiments.

5.3.2 *Expression of 'standard' surface markers*

When measuring the MFI of the surface markers in my standard flow cytometry panel, there was no clear difference in levels of expression between OA and IA synovial macrophages (Fig. 5.4). However, higher levels of CD14, CD45, CD16, CD11c and CD4 were measured in the healthy monocyte-derived macrophages compared to either OA or IA. Although these cells were generated from healthy blood, they likely better represent a monocyte-derived infiltrating macrophage, rather than a healthy tissue macrophage, due to their monocyte-derived *in vitro* culture. Importantly, synovial macrophages express expected markers (e.g. HLA-DR, CD14), and do not express other cell specific markers, such as CD1c or CD3.

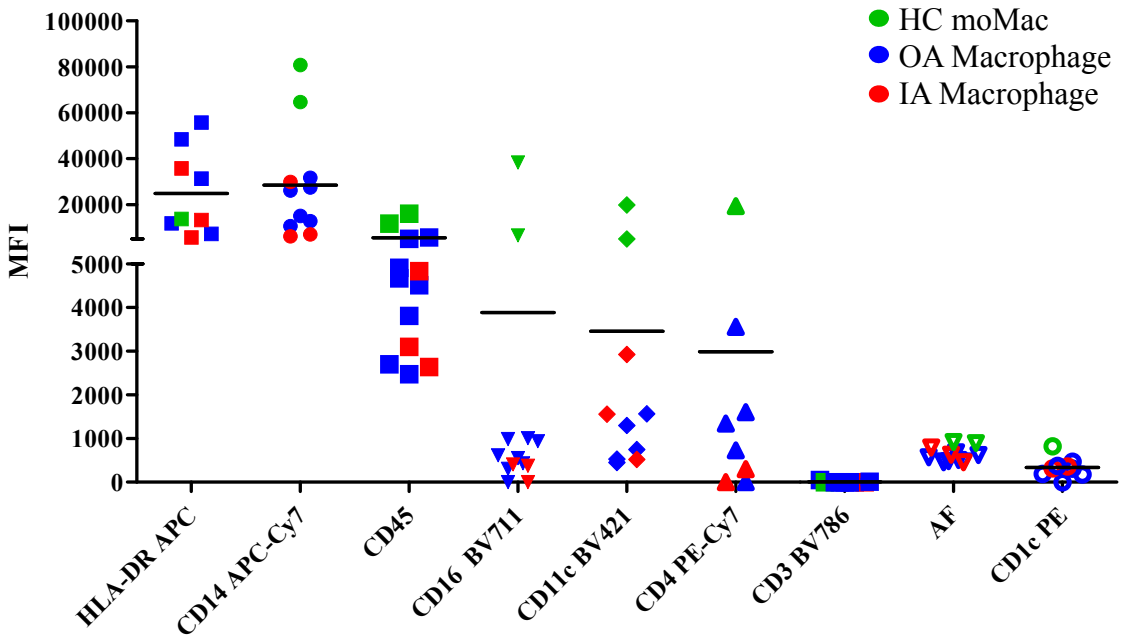

Figure 5.4: Expression of 'standard' surface antigens on synovial macrophages
Synovial tissue from OA total knee replacement and IA ultrasound guided biopsy was digested and analysed by flow cytometry using techniques described in Chapter 3. Expression of surface antigens included in FACS panel on healthy control (HC) monocyte-derived macrophages, OA and IA macrophages. Data are representative of 8-13 independent experiments.

5.3.3 *Expression of 'activation' surface markers*

To further characterise the surface marker phenotype of these synovial macrophages, antibodies that were not required for the identification of macrophages (CD3, CD4, CD11c, CD1c) were removed from the panel, and antibodies of interest added. This allowed the consistent identification of macrophages, and enabled specific questions to be addressed.

Expression levels of CD86 were similar between OA and IA synovial macrophages, and monocyte-derived macrophages (Fig. 5.5 A). However, higher levels of CD172α (Sirp-α), CCR2 and CCR7 were measured in the moMacs compared with the OA and IA synovial macrophages. Although not expressed to the same extent as moMacs, higher levels of all three of these markers were observed in OA compared to IA (Fig. 5.5 A). CD206 and FOLR2 were expressed at similar levels by both moMacs and OA macrophages. By contrast, IA macrophages expressed these markers at lower levels than both moMacs and OA macrophages. CD64 expression was similar between OA and IA, and although only measured on OA synovial macrophages, MCSF-R and CD83 were expressed (Fig. 5.5 A). When assessing the cell size (FSC-A) and structure (SSC-A) by flow cytometry, the OA macrophages had significantly higher FSC-A and SSC-A MFI as compared to synovial macrophages from IA patients (Fig. 5.5 B).

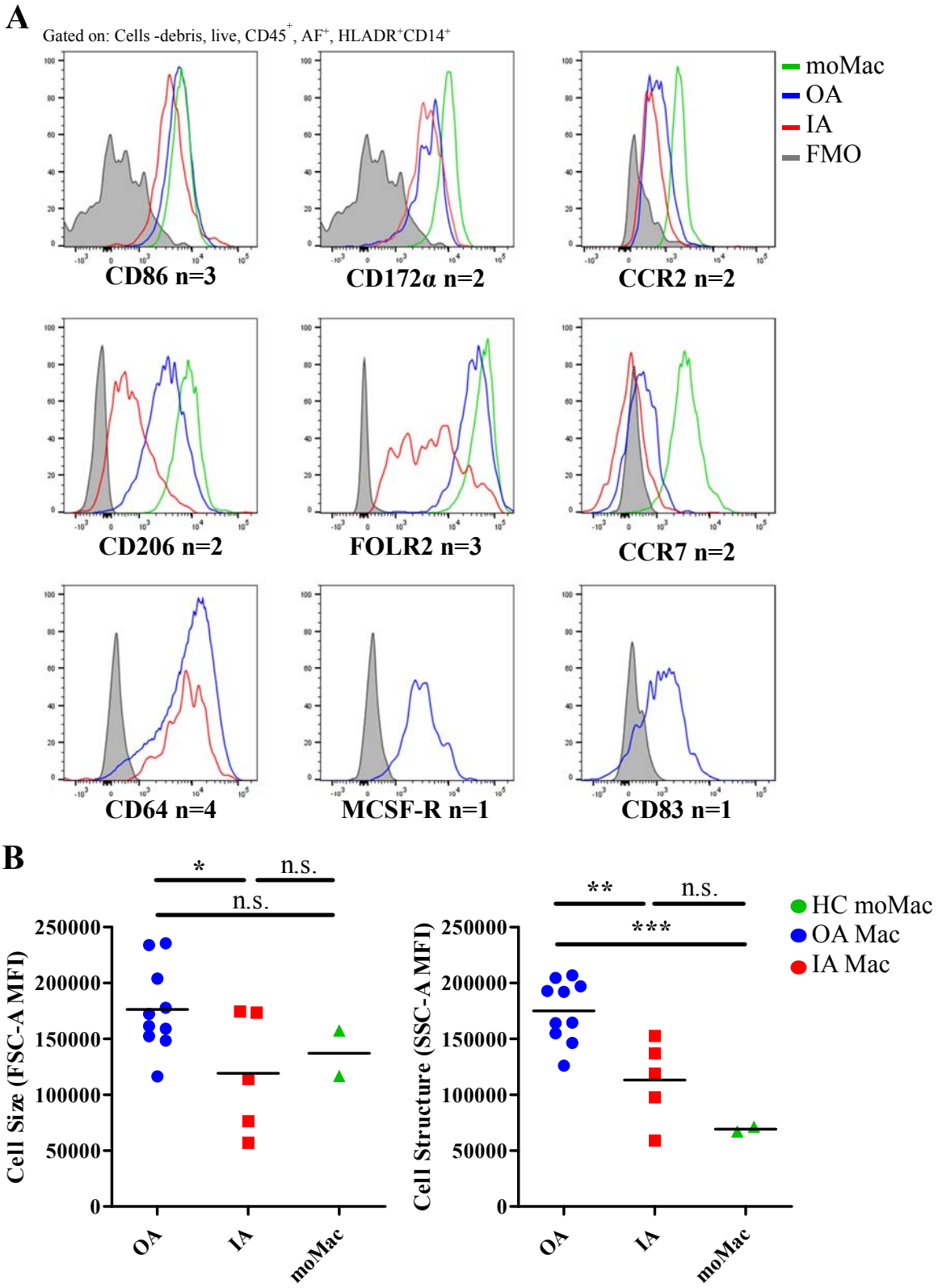

Figure 5.5: Expression of 'activation' surface antigens on synovial macrophages
Synovial tissue from OA total knee replacement and IA ultrasound guided biopsy was digested and analysed by flow cytometry using techniques described in Chapter 3. **A:** Expression of surface antigens on HC monocyte-derived macrophages, OA and IA macrophages. Data are representative of 1-4 independent experiments. **B:** Cell size and structure of HC monocyte-derived macrophages, OA and IA macrophages measured by FSC-A and SSC-A MFI. Data are representative of 17 independent experiments. **P ≤0.05, **P ≤0.01, ***P ≤0.001*.

5.4 Phagocytic capacity of synovial macrophages

As future studies will likely address the functional differences between synovial macrophages in different disease states, I next determined whether synovial macrophages retained functional ability after tissue digestion and cell sorting. Because phagocytosis is a typical function of macrophages, I measured their phagocytic ability utilising latex beads. moDC, which should have low phagocytic capacity, and moMacs, which should have high phagocytic capacity, were used as comparators.

5.4.1 *Flow cytometry analysis of phagocytosis*

When assessing the amount of latex beads phagocytosed by flow cytometry, moDC had a very low level of bead uptake, similar to that of the no-bead negative control (Fig. 5.6 A). In contrast, the moMacs had high levels of bead uptake, similar to that of the positive control, beads alone (Fig. 5.6 A). Synovial tissue macrophages had similar levels of phagocytosis as moMacs (Fig. 5.6 A). The levels of phagocytosis were next compared between moMacs and moDC generated from blood of either healthy controls or IA patients (Fig. 5.6 B). In both healthy and IA samples, moMacs had higher levels of phagocytosis than moDC (Fig. 5.6 B). IA moMacs had slightly lower levels of phagocytosis compared to healthy moMacs (Fig. 5.6 B). Unfortunately, I was unable to collect any OA blood at this stage of the project to carry out this experiment in parallel. When comparing OA synovial macrophages and cDC2, macrophages had a much higher efficiency for phagocytosis than cDC2 (Fig. 5.6 C).

Phagocytosis of the latex beads could be observed in the culture wells by light microscopy, demonstrated in Figure 5.6 C. Beads can be seen engulfed by macrophages in the positive condition, whereas they are absent in the negative condition. However, the presence of vacuoles in the macrophages could obscure true quantification by this method. Additionally, the latex beads could have been simply adhering to the surface of the cell rather than being phagocytosed, giving a false positive result by both flow cytometry and examination under a light microscope during culture.

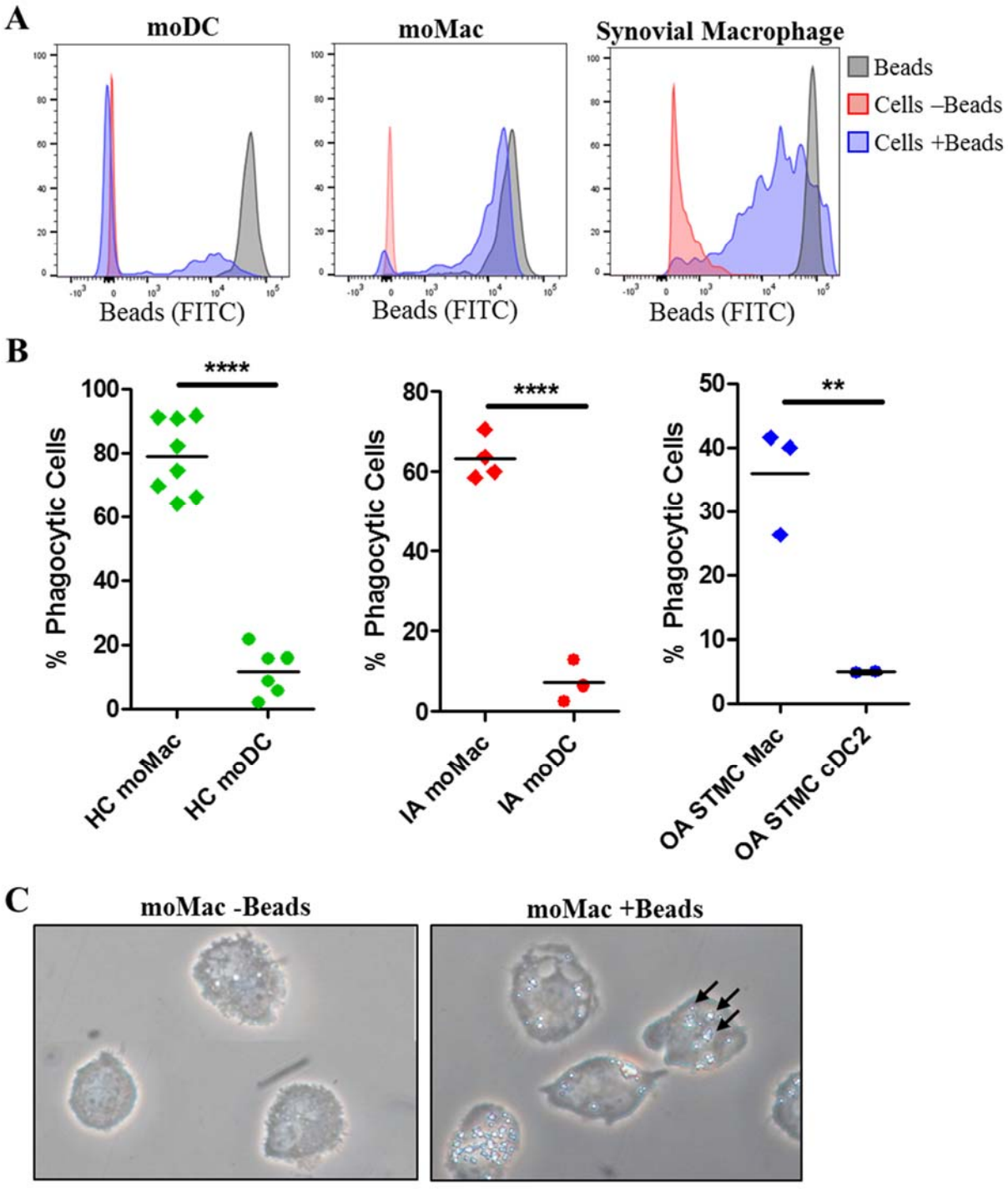

Figure 5.6: Flow cytometry measurement of phagocytosis by dendritic cells and macrophages
Synovial tissue from OA total knee replacement and IA ultrasound guided biopsy was digested and analysed by flow cytometry using techniques described in Chapter 3. **A:** Expression of latex bead fluorescence in FITC channel. Histograms depict cells incubated with beads (blue), cells incubated without beads (red), and beads alone (grey). Left panel depicts monocyte-derived DCs, middle panels depicts monocyte derived macrophages, right panel depicts synovial tissue macrophages. Data are representative of 3 independent experiments. **B:** Flow cytometry quantification of phagocytosis by monocyte-derived (left and middle) and synovial tissue (right) DCs and macrophages. Left graph depicts healthy donors (n=6-8), middle graph depicts IA donors (n=3-4) and right graph depicts OA donors (n=2-3). **C:** Images of monocyte derived macrophages incubated without (left panel) and with (right panel) latex beads. Arrows indicate beads. X100 Magnification. Data are representative of 8 independent experiments. $**P \leq 0.01$, $****P \leq 0.0001$.

5.4.2 *Immunofluorescent and confocal microscopy of phagocytosis*

To further assess latex bead engulfment by macrophages, immunofluorescence microscopy was conducted (Fig. 5.7). Interestingly, within the monocyte-derived macrophage condition, individual macrophages appeared to have different levels of phagocytosis (Fig. 5.7 A). A similar observation was seen with synovial macrophages (Fig. 5.7 B). Most of the beads were localized around the nucleus and within the outer membrane, suggesting that they were within the cell. However, as the presence of a small number of beads were overlaid with the nucleus, this again could suggest the possibly of beads simply adhering to the cell surface. To further confirm phagocytosis, confocal microscopy was conducted.

First, imaging was conducted using differential interference contrast (DIC), to provide high resolution images of macrophages (Fig. 5.8 A). This allowed the confirmation that the beads were not stuck to the outside of the cell membrane, however they could still be resting on the top membrane. To eliminate this possibility, serial images were taken through the cell (Z-stacks), and three-dimensional images recreated (Fig. 5.8 B & C). From examination of these re-constructed images, and the individual serial images (data not shown) it could be seen that the beads were located parallel to the nucleus, and within the cell membrane. This allowed me to confirm that these macrophages were indeed phagocytosing the beads.

This was an import preceding step to my gene expression analysis experiments. Although care has been taken in isolating these cells from tissue and subsequent purification, these experiments have allowed me to confirm that the cells are still functional once isolated.

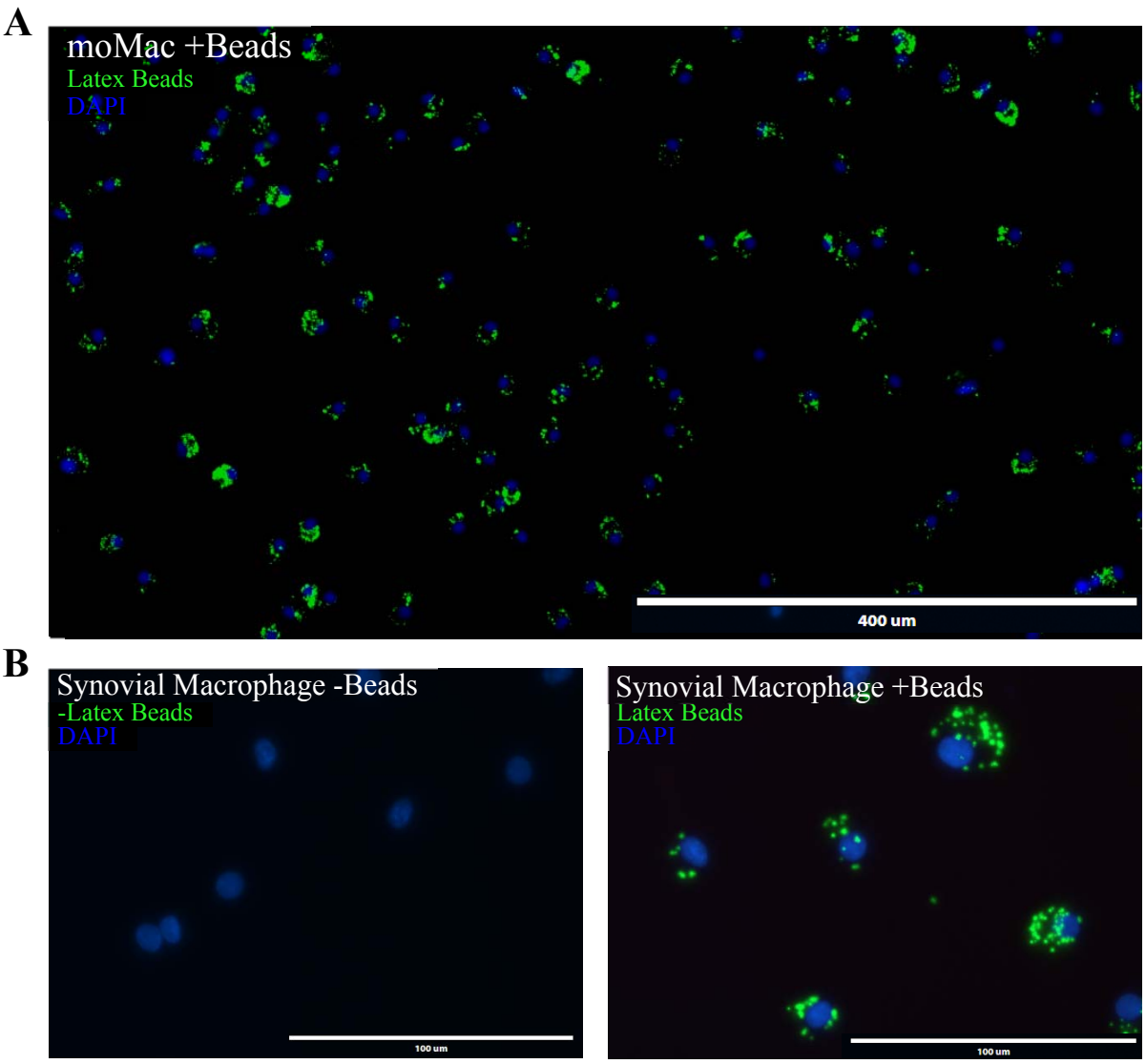

Figure 5.7: Phagocytosis of latex beads by synovial macrophages
Synovial tissue from OA total knee replacement was digested using techniques described in Chapter 3. Monocyte-derived macrophages were cultured following technique described in Chapter 2. Slides were prepared following methods outlined in Chapter 2. **A:** Immunofluorescent imaging of slide preparation at x40 magnification. **B:** Immunofluorescent imaging of slide preparation at x100 magnification. Left panel depicts cells incubated without latex beads. Right panel depicts cells incubated with latex beads. Data are representative of 2 independent experiments.

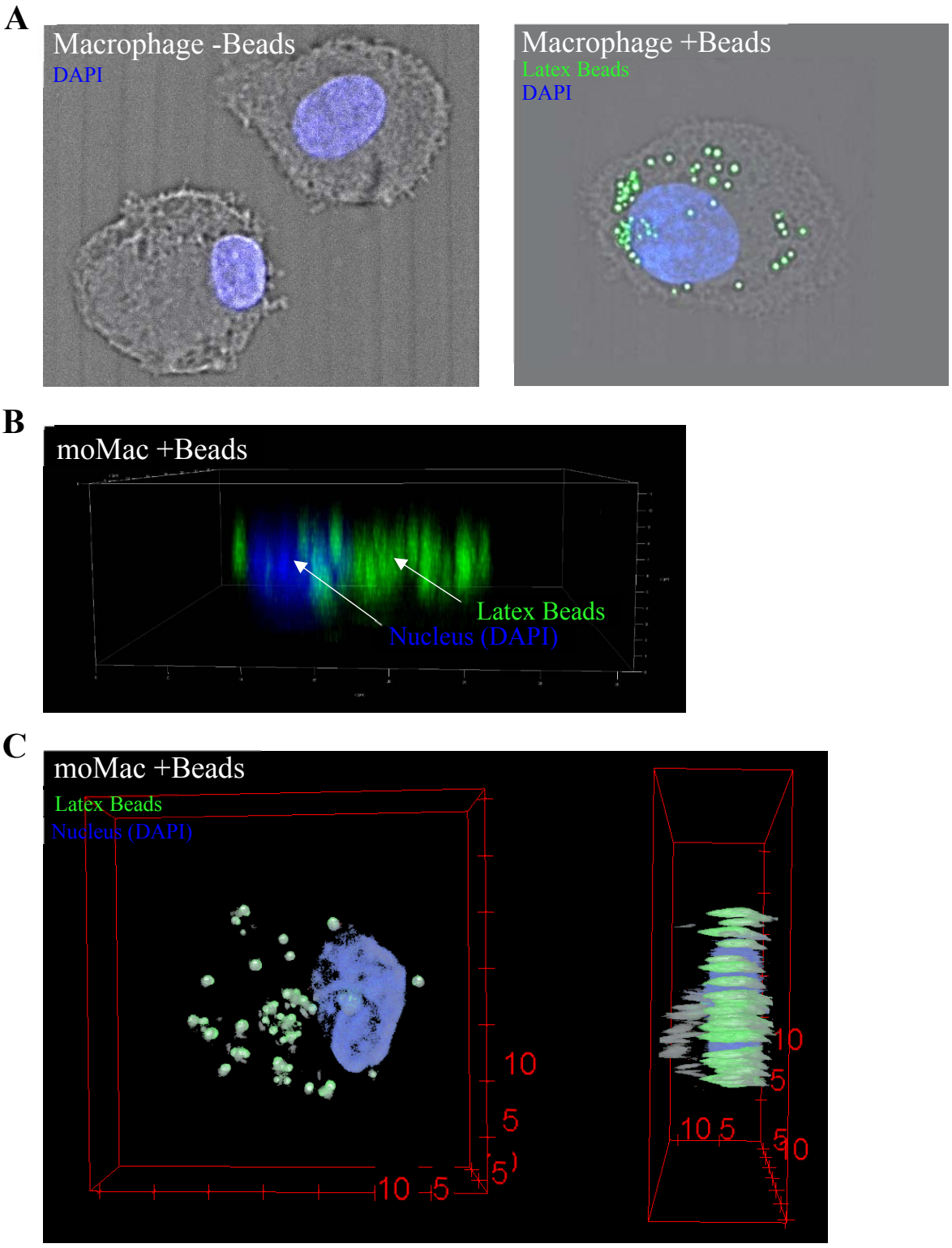

Figure 5.8: Confocal microscopy of phagocytosis by monocyte-derived macrophages
Monocyte-derived macrophages were cultured following techniques described in Chapter 2. Slides were prepared following methods outlined in Chapter 2. **A:** Confocal microscope image utilising differential interference contrast (DIC). Left panel depicts macrophages cultured without latex beads. Right panel depicts macrophages cultured with latex beads. **B:** Confocal Z stack reconstruction of 39 images. Blue areas indicate DAPI staining of nucleus. Green areas indicate latex beads. **C:** Confocal Z stack reconstruction animation of 39 images. Blue areas indicate DAPI staining of nucleus. Green areas indicate latex beads. Grey areas indicate cell membrane (DIC). Data are representative of 2 independent experiments.

5.5 Gene expression of synovial macrophages

I now know that these synovial macrophages are viable, pure, express expected surface markers and are functional after isolation. I next examined the transcriptomic profile of these synovial macrophages by RNA-sequencing. I aimed to do this by contrasting OA synovial macrophages with IA controls. This is a relatively new technique for our group and there are challenges associated with using tissue-derived cells. There were nine OA and three IA samples available for analysis. A summary of patient characteristics are presented in Table 5.1. The IA control group was heterogeneous, comprising one early and one established RA sample, and one PsA sample. Although this will inherently increase biological variance, the IA group was being used as an inflammatory control and therefore encapsulates a range of inflammatory arthritides. All IA samples were derived from wrist biopsies, whereas OA samples were taken from TKR surgery. The two disease cohorts were well matched for age, gender and BMI, with no significant differences (Table 5.1). However, the mean BMI of OA cohort, 36.3 (SD 4.7), is classed as obese, whereas the BMI of the IA cohort, 29.4 (SD 0.5) is classed as overweight. As previously discussed in Chapter 4, this will be taken into account during analyses, but was deemed as an acceptable difference owing to obesity being a risk factor for OA.

Both CRP and ESR were significantly higher in the IA patients. Again, this was expected as the clinical diagnosis for RA includes abnormal ESR or CRP measurements, and are likely due to differences in disease mechanisms. The median KL X-ray score recorded in our OA patients was 3.44. This suggests active OA disease in our cohort, showing multiple, moderately sized osteophytes, definite joint space narrowing, some sclerotic areas and possible bony end deformity (NICE, 2017). 11% and 33% of OA patients had previously undergone a meniscectomy or TKR, respectively. IA patients recruited showed a median DAS28 of 3.0. A DAS28 score of <3.2 represents a low disease activity (Fransen and van Riel 2005).

	OA (n=9)	IA (n=3)	Variation
Age (years; mean, SD)	61.7 (12.5)	48.3 (15.2)	n.s
% Females	100	100	n.s
BMI (mean, SD)	36.3 (4.7)	29.4 (0.5)	n.s
Disease Duration (years; median, SD)	4.5 (2.3)	N/A	N/A
Symptom Duration (weeks; median, SD)	N/A	18 (6)	N/A
CRP (mg/l; median, SD)	4.75 (5.8)	75.5 (52.5)	*
ESR (mm/hr; median, SD)	12.13 (5.7)	86.5 (39.5)	**
DAS28 (median, SD)	N/A	3 (0.3)	N/A
RF$^+$ (%)	N/A	33.3	N/A
CCP$^+$ (%)	N/A	33.3	N/A
KL X-ray Score (median, SD)	3.44 (0.7)	N/A	N/A
Joint (%R TKR)	33.3	N/A	N/A
% NIDDM	11.1	N/A	N/A
% Gout	11.1	N/A	N/A
% Previous Menisectomy	11.1	N/A	N/A
% Previous TKR +/- DTOS	33.3	N/A	N/A
OA Pattern (% bilateral, % unilateral)	66.6, 33.3	N/A	N/A
% No Medication (% medication)	77.7 (11.1 Warfarin, 11.1 Atorvastatin)	N/A	N/A
Joint Specific Pattern (% Pattern)	44.4 Medial, 33.3 Medial and patello-femoral, 22.2 Tricompartmental	N/A	N/A
Disease (% RA, % PsA)	N/A	(66.6, 33.3)	N/A

Table 5.1: Patient characteristics for synovial tissue macrophage RNA-sequencing analyses
For MØ RNA-seq, 9 OA patients and 3 IA patients were used. Patient data were collated and tabulated. As these patients were recruited from separate clinics, a number of clinical parameters were not available for each group. Some patient records were incomplete or unavailable, percentages therefore represent proportion of all disease specific patients used.

5.5.1 *Quality Control*

Data presented within this chapter are based on counts generated using methods outlined in Chapter 2. Counts with a low number (<0.5 Counts per million; CPM) were removed (data not shown). Counts per million were found to be consistent across disease groups (data not shown). No clear batch effect was present (Fig. 5.9 A). Next, I examined the library size (Fig. 5.9 B). Although all samples had good library sizes, X1_OA presents with a smaller library than the other samples. When plotting the relative log expression, X1_OA also shows an elevated ratio compared to the other samples (Fig. 5.9 C & D). RNA length was utilised as a covariate factor for pathway analyses.

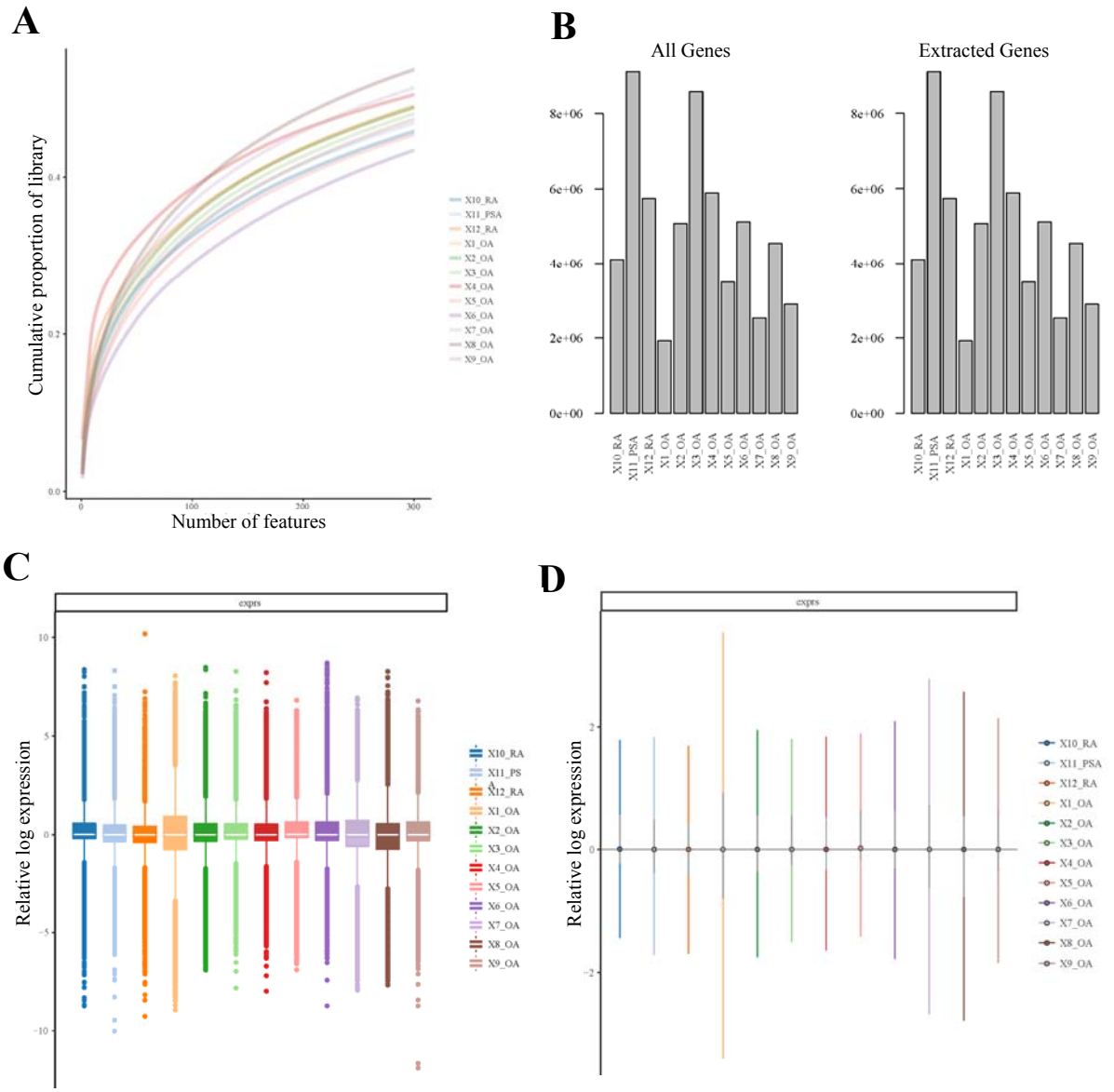

Figure 5.9: Quality control of synovial macrophage RNA-sequencing
RNA-sequencing of synovial macrophages and data analyses were conducted following methods described in Chapter 2. **A:** Assessment of batch effect plotting cumulative proportion of library size against number of features. **B:** **A**nalysis of library size plotted using relative log expression. Left panel depicts library sizes pre gene exclusion based upon low CPM values. Right plot depicts library sizes post gene exclusion based upon low CPM values. **C:** Full (**C**) and minimal (**D**) relative log expression ratio.

Using these raw counts, multidimensional scale (MDS) plots were used to initially visualise these data (Fig. 5.10 A). Despite the biological variance, the IA group cluster together. The OA group is highly dispersed, although a small group cluster close to the IA samples. Sample X1_OA clusters away from both IA and the rest of the OA samples. Because of this, the MDS plot was repeated without sample X1_OA (Fig. 5.10 A). This again showed the IA samples clustering together, and a heterogeneous range of OA samples. X6_OA, X3_OA and X4_OA can be seen on the left side of the leading logFC dimension (1) with the IA samples. Repeating without the IA samples further demonstrates heterogeneity with the OA samples (Fig. 5.10 A). A principle component analysis (PCA) plot was next generated of the same data (Fig. 5.10 B). Although similar to MDS plots, a PCA plot preserves covariance of data, and is useful for demonstrating local variation between samples. MDS plots preserve distance dimensionality allowing the interpretation of distance between data points. MDS plots are useful for identifying outliers in data as they demonstrate large differences better than local similarities. The PCA plot demonstrated similar clustering of IA samples, and similar heterogeneity of OA samples. Subsequent components do not demonstrate such separation (data not shown). As component one accounts for 39% of the dimensionality, subsequent components would not be expected to be useful. Due to consistent abnormalities in the quality and presentation of X1_OA, this sample was removed from the remaining analyses. For further analyses, these counts were computed to counts per million and normalised with edgeR. Expression levels were generated using Limma's 'voom' function. Counts per million were consistent pre-normalisation, and more so after normalisation (Appendix 5.1). Contrasts were built and differential expression analyses conducted using Limma.

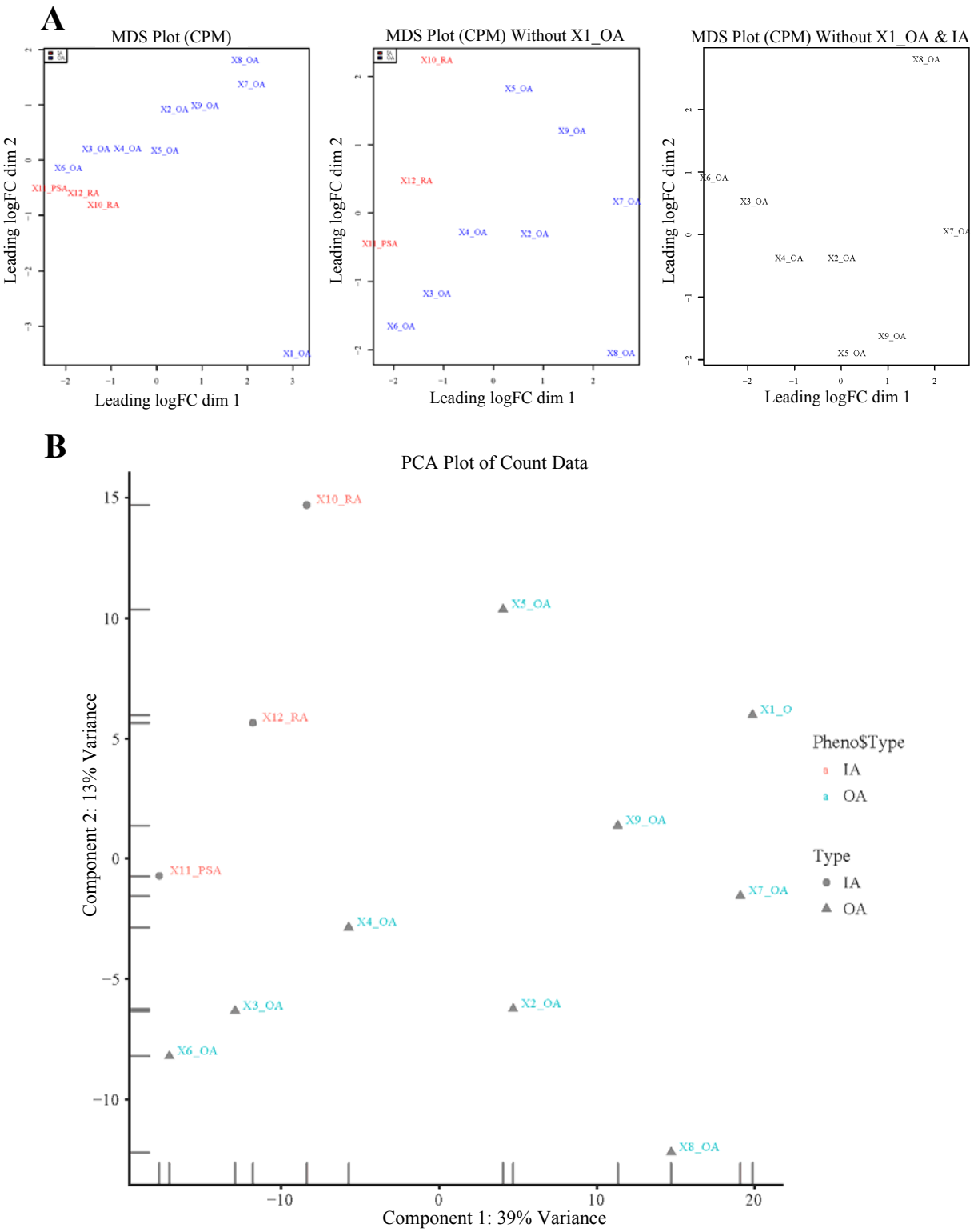

Figure 5.10: MDS and PCA analyses of synovial macrophage RNA-sequencing
RNA-sequencing of synovial macrophages and data analyses were conducted following methods described in Chapter 2. **A:** Multidimensional scale (MDS) plots of all samples (left panel), all samples minus X1_OA (middle panel), and OA samples minus X1_OA (right panel). **B:** PCA plot of all samples. Red text and circle identifies IA samples, blue text and triangle identifies OA samples.

5.5.2 *Expression of known macrophage gene signatures*

As a final validation step, I evaluated the expression of known macrophage genes, and non-macrophage genes in my data. As demonstrated, all samples lacked expression of genes associated with cell types including B-cells (B-cell receptor; BCR), DCs (CD1c), NK cells (Nuclear adhesion molecule; NCAM1), stromal cells (THY1) and T cells (T cell receptor alpha constant; TRAC) (Fig. 5.11). In contrast, all samples expressed genes associated with macrophages, including CD14, CD68, CSF1R, HLA-DRA and MARCO (Fig. 5.11).

Next, I considered the expression of known macrophage gene sets. Common M1 and M2 gene sets were composed from pre-existing gene sets and chemokine signatures (Martinez, Gordon et al. 2006, Beyer, Mallmann et al. 2012, Barros, Hauck et al. 2013, Italiani and Boraschi 2014, Roszer 2015, Saliba, Li et al. 2016, Gensel, Kopper et al. 2017). When addressing the expression of these gene sets by synovial macrophages isolated here, they do not clearly fit either M1 or M2 gene signatures (Fig. 5.12). Overall, all synovial macrophage samples appear to have lower levels of expression of M2 related genes compared to M1 (Fig. 5.12).

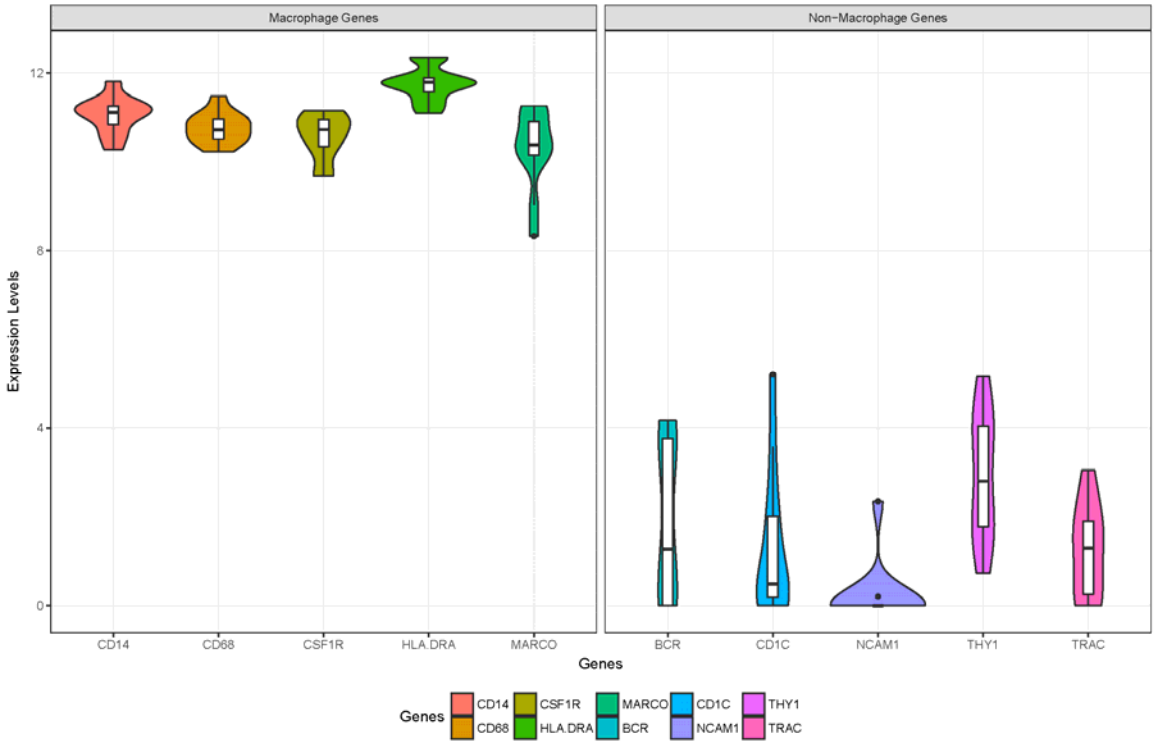

Figure 5.11: Expression of macrophage and non macrophage genes by synovial macrophages
RNA-sequencing of synovial macrophages and data analyses were conducted following methods described in Chapter 2. logCPM expression levels of macrophage genes (left panel) and B cell (BCR), DC (CD1c), NK cell (NCAM1), Stromal (THY1) and T cell (TRAC) genes (right panel).

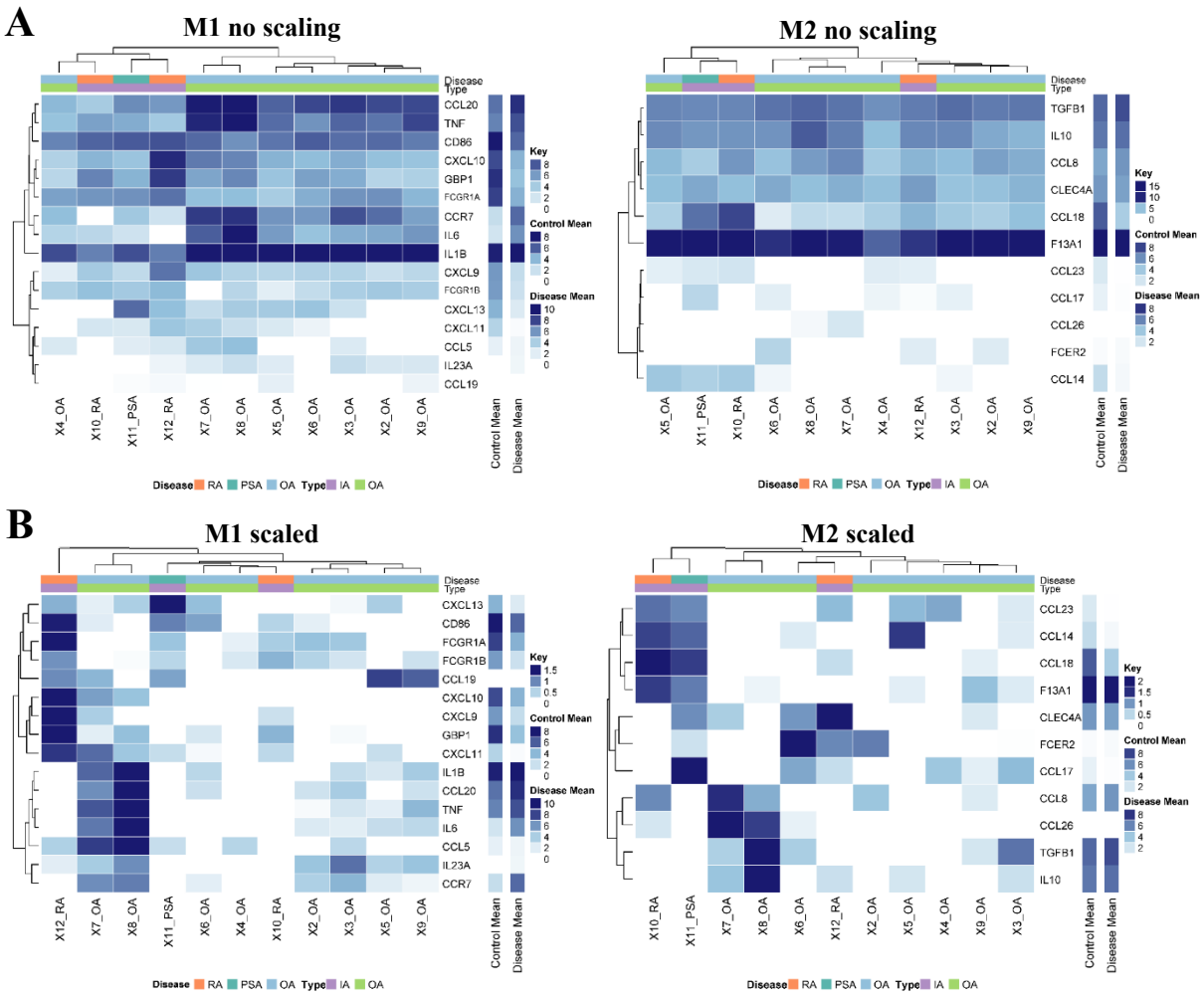

Figure 5.12: Expression M1 and M2 gene sets by synovial macrophages
RNA-sequencing of synovial macrophages and data analyses were conducted following methods described in Chapter 2. **A:** Hierachical clustering heat map based upon logCPM **e**xpression of M1 macrophages genes (left panel) and M2 macrophage genes (right panel). **B:** Hierachical clustering heat map with scaling of logCPM **e**xpression values of M1 macrophages genes (left panel) and M2 macrophage genes (right panel). Colours indicate gene-wise expression across 11 samples as per key (right). Top colour bar indicates disease group and type as per key (bottom).

5.5.3 *CD16$^+$ Macrophages*

Within the flow cytometry data, CD16$^+$ macrophages were observed in IA samples, which were only present in some OA samples (Appendix 5.2). I initially conducted differential gene expression analyses of sequenced macrophage samples with high and low amounts of CD16$^+$ macrophages. However, only one significantly differentially expressed gene (DEG) was observed (>1.5-FC; $p<0.05$, multiple test corrected) (Appendix 5.2). This gene was the non-protein encoding gene RP11-12601.5 (Appendix 5.2). The distribution of p-values from this differential gene expression analysis was plateaued suggesting a null-hypothesis (Appendix 5.2). Additionally, these samples did not cluster into CD16$^+$ high and low macrophage groups by MDS or PCA plot analyses (data not shown). Because of the statistical uncertainty of the

differences between these $CD16^+$ high and low groups, it was decided to discontinue with this analysis.

5.5.4 *IA v OA (Question 1)*

The first question I addressed was the difference in gene expression between IA and OA. From this first comparison, three protein encoding DEGs were observed (>1.5-FC; $p<0.05$, multiple test corrected) (Fig. 5.13 A). These genes were *IGFBP5*, *LRRN4CL* and *TKSU*, all under-expressed (>-4.5 FC) in the IA samples compared to OA (Fig. 5.13 B). As this is differential gene expression, the inverse that these genes are over-expressed in OA samples is equally true. When examining the p-value distribution for this question, an anti-conservative distribution is observed (Fig. 5.13 C). These genes are visually represented in a hierarchical clustering heat map (Fig. 5.14). As expected, the IA and OA groups are distinctly branched from one another.

To conduct pathway analyses, a larger set of DEGs was required. To achieve this, un-adjusted p-values (<0.05) were used (Fig. 5.15). Although this generates a greater array of significantly DEGs, these will only be used at an exploratory level due to the risk of false discovery. When presented in a heat map, this gene set also clusters IA separately to OA (Fig. 5.16). Additionally, samples X4_OA, X6_OA and X3_OA group separately from the other OA samples. Using these un-adjusted p-value DEGs, a range of significant ($p<0.01$) Kyoto Encyclopaedia of Genes and Genomes (KEGG) perturbed pathways in IA are noted (Fig. 5.17). Although under- and over-expressed KEGG pathways were analysed, the under-expressed fell short of any statistical acceptability (data not shown). Encouraging results of KEGG analyses include, but are not limited to, cytokine-cytokine receptor interaction, TNF signalling pathway, NF-kappa B signalling pathway, NOD-like receptor signalling, chemokine signalling and rheumatoid arthritis. All pathways reaching adjusted p-value <0.01 are shown in Appendices 5.7 – 5.34. KEGG pathway maps help to demonstrate how genes contribute to a particular pathway.

All of these analyses were repeated, removing the PsA sample from the IA disease group to reduce biological variation (data not shown). However, little difference in results were noted, and the PsA sample was included for all remaining analyses.

A

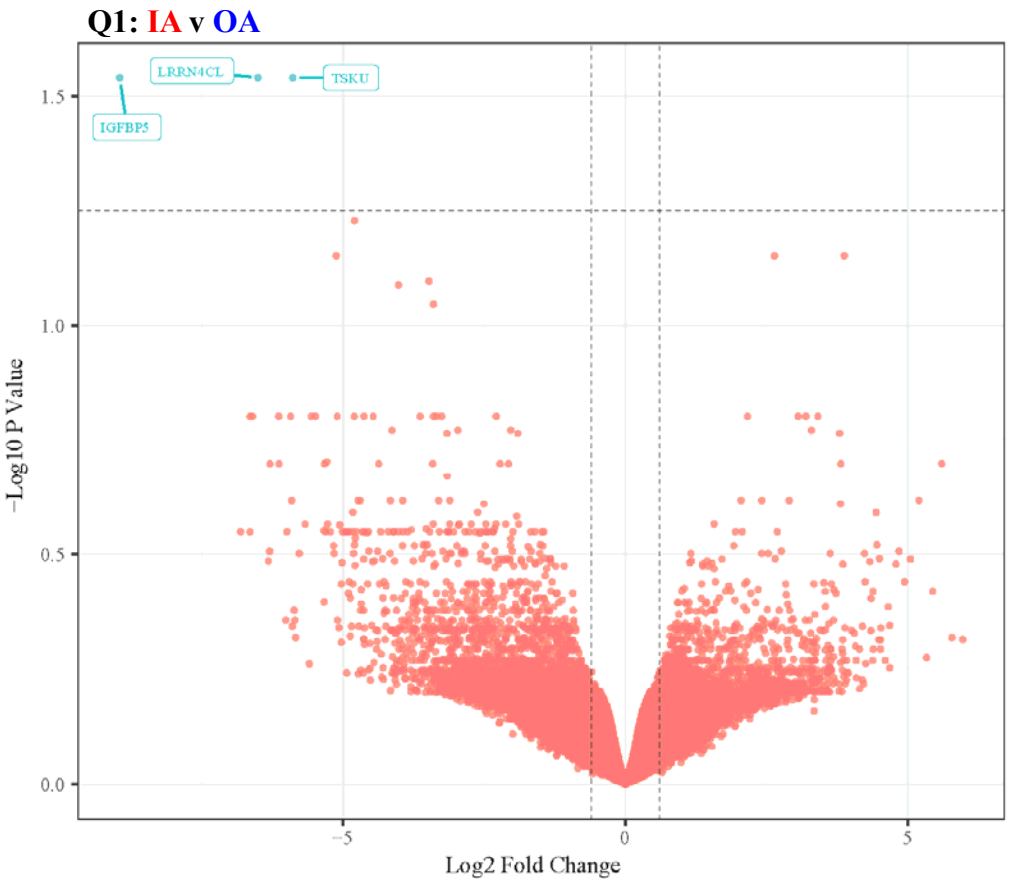

B

Gene	logFC	adj.P.Val
IGFBP5	-8.95887	0.028838
LRRN4CL	-6.51062	0.028838
TSKU	-5.89402	0.028838

Table 5.2: Question 1 DEGs

C

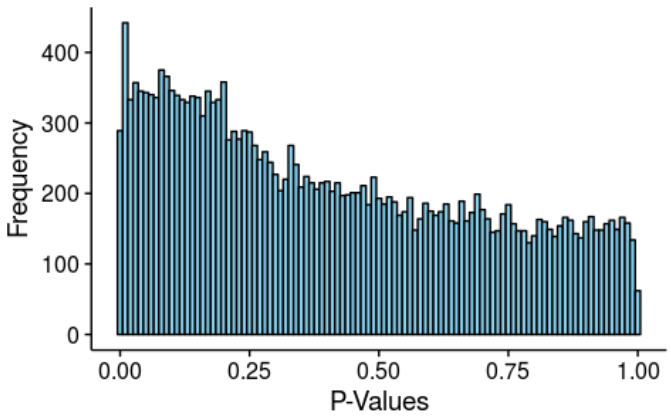

Figure 5.13: Question 1 (IA v OA) differential gene expression analyses
RNA-sequencing of synovial macrophages and data analyses were conducted following methods described in Chapter 2. **A:** Volcano plot identifying DEGs (>1.5-fold change; p<0.05, multiple test corrected). **B:** Table (5.2) of DEGs, log fold change and adjusted p-value from Question 1. **C:** p-value distribution of all DEGs from Question 1.

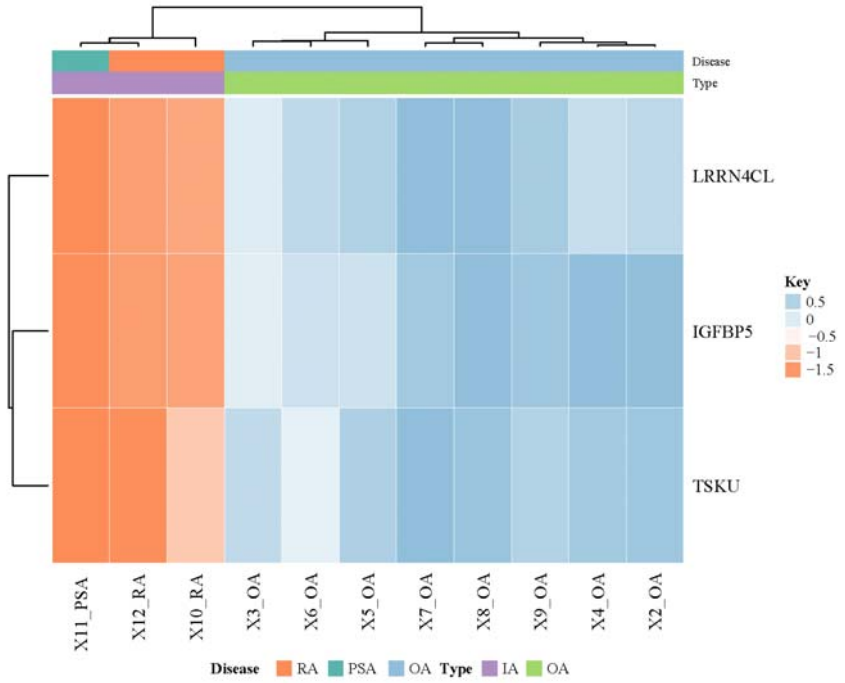

Figure 5.14: Heat map visualisation of DEGs from Question 1 (IA v OA)
RNA-sequencing of synovial macrophages and data analyses were conducted following methods described in Chapter 2. A hierarchical clustering heat map based on DEGs (>1.5-fold change; p<0.05, multiple test-corrected) from Question 1. Colours indicate gene-wise fold-change across 11 samples as per key (right). Top colour bar indicates disease group and type as per key (bottom).

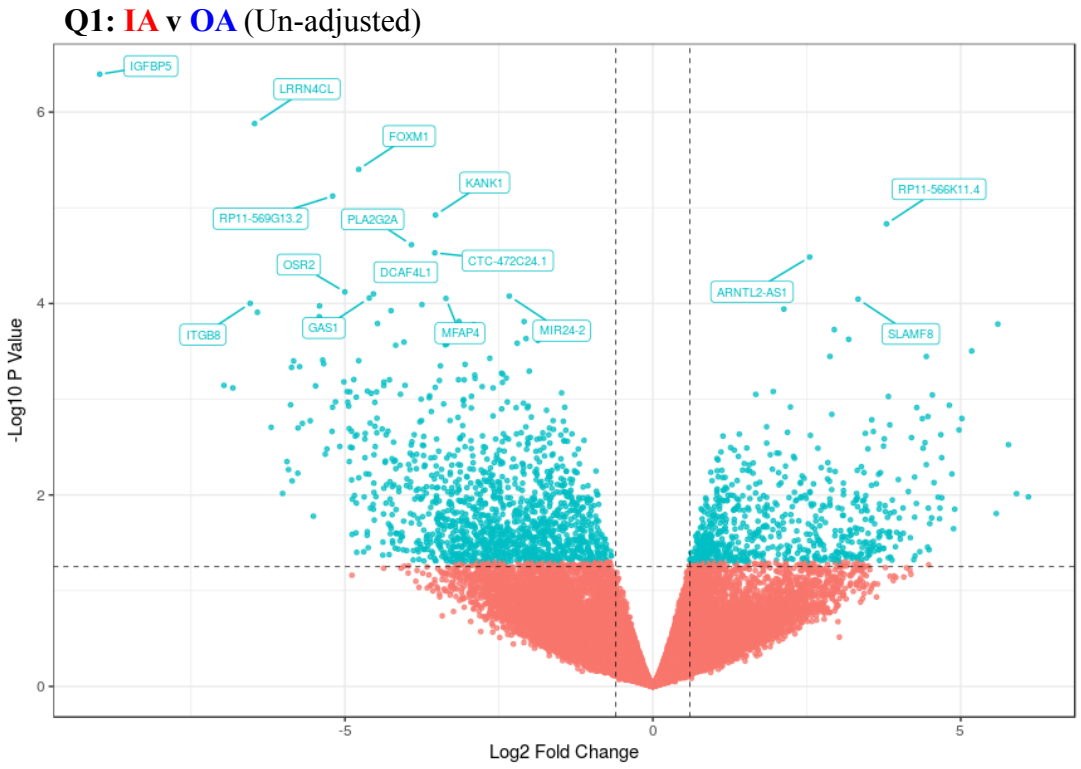

Figure 5.15: Un-adjusted differential gene expression analyses of Question 1 (IA v OA)
RNA-sequencing of synovial macrophages and data analyses were conducted following methods described in Chapter 2. Volcano plot identifying DEGs (>1.5-fold change; p<0.05, no multiple test correction).

Figure 5.16: Heat map visualisation of all DEGS from Question 1 (IA v OA)
RNA-sequencing of synovial macrophages and data analyses were conducted following methods described in Chapter 2. A hierarchical clustering heat map based on DEGs (>1.5-fold change) from Question 1. Colours indicate gene-wise fold-change across 11 samples as per key (right). Top colour bar indicates disease group and type as per key (bottom).

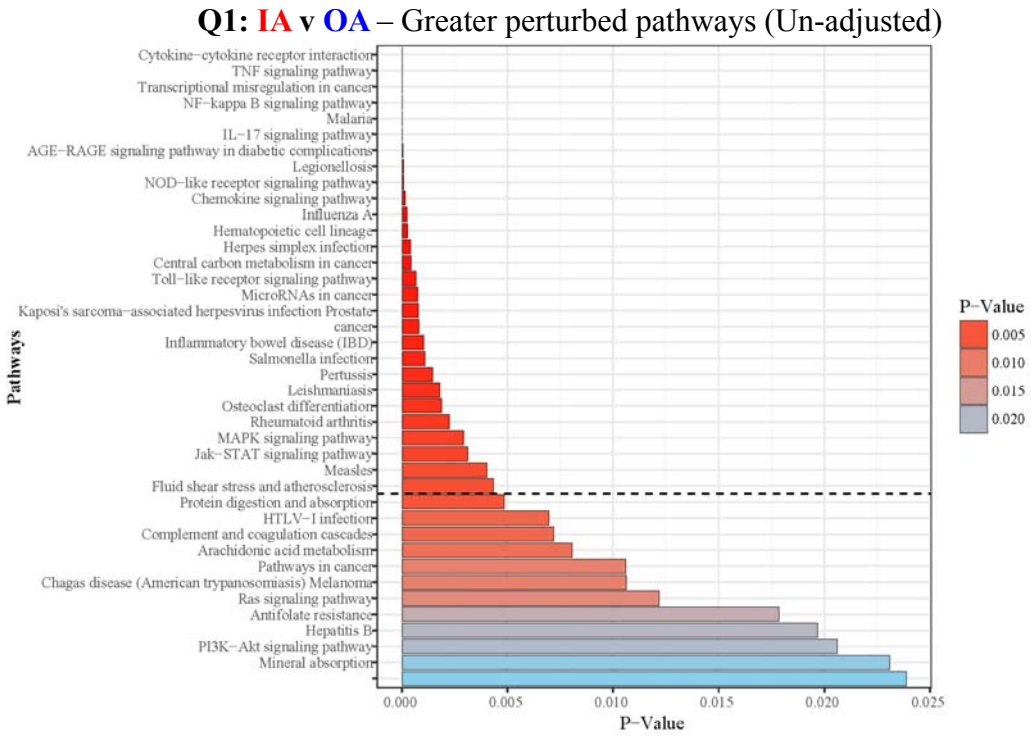

Figure 5.17: KEGG pathway analyses of un-adjusted DEGs from Question 1 (IA v OA)
RNA-sequencing of synovial macrophages and data analyses were conducted following methods described in Chapter 2. Perturbed KEGG pathways based upon DEGs from Question 1 (>1.5-fold change; p<0.05, no multiple test correction). Colour indicates p-value of pathway as per key.

5.5.5 *Identification of OA subgroups*

When examining the top 500 variably expressed genes between all samples, two distinct clusters are present (Fig. 5.18 A). One cluster contains the IA samples with X4_OA, X6_OA and X3_OA. The other group consists of the remaining OA samples. This segregation of OA samples remains true when removing IA samples from the analyses (Fig. 5.18 B), and when reducing to only the top 25 variable genes (Fig. 5.18 C). Using flow cytometry data acquired during fluorescence-activated cell sorting of these samples, percentages of cell subsets were calculated using methods discussed in Chapter 4. When these values are visualised in a heat map, hierarchical clustering of these same subgroups is again present (Fig. 5.18 D).

X3_OA, X4_OA and X6_OA, were also clustered closer to the IA samples in PCA and MDS plot analyses, based on the leading dimension (Fig. 5.10). To address the heterogeneity present with the OA group, I split the OA samples into two subgroups for the remaining analyses (Table 5.3). Contrasts were designed for further differential gene expression analysis of these subgroups (Table 5.4). Samples X3_OA, X4_OA and X6_OA that clustered closely to the IA samples are named group OA_1. Conversely, samples X2_OA, X5_OA, X7_OA, X8_OA and X9_OA that clustered distantly from the IA samples are named group OA_0.

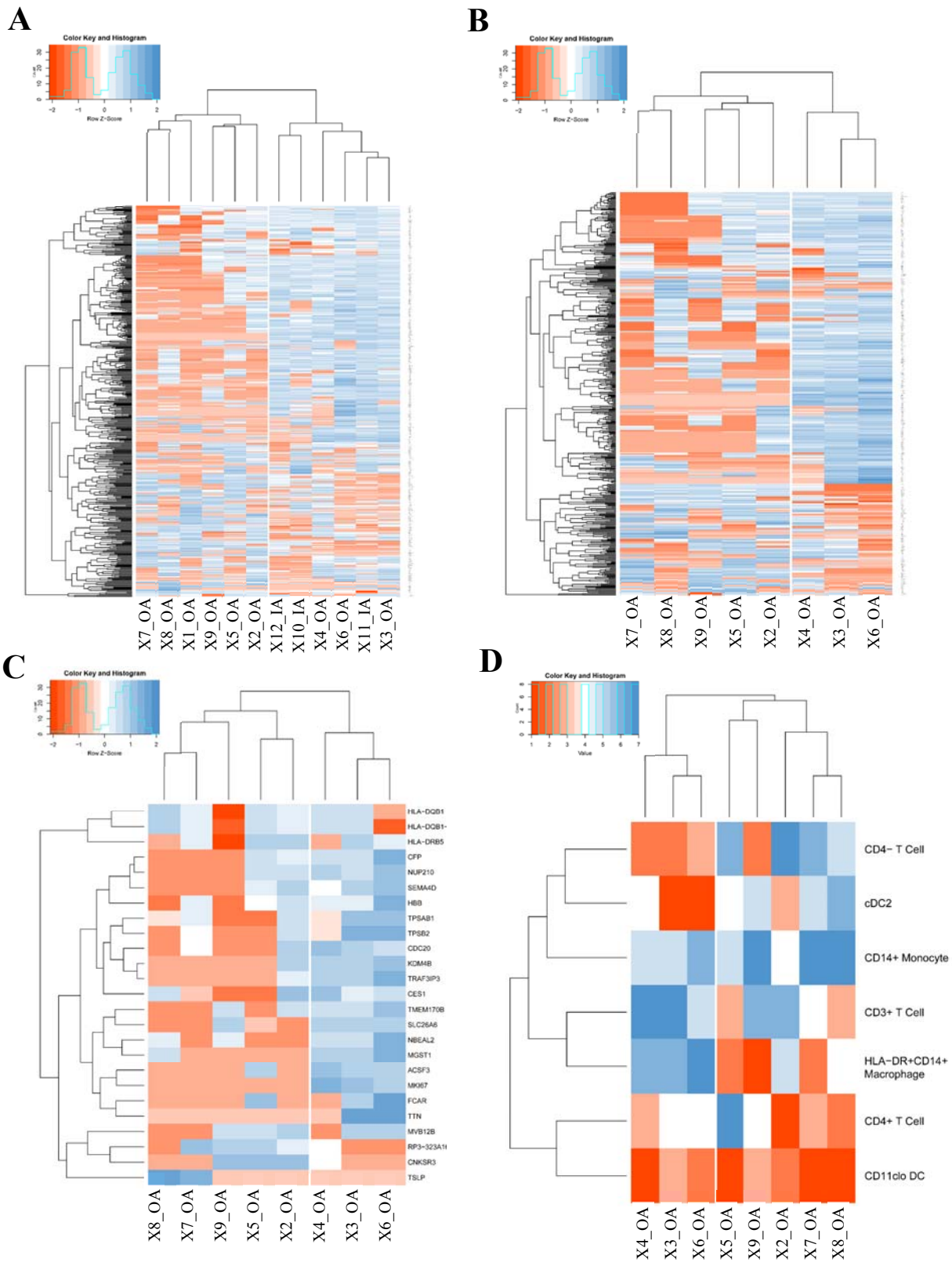

Figure 5.18: Identification of OA subgroups in RNA-seq and flow cytometry data sets
RNA-sequencing of synovial macrophages and data analyses were conducted following methods described in Chapter 2. Identification of cell subsets by flow cytometry was conducted following techniques described in Chapter 4. **A:** Hierarchical clustering heat map of the top 500 variable genes across all samples. **B:** Hierarchical clustering heat map of the top 500 variable genes across OA samples. **C:** Hierarchical clustering heat map of the top 25 variable genes across OA samples. Colours indicate gene-wise expression across samples as per key. **D: H**ierarchical clustering heat map of relative percentage (% of $CD45^{+}$) of cell subsets in samples. Colours indicate percentage across samples as per key.

Group	Sample
IA	X10_IA
	X11_IA
	X12_IA
OA_0	X2_OA
	X5_OA
	X7_OA
	X8_OA
	X9_OA
OA_1	X3_OA
	X4_OA
	X6_OA

Table 5.3: Re-designed sample grouping for differential gene expression analysis contrasts

Question	Comparison
Q1	IA v OA
Q2	OA_1 v IA
Q3	OA_0 v IA
Q4	OA_0 v OA_1

Table 5.4. Question contrast designs for differential gene expression analyses

5.5.6 *OA_1 v IA (Question 2)*

In previous analyses, OA_1 clustered closely with IA, and therefore differential gene expression analyses was unlikely to generate a great number of significant DEGs. Indeed, a small number of significant DEGs were observed (>1.5-FC; $p<0.05$, multiple test corrected) (Fig. 5.19). The volcano plot visualisation shows a high degree of striation, which suggest poor calculation of p-values (Fig. 5.19 A). This is often due to poor design contrast, incorrect hypotheses, or insufficient data. Poor p-value distribution was also observed (Fig. 5.19 C). This showed a bimodal and conservative distribution with a peak present at both the low and high end of the spectrum. These observations are likely due to the similarity of the two groups being tested. Significant DEGs are displayed in a heat map, which clusters into IA, OA_0 and OA_1 (Fig. 5.20). *IGFBP5* and *LRRN4CL* are under expressed in the IA group, as they were in Question 1. Using un-adjusted p-values, KEGG pathway analyses was repeated (Fig. 5.21). As there were still a relatively small number of DEGs, only 9 significant (<0.01) perturbed KEGG pathways were discovered. Full pathways are shown in Appendices 5.35 – 5.43.

A

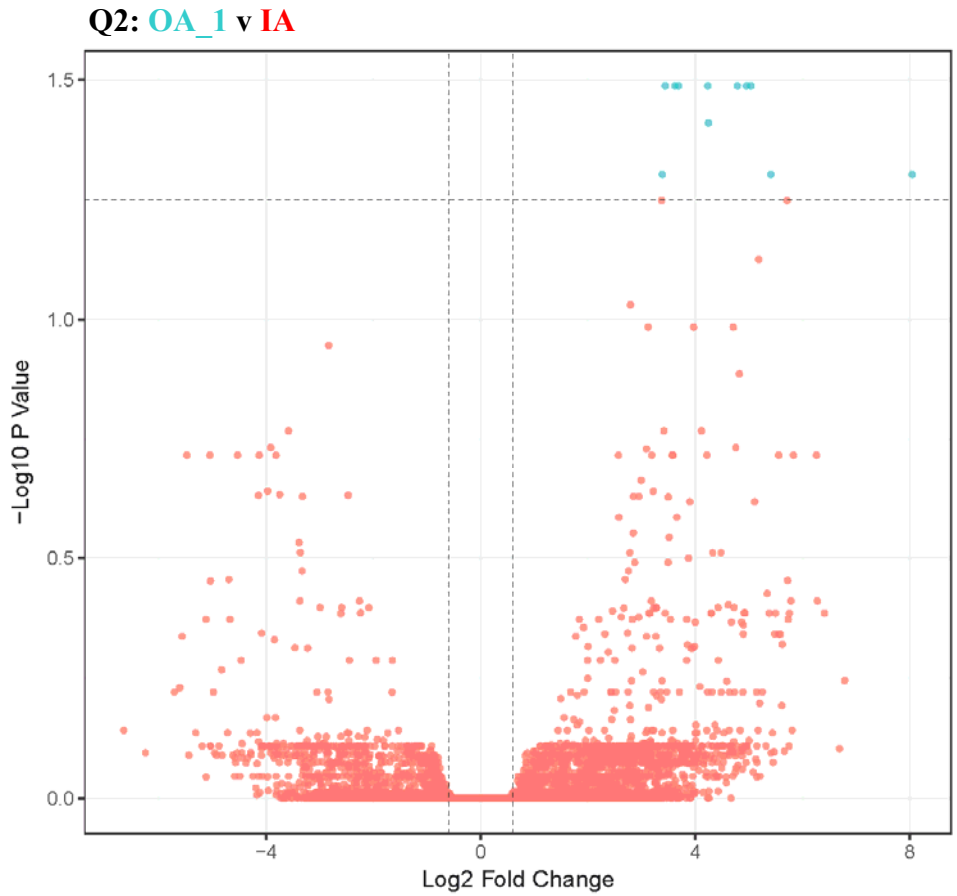

B

Gene	logFC	adj.P.Val
E2F8	5.039462	0.032499
CKAP2L	4.955639	0.032499
TMEM98	4.785574	0.032499
ZFP28	4.235747	0.032499
RSPO2	3.68798	0.032499
RP11-107E5.3	3.619163	0.032499
HOXA10-AS	3.442325	0.032499
HIST1H2AH	4.247155	0.038835
IGFBP5	8.047903	0.04976
LRRN4CL	5.409065	0.04976
RP11-57G10.8	3.386775	0.04976

Table 5.5: Question 2 DEGs

C

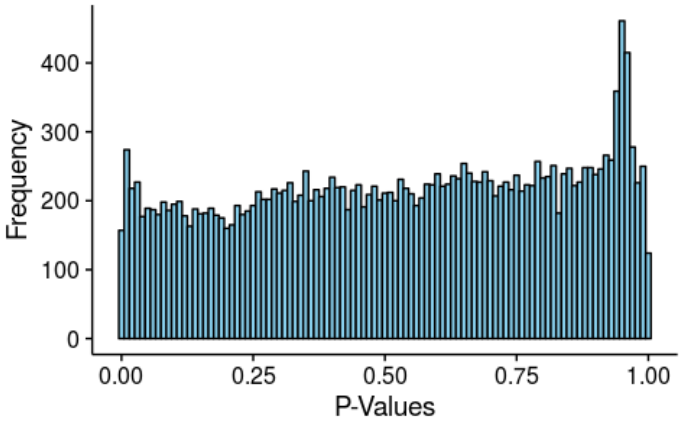

Figure 5.19: Question 2 (OA_1 v IA) differential gene expression analyses
RNA-sequencing of synovial macrophages and data analyses were conducted following methods described in Chapter 2. **A:** Volcano plot identifying DEGs (>1.5-fold change; $p<0.05$, multiple test corrected). **B:** Table (5.5) of DEGs, log fold change and adjusted p-value from Question 2. **C:** P-value distribution of all DEGs from Question 2.

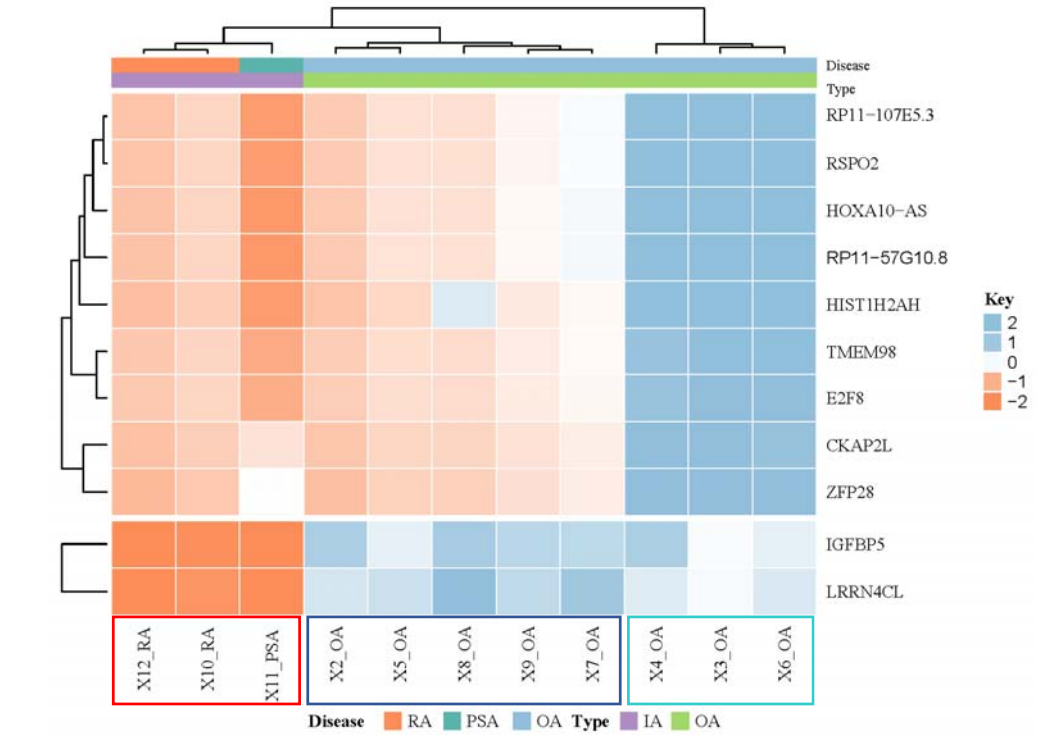

Figure 5.20: Heat map visualisation of DEGs from Question 2 (OA_1 v IA)
RNA-sequencing of synovial macrophages and data analyses were conducted following methods described in Chapter 2. A hierarchical clustering heat map based on DEGs (>1.5-fold change; p<0.05, multiple test-corrected) from Question 2. Colours indicate gene-wise fold-change across 11 samples as per key (right). Top colour bar indicates disease group and type as per key (bottom).

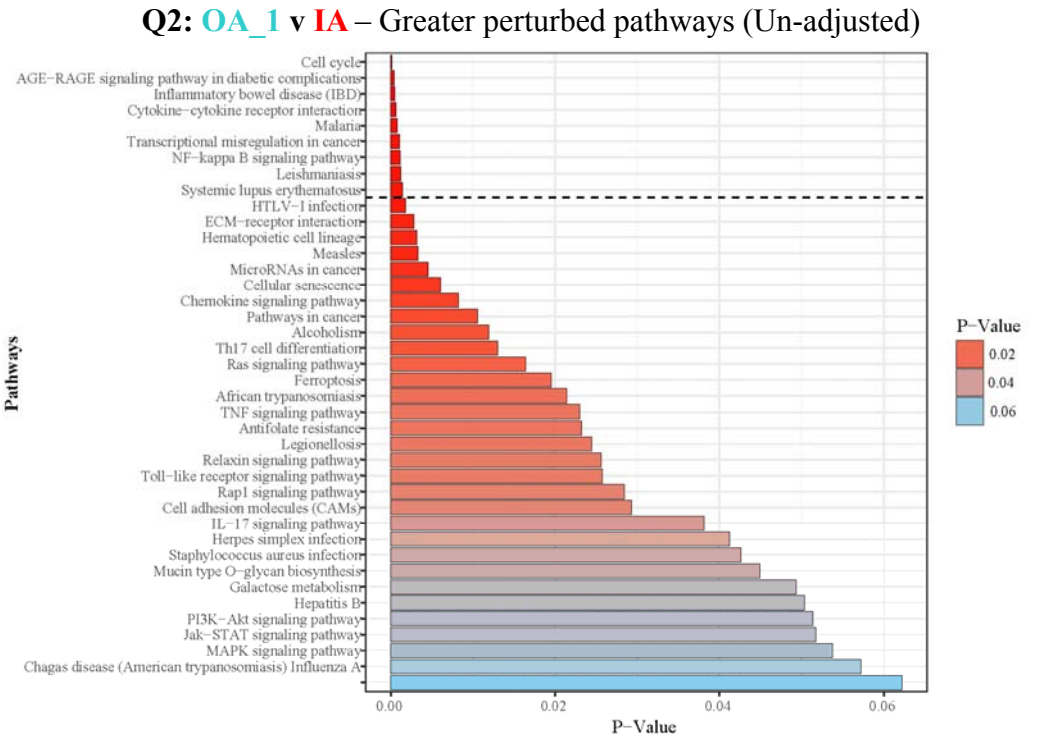

Figure 5.21: KEGG pathway analyses of un-adjusted DEGs from Question 2 (OA_1 v IA)
RNA-sequencing of synovial macrophages and data analyses were conducted following methods described in Chapter 2. Perturbed KEGG pathways based upon DEGs from Question 2 (>1.5-fold change; p<0.05, no multiple test correction). Colour indicates p-value of pathway as per key.

5.5.7 *OA_0 v IA (Question 3)*

I next carried out comparisons on the most distant groups, OA_0 and IA. Differential gene expression analyses yielded 138 DEGs (>1.5-FC; p<0.05, multiple test corrected) (Fig. 5.22). The p-value distribution for this question demonstrates consistent anti-conservative distribution (Fig. 5.22 C). When visualised in a heat map, three distinct groups are clustered matching those found in previous analyses (Fig. 5.23). Despite a higher number of DEGs, and a better statistical certainty in the question, KEGG pathway analyses was again conducted using un-adjusted p-values (Fig. 5.24). 15 significant (<0.01) perturbed KEGG pathways were discovered. All pathways reaching adjusted p-value <0.01 are shown in Appendices 5.44 – 5.58.

Owing to the greater number of significantly DEGs, gene set enrichment analyses could be performed using gene ontology database (GO). This used the adjusted p-values, and therefore has higher statistical significance than previous exploratory KEGG analyses. The p-value distribution of these GO terms demonstrated anti-conservative distribution (Appendix. 5.3). The DEGs and GO terms can then be linked using a Circos plot (Fig. 5.26). Circos plots visualise data in a circular layout, allowing the exploration between genes and GO term relationships. This demonstrates numerous genes involved in extracellular organisation, cartilage development, in addition to an array of other GO terms. In particular, it can be seen that individual genes such as *IGFBP5* contribute to a range of GO terms. In contrast, genes such as *TSKU* and *GPRC5A* contribute to a singular or <3 GO terms. When plotting biological process GO terms in a network visualisation, it is indicated that the gene *SMAD3* plays a role in many of these pathways (Fig. 5.26 A). Furthermore, when plotting these same networks in a different formation, it can be highlighted that the Extracellular Matrix Organisation pathway has the most interlinking roles with many of these additional pathways and genes (Fig. 5.26 B). Similarly, when plotting molecular function GO terms, the integrin binding and related pathways association with a smaller group of genes can be examined (Fig. 5.27).

A

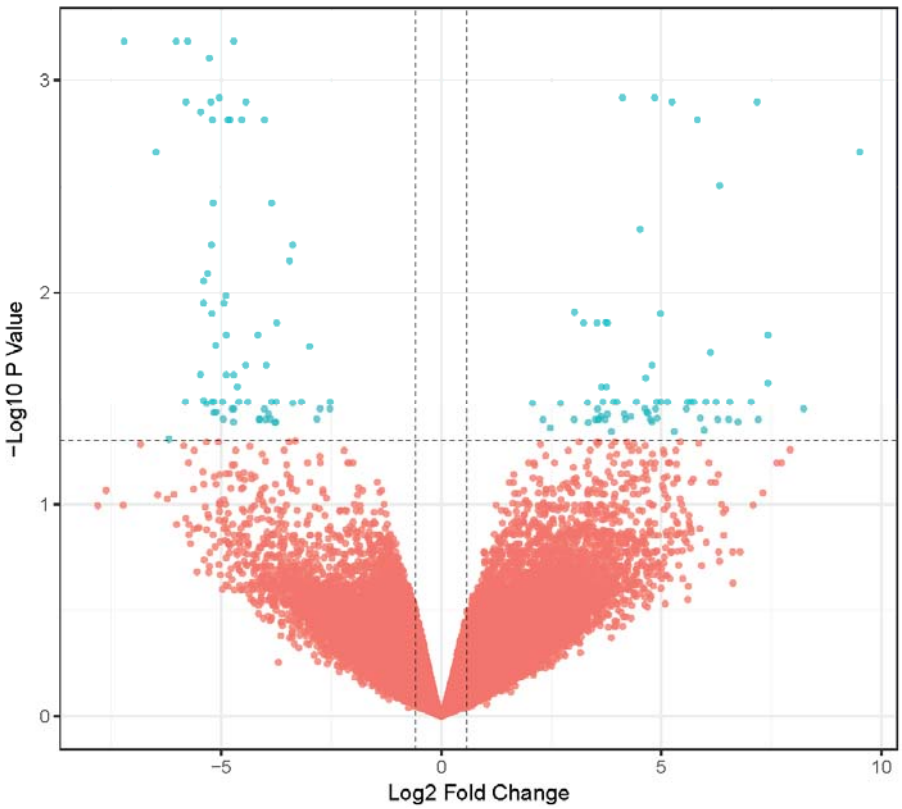

B

Gene	logFC	adj.P.Val
SLC25A29	-7.20296	0.000654
STOML1	-6.02295	0.000654
TRUB1	-5.76153	0.000654
CTRL	-4.71457	0.000654
TIGD6	-5.26707	0.000784
AC074117.10	-5.0431	0.001205
RP11-525G13.2	4.845674	0.001205
RP4-583P15.16	4.115736	0.001205
LRRN4CL	7.171548	0.001263
RP11-401P9.5	-5.80079	0.001263
AC097468.7	5.241024	0.001263
BAIAP2-AS1	-5.23265	0.001263
RP11-400F19.6	-4.43924	0.001263
DDX52	-5.46376	0.00141
RP11-569G13.2	5.816607	0.001532
CNOT3	-5.19758	0.001532
CIC	-4.84671	0.001532
SNAPC4	-4.79987	0.001532
C19orf35	-4.53139	0.001532
ORC6	-4.01449	0.001532
IGFBP5	9.505449	0.002177
FBXO31	-6.48117	0.002177
TSKU	6.32016	0.003119
ZNF202	-5.18207	0.003777
TMEM147-AS1	-3.85408	0.003777

Table 5.6: Question 3 DEGs

C

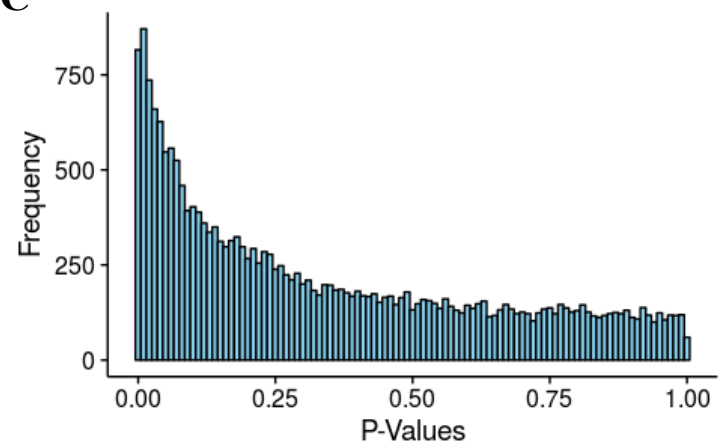

Figure 5.22: Question 3 (OA_0 v IA) differential gene expression analyses
RNA-sequencing of synovial macrophages and data analyses were conducted following methods described in Chapter 2. **A:** Volcano plot identifying DEGs (>1.5-fold change; p<0.05, multiple test corrected). **B:** Table (5.6) of DEGs, log fold change and adjusted p-value from Question 3. **C:** P-value distribution of top 25 (ordered by p-value) DEGs from Question 3.

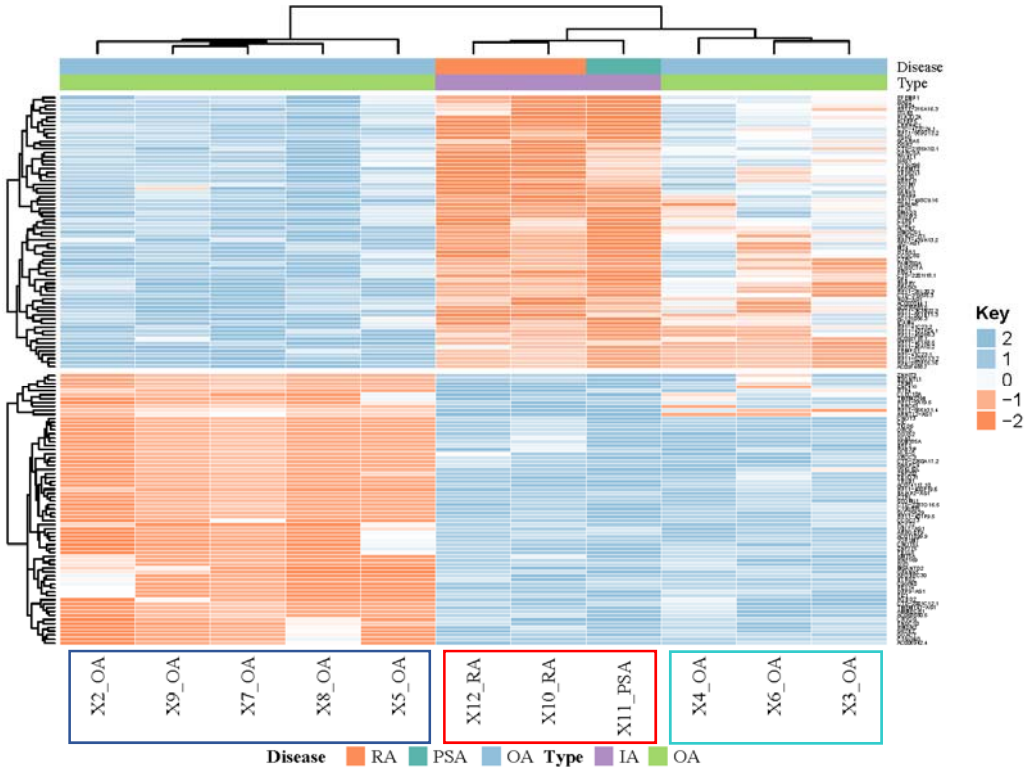

Figure 5.23: Heat map visualisation of DEGs from Question 3 (OA_0 v IA)
RNA-sequencing of synovial macrophages and data analyses were conducted following methods described in Chapter 2. A hierarchical clustering heat map based on DEGs (>1.5-fold change; p<0.05, multiple test-corrected) from Question 3. Colours indicate gene-wise fold-change across 11 samples as per key (right). Top colour bar indicates disease group and type as per key (bottom).

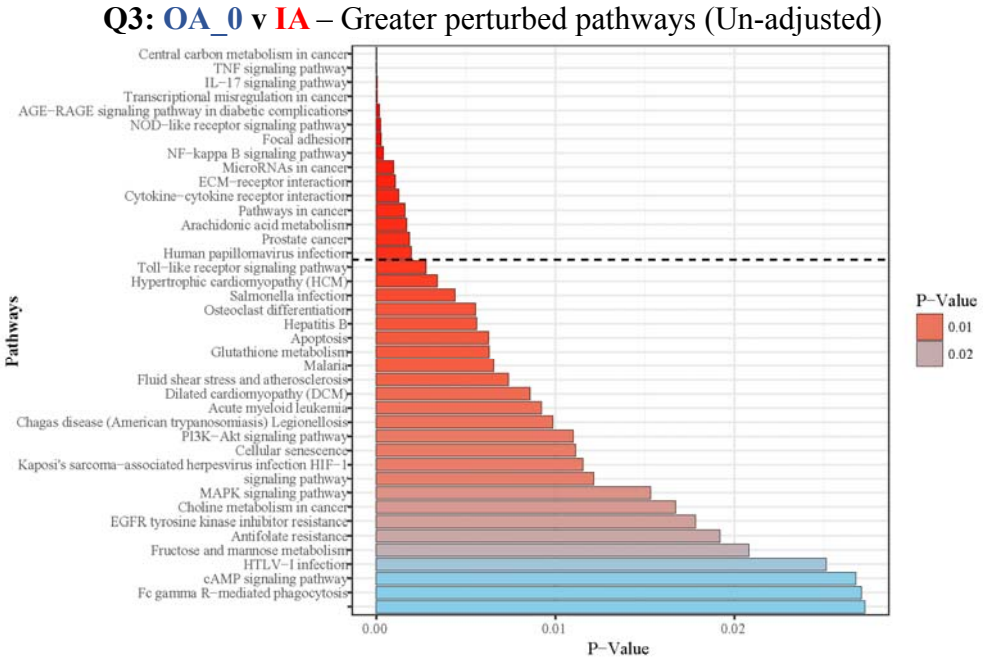

Figure 5.24: KEGG pathway analyses of un-adjusted DEGs from Question 3 (OA_0 v IA)
RNA-sequencing of synovial macrophages and data analyses were conducted following methods described in Chapter 2. Perturbed KEGG pathways based upon DEGs from Question 3 (>1.5-fold change; p<0.05, no multiple test correction). Colour indicates p-value of pathway as per key.

Q3: OA_0 v IA – Perturbed GO-terms (Adjusted)

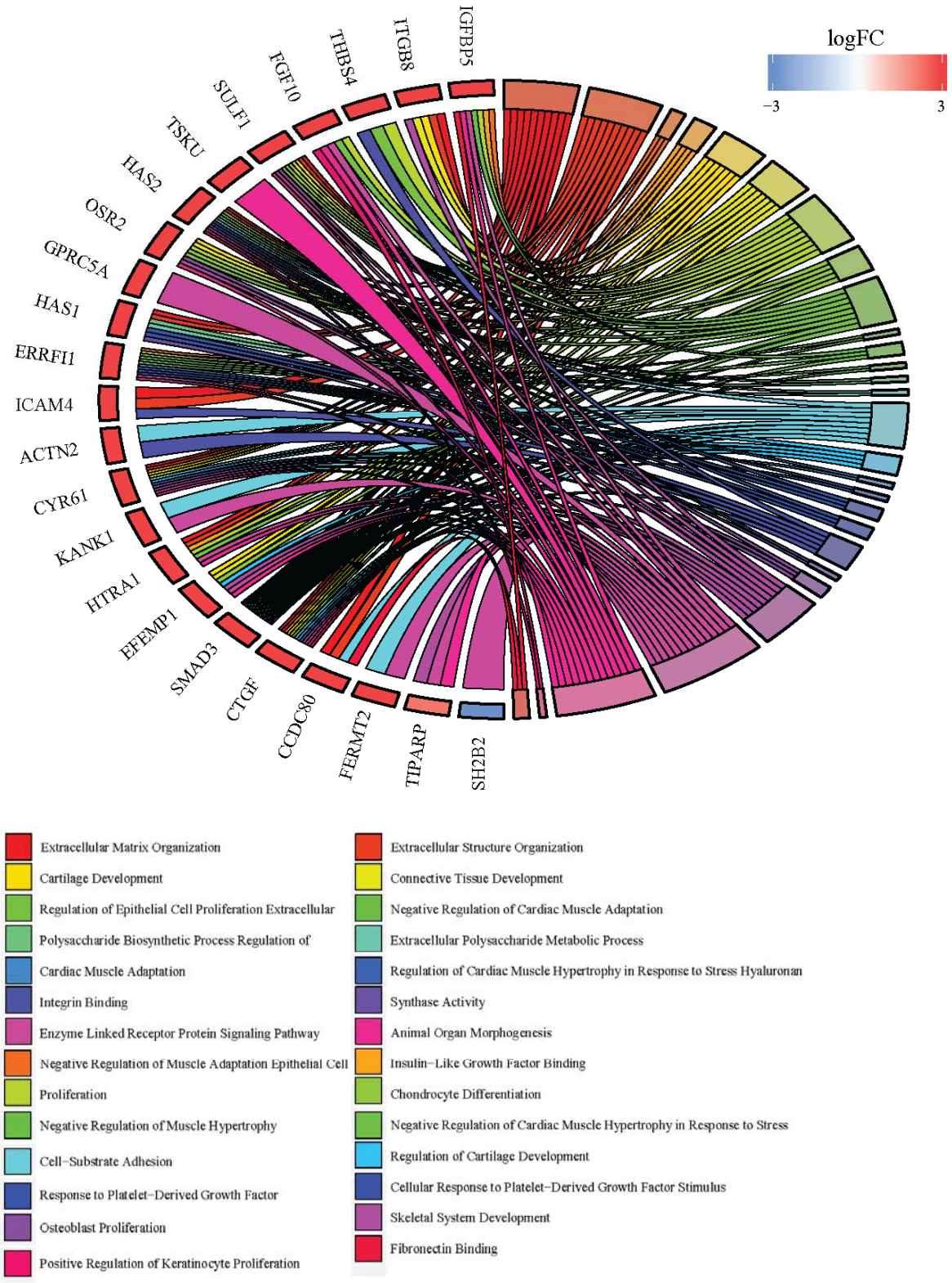

Figure 5.25: GO term circos plot of adjusted DEGs from Question 3 (OA_0 v IA)
RNA-sequencing of synovial macrophages and data analyses were conducted following methods described in Chapter 2. Perturbed GO terms passing adjusted p<0.05 and q-value FDR <0.25, based upon DEGs from Question 3 (>1.5-fold change; p<0.05, multiple test corrected). Pathway colour indicates GO pathway as per key (bottom). Gene colour indicates log fold change as per key (top).

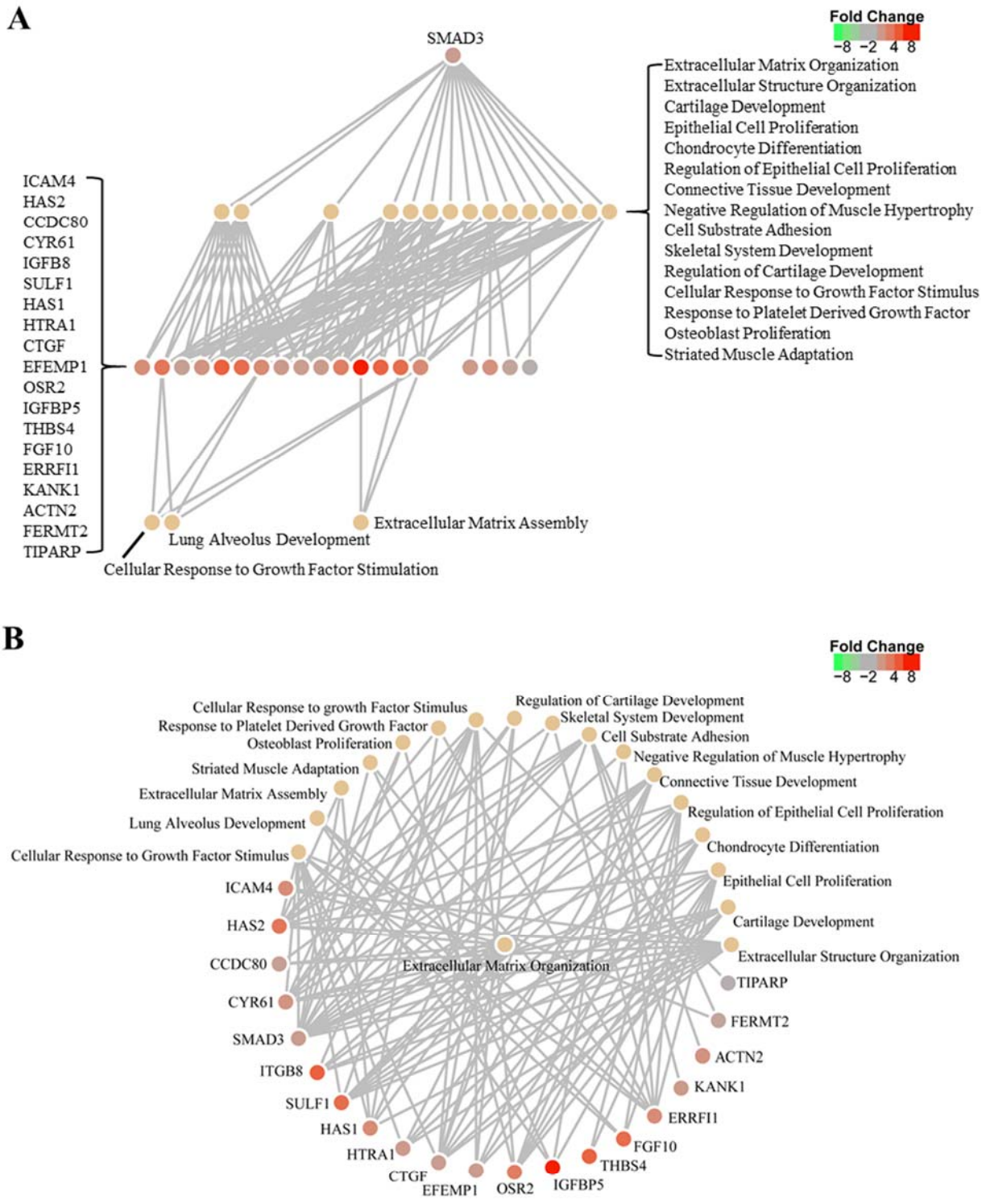

Figure 5.26: Network visualisation of tissue development GO terms from Question 3 (OA_0 v IA)
RNA-sequencing of synovial macrophages and data analyses were conducted following methods described in Chapter 2. Perturbed GO terms passing adjusted p<0.05 and q-value FDR <0.25, based upon DEGs from Question 3 (>1.5-fold change; p<0.05, multiple test corrected). Gene colour indicates fold change as per key. Visualisations utilising tree (**A**) and star (**B**) layouts. Gene and pathway lists are top to bottom representations of nodes in diagram left to right.

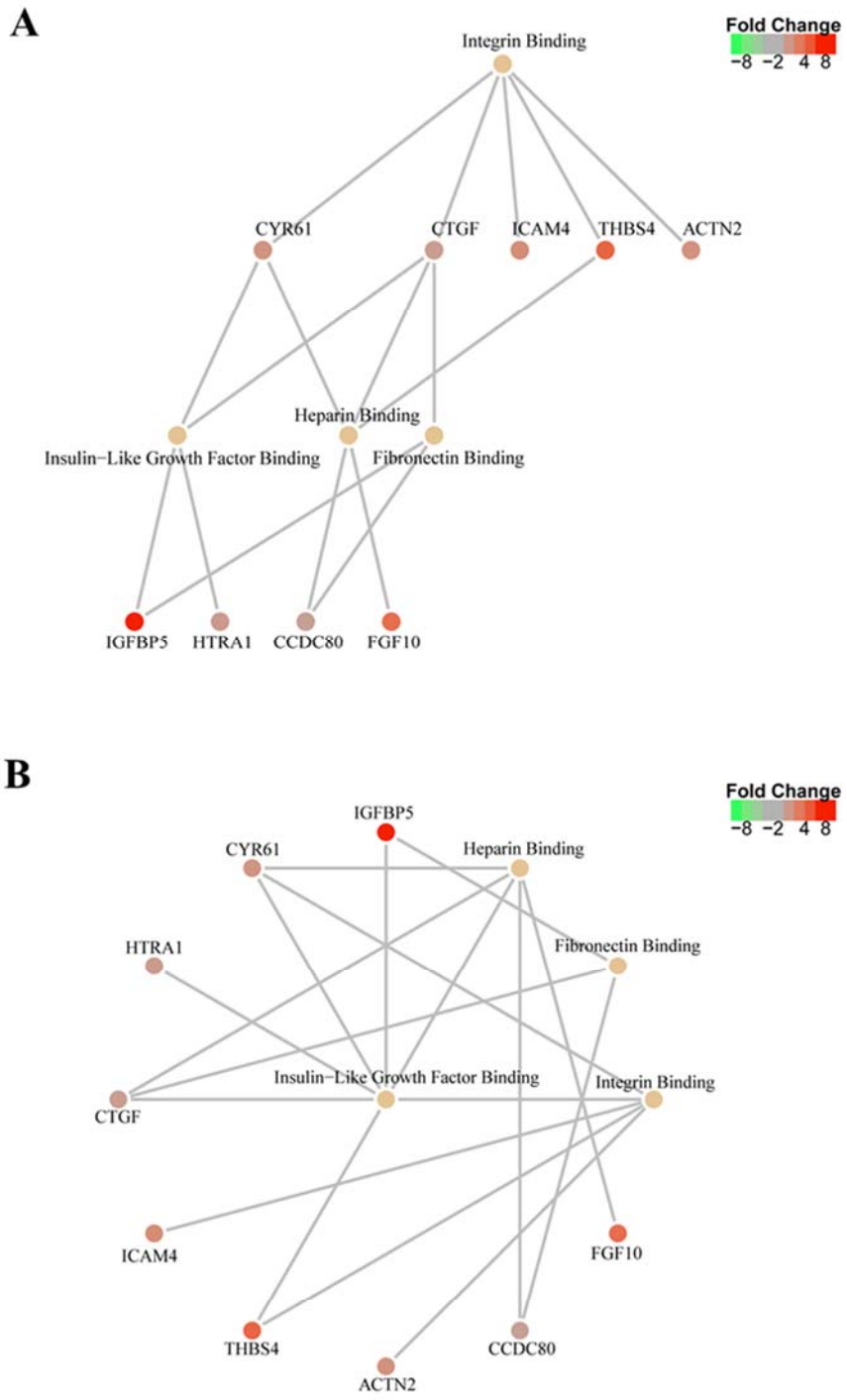

Figure 5.27: Network visualisation of integrin binding GO terms from Question 3 (OA_0 v IA)
RNA-sequencing of synovial macrophages and data analyses were conducted following methods described in Chapter 2. Perturbed GO terms passing adjusted p<0.05 and q-value FDR <0.25, based upon DEGs from Question 3 (>1.5-fold change; p<0.05, multiple test corrected). Gene colour indicates fold change as per key. Visualisations utilising tree (**A**) and star (**B**) layouts.

5.5.8 *OA_0 v OA_1 (Question 4)*

Finally, I compared both OA groups with each other. This yielded the biggest difference, with 155 significantly DEGs identified (>1.5-FC; $p<0.05$, multiple test corrected) (Fig. 5.28). The p-value distribution for this question demonstrates consistent anti-conservative distribution (Fig. 5.28 C). Visible in a heat map, the expression of these genes is highly consistent between both OA_0 and OA_1 (Fig. 5.29). The IA group expression of these genes is mixed. Despite a higher number of DEGs, and a better statistical certainty in the question, KEGG pathway analyses was again conducted using un-adjusted p-values (Fig. 5.30). No pathways meeting a significant threshold of (<0.01) were discovered.

As Question 4 also produced a larger array of significantly DEGs, gene set enrichment analyses was performed using adjusted p-values. The p-value distribution of these GO terms demonstrated anti-conservative distribution (Appendix. 5.4). The DEGs and GO terms can then be linked using a Circos plot (Fig. 5.31). This demonstrates numerous genes involved in cell cycle processes. Of note, *TTK*, *CDT1*, *XRCC3* and *PLK1* have roles in a large number of GO terms. It can be additionally visualised that *ASPM*, *KMT5A* and *KIFC* all have dual roles in mitotic cell cycle and cell cycle check point. When plotting these pathways and associated genes in a network visualisation, it is indicated the gene *CDT1* plays a role in many of these pathways (Fig. 5.32 A). Furthermore, when plotting these same networks in a different formation, it can be highlighted that the Mitotic Cell Cycle pathway has the most interlinking roles with many of these additional pathways and genes (Fig. 5.32 B).

A

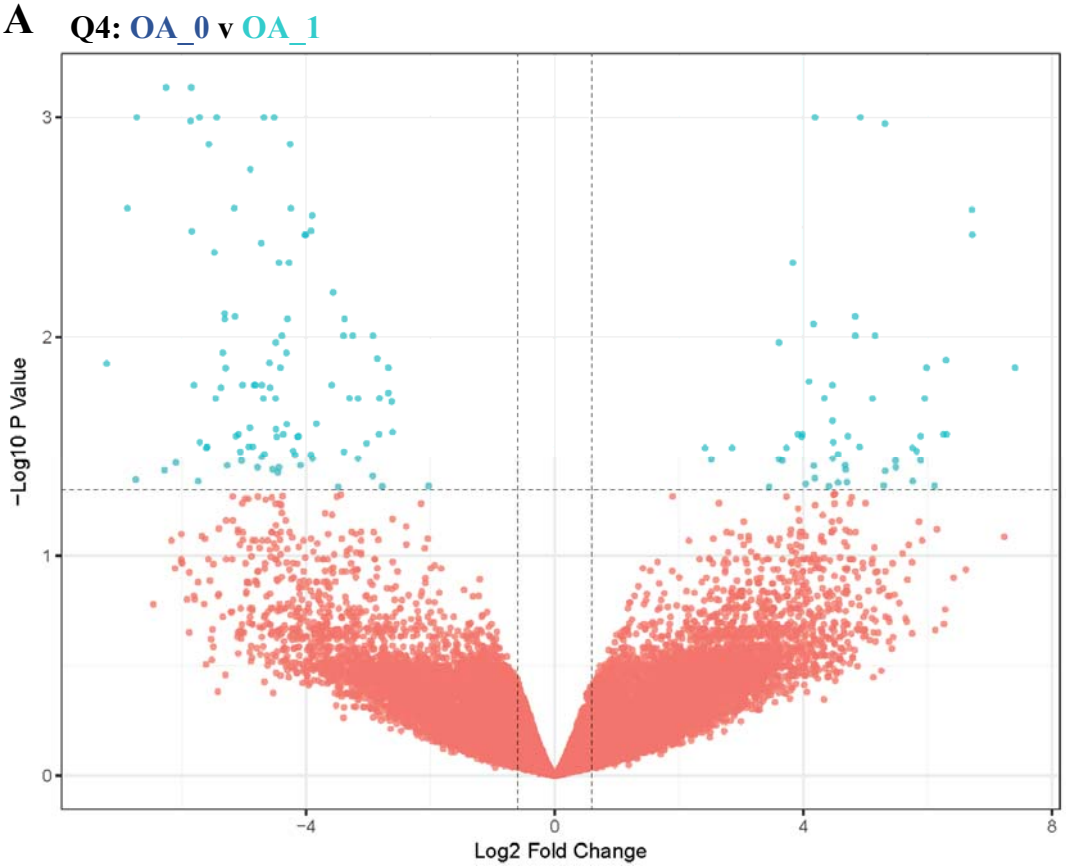

B

Gene	logFC	adj.P.Val
STOML1	-6.25188	0.000733
TIGD6	-5.84678	0.000733
SLC25A29	-6.72308	0.001003
BAIAP2-AS1	-5.71373	0.001003
SNAPC4	-5.43672	0.001003
RP11-525G13.2	4.915431	0.001003
TRUB1	-4.67736	0.001003
CTRL	-4.51275	0.001003
RP4-583P15.16	4.185494	0.001003
DDX52	-5.85665	0.001041
AC097468.7	5.310782	0.001072
CNOT3	-5.5626	0.001328
ORC6	-4.2563	0.001328
CIC	-4.89569	0.001724
BRF1	-6.87174	0.002599
RP11-401P9.5	-5.15452	0.002599
ZFP28	-4.24489	0.002599
SLC13A3	6.710747	0.002638
RP11-400F19.6	-3.90178	0.002801
FAM185A	-3.91765	0.003284
ULK1	-5.83789	0.003308
LPO	6.715284	0.003432
TMEM98	-4.02074	0.003432
AC074117.10	-4.00367	0.003432
CKAP2L	-4.71913	0.003749

Table 5.7: Question 4 DEGs

C

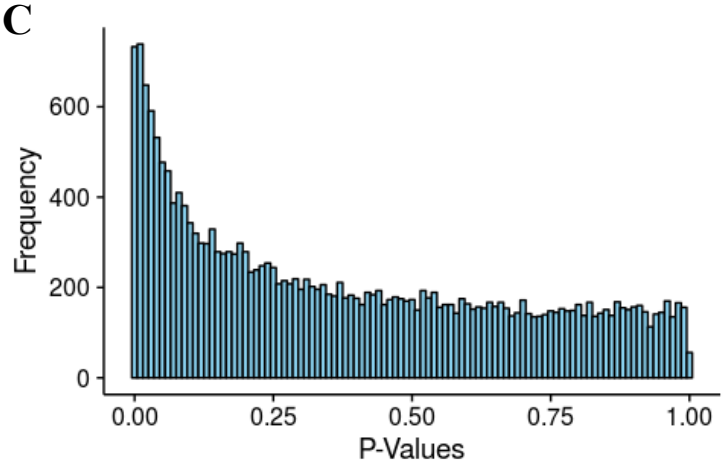

Figure 5.28: Question 4 (OA_0 v OA_1) differential gene expression analyses
RNA-sequencing of synovial macrophages and data analyses were conducted following methods described in Chapter 2. **A:** Volcano plot identifying DEGs (>1.5-fold change; p<0.05, multiple test corrected). **B:** Table (5.7) of DEGs, log fold change and adjusted p-value from Question 4. **C:** p-value distribution of top 25 (ordered by p-value) DEGs from Question 4.

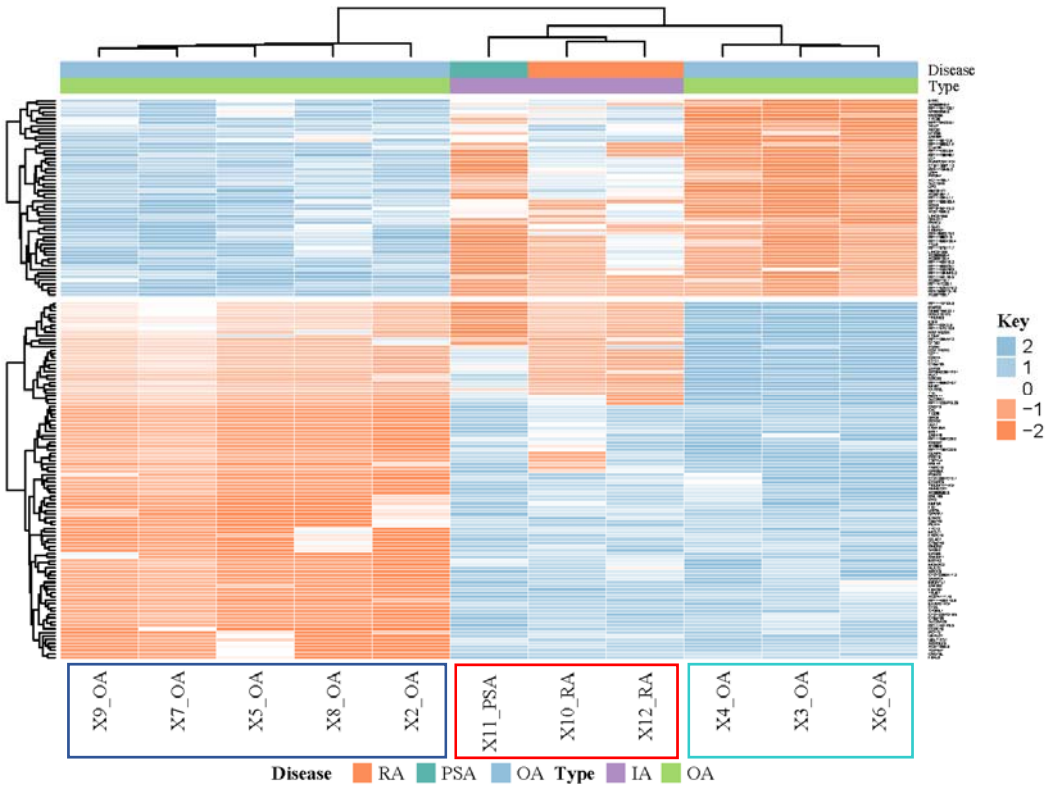

Figure 5.29: Heat map visualisation of DEGs from Question 4 (OA_0 v OA_1)
RNA-sequencing of synovial macrophages and data analyses were conducted following methods described in Chapter 2. A hierarchical clustering heat map based on DEGs (>1.5-fold change; p<0.05, multiple test-corrected) from Question 4. Colours indicate gene-wise fold-change across 11 samples as per key (right). Top colour bar indicates disease group and type as per key (bottom).

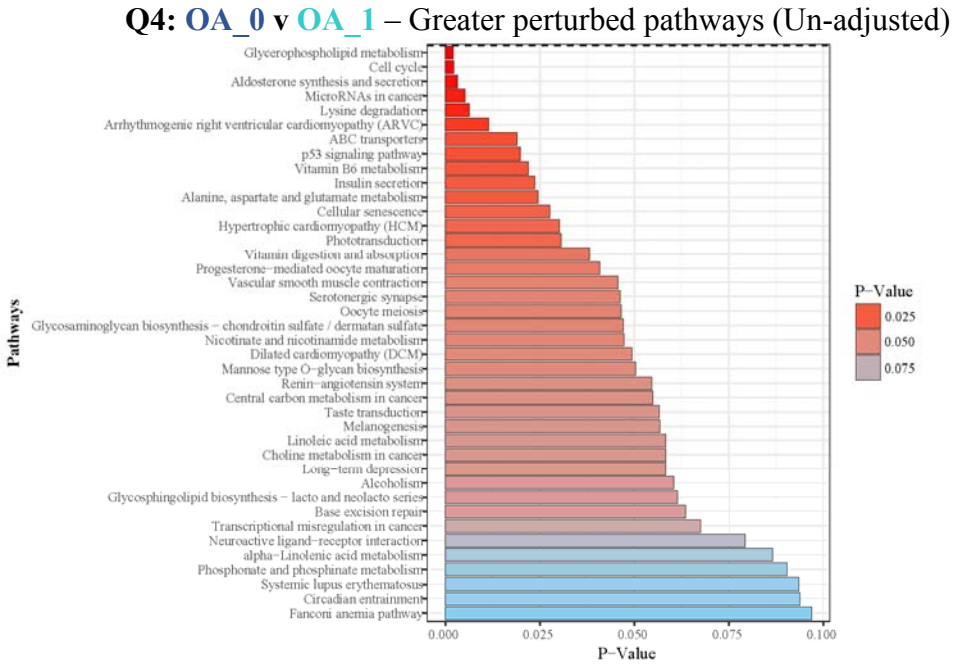

Figure 5.30: KEGG pathway analyses of un-adjusted DEGs from Question 4 (OA_0 v OA_1)
RNA-sequencing of synovial macrophages and data analyses were conducted following methods described in Chapter 2. Perturbed KEGG pathways based upon DEGs from Question 4 (>1.5-fold change; p<0.05, no multiple test correction). Colour indicates p-value of pathway as per key.

Q4: OA_0 v OA_1 – Perturbed GO-terms (Adjusted)

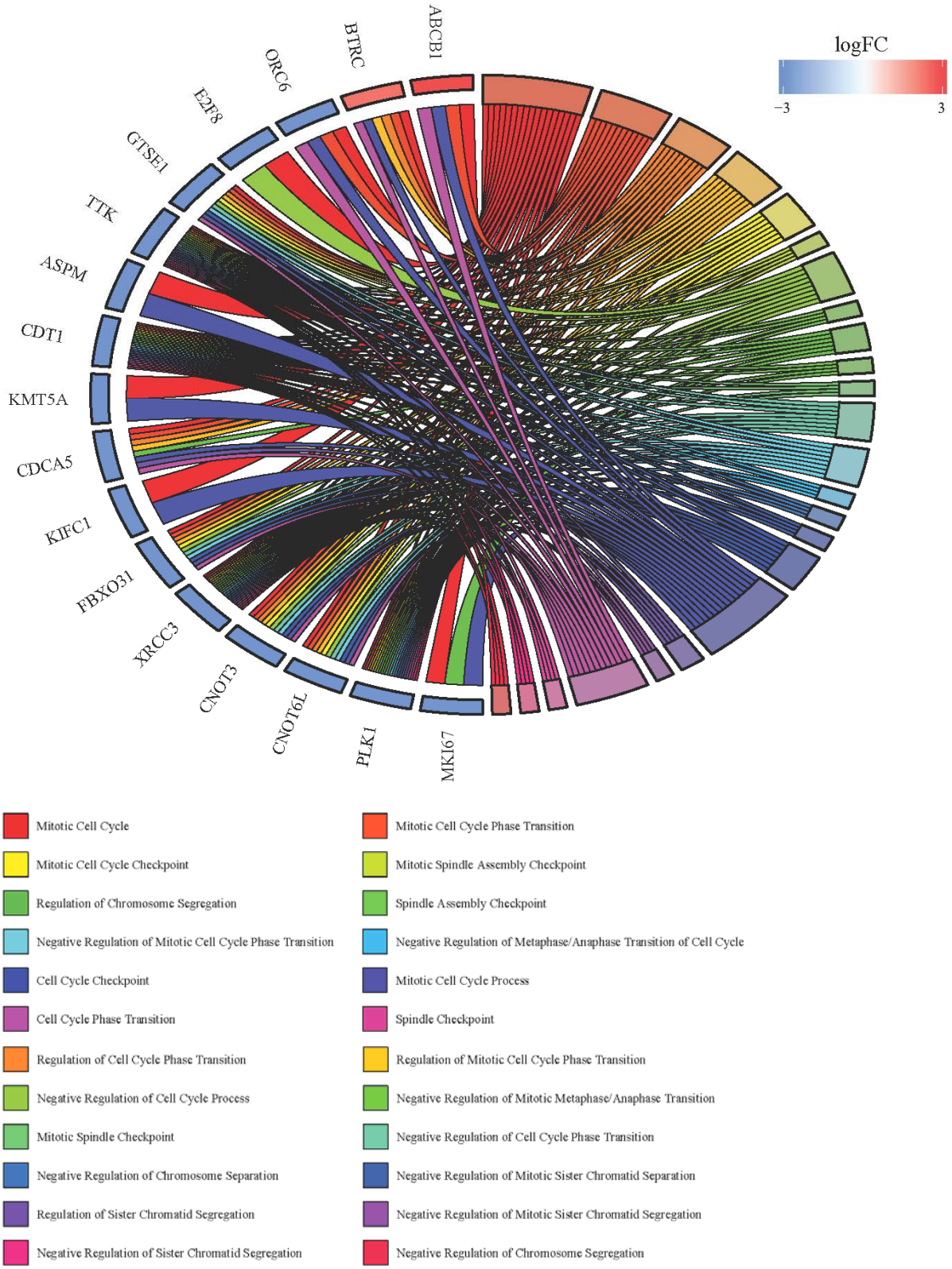

Figure 5.31: GO term circus plot of adjusted DEGs from Question 4 (OA_0 v OA_1)
RNA-sequencing of synovial macrophages and data analyses were conducted following methods described in Chapter 2. Perturbed GO terms passing adjusted p<0.05 and q-value FDR <0.25, based upon DEGs from Question 4 (>1.5-fold change; p<0.05, multiple test corrected). Pathway colour indicates GO pathway as per key (bottom). Gene colour indicates log fold change as per key (top).

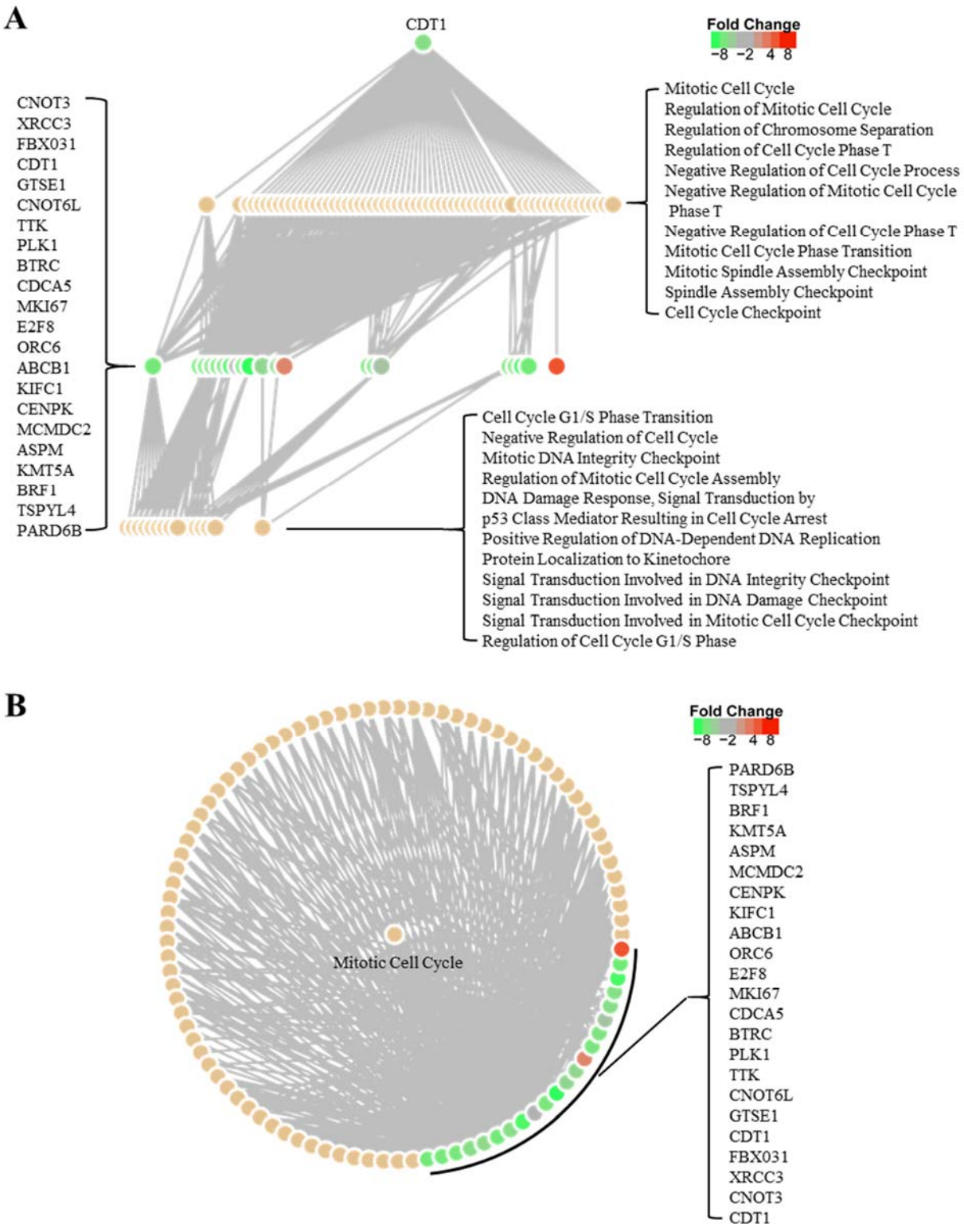

Figure 5.32: Network visualisation of cell cycle GO terms from Question 4 (OA_0 v OA_1)
RNA-sequencing of synovial macrophages and data analyses were conducted following methods described in Chapter 2. Perturbed GO terms passing adjusted p<0.05 and q-value FDR <0.25, based upon DEGs from Question 4 (>1.5-fold change; p<0.05, multiple test corrected). Gene colour indicates fold change as per key. Visualisations utilising tree (**A**) and star (**B**) layouts. **A:** Gene and pathway lists are top to bottom representations of nodes in diagram left to right. **B:** Gene list is representative of nodes in diagram top to bottom. Full pathway list (Appendix 5.4) is representative of nodes in diagram right to bottom, anti-clockwise.

5.5.9 *Overlap*

In order to determine the concordance of DEGs between questions, a Venn diagram was used to visualise the DEGs generated (Fig. 5.33). Between the comparison of whole OA and IA (Question 1), *TSKU* was shared with OA_0 (Fig. 5.33 B). *IGFBP5* and *LRRN4CL* were both differentially expressed in Questions 1-3. However, these two genes were not significantly differentially expressed in Question 4, suggesting they are ubiquitously expressed by all OA samples (Fig. 5.33 C). The remaining genes were exclusive to each question. The 85 DEGs unique to Question 4 exhibited strong cell cycle functional pathways (Fig. 5.33 C). 75 DEGs from Question 3 were exclusive to OA_0, representing extracellular matrix and cartilage development related pathways and SMAD/RUNX functioning (Fig. 5.33 C). 61 DEGs were shared between Question 3 & 4, and although did not have a strong consistent pathways signature, again showed cell cycle related pathways, in addition to RNA III Polymerisation (Fig. 5.33 C).

5.6 Clinical analyses

To assess whether the distribution of samples by gene expression could be explained by clinical factors, a density plot was used to demonstrate these relationships (Fig. 5.34). None of the clinical factors collected demonstrated a log10 variance of 1 (100% variance), and all samples present values above this threshold suggesting negative percentage variance. Although ESR presented with a proportionately large density, this remains relatively low, explaining <15% of variance. Additionally, ESR did not demonstrate a log10 variance of 1. Overall, this co-variate analysis demonstrates that none of the clinical data collected have a substantial explanatory power for the genes measured and variances observed in this data-set.

A

Question	Comparison	DEGs
Q1	IA v OA	3
Q2	OA_1 v IA	11
Q3	OA_0 v IA	138
Q4	OA_0 v OA_1	155

Table 5.8: All question DEGs

B

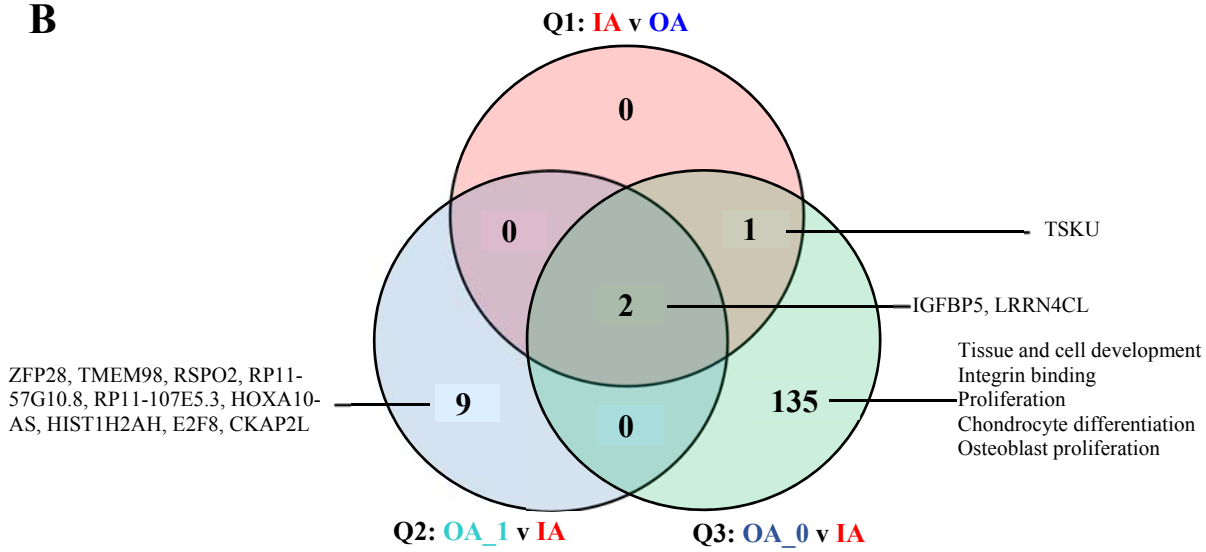

C

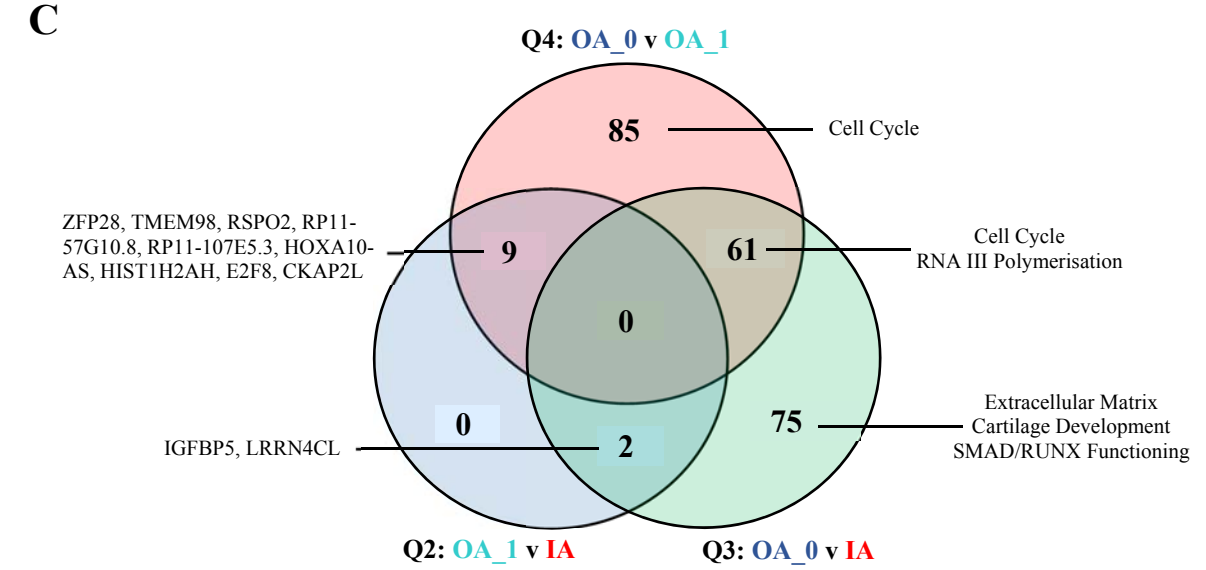

Figure 5.33: Concordance of DEGs identified across all questions
RNA-sequencing of synovial macrophages and data analyses were conducted following methods described in Chapter 2. **A:** Table (5.6) of DEGs, log fold change and adjusted p-value from all questions. **B:** Venn diagram depicting degree of concordance between DEGs (>1.5-fold change; p<0.05, multiple test corrected) identified in questions 1, 2 & 3. **C:** Venn diagram depicting degree of concordance between DEGs (>1.5-fold change; p<0.05, multiple test corrected) identified in Questions 2, 3 & 4.

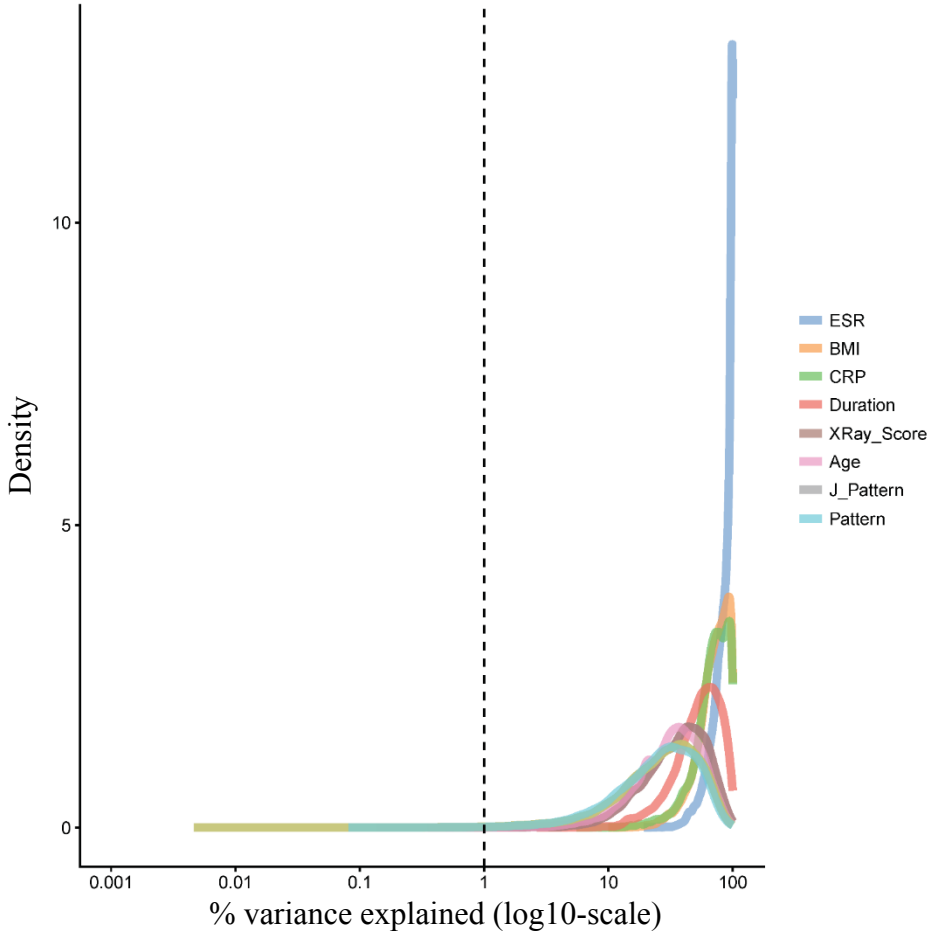

Figure 5.34: Density plot of variance explained by clinical data
Density plot of the percentage variance (log10) normalised counts across all genes. Each line corresponds to a clinical factor and represents the distribution of percentages. Those aligning with the dashed line corresponding to log10 1 on the X axis demonstrate 100% variance. Those with a high proportion of density demonstrate hierarchical clustering of samples based on gene expression data, such as seen in PCA analyses.

5.7 Discussion

Within Chapter 5, I set out to examine the phenotype, function and gene expression of synovial macrophages in OA patients. This encompassed wide-ranging and advanced techniques including, flow cytometry, FACs, *in vitro* assays, RNA-isolation and RNA-sequencing. Through this, I aimed to provide a novel in-depth analysis of synovial macrophages in OA synovial tissue.

The gating strategy for the accurate identification and purification of synovial macrophages had already been developed, discussed in Chapter 4. However, for Chapter 5 I began by testing a gating strategy developed by Professor Matthew Collin for the identification of inflammatory monocyte and macrophage subsets in healthy and inflammatory (graft-versus- host disease; GvHD) dermis. The first method was the identification of an inflammatory monocyte subset. Although my flow cytometry panel was not optimised for this gating strategy, I was still able to identify these monocyte subsets in previously acquired samples. When applied to OA and IA synovium samples, a larger proportion of monocyte '2' were identified in the IA samples compared to OA. This matches the observation seen in healthy versus GvHD dermis. A second strategy allows the identification of resident and inflammatory macrophages based on CD11c expression. This demonstrated a higher proportion of resident macrophages in OA synovium samples and conversely a higher proportion of inflammatory macrophages in IA samples. With the inclusion of auto-fluorescence into this strategy, I was able to eliminate non-auto-fluorescent cell contamination, likely monocytes and DCs. Although I only had data for one additional surface marker for these samples, it was shown that 'inflammatory' macrophages indeed had higher expression of CD86, a co-stimulatory marker often associated with inflammation. This gating strategy may present a novel method that will aid in our understanding of resident macrophages and, potentially, monocyte-derived inflammatory macrophages. As this strategy was recently developed, it was left for future work.

When examining the surface markers within my FACs panel on synovial macrophages, they expressed macrophage- and myeloid-markers and did not express markers associated with other cell types. This aided in confirming the purity of these cell-sorted synovial macrophages. Healthy moMacs expressed higher levels of CD14, CD45, CD16, CD11c and CD4. As this cell type represents a monocyte-derived macrophage, it is interesting to note higher levels of CD11c, the marker used in the previous analyses for the identification of inflammatory macrophages. Furthermore, when assessing a select panel of 'activation' markers, monocyte-derived macrophages also had increased expression of CD172α, CCR2 and CCR7. These have all previously been reported as markers of moMacs, giving me confidence in these data (Italiani

and Boraschi 2014, Yang, Zhang et al. 2014, Bian, Shi et al. 2016). Folate receptor 2 (FOLR2) has been previously used as a marker of activated synovial macrophages in an imaging study (Kraus, McDaniel et al. 2016). Here I measured increased expression in both my moMacs and OA macrophages compared to IA. A similar observation was also recorded for CD206, mannose receptor, which is associated with tissue repair-like M2 macrophages (Martinez and Gordon 2014).

Although care was taken in optimising the isolation and purification of these synovial macrophages, it was important to ensure that these cells were still functional once isolated. Through incubation of macrophages with latex beads, I was able to measure phagocytic capacity by flow cytometry. Using confocal microscopy, I confirmed engulfment of latex beads as opposed to adherence to the cell membrane. Healthy moMacs, IA moMacs and OA synovial macrophages were shown to have a superior capacity of phagocytosis than their DC counterparts. This data overall demonstrated that despite the stresses of mechanical and enzymatic digestion, in addition to FACs, once isolated these macrophages are still functional.

For gene expression analyses, patient cohorts were matched well between disease type with similar age and sex. Differences in BMI, CRP and ESR were deemed acceptable, as these have been identified as known risk factors or disease-specific consequences. The OA group had active OA disease, assessed by KL scoring of radiographic images. The IA group had a low disease activity score of 3.0 (SD: 0.3). However this was close to a moderate disease activity score, classed as between >3.2 and ≤5.1.

Through both MDS and PCA analyses, the three IA samples grouped together, away from the OA samples. However, the OA samples could be split along the leading dimension in all analyses. These analyses suggest heterogeneity within the OA samples. This heterogeneity is not seen in the IA samples, despite the biological variation of disease types. Secondly, a group of OA samples appear to cluster closer to the IA samples, and further from the remaining OA samples. Together, these observations suggest the macrophages isolated from OA patients are heterogenous, and that a subset of these macrophage samples may have a gene signature more closely matched to those isolated from IA patients.

Subsequently, I assessed whether these synovial macrophages had a gene signature homologous to previously described macrophage phenotypes. When addressing M1 and M2 macrophage gene signatures, no clear conformity was found of either all synovial macrophages, or discrimination between OA and IA samples. X9_OA, X5_OA, X7_OA and X8_OA (all from the OA_0 group) had high expression of a number of these M1 genes. Notably, all IA

macrophage samples had lower levels of expression of genes commonly associated with inflammation and RA such as TNF, IL6 and IL1B, whereas the OA samples had higher levels of expression of these genes. Conversely, most synovial macrophages did not express M2-related genes, however two IA samples had higher levels of expression of a small group of these M2 genes. Although IA is an inflammatory condition, the macrophages present in the synovium may not actively express these inflammation-related genes. Overall, these data suggest that while the M1/M2 macrophage activation paradigm is useful, it may not be relevant in the context of tissue-derived macrophages from our samples.

I next assessed the differing gene signatures of synovial macrophages isolated from OA and IA patients. After performing differential gene expression analysis, there were three significantly DEGs after Benjamini-Hochberg correction. These were under-expressed in the IA samples and therefore over-expressed in the OA samples. Although I expected to find greater numbers of significantly DEGs between these groups, the p-value distribution of the DEGs did not suggest a null-hypothesis. The three significantly DEGs were *IGFBP5*, *LRRN4CL* and *TSKU*.

To conduct exploratory pathway analyses, unadjusted p-values were used to generate a large enough repository of logFC DEGs. When all unadjusted DEGs were visualised in a heat map, the IA samples clustered separately as expected due to the question design. However, it was noted that the same three OA samples observed in the MDS and PCA analyses again clustered separately from the remaining OA samples. From this visualisation, the heterogeneity of OA samples, and homology of IA samples is clear.

The KEGG pathways generated that were statistically significant were all over expressed in the IA group. 28 pathways were statistically significant ($p<0.01$). It is important to consider that this was performed on un-adjusted p-values and is exploratory. However, a number of pathways generated are already implicated in the pathogenesis of IA and give confidence in this data. These include cytokine-cytokine, TNF, NF-kappa B, IL-17, NOD-like receptor, chemokine, toll-like receptor, rheumatoid arthritis, MAPK and JAK-STAT pathways. Results such as malaria, and cancer related pathways should be treated with caution. These could be significant due to the nature of using un-adjusted p-values. However, especially in the cancer field, there is often a greater array of data in these diseases, and their presentation in this analyses rather reflects a component of this pathway being active within our samples. For example, when examining the pathview of inflammatory bowel disease, this suggests an over expression of MHCII, TLRs, cytokines and STAT signalling, all relevant in the context of macrophages and IA. As this analysis was exploratory, it was not considered in any more detail.

Owing to the lack of significant differences observed between the IA and OA samples, I hypothesised that this was limited due to the heterogeneity observed within the OA samples. It was thought that the biological variation within the OA samples was masking the difference with the IA samples. Paired with the observation that a subgroup of OA samples appeared more similar to IA, I decided to investigate this heterogeneity further.

Through visualising the top 500 and 25 genes, with and without inflammatory samples, this same clustering of three OA samples was present. In these analyses, these samples clustered within the IA samples, rather than in their own cluster. When this analyses was applied to the flow cytometry dataset for these samples, a similar clustering was observed (Fig. 5.17). Due to the consistent evidence for heterogeneity in OA, and the appearance of a sub group consisting of X3_OA, X4_OA and X6_OA, three additional question were asked. The aim of these questions was to segregate the OA samples and compare with the IA samples. This allowed me to reduce the biological variation within the OA samples when comparing with IA. In addition, I aimed to identify gene expression differences between these two OA groups.

The first question was to compare the OA_1 group that had previously clustered closely with IA samples, to the IA samples. Although this resulted in 11 significantly over expressed genes, visualisation of the data and analysis of the p-value distribution suggested that this question was designed poorly. This could be owing to a high similarity between the two groups, or a lack of repeats. However, within the significantly DEGs, *IGFBP5* and *LRRN4CL* were again up regulated in the OA samples. The most statistically significant DEG was *E2F8*. *E2F8* has roles in the regulation of cell cycle, promoting cell proliferation and has been previously reported in OA chondrocytes (Ye, Guo et al. 2016, Alshenibr, Tashkandi et al. 2017). Other genes overexpressed include *TMEM98* and *RSPO2*. *TMEM98* is a regulator of MMPs, can promote Th1 cells and can regulate cell invasion and migration (Fu, Cheng et al. 2015, Mao, Chen et al. 2015). *RSPO2* is a member of the R-spondin family, which have been widely implicated in OA (Abed, Chan et al. 2011, Jin and Yoon 2012, Nakajima, Kou et al. 2016).

Exploratory pathway analyses was performed again on un-adjusted p-values. 9 statistically significant KEGG pathways were generated. Again, those that are immediately relevant to the experiment as a whole include cytokine-cytokine receptor and NF-kappa B. Pathways such as AGE-RAGE, inflammatory bowel disease, malaria, cancer transcription and other inflammatory diseases that were observed in the previous question are again perturbed here. It is again likely that this is a result of the exploratory nature of these analyses, or generic cell mechanisms which are cross relevant to this experimental set-up. Of note, Cell cycle pathway was the highest significant result in the OA samples, similarly to the GO term analyses.

Within Question 2, it is likely that a lack of statistical significance is due to the similarity of this OA sub group (OA_1) and the IA samples. Although the results are not of the highest statistical significance, these help to validate this data set as a whole and give confidence in its quality.

Question 3 addressed the difference between the second OA group (OA_0) the IA group. It was clear after visualisation of the data and p-value distribution, that there were a greater number of significant differences between these two groups. There were 138 significantly DEGs (adjusted). This would again suggest that the OA samples are heterogeneous, and that the biological variation within all OA samples was masking the difference in Question 1 (IA v OA). True to the hypothesis, many of the DEGs were very biologically relevant with roles in either OA, cartilage development, RA, macrophages or cell signalling.

Despite the greater amount of significantly DEGs, KEGG pathway analyses again required a greater number of genes to reach statistical significance. Many of the previously relevant pathways were again observed in this analysis. Although KEGG analyses were performed on un-adjusted p-values, a number of significant GO terms were found based on the adjusted p-value DEGs. Many of these GO terms are relevant to OA, including extracellular matrix and structure organisation, osteoblast proliferation, cartilage and connective tissue development and roles in other tissue engineering. When network analysis was performed on the GO terms, the relation of the most significant GO terms and genes can be more intuitively visualised. Once more, we see many tissue engineering pathways in addition to binding pathways. Utilising network visualisations, *SMAD3* was highlighted as having roles in many of the GO terms, in addition to the importance of the Extracellular Matrix Organisation pathway in this question. Additionally, *IGFBP5* was again identified, and was associated with integrin and insulin binding pathways.

The final question addressed the difference between the two OA groups. This yielded the largest amount of significantly DEGs, 155, with a good p-value distribution. Once again, despite the greater amount of significantly DEGs, KEGG pathway analyses required a greater number of genes to reach statistical significance. In this analysis, there were no pathways that fell below a significant value of 0.01. Although KEGG analyses were performed on un-adjusted p-values, a number of significant GO terms were found based on the adjusted p-value DEGs. Interestingly, when performing GO term analyses, a strong cell cycle gene signature was present in the pathways, which was again seen in network analyses. *CDT1* was highlighted as having roles in many cell cycle processes. *CDT1* encodes the DNA replication factor Cdt1 protein, involved in the formation of the DNA pre-replication process. The *CDT1* gene is involved in the cell cycle

and has been previously been reported to be highly expressed in scleroderma patients (Milano, Pendergrass et al. 2008).

The analysis of Question 4 strongly supports the premise that there are two distinct groups within the OA samples. Interestingly, there were greater differences measured between these two OA groups, than when contrasting OA_1 against IA, or contrasting all OA samples against IA. Question 3 yielded a similar result to Question 4 with a relatively large amount of significant DEGs presenting between OA_0 and IA. These differences again suggest that the biological variation in OA samples, or the similarity of IA and OA_1, was masking differences in previous analyses.

All of these data highlight a level of heterogeneity in OA synovial macrophages. *IGFBP5* and *LRRN4CL* were significantly over-expressed in all OA groups tested as compared to IA, suggesting these genes are uniquely expressed in the OA macrophages. Previously published literature on *LRRN4CL* are limited to its generic expression in human tissues. However, there is much research surrounding insulin growth factor binding proteins (IGFBP).

IGFBP5 has roles in controlling cell survival, differentiation and apoptosis and is often implicated in tumour biology (Salih, Tripathi et al. 2004, Sureshbabu, Okajima et al. 2012). The role of IGFBPs in OA is unclear. In a canine model of OA, inhibition of IGFBP5 proteases improved the structure of the joint during OA development (Clemmons, Busby et al. 2002). It was suggested that the inhibition of complement C1s in human OA synovial fluid reduced *IGFBP5* cleavage and that this mechanism may promote a cartilage repair response (Busby, Yocum et al. 2009). Conversely, IGFBPs have been found increased in chondrocytes in human OA, with a positive correlation of histological joint destruction and IGFBP levels (Olney, Tsuchiya et al. 1996). Downregulation of *IGFBP5* has also been associated with the upregulation of TNFα-induced NF-kappa B signalling in synovial fibroblasts, promoting IL6 production (Hong, You et al. 2017). Furthermore, in an animal model of sepsis, and in response to LPS stimulation, *IGFBP5* expression was shown to be reduced (Lang, Krawiec et al. 2006).

There is less research surrounding the specific function of *IGFBP5* in macrophages, and to my knowledge, none in the context of synovial macrophages in OA. In murine macrophages, *IGFBP5* has been shown to reduce expression of inflammatory markers and oxidative stress, including F4/80, MAC1 and TGFβ mRNA (Sokolovic, Montenegro-Miranda et al. 2012). Similarly, *IGFBP5* has been shown to reduce local inflammation in animal models of periodontitis through the negative regulation of NF-kappa B signalling (Liu, Wang et al. 2015). As IGFBP5 was over-expressed in OA macrophages, and therefore under-expressed in IA

macrophages, this could reflect a less inflammatory environment in OA compared to IA. Furthermore, in Question 3, *IGFBP5* had the highest logFC change (LogFC = 9.51) representing a significant overexpression in OA_0 compared with IA. As OA_0 macrophages consistently clustered separately from both IA and OA_1 macrophages, this large over expression could again reflect a less inflammatory environment. Perhaps the expression of *IGFBP5* seen in these OA macrophages, particularly OA_0, is a cellular mechanism contributing directly to the reduction of local synovial inflammation. Conversely, these macrophages could simply be reflecting the inflammatory or non-inflammatory environment in which they are found.

High temperature requirement serine protease A1 (*HTRA1*) is a serine protease previously considered to degrade *IGFBP5*. However, it is now thought that the high affinity of C1s for *IGFBP5* results in this degradation (Clemmons, Busby et al. 2002, Busby, Yocum et al. 2009). Nevertheless, upregulation of *HTRA1* has also been demonstrated following cartilage damage in animal models of OA (Tsuchiya, Yano et al. 2005, Grau, Richards et al. 2006). Although the primary source of *HTRA1* in the synovium is thought to be fibroblasts, *HTRA1* is upregulated (non-statistically significant) in OA macrophages compared to IA macrophages (Question 1 – LogFC = -3.16), and significantly upregulated in OA_0 macrophages (Question 3 - LogFC = 3.71; p value = 0.03, multiple test corrected). In agreement with this, *HTRA1* has previously been measured at higher levels in the synovial fluid of OA patients compared to RA patients and non-arthritic controls (Grau, Richards et al. 2006). Treatment of synovial fibroblasts with *HTRA1* increases the production of cartilage catabolic MMP1 & 3 (Grau, Richards et al. 2006). This induction of MMPs was generated directly, and indirectly through the production of fibronectin fragments through fibronectin degradation. The immunohistochemical expression of *HTRA1* in synovial tissue has been used as a biomarker for OA progression, specifically cartilage damage (Grau, Richards et al. 2006, Larkin, Kartchner et al. 2013). However, the mechanism for *HTRA1* upregulation, and its cellular source in OA is unknown. Perhaps an increased expression of *HTRA1* in OA macrophages, particularly macrophages from OA_0 synovium in this instance, induces MMP production by synovial fibroblasts, which in turn contributes to the cartilage destruction characteristic of OA.

EFEMP1, also referred to as fibulin-3, was significantly over-expressed in OA_0 macrophages compared with IA macrophages. *EFEMP1* has been reported to inhibit angiogenesis, as well as being a negative regulator of chondrogenesis (Albig, Neil et al. 2006, Wakabayashi, Matsumine et al. 2010). A correlative link between *EFEMP1* and OA progression has been previously reported (Henrotin, Gharbi et al. 2012). Furthermore, the detection of fibulin-3 fragments has

shown to be a prognostic biomarker for the development of knee OA in overweight and obese middle age women (Runhaar, Sanchez et al. 2016). However, the role of *EFEMP1* in macrophages in synovial tissue remains unclear. *EFEMP1* expression in the OA_0 macrophages may function as a negative regulator of chondrogenesis, and therefore a failing repair mechanism after cartilage destruction through chronic mechanical damage and other catabolic factors such *HTRA1* signalling and MMP production previously discussed.

SMAD3 was also over-expressed in OA_0. *SMAD3* functions as a transcriptional modulator coding for an intracellular molecule that translocates TGF-β signal to the nucleus. Previous work in our department (Musculoskeletal Research Group) has investigated a molecular *SMAD3* SNP loss of function mutation in OA knees and hips (Raine, Reynard et al. 2014). An increase of *SMAD3* expression was observed in OA knees compared with hips. They postulated allelic expression effects of relevance to OA. Indeed, there is much molecular literature investigating the association of *SMAD3* and OA (Yao, Wang et al. 2003, Aref-Eshghi, Zhang et al. 2014, Su, Yang et al. 2015). SMAD3 and TGFβ signalling have also been implicated in tissue repair M2-like macrophages, particularly in environments of fibrosis and tissue damage (Kalinina, Agrotis et al. 2004, Gong, Shi et al. 2012, Rocher and Singla 2013, Eichenfield, Troutman et al. 2016, Loboda, Sobczak et al. 2016). Treatment with Bone morphogenetic protein-7 (BMP-7), a TGF-β signalling protein, in an animal model of OA resulted in improved cartilage repair through reduction of catabolic factors of cartilage destruction (MMPs and aggrecanase) (Badlani, Oshima et al. 2009). The loss of SMAD2/3 signalling in favour of SAD1/5/8 further progresses OA joint damage through chondrocyte differentiation (van der Kraan, Blaney Davidson et al. 2009). SMAD2/3 signalling is thought to inhibit *RUNX2*, a contributing factor for this chondrocyte differentiation (van der Kraan, Blaney Davidson et al. 2009). RUNX2 is under-expressed in OA_0 macrophages in both Questions 3 and 4 (Q3: LogFC = -1.39; Q4 LogFC = -2.12). Although these changes in expression are not statistically significant, they are consistent with the negative association of *SMAD3* with *RUNX2*, in addition to the negative regulation of chondrogenesis by *EFEMP1*. The upregulation of *SMAD3* in the synovial macrophages of OA_0 is likely a tissue repair response to chronic mechanical joint damage. However, this may be an additional failing mechanism since these patients are at end stage OA.

In contrast, the top GO terms from Question 4 (OA_0 vs OA_1) yielded a consistent cell cycle phenotype. The top genes contributing to this were mostly over-expressed in the OA_1 group. Notably, *MKi67* gene was highly over-expressed by this group (LogFC -7.2 in OA_0). *MKi67* encodes for Ki67, a nuclear protein associated with cell proliferation. Although Ki67 has been

previously shown to be correlated with OA Research Society International (OARSI) histological grading, no correlation was shown with CD68 macrophages in OA (Koller, Waldstein et al. 2017). This was attributed to the inclusion of only biomechanical degenerative joint disease, suggesting a lack of inflammatory involvement in these samples. To confirm synovial macrophages isolated from OA synovium expressed Ki67, I stained for Ki67 by flow cytometry (Appendix 5.6). Positive expression was seen, but this was not clear. As Ki67 is a nuclear marker and requires permeabilisation of cells, it can be difficult to stain by flow cytometry. This staining of Ki67 would need to be repeated with an optimised staining protocol. Additionally, many other genes with involvement in cell cycle and proliferation were upregulated in OA_1 macrophages compared to OA_0 macrophages including *E2F8* and *CDT1* which have been shown promote cell proliferation through modulation of G1/S phase (Deng, Wang et al. 2010, Zhang, Xing et al. 2012, Pozo and Cook 2016, Ye, Guo et al. 2016). It is likely that OA_1 macrophages are undergoing proliferation. The tissue environment which may be modulating this is unclear. The *CTRL* gene encodes the enzyme Chymotrypsin-like protease (CTRL-1), and is highly overexpressed in OA_1 compared to OA_0. *CTRL* has been shown to be enhanced after stimulation with LPS. Additionally, when *CTRL* stimulation is blocked, macrophages reduce their expression of inflammatory mediator genes, Nitric Oxide (NO) production and TNF-α secretion (Maa, Chang et al. 2008, Reis, Guan et al. 2011). As *CTRL* is highly expressed in OA_1 macrophages, this could be in response to an inflammatory environment, and these macrophages then subsequently contribute to this inflammatory environment through the *CTRL* dependent production of inflammatory mediators. Local proliferation of macrophages in tissue, rather than monocytic recruitment from blood, has been reported to be Th2/IL-4-type inflammation driven (Jenkins, Ruckerl et al. 2011). This could be further mediated by factors such as *CTRL* expression controlling enhanced production of inflammatory mediators, providing a positive feedback loop further contributing to this inflammatory environment. Taken together, these analyses are suggestive of a cell cycle gene signature in OA_1 macrophages, which is likely to be driven by a specific, potentially inflammatory tissue environment in this group of OA patients.

Unc-51 like-kinase 1 (*ULK1*) is a protein encoding gene which is a key inducer of autophagy, through mTOR signalling (Zhang, Vasheghani et al. 2015). In OA, it is thought that mTOR regulation of *ULK1* may contribute to catabolic and anabolic factors in cartilage, however these specific mechanisms are unclear (Zhang, Vasheghani et al. 2015). In contrast, it has been reported that this *ULK1* mediated authophagy is protective of cartilage, and that an ageing related loss of expression results in OA development (Carames, Taniguchi et al. 2010). In RA, expression of *ULK1* has previously been associated with disease activity, and measures of

ULK1 and *RUNX2* being used as predictors and measures of response to rituximab and methotrexate (Tchetina, Pivanova et al. 2016, Tchetina, Demidova et al. 2017). *ULK1* is significantly over expressed in both IA and OA_1 macrophages when compared with to OA_0 macrophages. This difference is not seen when contrasting IA and OA_1 macrophages. Additionally as previously mentioned, *RUNX2* is overexpressed (LogFC = -2.12) in OA_1 macrophages compared to OA_0 macrophages, although not statistically significantly. These observations again suggest a similarity between OA_1 macrophages and IA macrophages. Furthermore, with further validation, expression of *ULK1* may prove a useful tool for identifying OA patients which may respond treatments commonly used in RA.

Previous research into *ULK1* expression in the tissues of OA patients has been limited to histological analysis of cartilage and western blotting of chondrocytes (Carames, Taniguchi et al. 2010). The authors suggest that in the quantification of *ULK1* expression in cartilage, the assessment may be conflicted by cell clusters localised in the middle and deep zones. This yielded inconsistent results with western blot analyses. Overall, reduced expression of *ULK1* was measured in both mild and established OA groups compared the healthy controls. However histological analysis of cartilage showed lowest *ULK1* expression in mild OA, whereas through western blotting of chondrocytes, *ULK1* expression in established OA was significantly lower than both mild OA and normal controls. It could be postulated that this is due to technical variances in measurement, as well as the biological variance of measuring whole cartilage expression and expanded chondrocytes. This was not discussed by the authors. A significant decrease of *ULK1* was observed after surgically induced OA compared to sham surgery in murine knee joints. In my analyses of synovial macrophages, *ULK1* is highly over-expressed in both IA and OA_1 macrophages in differential gene expression analyses. Although this over-expression in OA_1 and IA macrophages was the primary interest, when examining gene reads, *ULK1* is absent from all OA_0 samples, with counts measured in all OA_1 and IA samples. Since all OA samples were derived from end stage OA patients, and there was no significant variation of age between OA groups, this is unlikely to be an age or disease activity associated decrease of *ULK1* expression in OA_0. It could be postulated that a previous lack of OA patient stratification (other than disease activity or age), results in inaccurate data. Rather than OA patients having decreased expression of *ULK1*, a subset of OA patients may completely lack expression in synovial macrophages (OA_0). It would be interesting to see if these patients additionally lack *ULK1* expression in cartilage and chondrocytes. Since *ULK1* is an inducer of autophagy, a complete lack of *ULK1* expression in OA_0 patients could result in reduced levels of autophagy and subsequent increased chondrocyte cell death. It has been previously suggested that Rapamycin, a specific inhibitor of mTOR signalling, could enhance autophagy and prevent

chondrocyte death (Li, Zhang et al. 2016). By stratifying patients via lack of *ULK1* expression, this treatment could potentially restore autophagy functioning in these patients and prevent OA cartilage damage.

A limitation of this gene expression experiment is the sample size. In RNA-sequencing experiments using human samples, a group of 12 repeats is typically recommended. After the removal of one low quality sample, and the subsequent identification of two endotypes within my OA cohort, the number of repeats for each group was greatly reduced. Although statistically significant and acceptable results were still generated, a larger sample size would have allowed for greater statistical certainty in exploratory analyses. Additionally, the cells used for RNA-sequencing were tissue-derived, and had therefore undergone isolation, and subsequent FACS. Despite optimising a digestion protocol that results in high viability and retained functionality, the gene expression signature of these cells will inevitably have been influenced. However, the design of this experiment was to compare synovial macrophages between disease type, thereby eliminating technical differences in isolation. This therefore gives me confidence that the data generated are biologically relevant.

These results show that using the techniques optimised in Chapter 3, it is possible to carry out advanced technical analyses of cell subsets from synovial tissue. RNA-sequencing identified the possibility of two distinct macrophage endotypes in OA. These have functionally different gene signatures consisting of either cell cycle mechanisms or cartilage and tissue engineering, summarised in Figure 5.35. It can be postulated that the differing disease environments between the arthritic joints of these OA patients is driving two different polarisation states of these macrophages. Although it is likely that these macrophages also contribute to disease pathogenesis, the specifics of this are less clear.

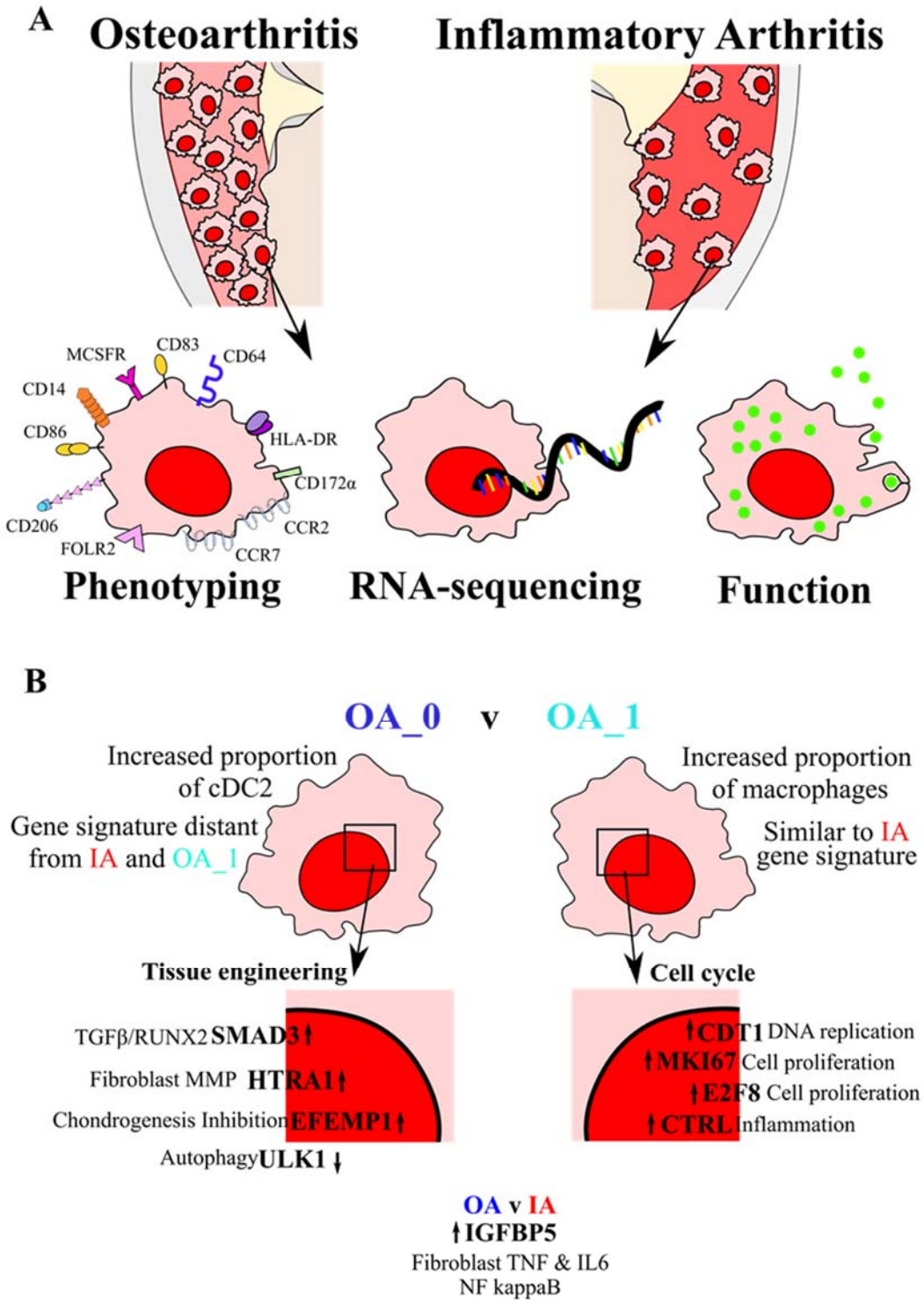

Figure 5.35: Illustrative summary of Chapter 5 results
Depiction of the main findings from Chapter 5. **A:** Summary of the main experiments conducted in Chapter 5. Synovial macrophages isolated form OA and IA patients were phenotyped by flow cytometry, gene expression determined by RNA-sequencing and functional capability assessed. **B:** Identification of two OA endotypes determined by macrophage gene expression.

Chapter 6. Thesis summary and general discussion

6.1 Thesis Summary

OA represents a huge burden on patients and society. As there are no disease-modifying treatments, there is a major unmet clinical need for OA patients. Inflammation has become recognised as a key mediator of OA pathogenesis (Haywood, McWilliams et al. 2003, Baker, Grainger et al. 2010, Sellam and Berenbaum 2010, Roemer, Crema et al. 2011, Scanzello and Goldring 2012). In particular, there is an emerging body of evidence supporting the role of synovial macrophages in OA pathogenesis (Haywood, McWilliams et al. 2003, Blom, van Lent et al. 2004, Benito, Veale et al. 2005, Bondeson, Blom et al. 2010, Kraus, McDaniel et al. 2016, Manferdini, Paolella et al. 2016, Wu, McNeill et al. 2017). However, technical barriers have thus far limited high resolution and in-depth analyses of these cells.

Three overarching aims were designed to assess the hypothesis that there is heterogeneity at the cellular and molecular level in the synovial tissue of osteoarthritis patients, particularly within synovial macrophages. Further understanding the specific tissue environments modulating this heterogeneity could lead to improved patient stratification and the modification of treatment strategies for OA patients. The first aim was to develop technical protocols to allow the successful isolation, identification and purification of immune cell populations from synovial tissue. The second aim involved the enumeration of immune cell subsets using both manual and computational analyses. The final aim was to conduct in-depth analyses on synovial macrophages, encompassing surface marker phenotyping, functional analyses and gene expression by RNA-sequencing. Supporting data for the contribution of synovial macrophages to OA disease were found, in addition to the stratification of OA macrophages into two endotypes.

Through the assessment of published and established protocols, I developed a digestion protocol suitable for synovial tissue (Chapter 3). After mechanical digestion, synovial tissue was exposed to a suboptimal concentration of the enzyme cocktail liberase for three, 45min-digestion rounds in a shaking incubator, with filtration after each digestion round. This protocol ensured that cells were only exposed to a low concentration of liberase at any time during the digestion process, resulting in minimal cleavage of the extracellular antigens tested and high viability of cells. The multiple digestion rounds were necessary to obtain sufficient cell yields. The combination of a carefully constructed 12-colour flow cytometry panel and optimised FACs allowed the purification of synovial tissue immune cell subsets of interest, namely HLA-DR^+CD14^+ macrophages, cDC2s, $CD14^+$ monocytes and $CD4^+$ T cells.

For enumeration of the immune cell subsets present in the peripheral blood and synovial tissue of OA and IA patients, both manual methods and computational analyses were employed (Chapter 4). viSNE produced an informative visual representation of these high parameter data, whereas CITRUS provided useful quantitative analyses of cell clusters. Although these types of analyses are becoming typically used in the analysis of mass cytometry data, they have also been previously applied to flow cytometry data. Examples of this include the identification of cell subsets as well as the contrast of healthy and cancerous tissues (Amir el, Davis et al. 2013, Bruggner, Bodenmiller et al. 2014, Guilliams, Dutertre et al. 2016, Acuff and Linden 2017). Increased immune cell infiltration was observed in the IA synovial samples compared to OA. However, an increase in the proportion of macrophages was observed in OA synovial tissue compared to IA. This was mirrored by an increased proportion of T cells in the synovial tissue of IA. There has been little previous research directly comparing synovial tissue cell subsets between OA and IA, particularly using the techniques described here. This observation may support the premise that synovial macrophages play a role in the OA pathogenesis. Although potentially interesting findings were uncovered in the correlation of clinical and immunological information, these did not meet statistical acceptability, and were ultimately limited by the sample size.

An in-depth analysis was conducted on synovial tissue macrophages (Chapter 5). This involved the phenotyping of their surface markers by flow cytometry, assessment of functionality, and measurement of gene expression by RNA-sequencing. Synovial macrophages were pure and expressed expected surface markers, such as HLA-DR, CD14 and CD45. Increased expression of a number of surface markers, including CD206, FOLR2 and CD86 was noted in OA samples compared to IA samples. Together with their increased proportion in OA synovial tissue, these observations may suggest OA synovial tissue macrophages have an alternative activation state compared to IA synovial tissue macrophages. This could reflect the modulating effect of these differing tissue environments in arthritic joints between disease types. A flow cytometry gating strategy for the identification of ‘resident’ and ‘inflammatory’ macrophages in healthy and GvHD dermis was applied to OA and IA synovial tissue samples. This demonstrated increased proportions of ‘resident’ macrophages in the synovial tissue of OA patients compared to IA. However, in OA, the ratio of ‘resident’ and ‘inflammatory’ macrophages was variable, with some OA patients showing a similar proportion to IA patients. Observations in the IA synovium samples are consistent with the inflammatory dermis, where increased proportions of ‘inflammatory’ macrophages are also observed in patients with graft versus host disease (Collin group, manuscript in preparation). It is possible that the well described inflammatory environment in IA synovial tissue is driving the recruitment of monocytes and their

differentiation into inflammatory monocyte-derived cells. Although a high ratio of 'inflammatory' to 'resident' macrophages was not seen in the OA cohort as a whole, a subset of these patients had proportions of 'inflammatory' macrophages similar to those seen in IA. In addition to identifying heterogeneity in OA patients, this could suggest that the OA patients with a similar proportion of 'inflammatory' macrophages as IA patients, have a more inflammatory OA disease phenotype. This strategy presented a potentially novel method for the identification of resident and inflammatory, infiltrating macrophages in synovial tissue. Due to the recent development of this strategy, further assessment needs to be conducted. However, when applied to the flow cytometry data-set of sequenced macrophage samples, there was no clear difference in monocyte or macrophage subsets between the three disease groups tested (IA, OA_0 and OA_1) (Appendix 6.1). A number of experiments will therefore be carried out to further characterise these resident and infiltrating macrophages in synovial tissue. As this identification was based solely on the low and high expression of CD11c, it would be important to validate these cells' ontogeny. Although there is no definitive marker of human monocyte-derived macrophages, CCR2 has been previously identified as a marker for the recruitment of monocytes and DCs into tissues (Daigneault, Preston et al. 2010, Italiani and Boraschi 2014, Yang, Zhang et al. 2014, Bernardo, Durant et al. 2016, Gordon and Pluddemann 2017). The measurement of CCR2 and other candidate markers such as CD11b and CX3CR1, in addition to functional assessment such as migratory capability and differential response to stimulus may aid in the identification of monocyte-derived macrophages in synovial tissue.

Functionality of purified macrophages was assessed by phagocytosis of latex beads using confocal microscopy. This demonstrated that synovial macrophages can still phagocytose after tissue digestion and FACs. This was a crucial step in ensuring functionality before conducting gene-expression and future functional assays. RNA-sequencing was conducted on OA synovial macrophages with IA macrophages used as a control group. This confirmed heterogeneity of synovial macrophages in OA patients. Macrophages from OA had varied gene expression, and could be split into two endotypes (Figure 5.35). These groupings were also segregated by hierarchical clustering of immune cell subset percentages determined by flow cytometry, demonstrating an increased proportion of macrophages in OA_1 and increased cDC2s in OA_0. OA_1 samples were similar to IA samples, where macrophages presented a cell cycle gene signature. OA_0 macrophages were distinct from both IA and OA_1 macrophages, demonstrating a gene signature rich in tissue engineering pathways. These different macrophage endotypes did not correlate with any of the clinical data collected. As none of the clinical data were found to be a confounding factors, this suggests these endotypes are not caused by factors measured such as age, obesity and gender.

A number of limitations were identified in this project. These included the use of tissue digestion, use of tissue samples from both knees and wrists, small sample sizes and use of only end-stage OA disease samples. However, all of these were deemed either unavoidable and effects minimised (digestion of tissue), acceptable (different tissue sites), or an area to be developed in future work (small sample sizes). For this project, the use of end-stage OA samples was unavoidable, but it has been recognised that to further understand the pathogenesis of OA, samples from earlier stages of disease will be essential.

When designing future experiments to further characterise the OA subgroups identified here, a number of factors need to be considered. As only synovial tissue from end-stage OA has been used in this thesis, the data presented may only represent end-stage disease. When further investigating disease mechanisms and pathogenesis, it will be essential to sample synovial tissue from multiple stages of disease to provide a better representation of pathogenesis. In addition, larger sample sizes would be beneficial. Although clinical analyses have been conducted, access to this data has been limited. It will also be crucial to collect a specific set of clinical data from these patients. This additional information could include patient pain and joint mobility, general quality of life scores and a standardised, surgeon reported synovial tissue colouring score. Ideally, these data will be collected pre-, at time of, and post- sample collection and include patient reported outcome measures in the occurrence of medical intervention. Determining the relationship between the clinical data of OA patients with immunological data will aid in measuring patients' response to clinical interventions as well as defining new diagnostic markers and the modification of treatments strategies for OA patients.

As discussed in Chapter 4, it would be useful to fully validate the enumeration of synovial tissue cell subsets. Immunofluorescence imaging of tissue sections would be a valuable technique to approach this. Additionally, it would be interesting to explore the use of imaging by mass cytometry. Cytof Imaging Mass Cytometry technology currently allows the staining of up to 32 proteins in a single tissue section, and it is envisaged that this could reach up to 100 proteins once isotypes and antibodies are developed. In addition to the enumeration of cells, this approach would allow the staining of potential biomarkers for OA subgroups identified by my gene expression experiment. Furthermore, the visualisation of cell location to both tissue structure in these arthritic joints, and to multiple other cell subsets, would aid in the understanding of cell-cell mechanisms in these differing pathologies. When designing an experiment encompassing this technique, it would be important to include the analyses of both tissue sections and matched peripheral blood samples. Although being able to identify patients by synovial tissue is useful and could be translated to minimally invasive biopsies, it would be

advantageous to be able to stratify these patients using peripheral blood samples only. However, since OA is not a systemic disease, it is likely that using peripheral blood would not be useful. Despite this, the use of minimally invasive biopsies for the stratification of patients for disease modifying treatment, preventing unnecessary total joint replacement, is acceptable. This would first require the identification of select markers in tissue for the consistent identification of these OA subgroups, and then the correlation with blood samples to identify similar markers. Finally, a large cohort size, in addition to samples obtained from multi-stages of OA, will be crucial to any future work. Being able to identify these patients consistently and easily would aid in the modification of their treatment strategies due to the better understanding of the disease processes that take place in the affected joint(s).

It would be useful to determine the cytokine production of synovial macrophages. Although cytokine genes were expressed by the synovial macrophages assessed in my gene expression experiment (data not shown), these were not observed through differential gene expression analysis. This is likely owing to the small sample size. Alongside synovial macrophages, the cytokine profiles of whole synovial tissue, in addition to the adipokine contribution from the fat pad, will aid in fully understanding the tissue specific environments in these patients, and how this may modulate cellular pathogenesis. Since the functionality of macrophages appears to be retained after digestion and FACs, it will be useful to carry out further functional experiments on these cells. In addition to assessing macrophage cytokine production in response to stimuli, this may encompass mixed lymphocyte reactions and proliferation assays.

Overall, the techniques developed here have allowed the advanced technical analyses of synovial tissue cell subsets, in particular synovial tissue macrophages in OA patients. This level of analyses in the context of OA and macrophages is novel, can be applied to a range of synovial samples, and provides many directions for new hypotheses and future work.

6.2 General Discussion

With the identification of synovial macrophage subgroups in OA, it would be interesting to assess the functional differences and cellular mechanisms of pathogenesis between them. This would aid in the understanding of macrophage contribution to OA pathogenesis. From the study of gene expression and subsequent pathway analyses, the unique gene signatures suggest how these macrophages from OA patients, and their specific tissue environments may differ, summarised in Figure 6.1.

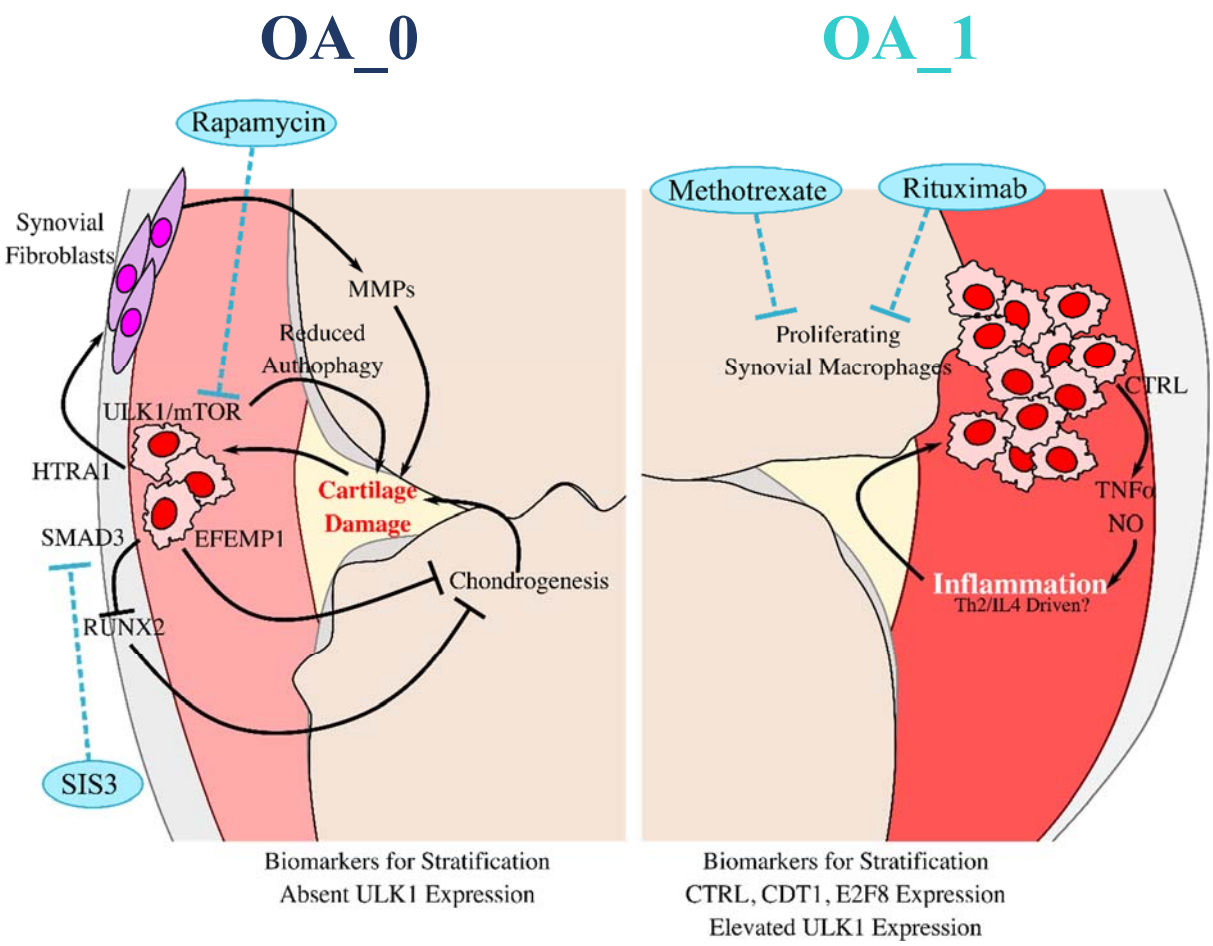

Figure 6.1: OA_0 and OA_1 synovial macrophages
Depiction of potential mechanism of disease pathogenesis in OA_0 and OA_1. OA_0 tissue environment is likely centred around cartilage damage and degradation, one of the key characteristics of OA. Synovial macrophages present have aberrant tissue repair mechanisms, which results in further cartilage damage. Additionally, these macrophages may also contribute directly to cartilage damage through the mediation of MMP release by synovial macrophages, and reduced autophagy. SIS3 inhibition of *SMAD3* and Rapamycin inhibition of mTOR signalling may prove useful methods of reinstating chondrogenesis and autophagy in these patients, promoting cartilage repair. Biomarkers in synovial tissue for these patients could include a lack of *ULK1* expression. OA_1 tissue environment is likely to be inflammatory, similar to that seen in IA patients. This inflammatory environment likely polarises synovial macrophages into a proliferative capacity. These highly proliferative macrophages may then further contribute to inflammation through the release of TNFα and NO. Methotrexate and Rituximab may be useful therapeutic approaches for these patients, halting cell cycle at G1/S phase. *ULK1* may be a useful predictor for treatment response in these patients. Biomarkers for stratification of these patients could include the expression of *CTRL*, *CDT1*, *E2F8* and *ULK1*.

IGFBP5 was significantly overexpressed in OA macrophages compared to IA macrophages, particularly in OA_0 macrophages. Since *IGFBP5* is associated with the negative regulation of inflammatory mediators, this over expression in OA macrophages, particularly OA_0 macrophages, could reflect a less inflammatory tissue environment compared to IA. OA_1 may demonstrate an inflammatory environment similar to that of IA. Likewise, over expression of *HTRA1* is observed in OA_0 macrophages compared to IA. *HTRA1* can modulate synovial fibroblasts to produce cartilage catabolic MMPs. Alongside the observed over-expression of *EFEMP1*, potentially acting as a negative regulator of chondrogenesis, this could demonstrate a potential mechanism of cartilage destruction, and subsequent failure of cartilage repair in these OA_0 patients. *SMAD3* was also observed to be over-expressed, and *RUNX2* to be possibly under expressed in OA_0 macrophages compared to IA and OA_1 macrophages. This may be an additional failing, tissue repair mechanism.

The over-expression of *ULK1* in IA and OA_1 macrophages compared to OA_0 macrophages was initially of interest. However, it became clear that this was actually a complete lack of expression of *ULK1* in OA_0 macrophages. *ULK1* is protective of cartilage, and could present another mechanism of cartilage destruction through reduced autophagy and increased chondrocyte death. As *ULK1* can be negatively regulated by mTOR activity, it could be postulated that inhibition of mTOR activity may promote *ULK1* expression in OA_0. This could ultimately lead to the restoration of autophagy, and resolution of cartilage damage. Rapamycin targets mTOR and treatment has been shown to significantly decrease cartilage degradation and furthermore decrease *ADAMTS5* and IL-1β expression in cartilage murine OA (Carames, Hasegawa et al. 2012). Similar results have been observed in murine OA studies (Cejka, Hayer et al. 2010, Takayama, Kawakami et al. 2014). However, there is no evidence for its involvement in human OA. Another direction for therapeutic options is the TGFβ/SMAD3 signalling pathways. There are many therapies for the blocking of TGFβ, however these may not be specific. SIS3 is a specific inhibitor of *SMAD3* phosphorylation and gene expression, without affecting *SMAD2*. Upregulation of type 1 collagen by scleroderma fibroblasts with SIS3 treatment has been previously observed (Jinnin, Ihn et al. 2006). However, there is no evidence of the application of SIS3 in the context of OA. This could prove an additional mechanism for the restoration of autophagy in these OA_0 patients. To functionally assess the contribution to, or inhibition of, cartilage degradation by macrophages in the OA_0 group, a modified version of a previously described *in vitro* cartilage degradation assay could be performed (Jetten, Roumans et al. 2014, Radwan, Wilkinson et al. 2015). The culture of synovial tissue cells and bovine cartilage discs, with the presence or depletion of these

macrophages could reveal the true extent of their contribution to cartilage damage, or restoration.

OA_1 macrophages were similar to IA macrophages, and genes expressed had a strong association with cell cycle processes. The over expression of *MKi67* in OA_1 macrophages compared to OA_0 macrophages was of particular interest since it encodes a well associated protein of cell proliferation, Ki67. The over expression of *E2F8* and *CDT1,* which have been shown to promote cell proliferation through the modulation of G1/S phase, were also of interest. These samples additionally had a higher proportion of macrophages compared with OA_0 samples, assessed by flow cytometry. The observation of a higher proportion of macrophages in OA_1 is likely owing to increased rates of macrophage proliferation within these samples, suggested by their gene expression. As OA_1 macrophage samples were similar in gene expression to IA macrophages, this macrophage proliferation could be in response to immune cell driven inflammation within the joint. Over-expression of *CTRL* in OA_1 macrophages compared to OA_0 macrophages may reflect a more inflammatory environment, and result in the further contribution to this inflammatory environment, creating a positive feedback loop.

It would be interesting to test the differential effects of therapeutic drugs on these cells, which may translate to better stratification of OA patients for clinical trials. For example, methotrexate, a repurposed cancer drug used first line in RA patients, is a competitive inhibitor of dihydrofolate reductase (DHFR), halting cell cycle at S phase. Since OA_1 macrophages may be actively proliferating with specific modulation at the G1/S phase, methotrexate treatment could be used to inhibit this cell proliferation, and subsequently reduce inflammation. Previous trials of methotrexate treatment in OA patients have demonstrated mixed success, which could be explained by heterogeneity in OA macrophages observed here (Wenham, Grainger et al. 2013, Abou-Raya, Abou-Raya et al. 2014). As methotrexate has associated side effects, it would be desirable to identify patients that would respond well to this drug, before commencement of treatment. It will be interesting to see results from the ARUK multi-centre 'PROMOTE' study assessing pain reduction and synovitis in OA patients with methotrexate treatment. To initially assess the efficacy of methotrexate treatment on these macrophages, the *in vitro* culture of macrophages from OA subgroups +/- soluble methotrexate and assessment of resultant proliferation would be intriguing. Similar cultures have previously been conducted in macrophages and stromal cell cultures but not in the context of OA heterogeneity (Neurath, Hildner et al. 1999, Minaur, Jefferiss et al. 2002, Lo, Steer et al. 2011). Although *ULK1* expression was absent in OA_0 macrophages, as no healthy controls were used it is unknown whether the levels measured in OA_1 and IA macrophages are elevated. If these levels are

indeed elevated, *ULK1* expression could provide a useful identifier for OA patients which may respond to methotrexate treatment, as well as rituximab.

Taken together, these data suggest that there are divergent synovial tissue environments between OA_0 and OA_1 patients. It is likely that these environments specifically modulate synovial macrophages to differing polarisation states. OA_1 appears to be particularly inflammatory, whereas OA_0 is likely to be centred around cartilage degradation, possibly a result of chronic mechanical damage. Within OA_0 macrophages there are aberrant tissue repair mechanisms, in addition to factors which may directly contribute to cartilage degradation. OA_1 macrophages are highly proliferative, reflected by their gene signature, in addition to increased proportions in the synovium measured by flow cytometry. It is likely that the inflammatory synovial environment directly contributes to these macrophages' proliferative capacity, but there is scope for a positive feedback loop whereby these macrophages further exacerbate synovial inflammation.

With the identification of these OA endotypes, it is now possible to further investigate the specific cellular mechanisms of disease pathogenesis. After validation of these endotypes, it will be important to identify biomarkers to aid in the accurate identification of these patients. Once identified, these biomarkers should be detectable in the peripheral blood or synovial tissue in clinical application. Once this identification has been established, recommendations for treatment modification can be made based on the functional cellular pathogenesis of each endotype. This could ultimately result in disease modification in patients with OA, which has previously been unachievable, likely owing to the heterogeneity within this disease.

Appendices

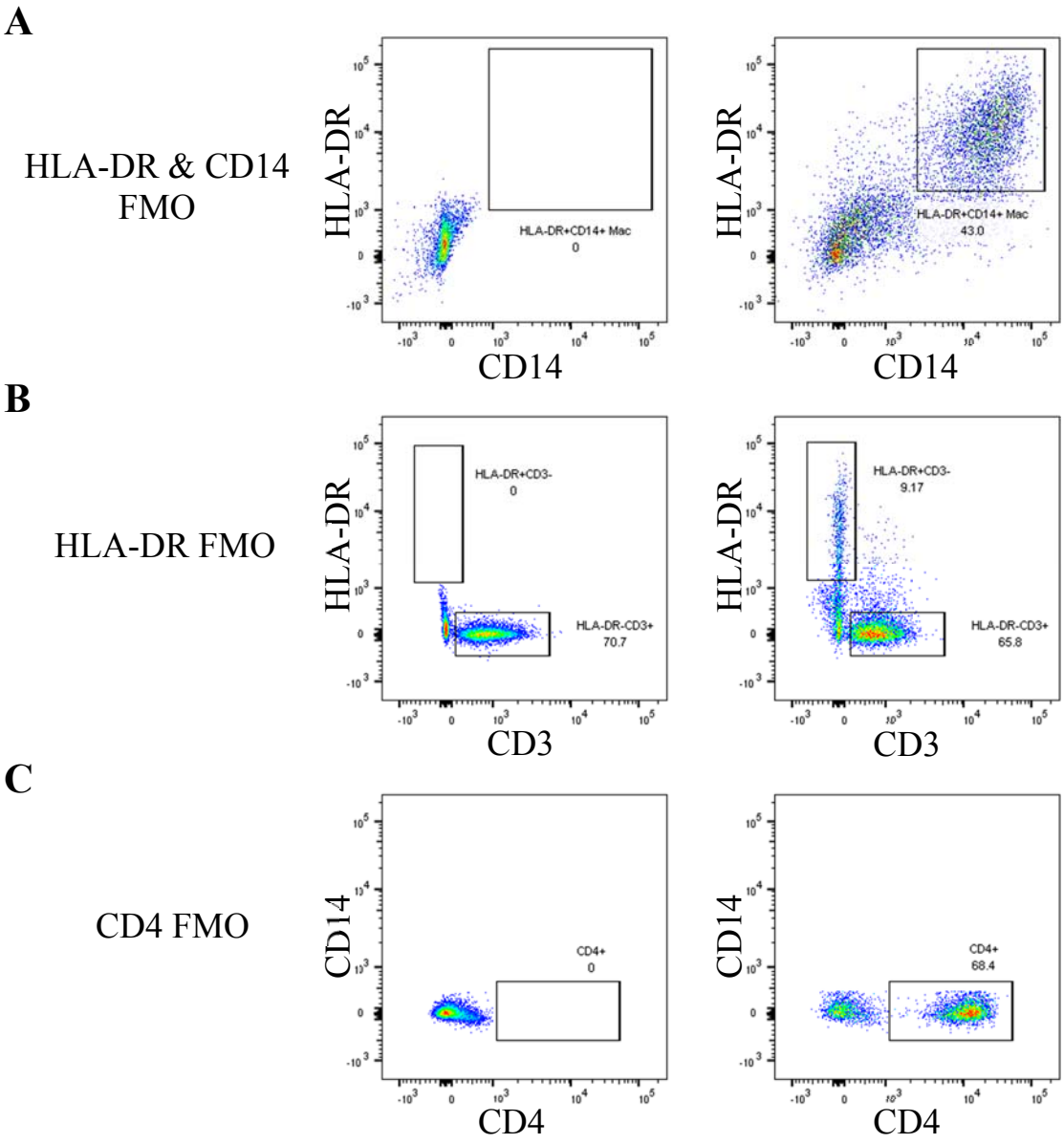

Appendix 2.1: FMOs for gating strategy
Synovial tissue from OA total knee replacement was digested using the optimised protocol shown in Figure 3.6. Single cell suspension was divided into two before flow cytometry antibody staining. Flow cytometry panel shown in Figure 3.16 was used. Left hand panels depict FMO. Right hand panels depict antibody staining. **A:** Sample with and without HLA-DR and CD14 antibodies. **B:** Sample with and without HLA-DR antibody. **C:** Sample with and without CD4 antibody. Data are representative of two independent experiments.

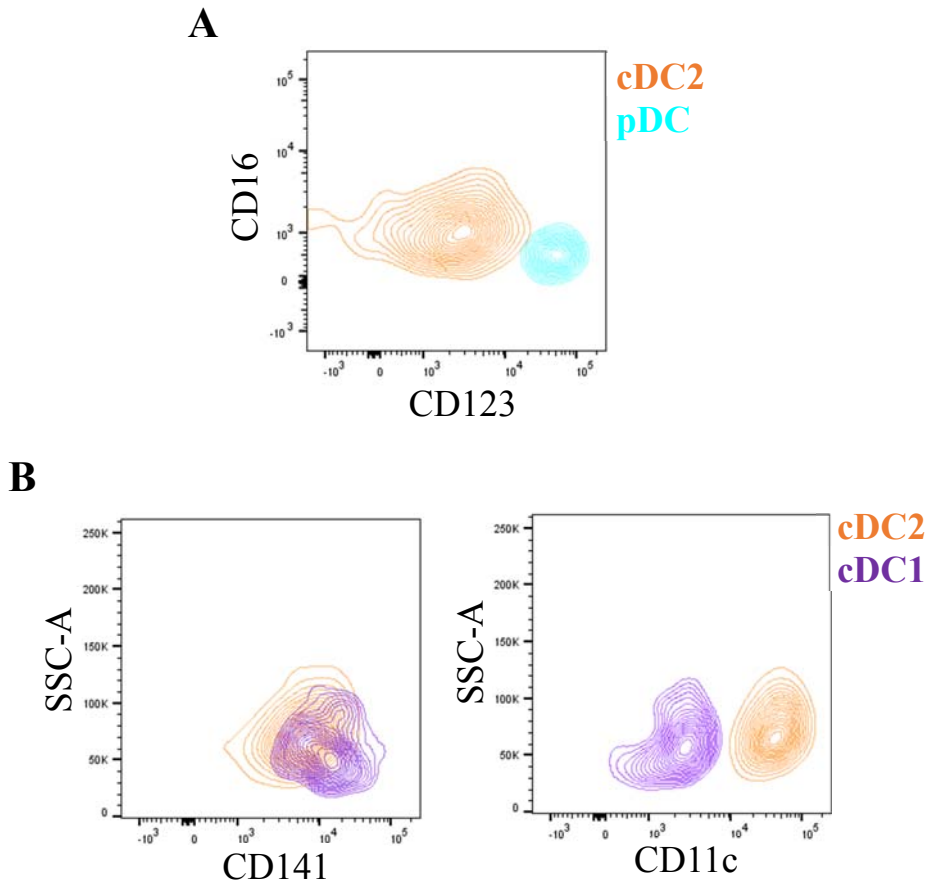

Appendix 3.1: pDC and cDC1 identification
Synovial tissue from OA total knee replacement was digested using the optimised protocol shown in Figure 3.6. **A:** Expression of CD123 on cDC2 and pDC. **B:** Expression of CD141 (left panel) and CD11c (right panel) on cDC2 and cDC1.

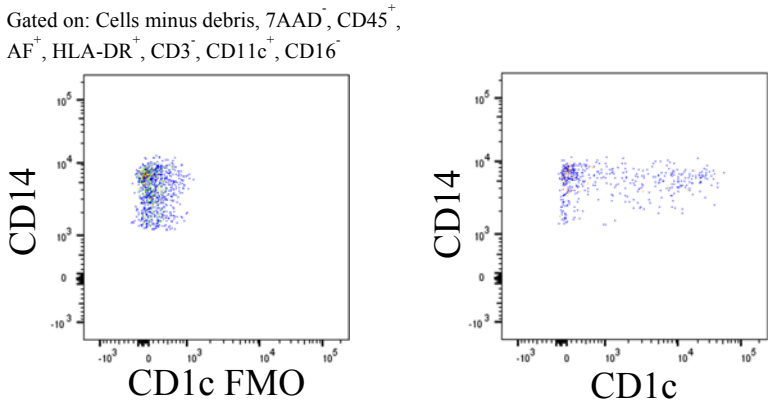

Appendix 3.2: CD1c FMO
Synovial tissue from OA total knee replacement was digested using the optimised protocol shown in Figure 3.6. Single cell suspension was divided into two before flow cytometry antibody staining. Flow cytometry panel shown in Figure 3.17 was used. Left hand panel depicts FMO. Right hand panel depicts antibody staining. Data are representative of one experiment.

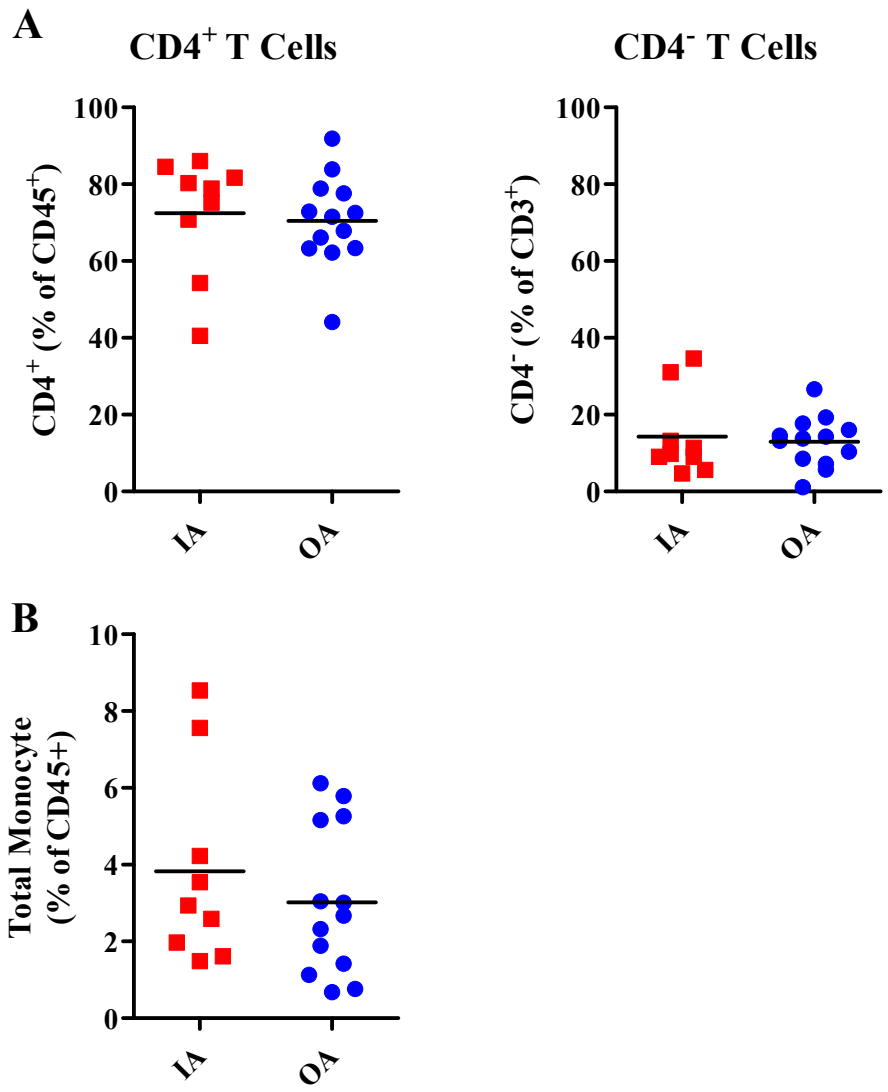

Appendix 4.1: Quantification of immune cell subsets in peripheral blood
PBMCs were isolated from peripheral blood of OA total knee replacement and IA ultrasound guided biopsy patients. PBMCs were analysed by flow cytometry using techniques described in Chapter 3. **A:** Proportion of $CD4^+$ and $CD4^-$ T-cells in IA and OA peripheral blood. **B:** Proportion of total monocytes in IA and OA peripheral blood. *n=23*.

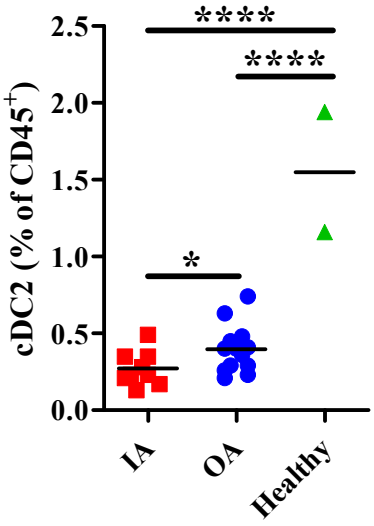

Appendix 4.2: Quantification of cDC2 in disease and healthy blood
PBMCs were isolated from peripheral blood of OA total knee replacement and IA ultrasound guided biopsy patients in addition to healthy volunteers. Proportion of cDC2 cells in IA, OA and healthy blood. Data presented as % of CD45+ cells. *n=24. *P≤0.05, ****P≤0.0001.*

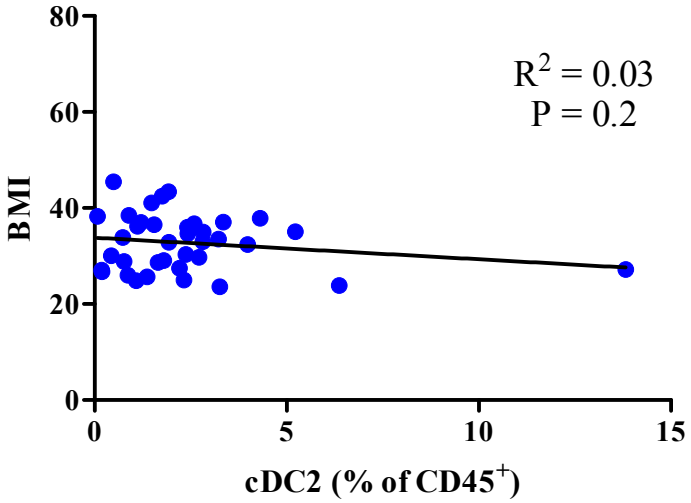

Appendix 4.3: Correlation of cDC2 and BMI
Synovial tissue from OA total knee replacement and IA ultrasound guided biopsy was digested and analysed by flow cytometry using techniques described in Chapter 3. Correlation of BMI and cDC2 as % of $CD45^+$ cells. *Linear regression: R2 = 0.03. P = 0.2.*

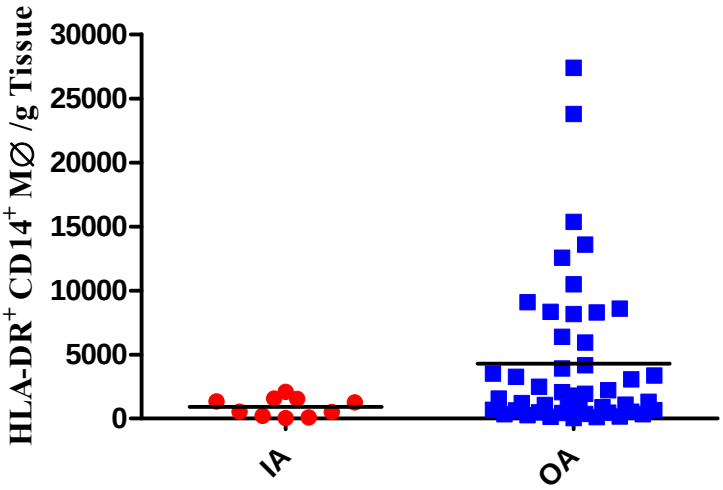

Appendix 4.4: Quantification of HLA-DR^+CD14^+ Macrophage in synovial tissue
Synovial tissue from OA total knee replacement and IA ultrasound guided biopsy was digested and analysed by flow cytometry using techniques described in Chapter 3. Quantity of HLA-DR^+CD14^+ Macrophage in IA and OA synovial tissue. Data presented as cells per gram of tissue.

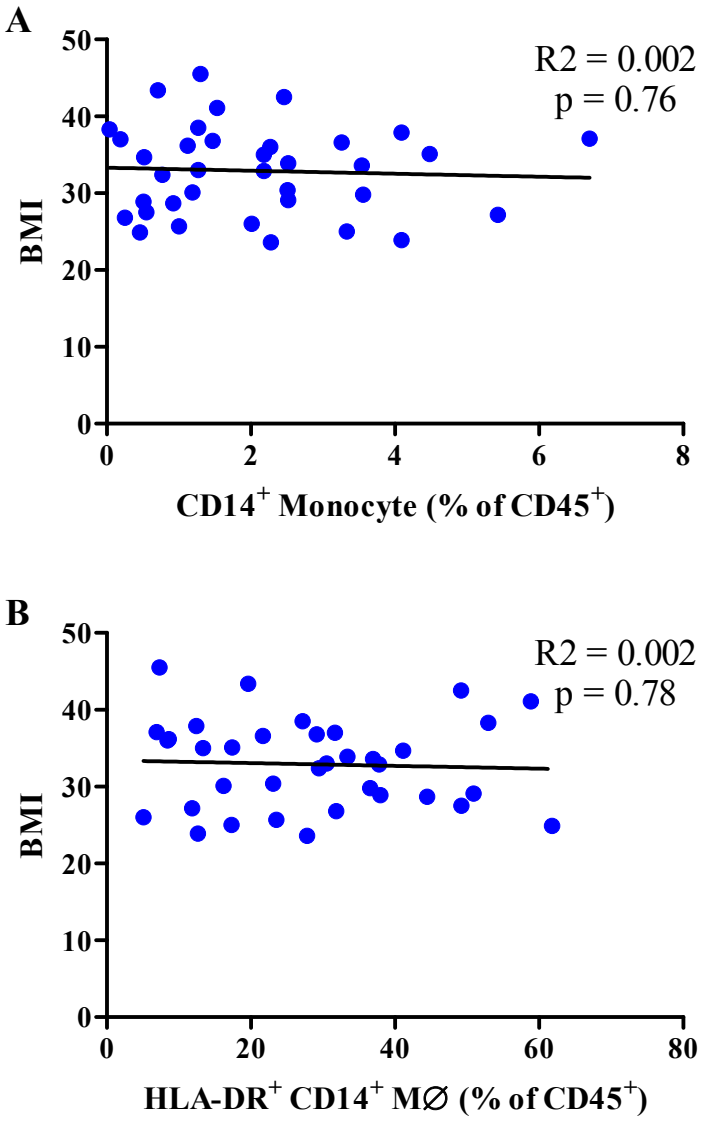

Appendix 4.5: Correlation of HLA-DR$^+$CD14$^+$ MØ and CD14$^+$ monocytes with BMI
Synovial tissue from OA total knee replacement and IA ultrasound guided biopsy was digested and analysed by flow cytometry using techniques described in Chapter 3. **A:** Correlation of BMI and CD14$^+$ monocytes as % of CD45$^+$ cells. *Linear regression: R2 = 0.002. P = 0.76.* **B:** Correlation of BMI and HLA-DR$^+$CD14$^+$ MØ as % of CD45$^+$ cells. *Linear regression: R2 = 0.002. P = 0.78.*

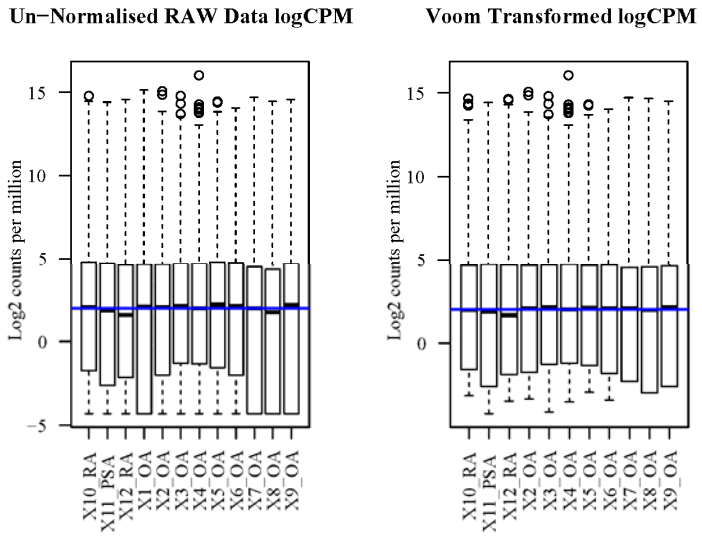

Appendix 5.1: Normalisation of counts

RNA-sequencing of synovial macrophages and data analyses were conducted following methods described in Chapter 2. Normalisation of counts was conducted using Limma's Voom function. Left panel depicts counts pre- normalisation. Right panel depicts counts post- normalisation

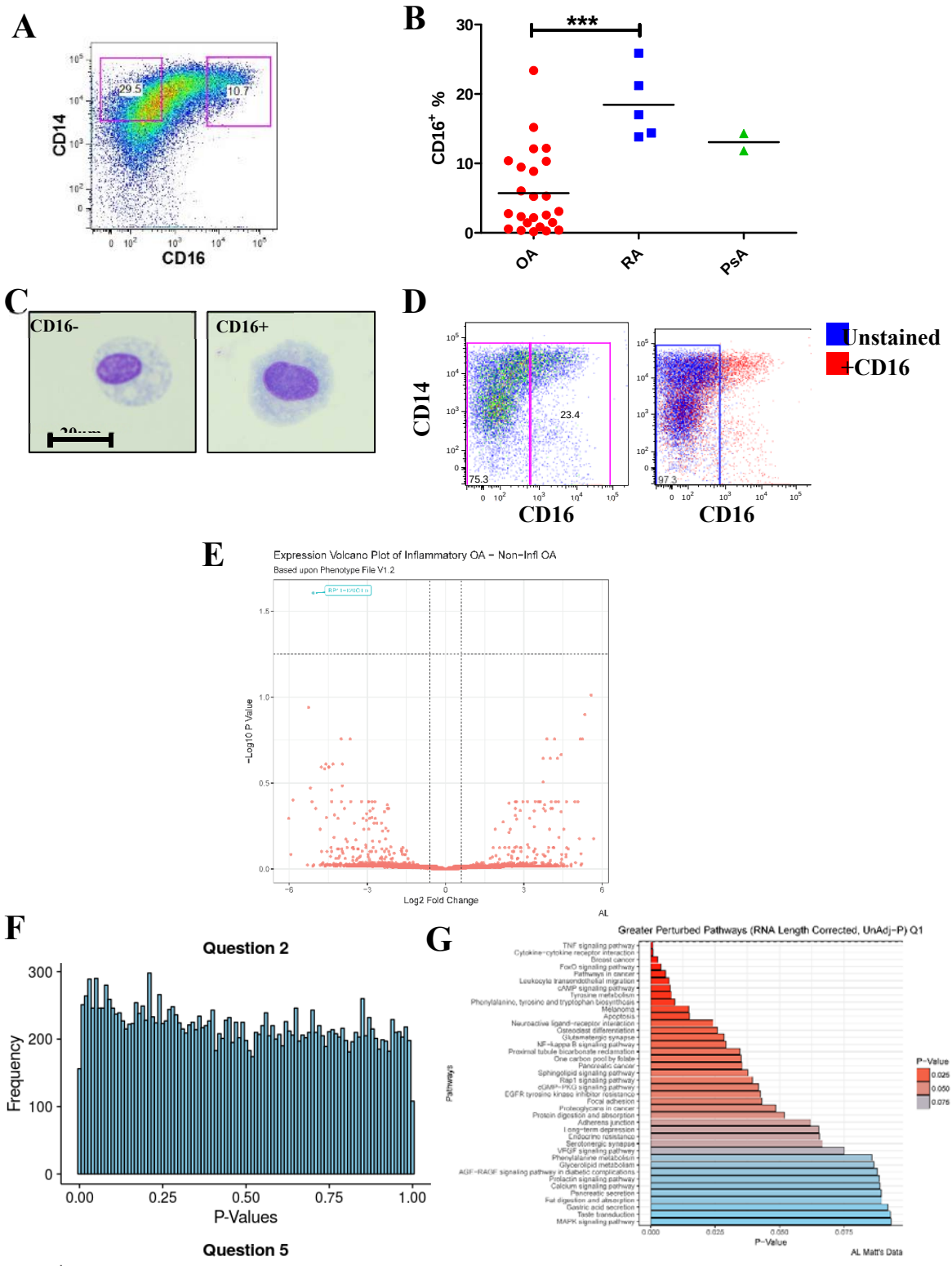

Appendix 5.2: CD16^{+} Macrophages in synovial tissue

Synovial tissue from OA total knee replacement and IA ultrasound guided biopsy was digested and analysed by flow cytometry using techniques described in Chapter 3. **A:** Identification of a CD16^{+} MØ population present in synovial tissue samples. **B:** Percentage of CD16^{+} MØs present in samples of different disease groups. **C:** Morphological analysis of CD16^{+} and CD16^{-} MØ by cytospin and giemsa staining. **D:** Verification of CD16 staining in MØ population using unstained control. **E:** Volcano plot of DEGs between CD16^{+} and CD16^{-} OA patients. **F:** Distribution of p-values. **G:** KEGG pathway analyses on un-adjusted p-values. *** $P = 0.0001$.

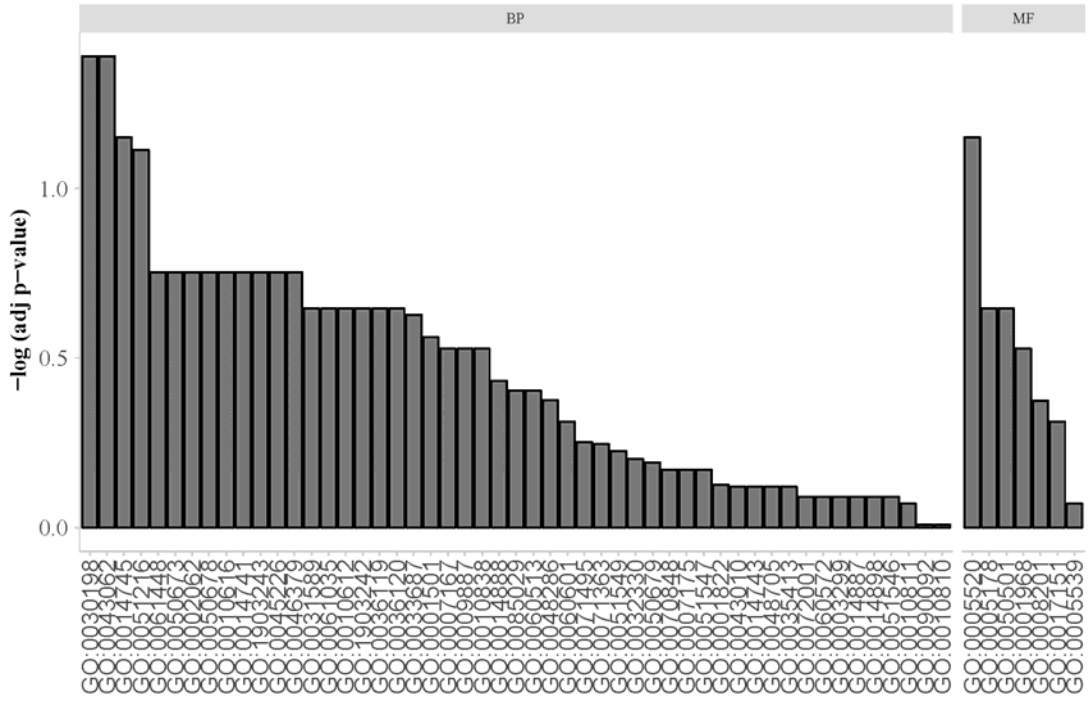

Appendix 5.3: Distribution GO term p-values from Question 3
RNA-sequencing of synovial macrophages and data analyses were conducted following methods described in Chapter 2. Perturbed GO terms passing adjusted p<0.05 and q-value FDR <0.25, based upon DEGs from Question 3 (>1.5-fold change; p<0.05, multiple test corrected).

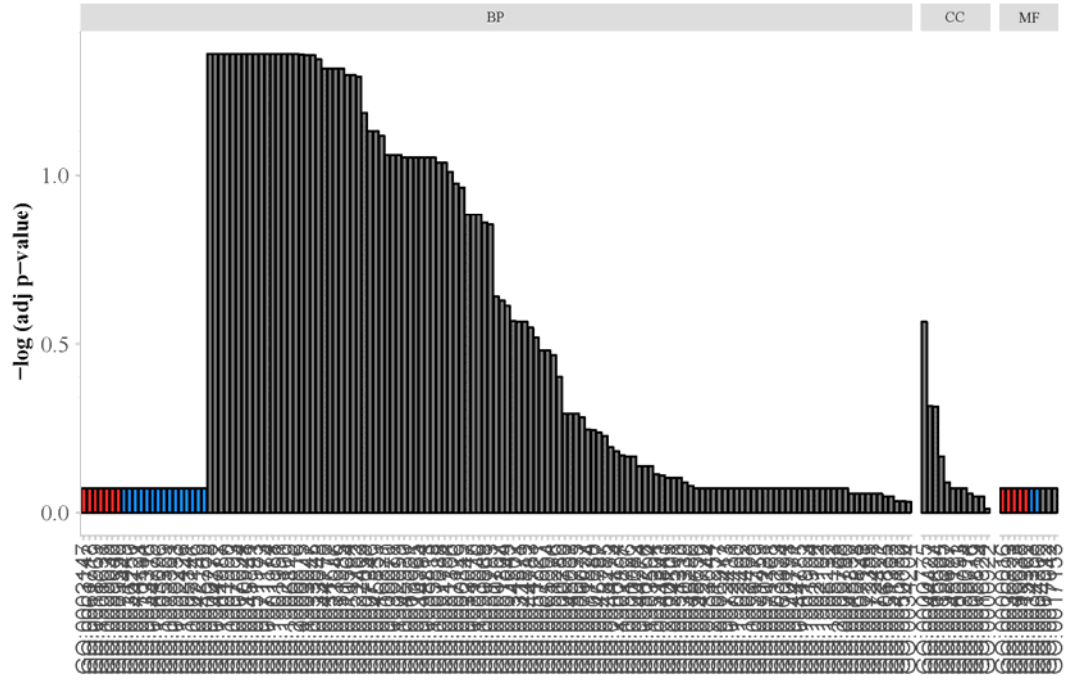

Appendix 5.4: Distribution GO term p-values from Question 4
RNA-sequencing of synovial macrophages and data analyses were conducted following methods described in Chapter 2. Perturbed GO terms passing adjusted p<0.05 and q-value FDR <0.25, based upon DEGs from Question 4 (>1.5-fold change; p<0.05, multiple test corrected).

Pathways 1-37	Pathways 38-74
Mitotic Cell Cycle Checkpoint	Regulation of Nuclear Division
Regulation of Mitotic Cell Cycle	Regulation of Mitotic Sister Chromatid Segregation
Regulation of Chromosome Separation	Chromosome Separation
Regulation of Cell Cycle Phase T	Protein Localization to Chromosome
Negative Regulation of Cell Cycle Process	Mitotic Nuclear Division
Negative Regulation of Mitotic Cell Cycle Phase T	Mitotic G1 DNA Damage Checkpoint
Negative Regulation of Cell Cycle Phase T	Mitotic G1/S Transition Checkpoint
Mitotic Cell Cycle Phase Transition	Meiotic Cell Cycle
Mitotic Spindle Assembly Checkpoint	G1 DNA Damage Checkpoint
Spindle Assembly Checkpoint	Protein-DNA Complex Assembly
Cell Cycle Checkpoint	DNA Damage Checkpoint
Mitotic Spindle Checkpoint	Positive Regulation of Cell Cycle
Cell Cycle Checkpoint	Protein-DNA Complex Subunit Organization
Negative Regulation of Mitotic Metaphase/Anaphase Transition	DNA Recombinase Assembly
Negative Regulation of Metaphase/Anaphase Transition of Cell Cycle	Double-strand Break Repair via Synthesis-Dependent Strand Annealing
Negative Regulation of Chromosome Separation	DNA Repair Complex Assembly
Regulation of Mitotic Sister Chromatid Separation	Mitotic Metaphase Plate Congression
Regulation of Sister Chromatid Segregation	Mitotic DNA Damage Checkpoint
Regulation of Mitotic Sister Chromatid Segregation	G1/S Transition of Mitotic Cell Cycle
Chromosome Segregation	Negative Regulation of G1/S Transition of Mitotic Cell Cycle
Negative Regulation of Sister Chromatid Segregation	Cell Division
Negative regulation of Chromosome Segregation	Negative Regulation of Cell cycle G1/S Phase Transition
Spindle Checkpoint	Cell Cycle G1/S Phase Transition
Mitotic Sister Chromatid Segregation	Negative Regulation of Cell Cycle
Regulation of Mitotic Metaphase/Anaphase Transition	Mitotic DNA Integrity Checkpoint
Regulation of Metaphase/Anaphase Transition of Cell Cycle	Regulation of Mitotic Cell Cycle Assembly
Metaphase/Anaphase Transition of Mitotic Cell Cycle	DNA Damage Response, Signal Transduction by p53 Class Mediator Resulting in Cell Cycle Arrest
Regulation of Mitotic Sister Separation	Positive Regulation of DNA-Dependent DNA Replication
Metaphase/Anaphase Transition of Cell Cycle	Protein Localization to Kinetochore
Regulation of Chromosome Separation	Signal Transduction Involved in DNA Integrity Checkpoint
Negative Regulation of nuclear Division	Signal Transduction Involved in DNA Damage Checkpoint
Sister Chromatid Segregation	Signal Transduction Involved in Mitotic Cell Cycle Checkpoint
Meiotic Nuclear Division	Regulation of Cell Cycle G1/S Phase
Mitotic Sister Chromatid Separation	Establishment of Chromosome Localisation
DNA Integrity Checkpoint	Spindle Organization
Meiotic Cell Cycle Process	RNA Destabilisation
Positive Regulation of Cell Cycle Process	Synaptonemal Complex Organisation

Appendix 5.5: GO term pathways for Question 5 network analysis. GO terms passing adjusted $p<0.05$ and q-value FDR <0.25, based upon DEGs from Question 4 (>1.5-fold change; $p<0.05$, multiple test corrected).

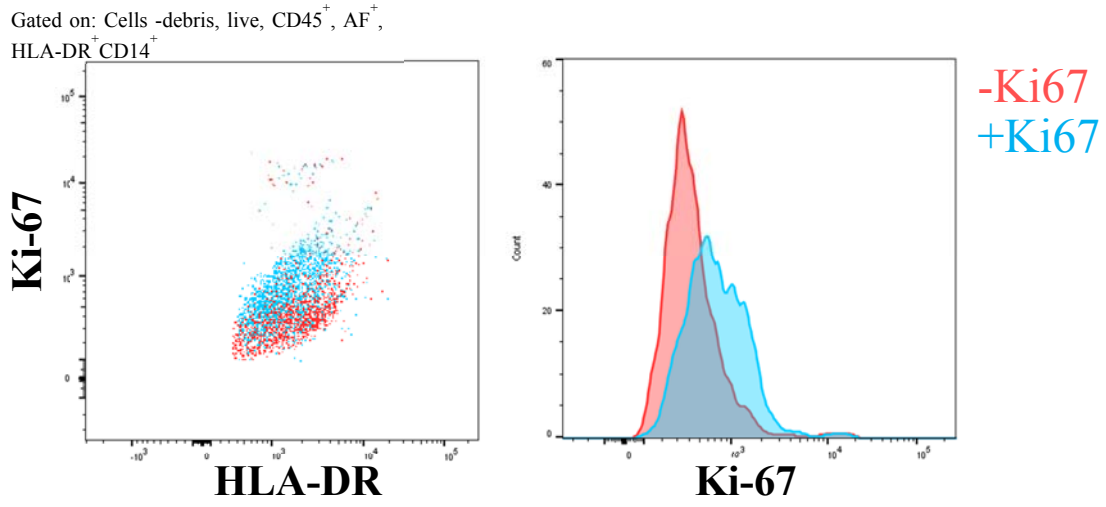

Appendix 5.6: Expression of Ki-67 on synovial macrophages
Synovial tissue from OA total knee replacement was digested and analysed by flow cytometry using techniques described in Chapter 3. Expression of Ki-67 on OA synovial macrophages. Left panel depicts overlay dotplot of sample stained with and without Ki-67. Right panel depicts histograms of Ki-67 expression on synovial macrophages. Data are representative of 1 experiment.

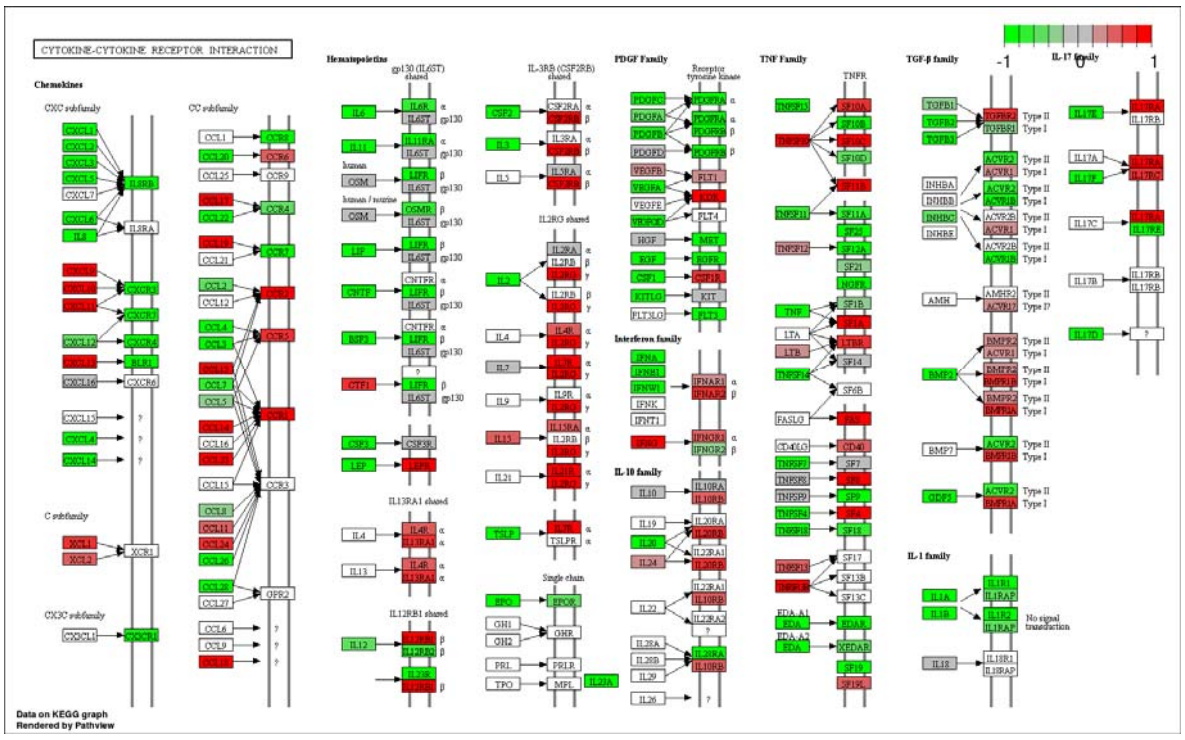

Appendix 5.7: Cytokine-Cytokine Receptor Interaction KEGG pathway
Greater perturbed KEGG pathway from Question 1 (IA v OA)

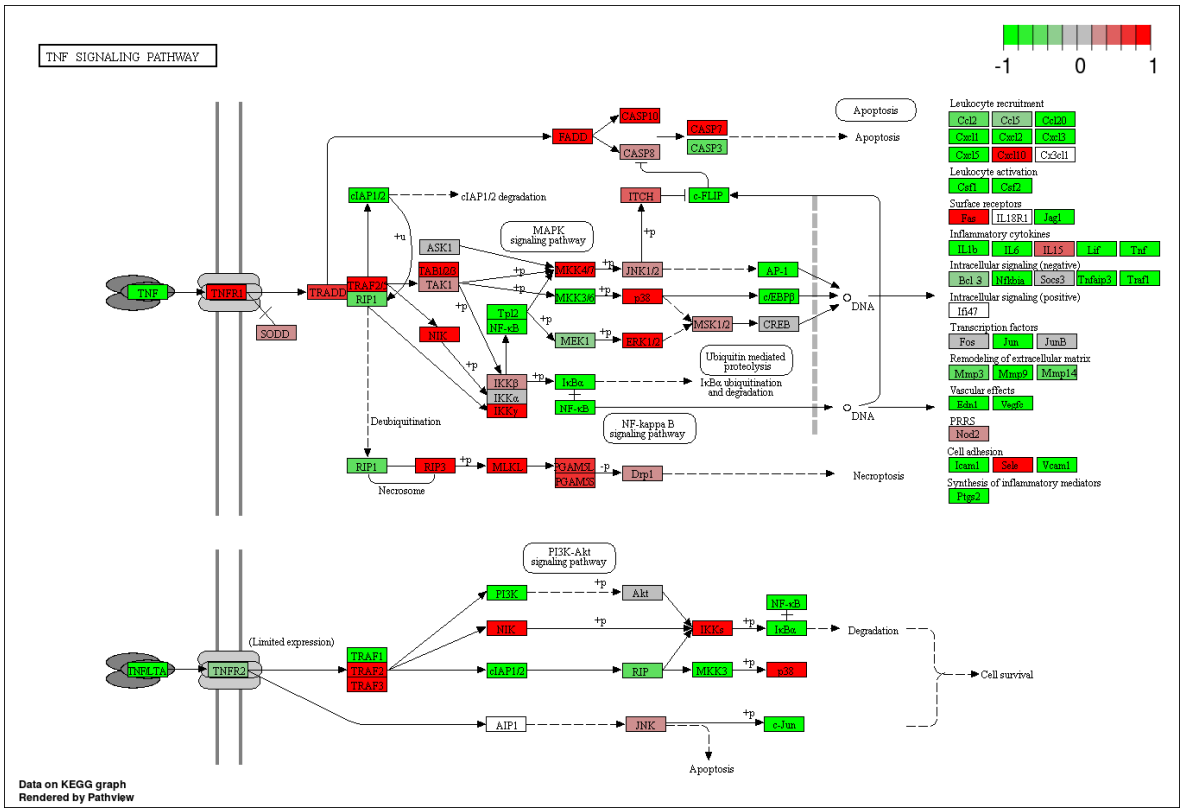

Appendix 5.8: TNF Signalling KEGG pathway
Greater perturbed KEGG pathway from Question 1 (IA v OA)

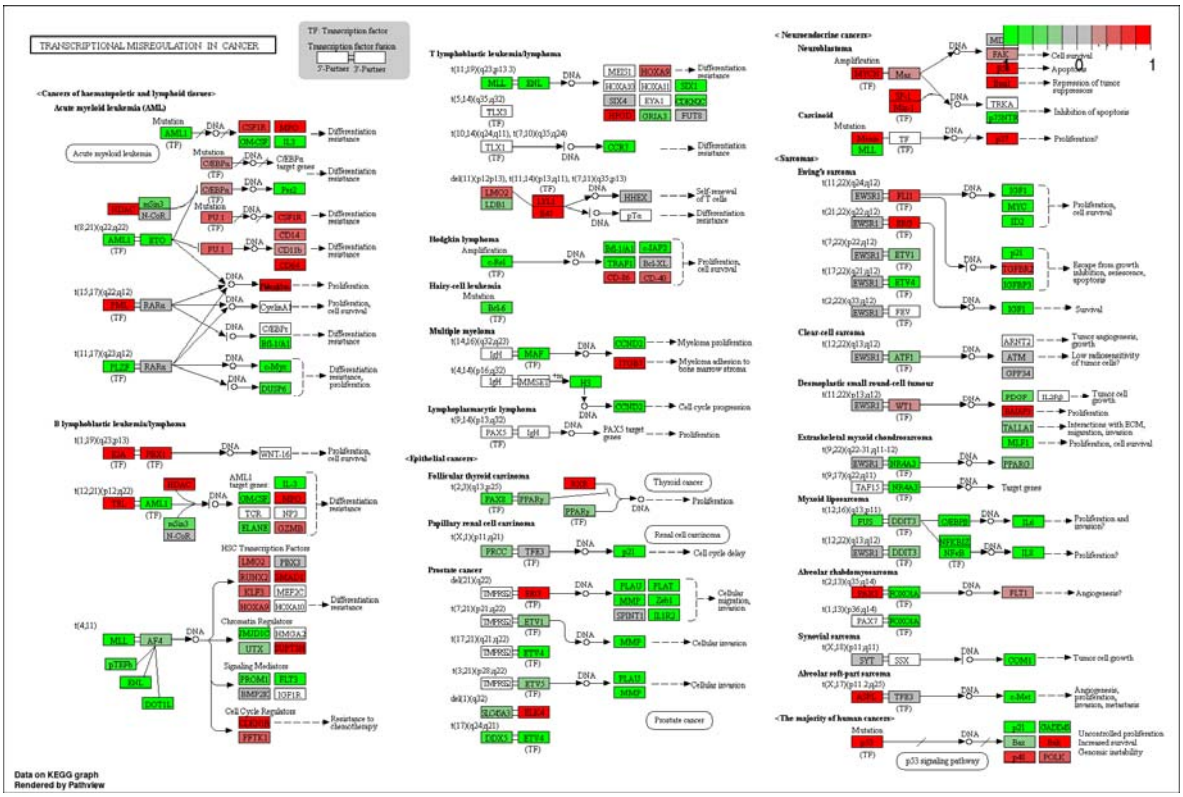

Appendix 5.9: Transcriptional Misregulation in Cancer KEGG pathway
Greater perturbed KEGG pathway from Question 1 (IA v OA)

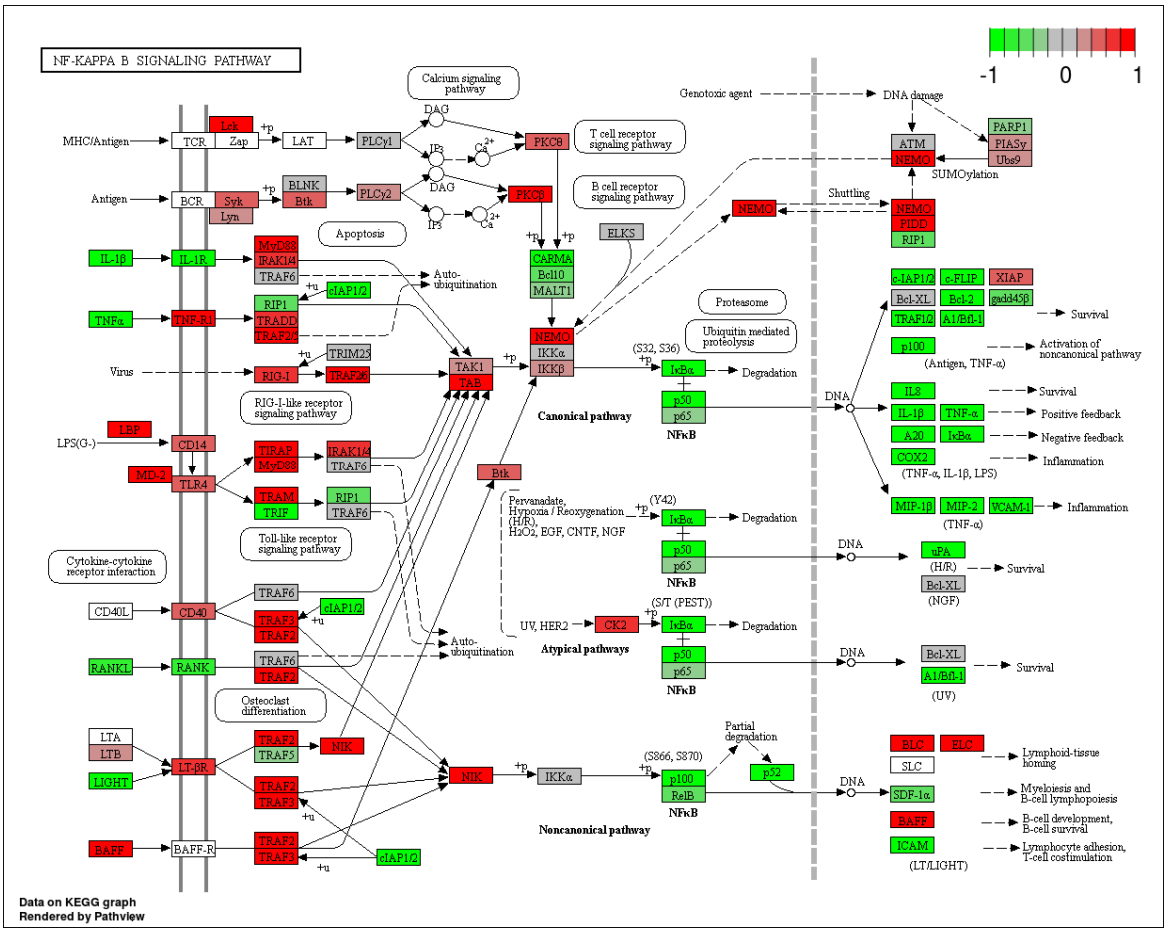

Appendix 5.10: NF-Kappa B KEGG pathway
Greater perturbed KEGG pathway from Question 1 (IA v OA)

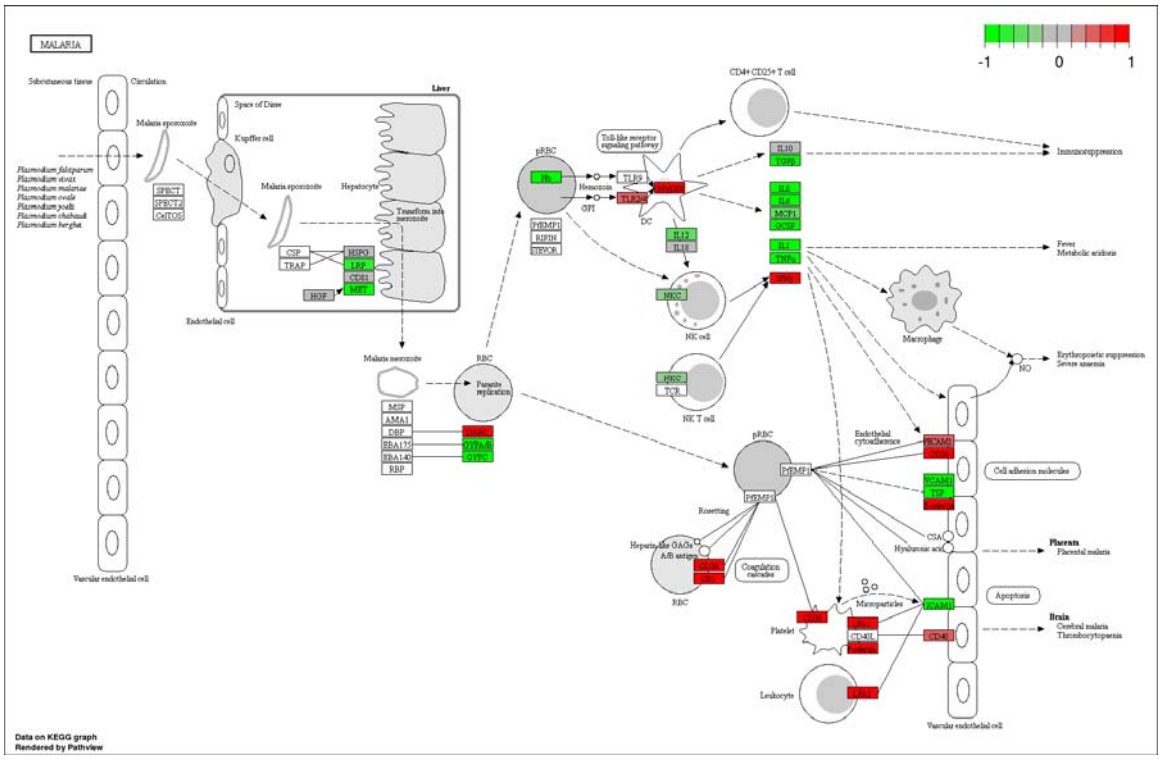

Appendix 5.11: Malaria KEGG pathway
Greater perturbed KEGG pathway from Question 1 (IA v OA)

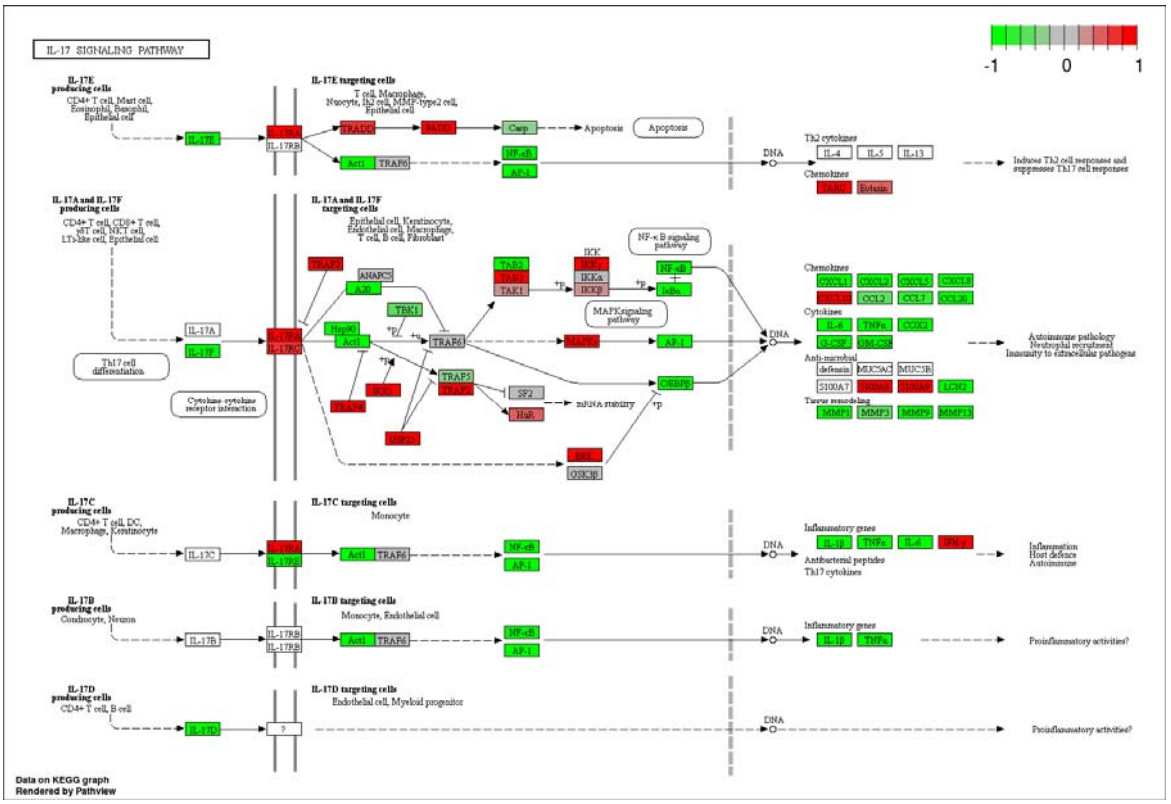

Appendix 5.12: IL-17 Signalling KEGG pathway
Greater perturbed KEGG pathway from Question 1 (IA v OA)

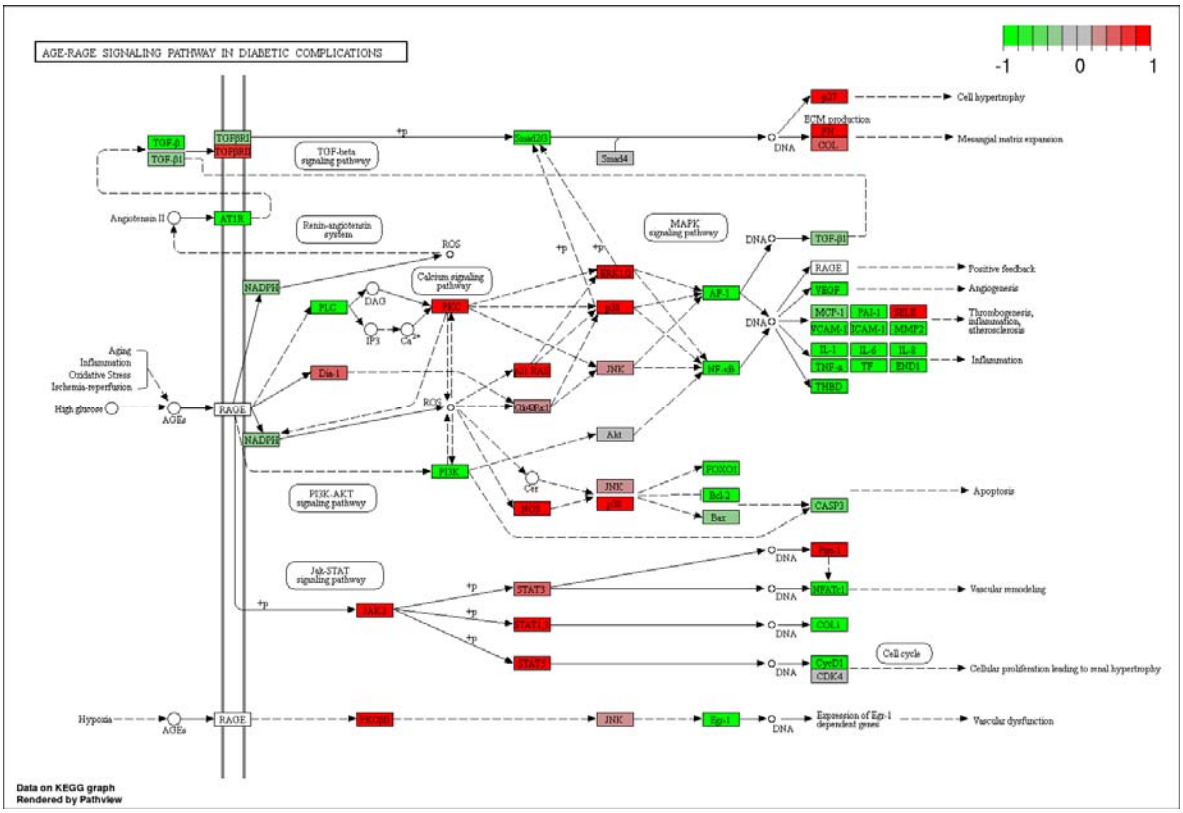

Appendix 5.13: AGE-RAGE Signalling Pathway in Diabetic Complications KEGG pathway
Greater perturbed KEGG pathway from Question 1 (IA v OA)

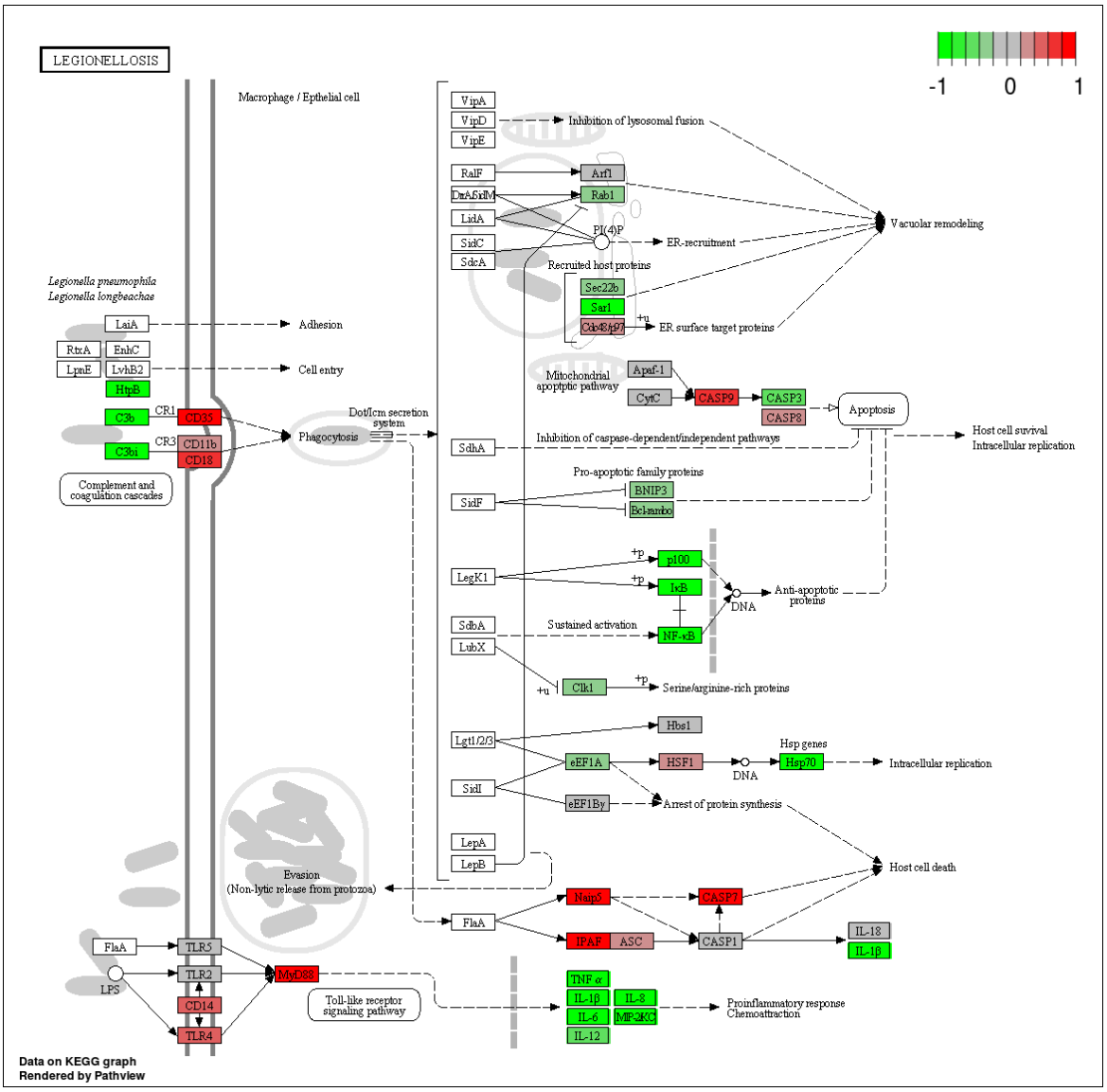

Appendix 5.14: Legionellosis KEGG pathway
Greater perturbed KEGG pathway from Question 1 (IA v OA)

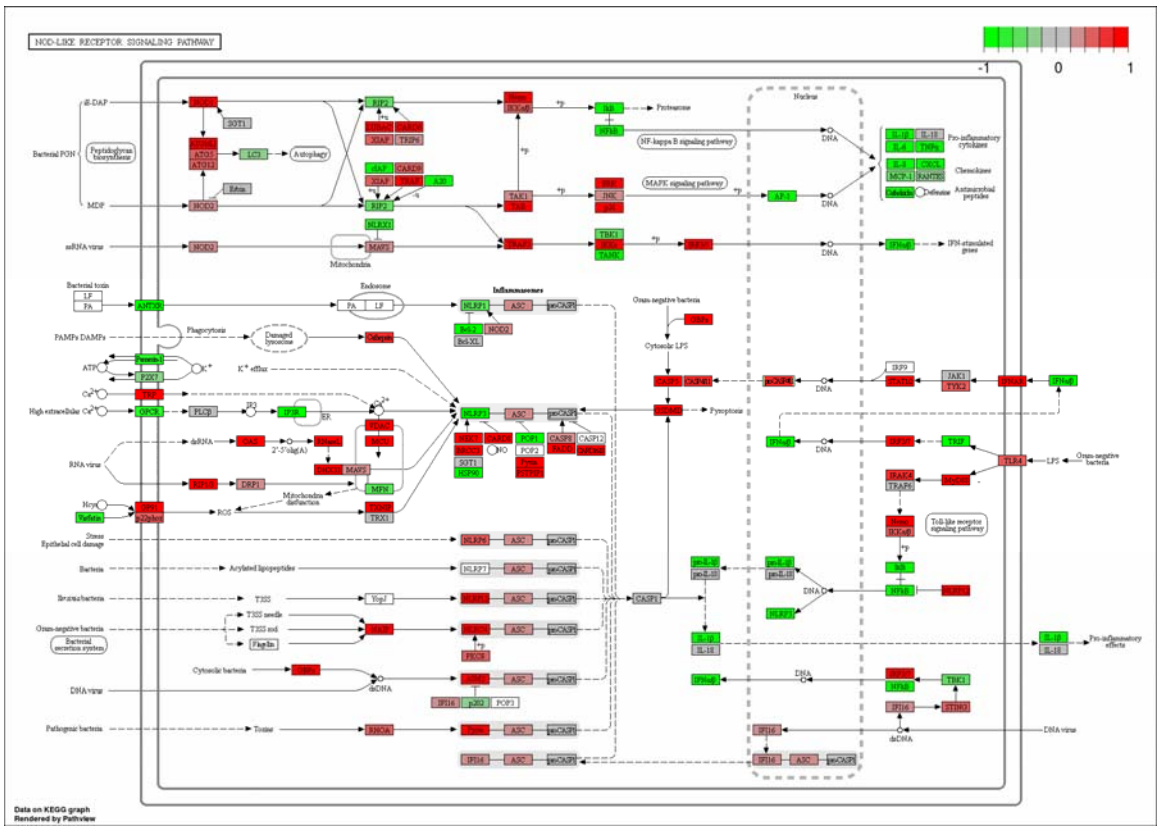

Appendix 5.15: NOD-like Receptor Signalling KEGG pathway
Greater perturbed KEGG pathway from Question 1 (IA v OA)

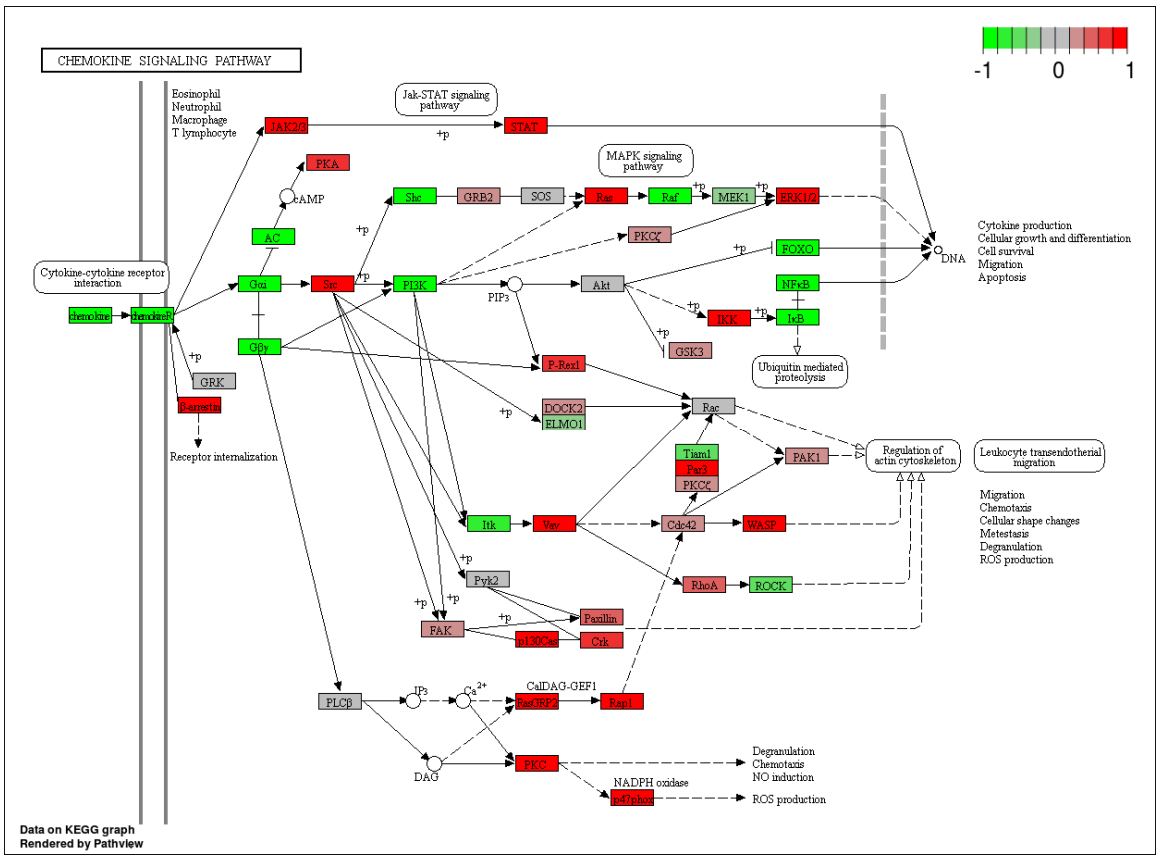

Appendix 5.16: Chemokine Signalling KEGG pathway
Greater perturbed KEGG pathway from Question 1 (IA v OA)

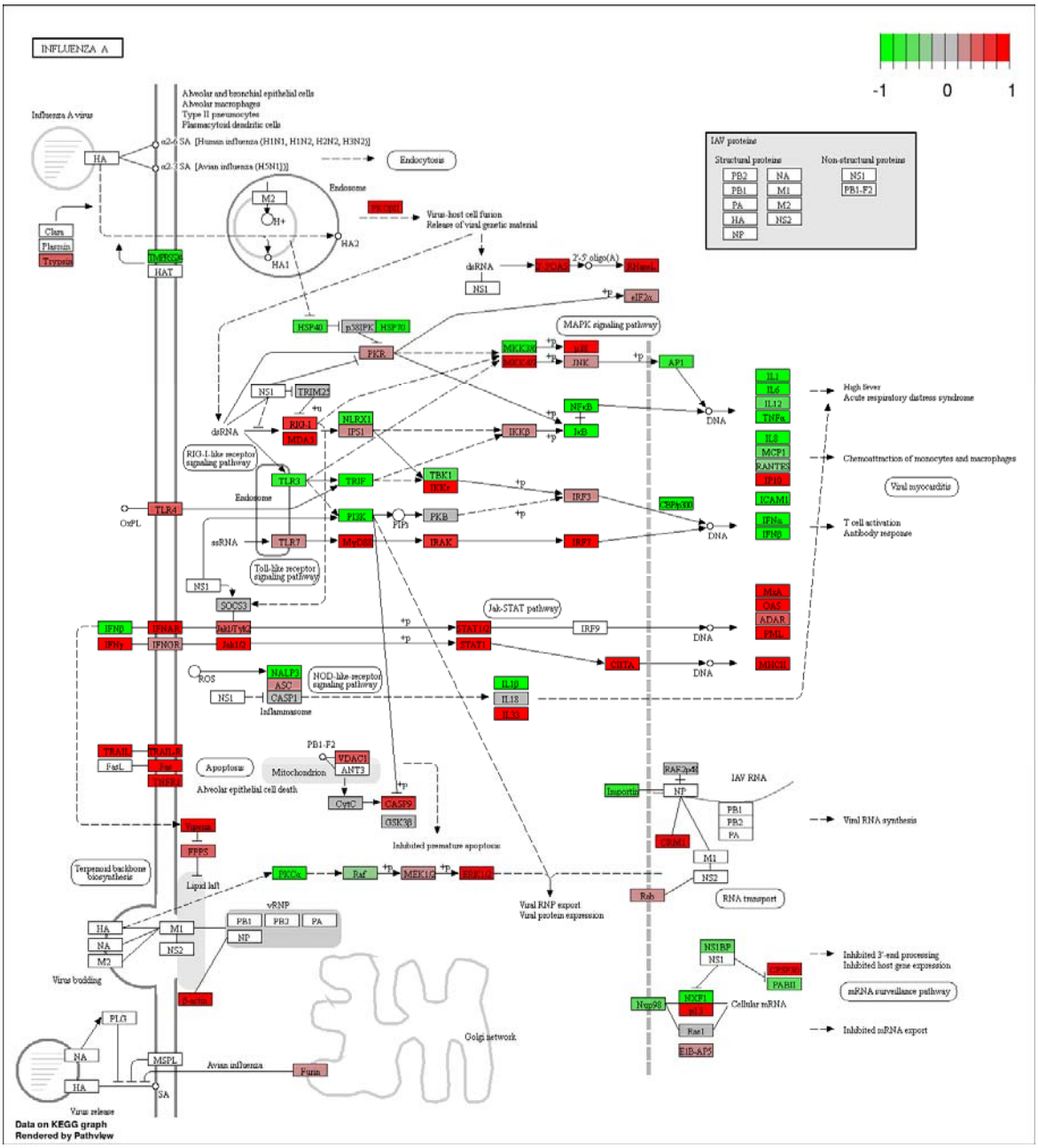

Appendix 5.17: Influenza A KEGG pathway
Greater perturbed KEGG pathway from Question 1 (IA v OA)

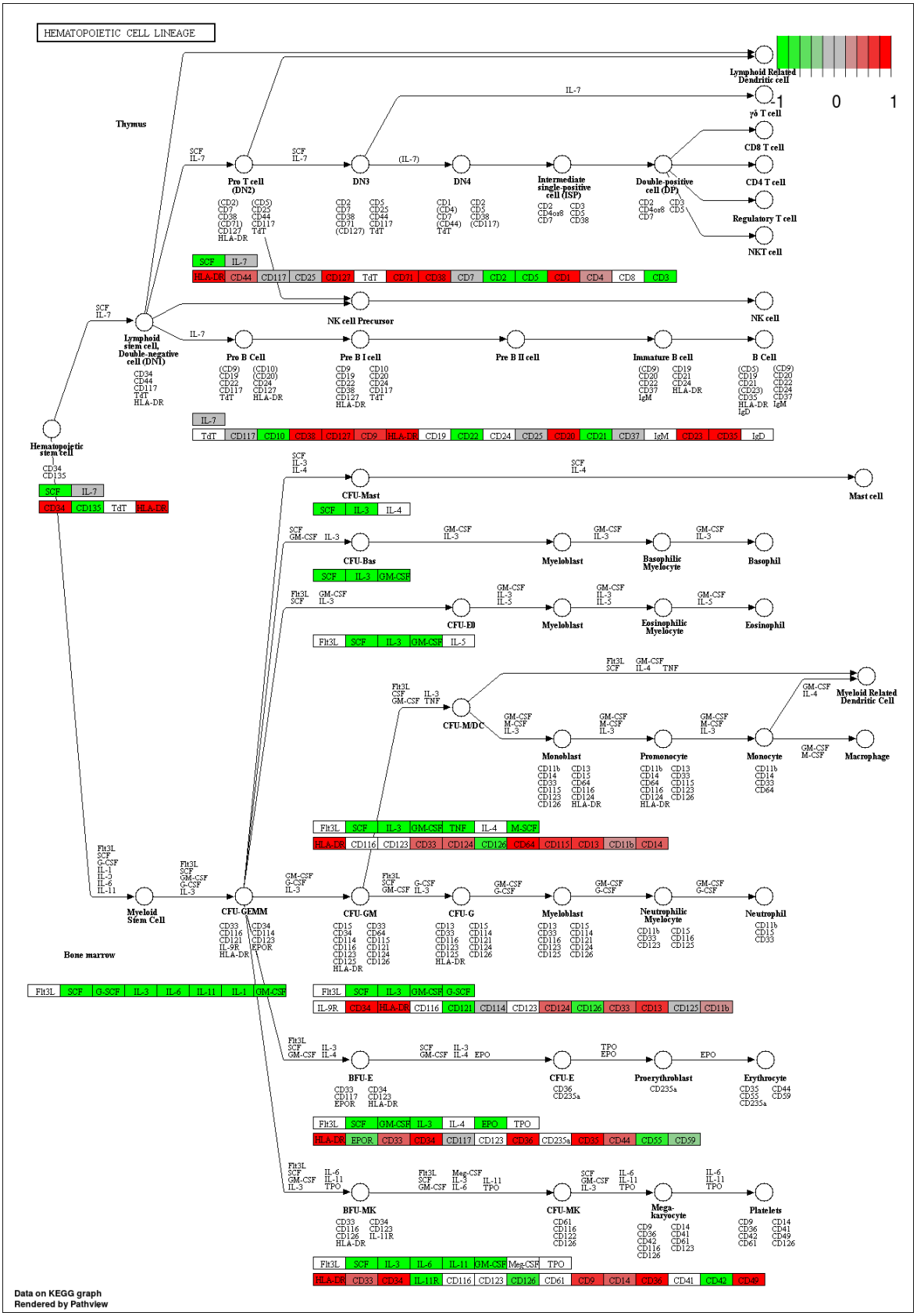

Appendix 5.18: Hematopoietic Cell Lineage KEGG pathway
Greater perturbed KEGG pathway from Question 1 (IA v OA)

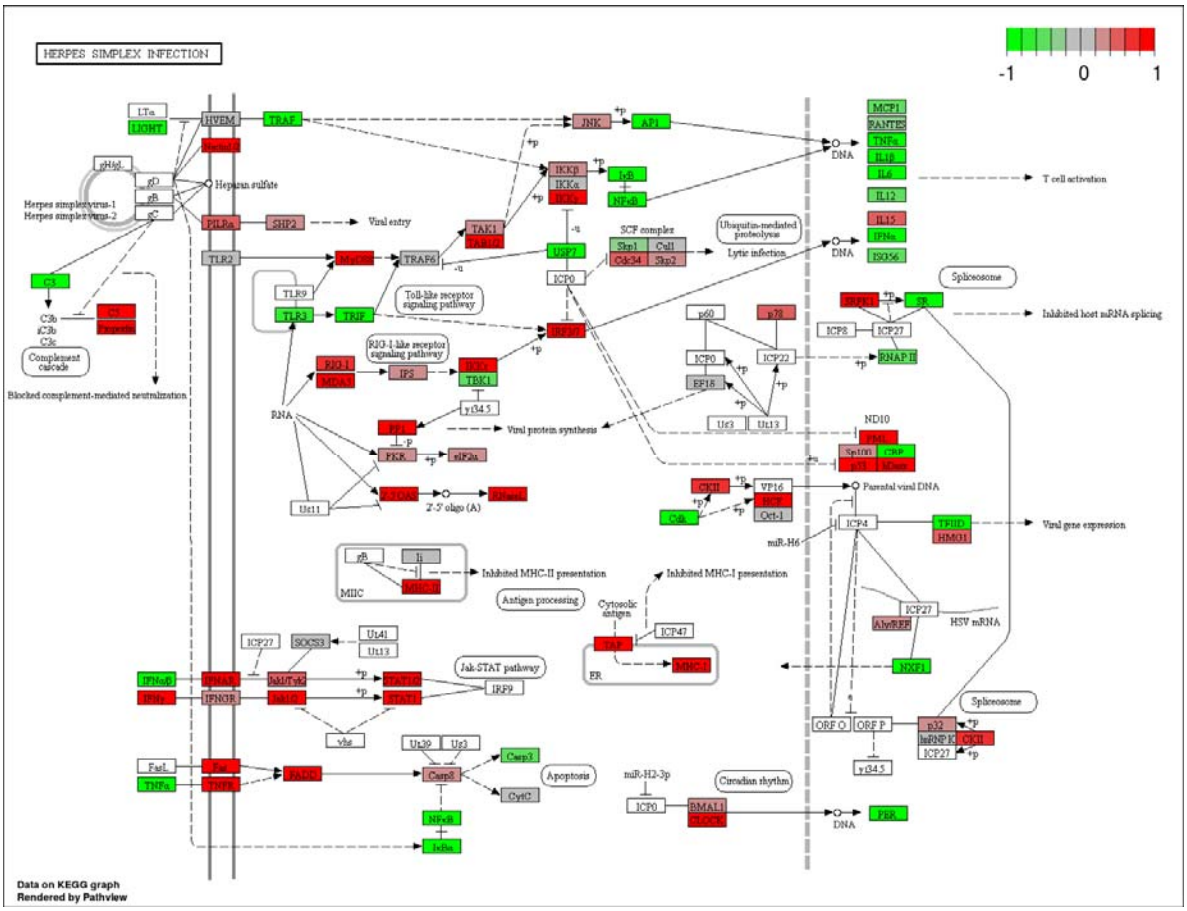

Appendix 5.19: Herpes Simplex Infection KEGG pathway
Greater perturbed KEGG pathway from Question 1 (IA v OA)

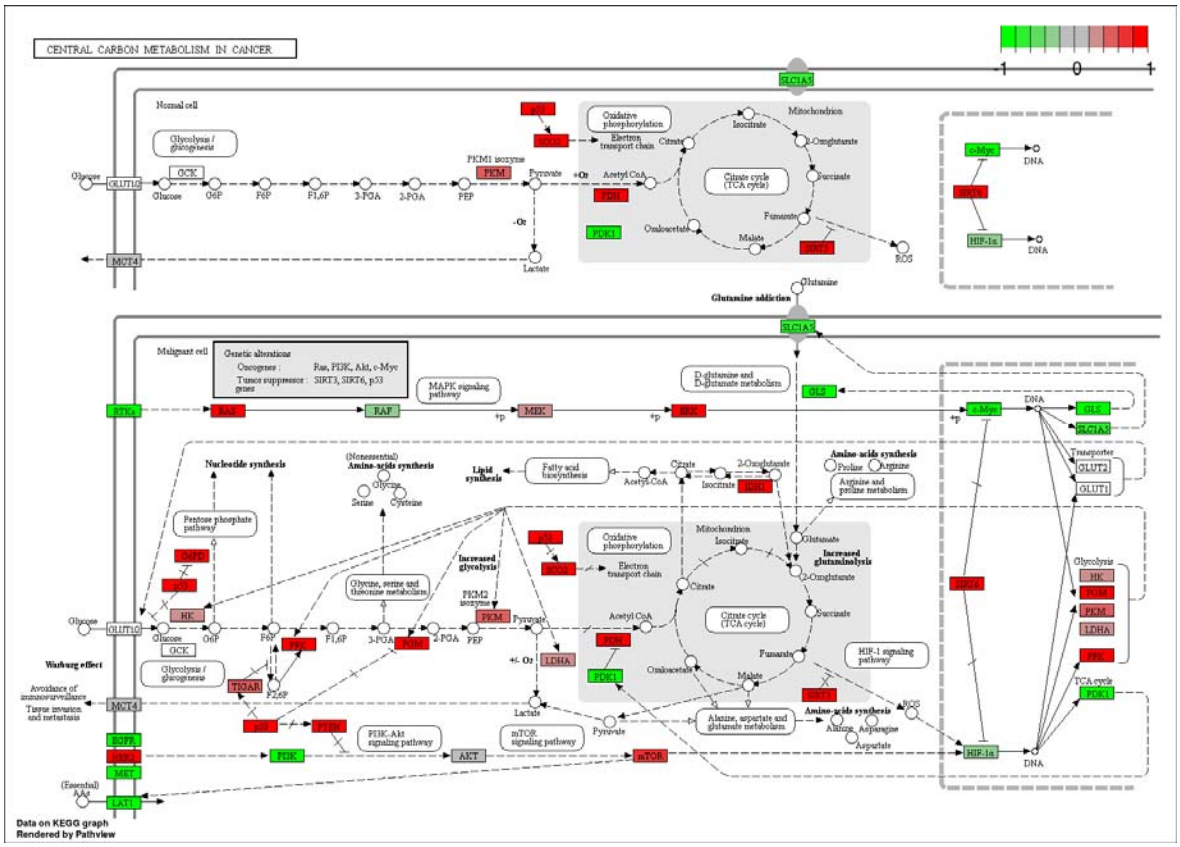

Appendix 5.20: Central Carbon Metabolism in Cancer KEGG pathway
Greater perturbed KEGG pathway from Question 1 (IA v OA)

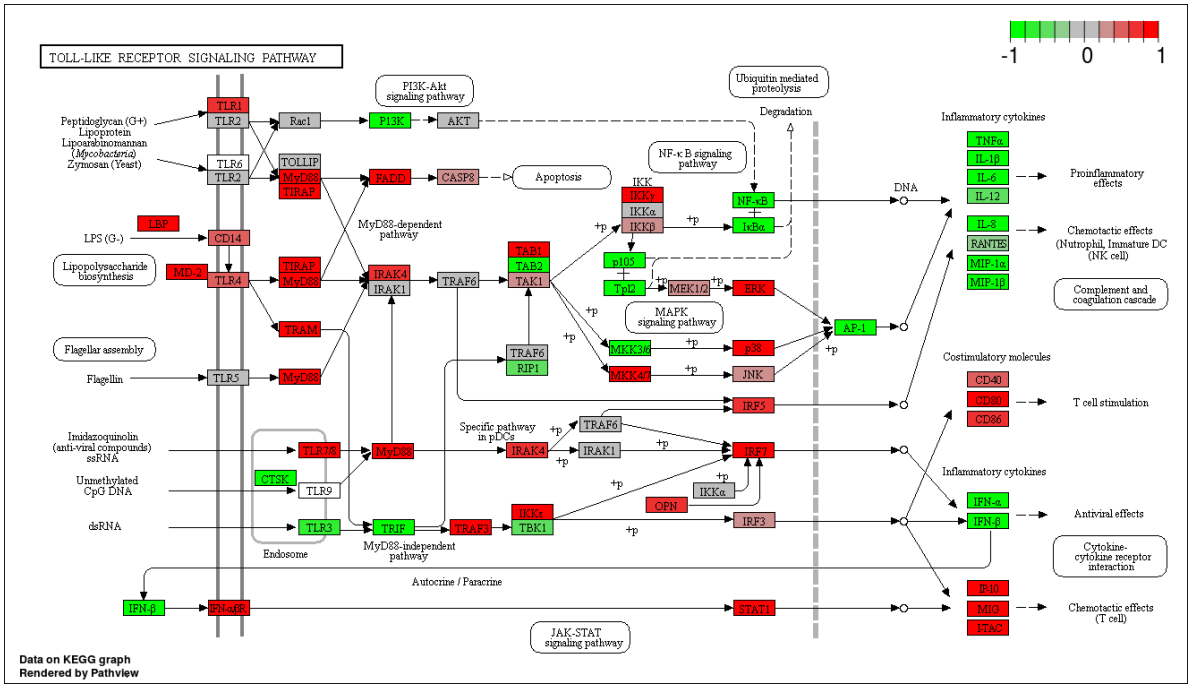

Appendix 5.21: Toll-like Receptor Signalling KEGG pathway
Greater perturbed KEGG pathway from Question 1 (IA v OA)

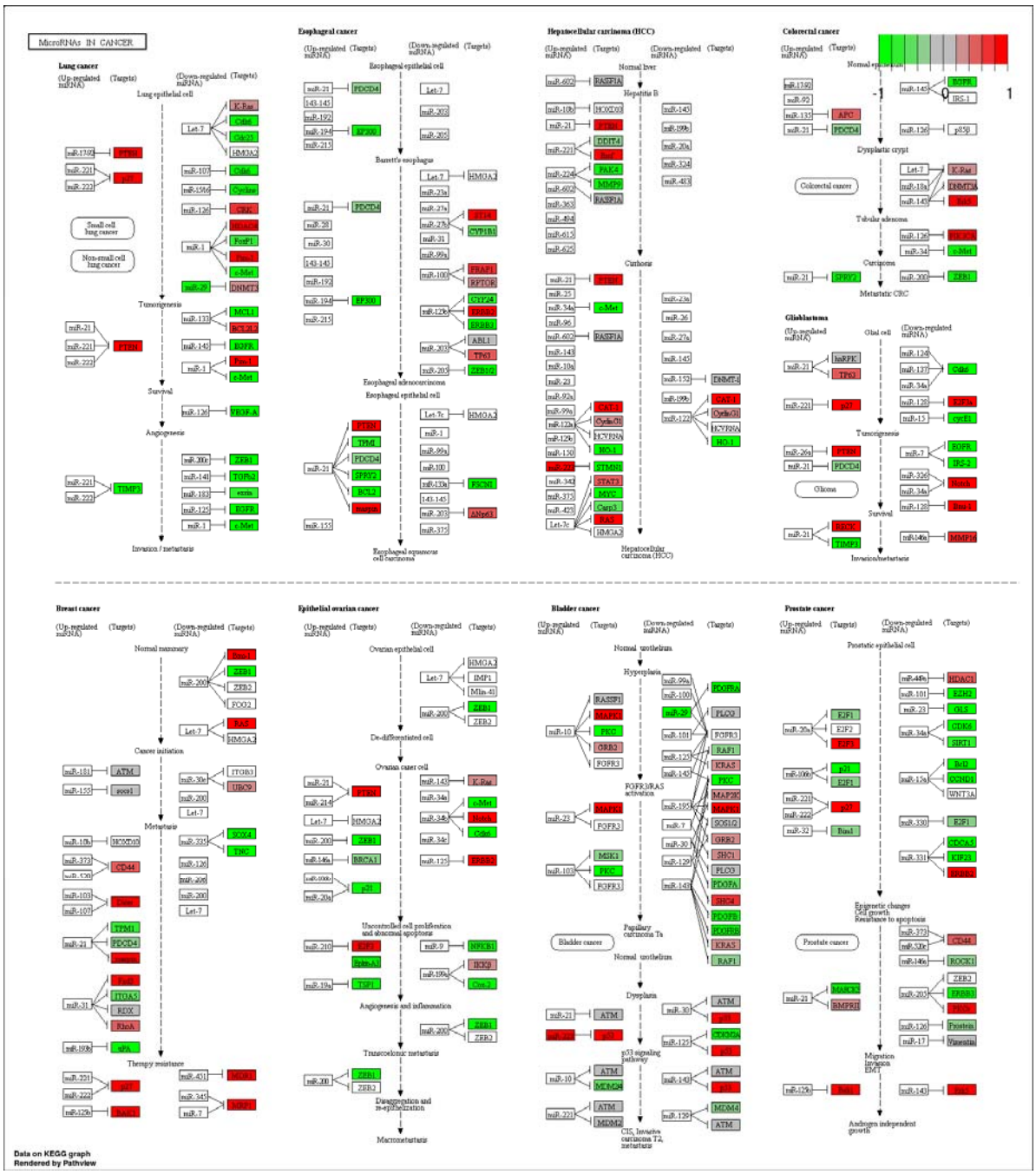

Appendix 5.22: MicroRNAs in Cancer KEGG pathway
Greater perturbed KEGG pathway from Question 1 (IA v OA)

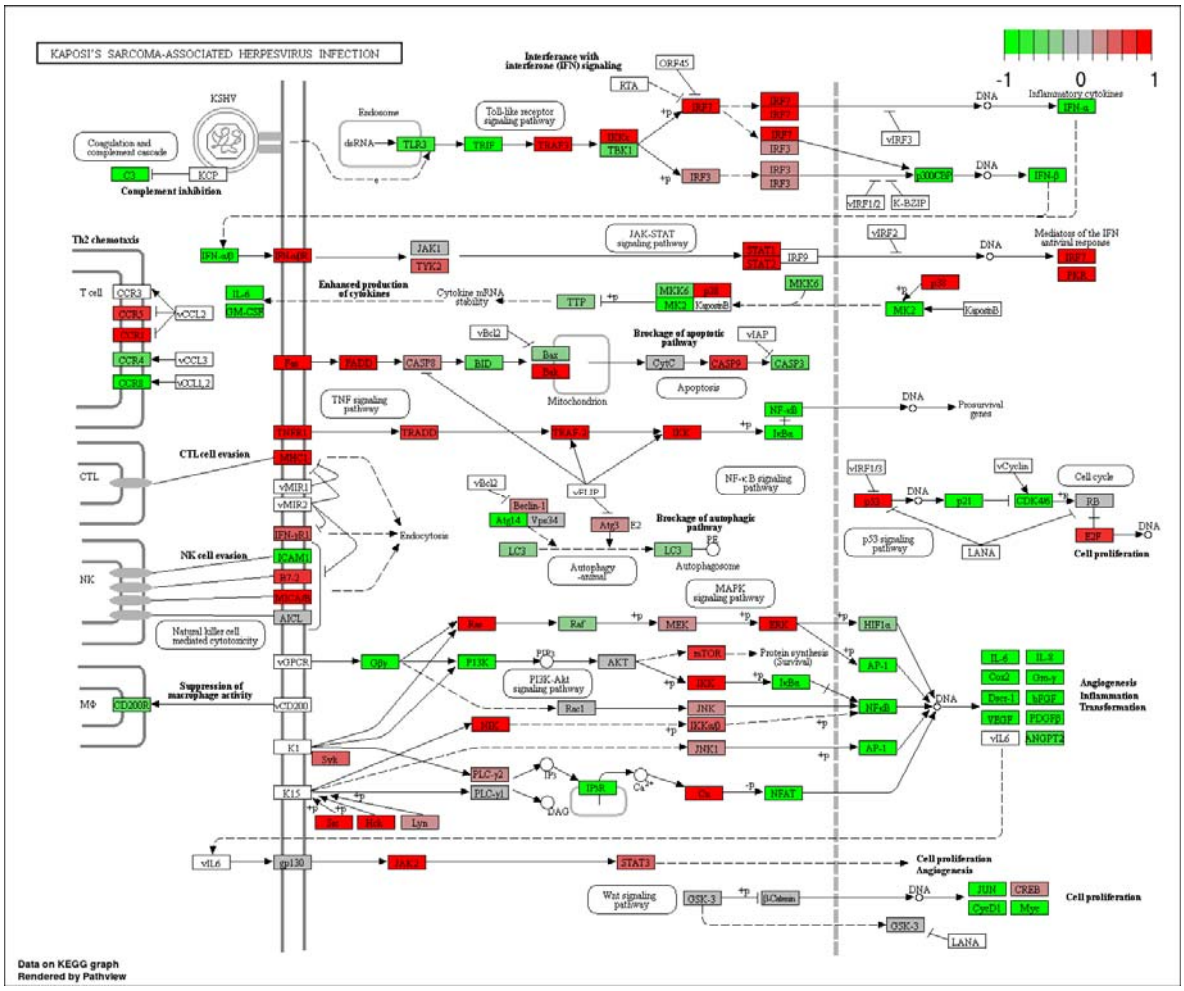

Appendix 5.23: Kaposi's Sarcoma-associated Herpesvirus Infection KEGG pathway
Greater perturbed KEGG pathway from Question 1 (IA v OA)

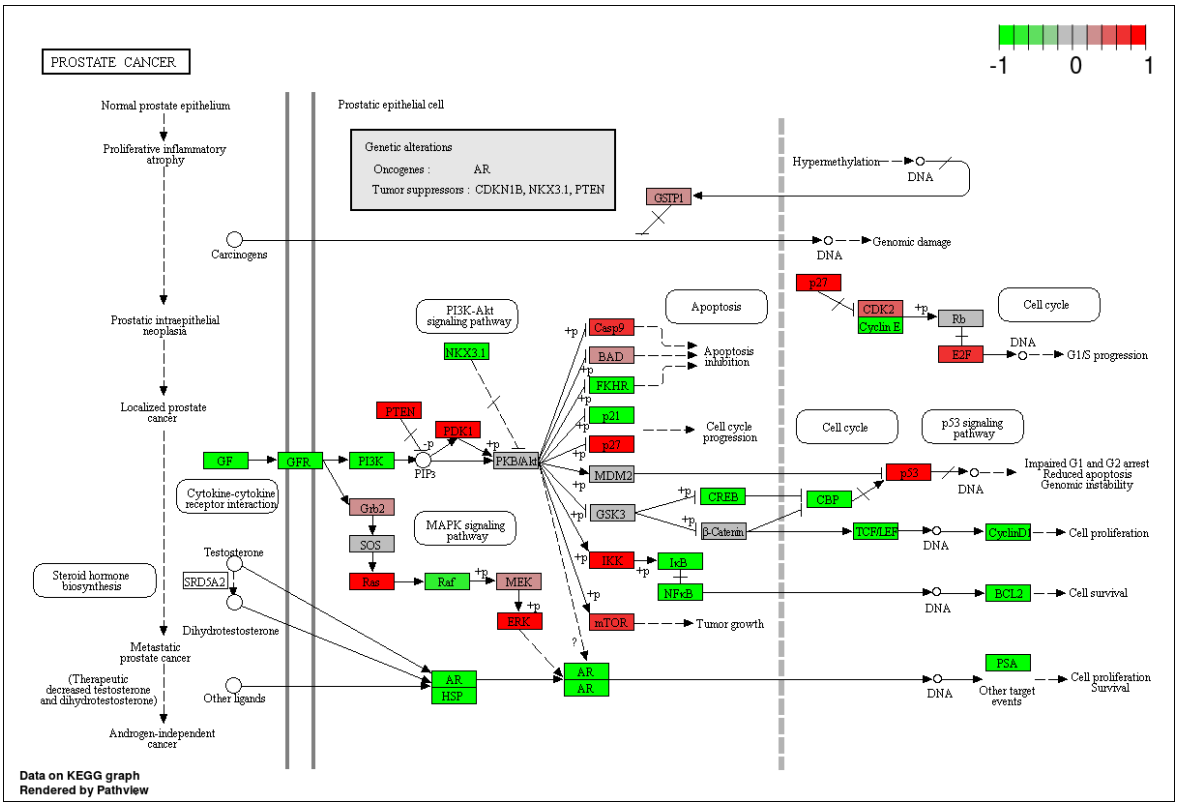

Appendix 5.24: Prostate Cancer KEGG pathway
Greater perturbed KEGG pathway from Question 1 (IA v OA)

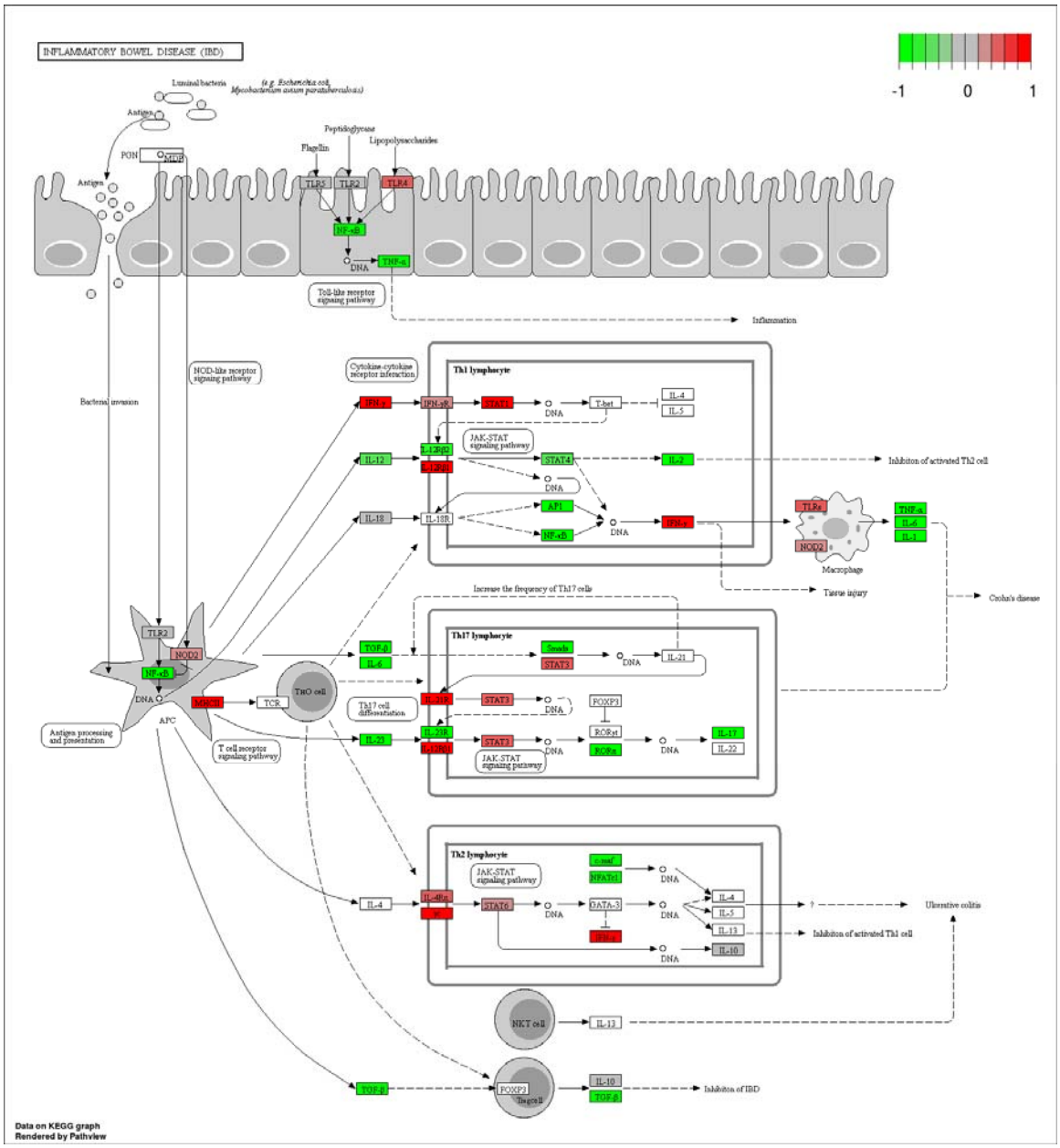

Appendix 5.25: Inflammatory Bowel Disease (IBD) KEGG pathway
Greater perturbed KEGG pathway from Question 1 (IA v OA)

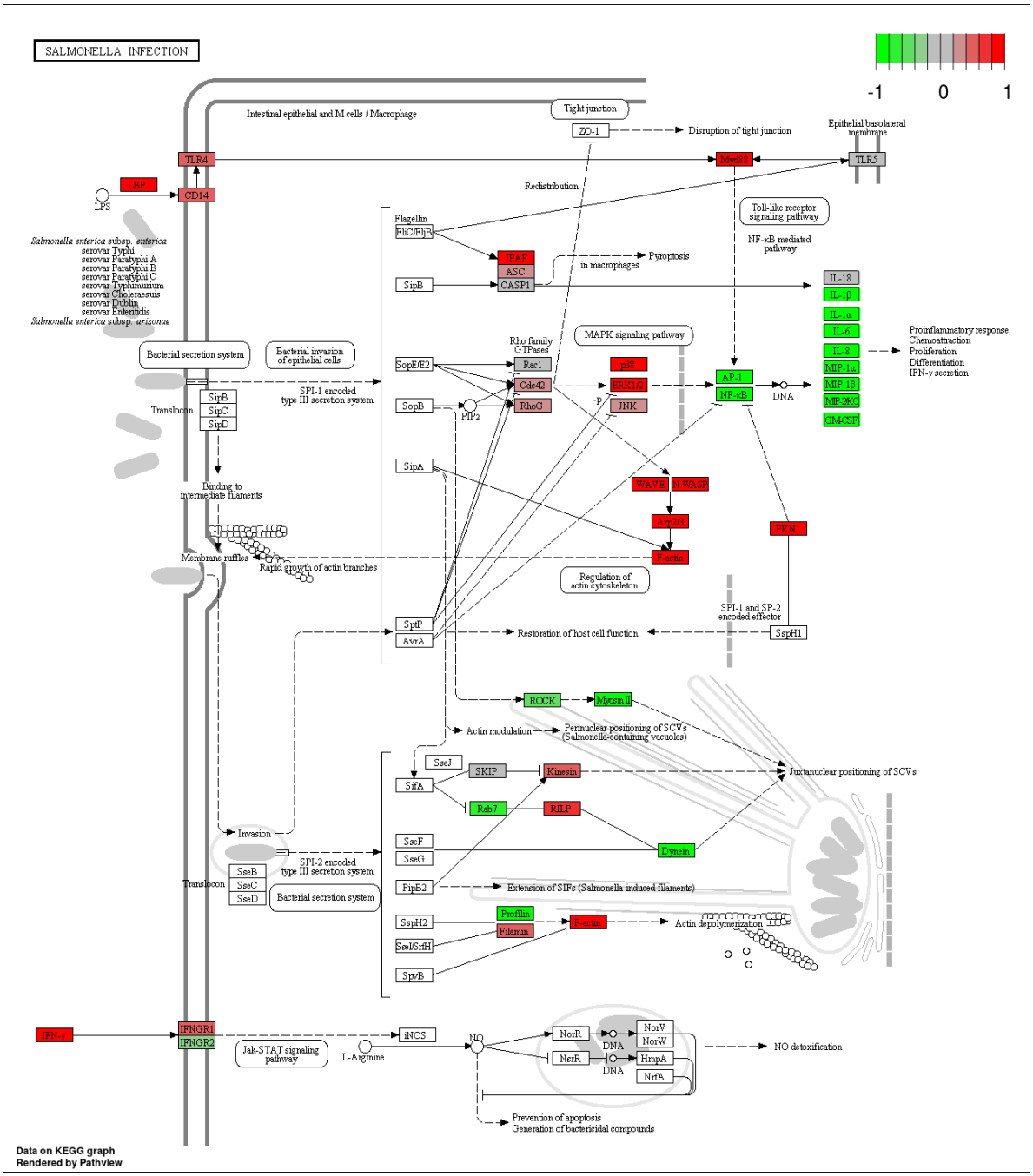

Appendix 5.26: Salmonella Infection KEGG pathway
Greater perturbed KEGG pathway from Question 1 (IA v OA)

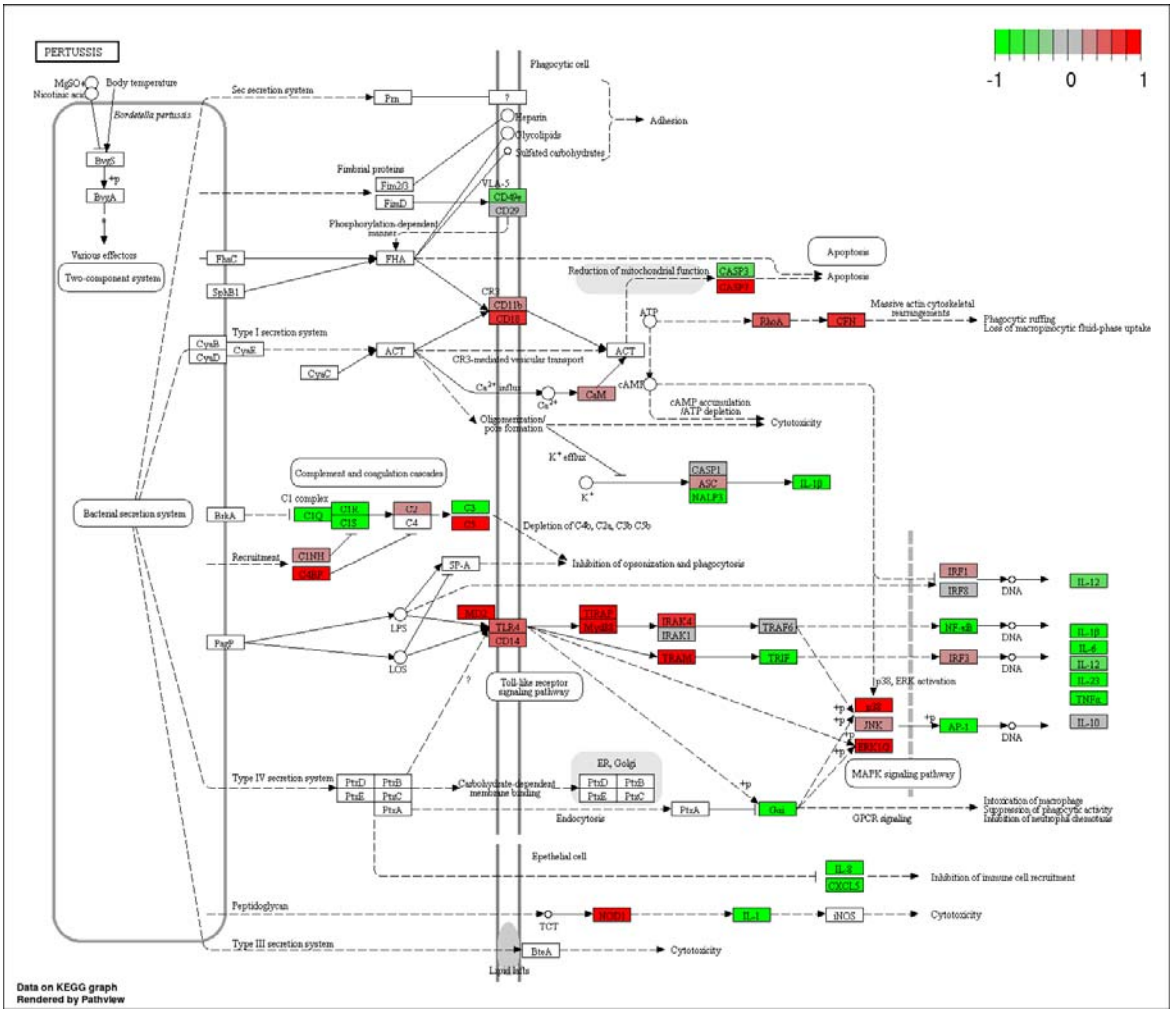

Appendix 5.27: Pertussis KEGG pathway
Greater perturbed KEGG pathway from Question 1 (IA v OA)

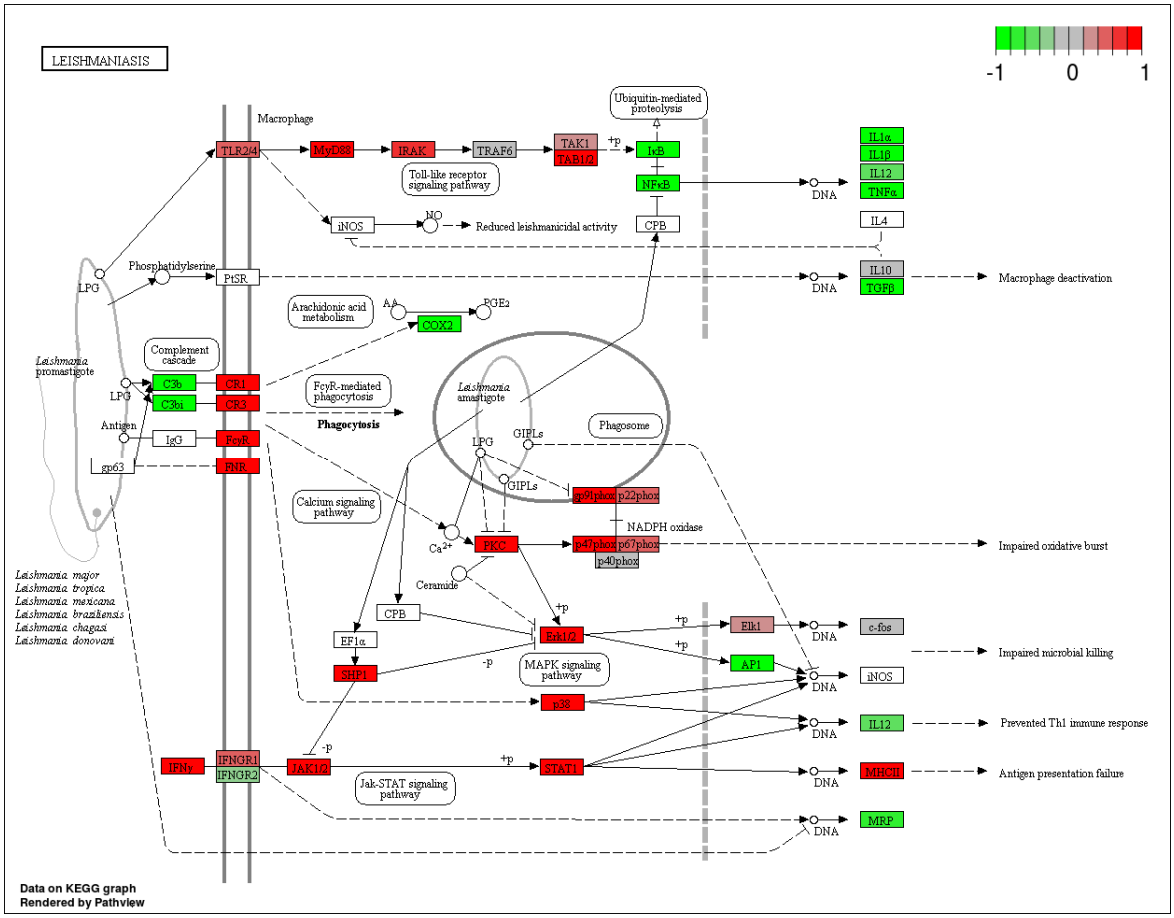

Appendix 5.28: Leishmaniasis KEGG pathway
Greater perturbed KEGG pathway from Question 1 (IA v OA)

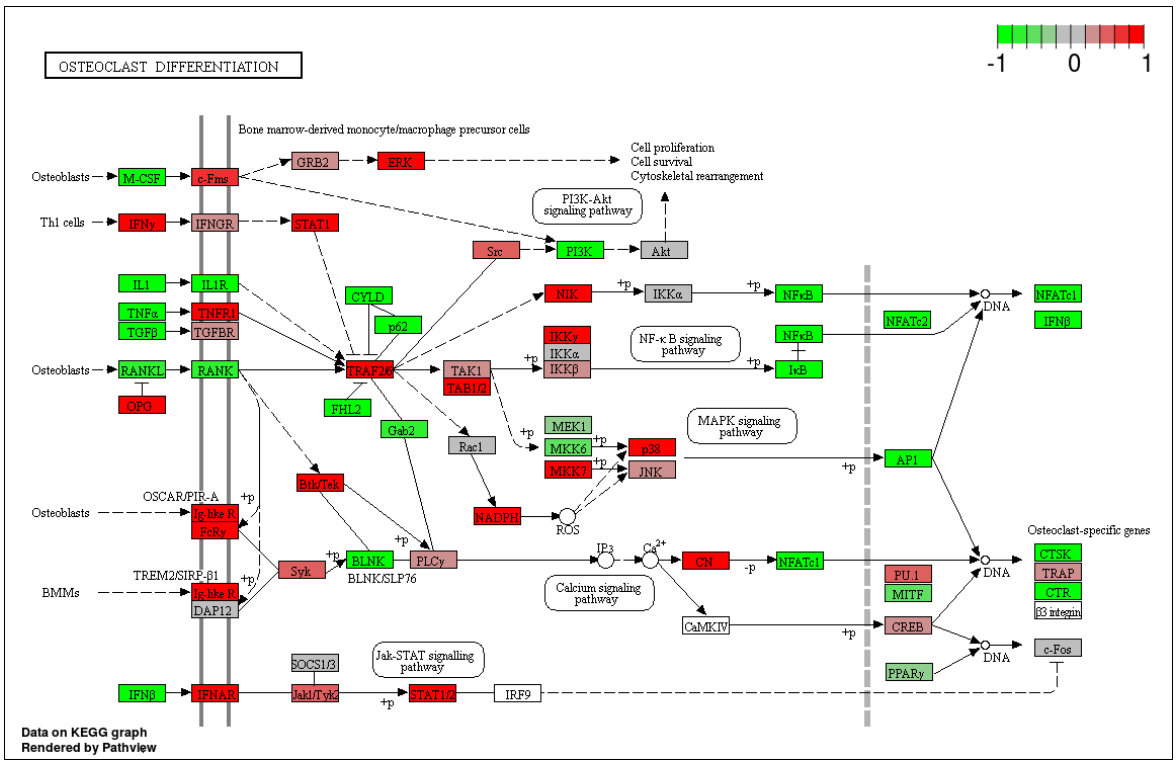

Appendix 5.29: Osteoclast Differentiation KEGG pathway
Greater perturbed KEGG pathway from Question 1 (IA v OA)

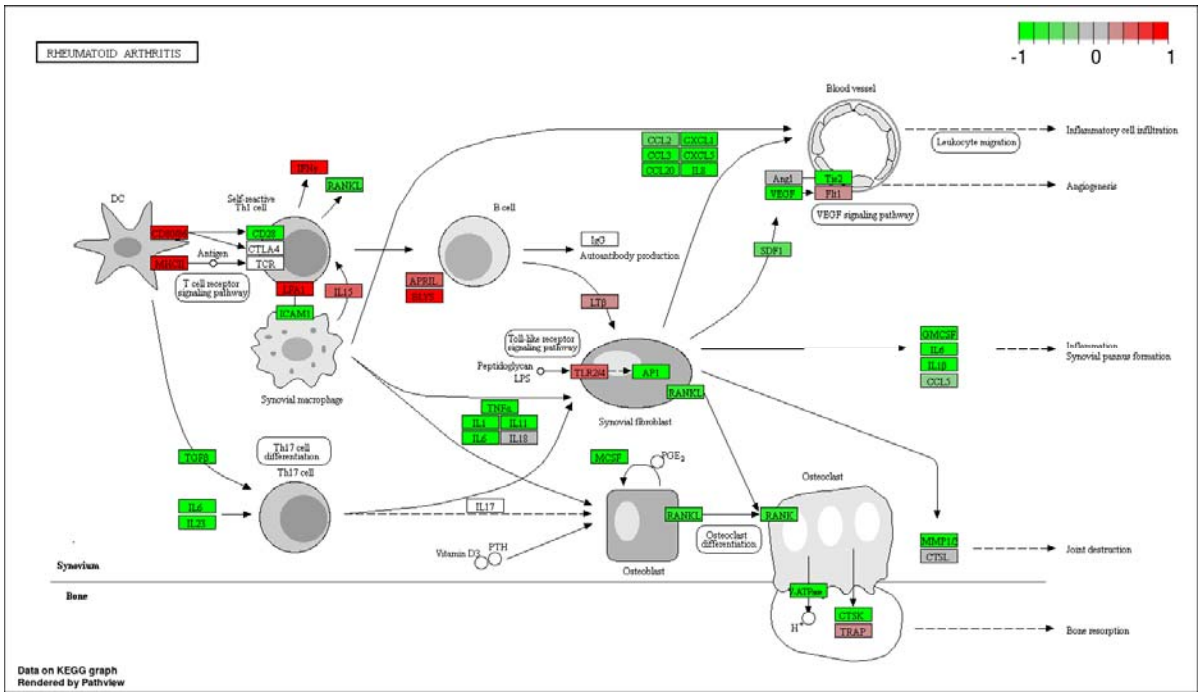

Appendix 5.30: Rheumatoid Arthritis KEGG pathway
Greater perturbed KEGG pathway from Question 1 (IA v OA)

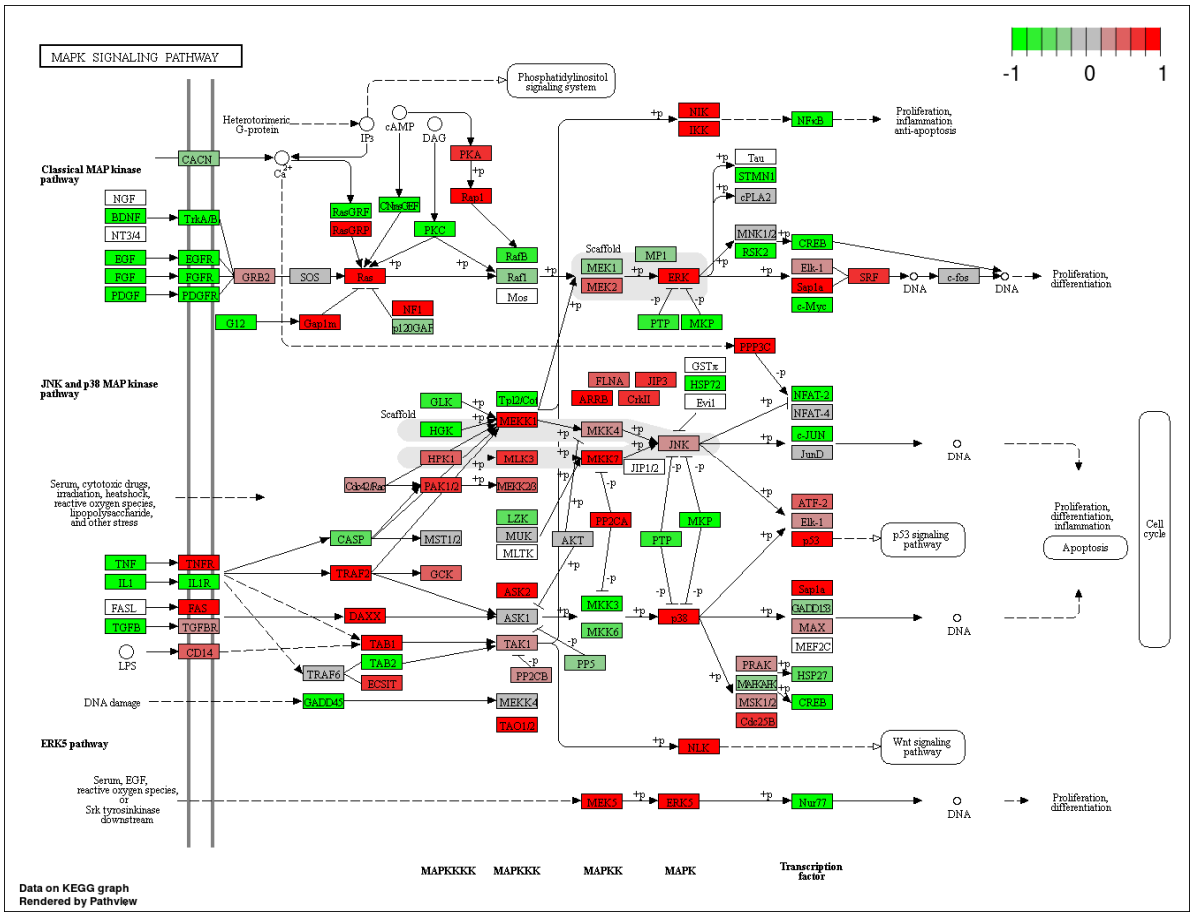

Appendix 5.31: MAPK Signalling KEGG pathway
Greater perturbed KEGG pathway from Question 1 (IA v OA)

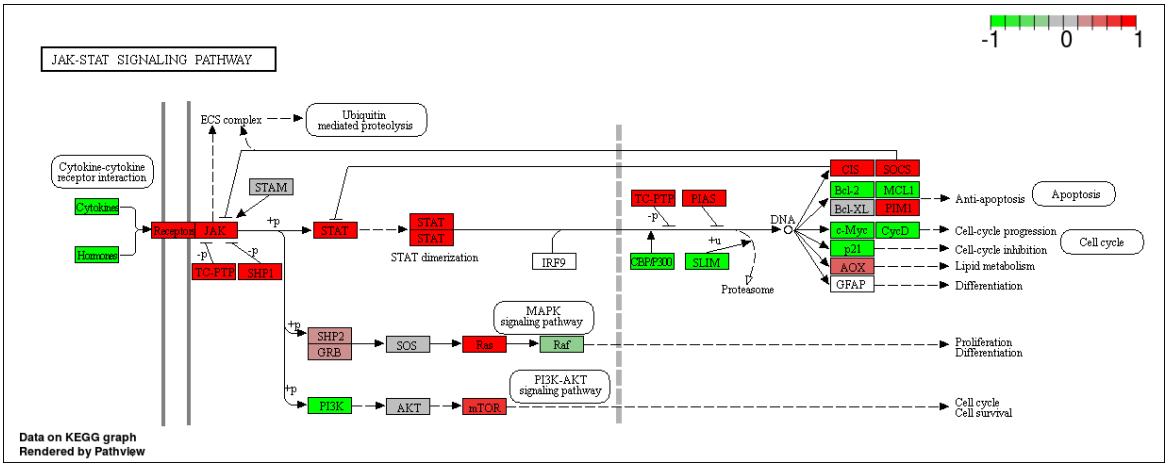

Appendix 5.32: Jak-STAT Signalling KEGG pathway
Greater perturbed KEGG pathway from Question 1 (IA v OA)

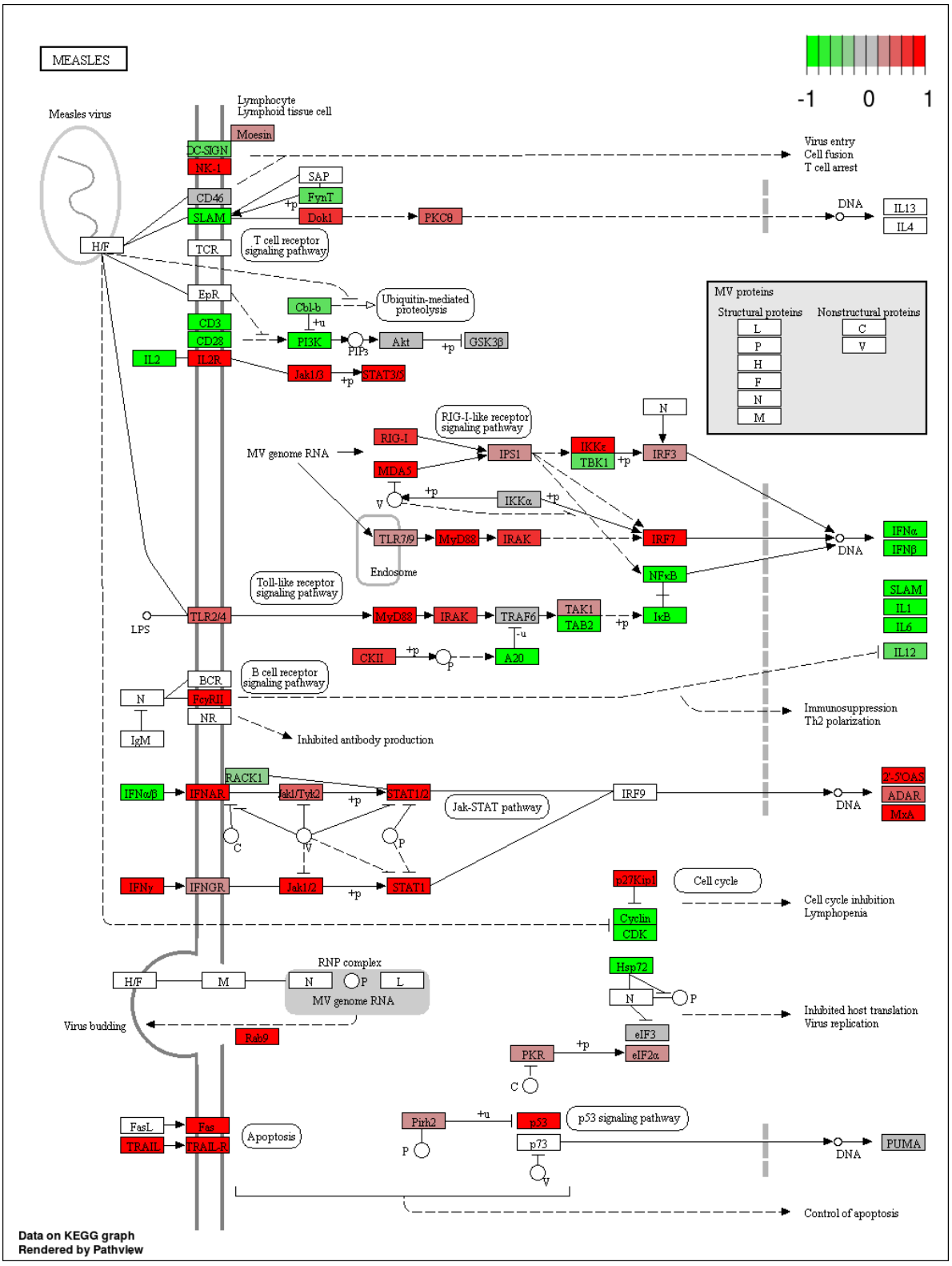

Appendix 5.33: Measles KEGG pathway
Greater perturbed KEGG pathway from Question 1 (IA v OA)

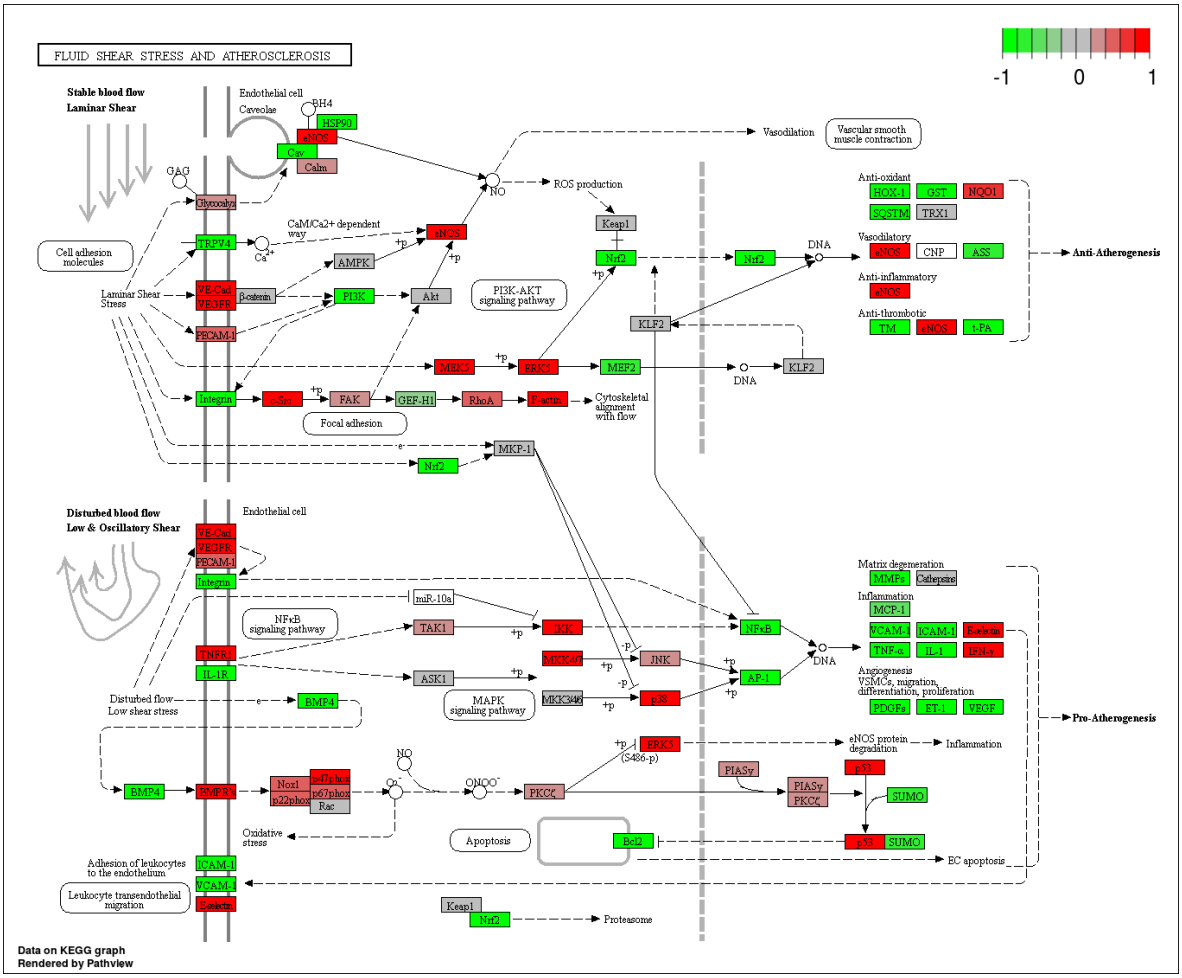

Appendix 5.34: Fluid Shear Stress and Atherosclerosis KEGG pathway
Greater perturbed KEGG pathway from Question 1 (IA v OA)

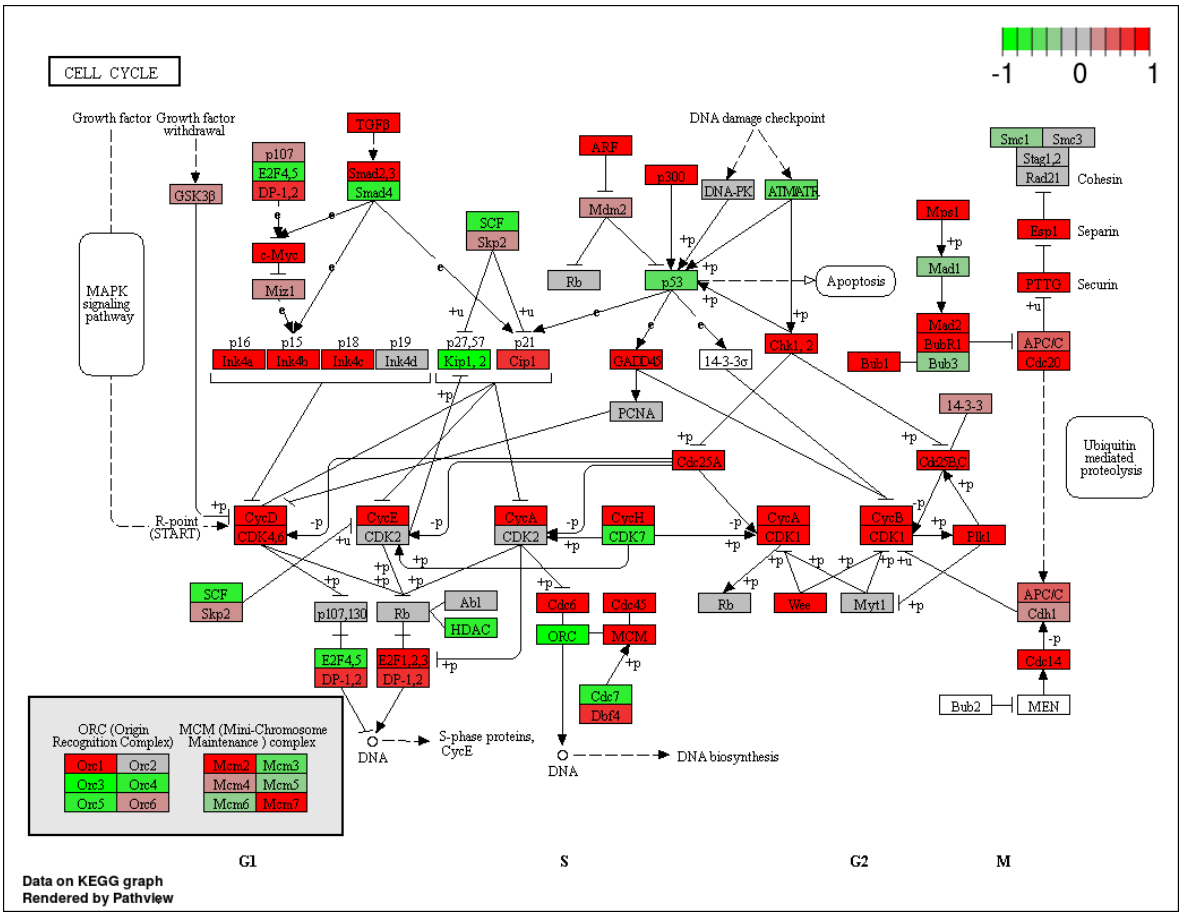

Appendix 5.35: Cell Cycle KEGG pathway
Greater perturbed KEGG pathway from Question 2 (OA_1 v IA)

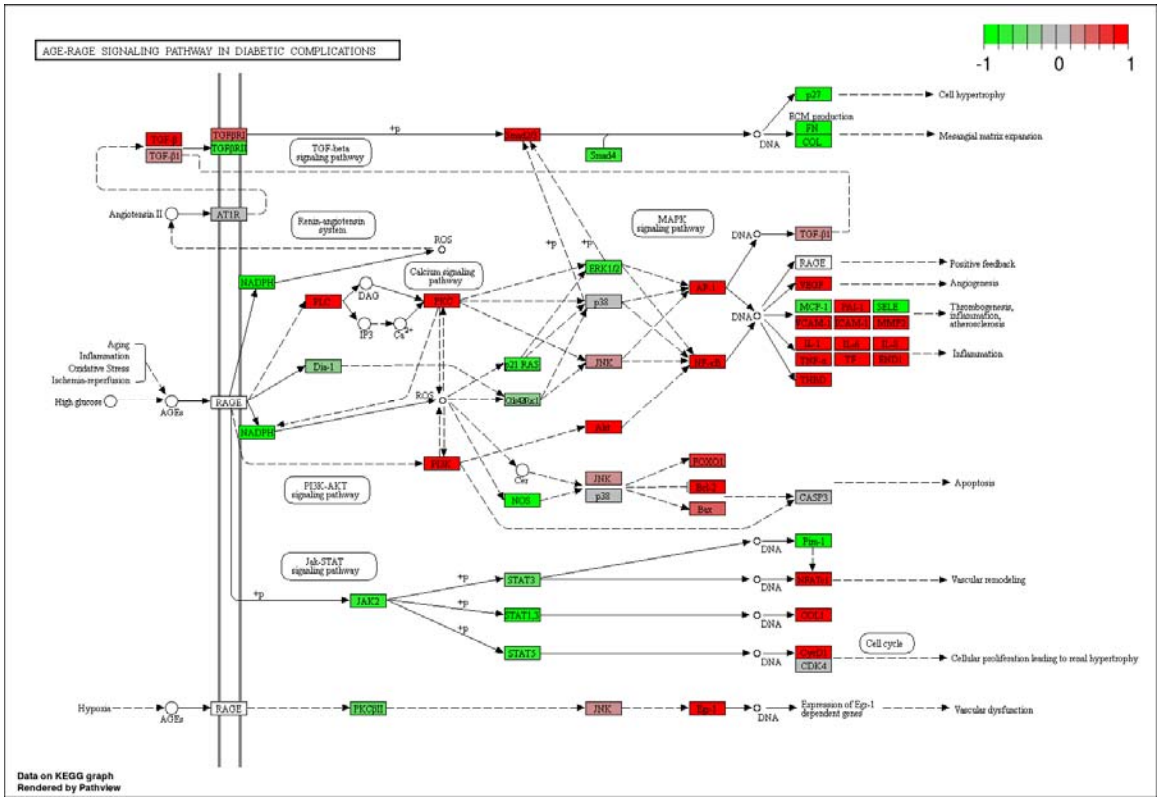

Appendix 5.36: AGE-RAGE Signalling Pathway in Diabetic Complications KEGG pathway
Greater perturbed KEGG pathway from Question 2 (OA_1 v IA)

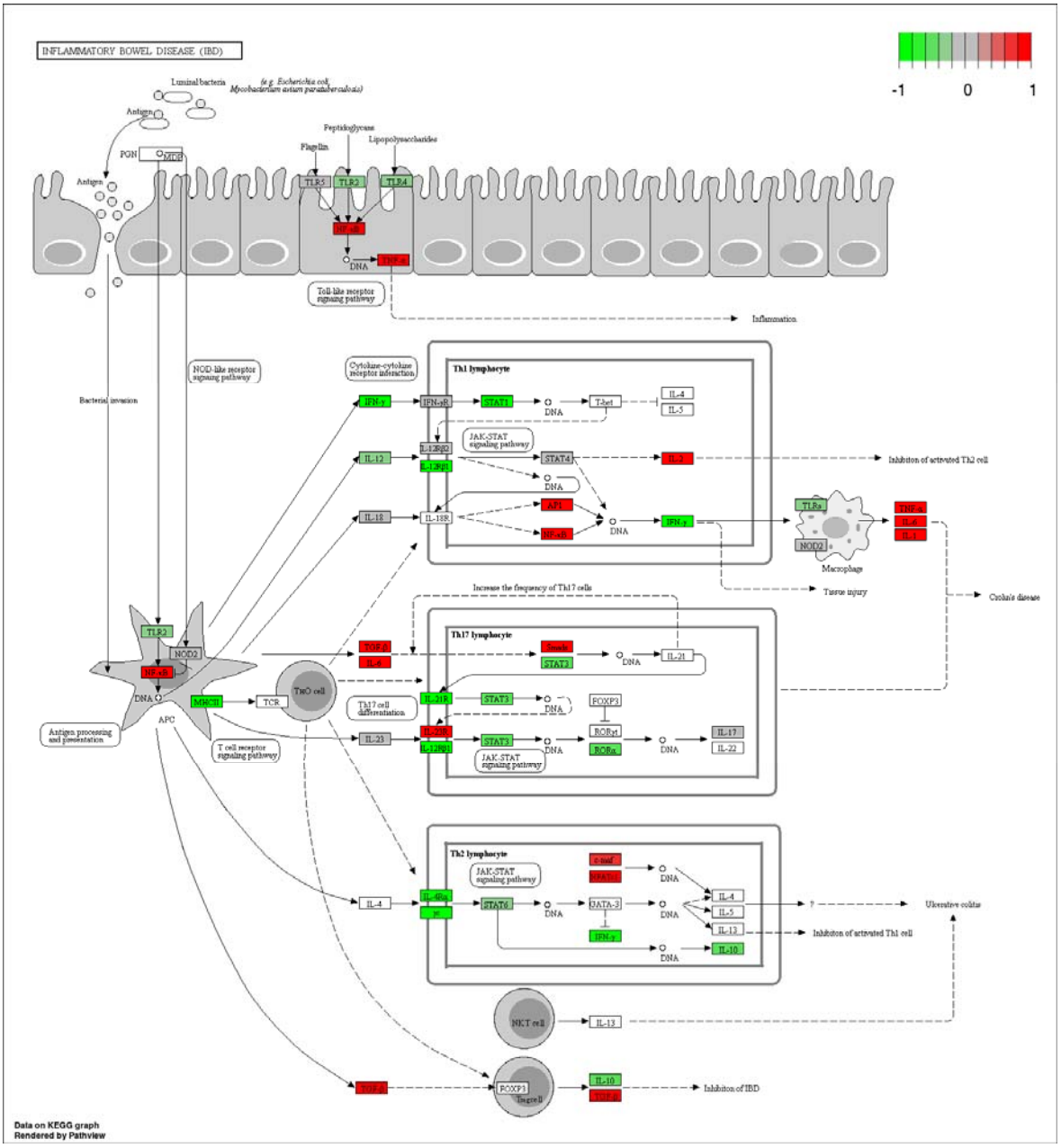

Appendix 5.37: Inflammatory Bowel Disease (IBD) KEGG pathway
Greater perturbed KEGG pathway from Question 2 (OA_1 v IA)

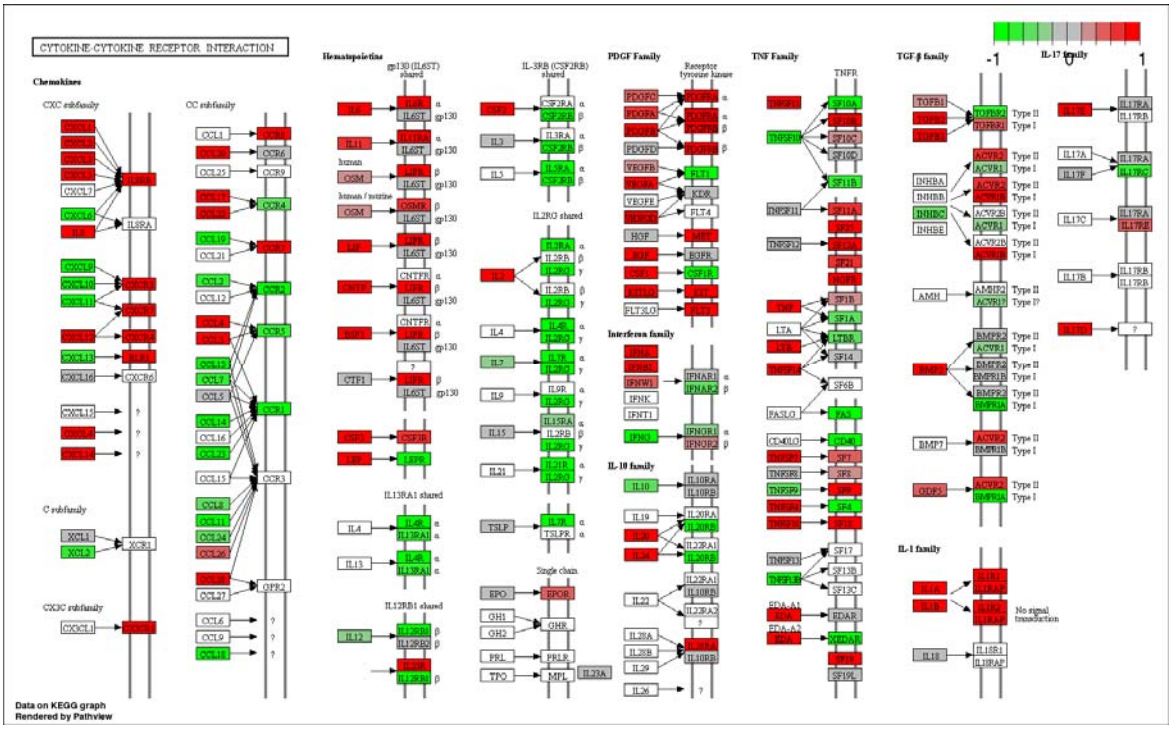

Appendix 5.38: Cytokine-Cytokine Receptor Interaction KEGG pathway
Greater perturbed KEGG pathway from Question 2 (OA_1 v IA)

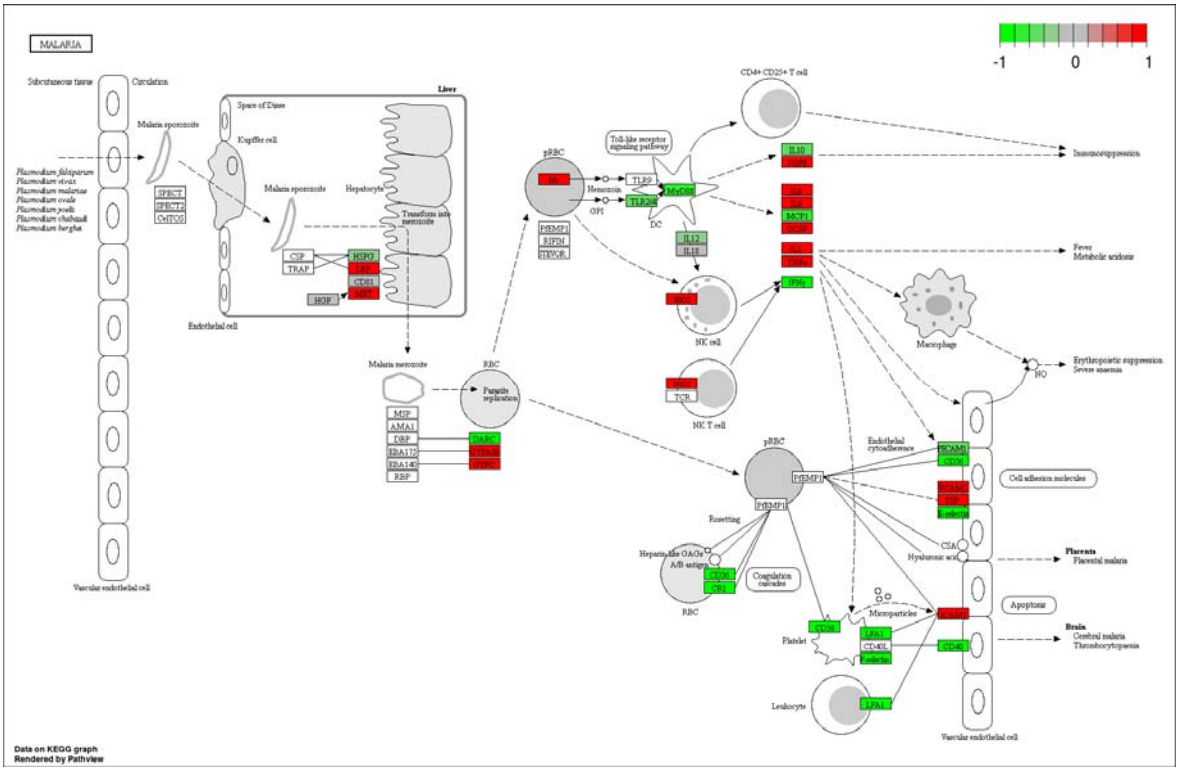

Appendix 5.39: Malaria KEGG pathway
Greater perturbed KEGG pathway from Question 2 (OA_1 v IA)

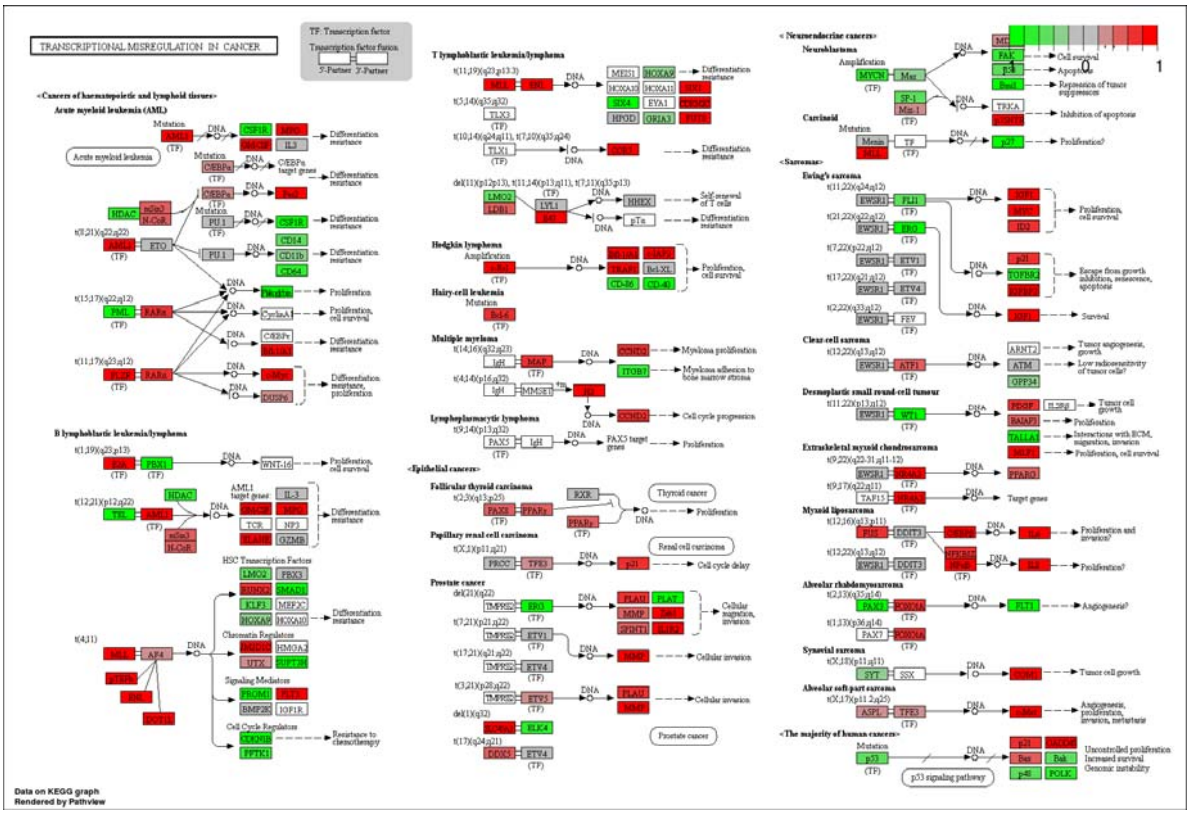

Appendix 5.40: Transcriptional Misregulation in Cancer KEGG pathway
Greater perturbed KEGG pathway from Question 2 (OA_1 v IA)

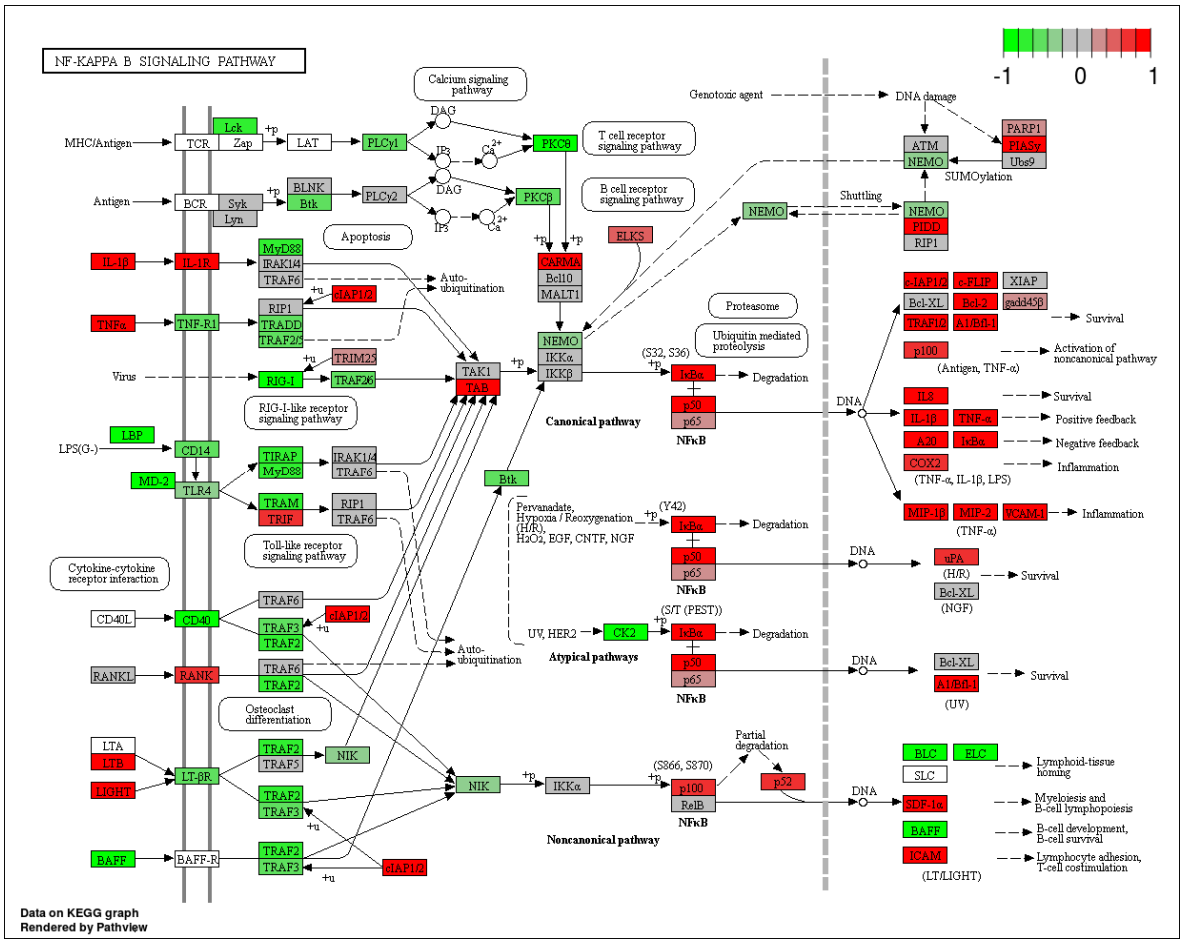

Appendix 5.41: NF-Kappa B Signalling KEGG pathway
Greater perturbed KEGG pathway from Question 2 (OA_1 v IA)

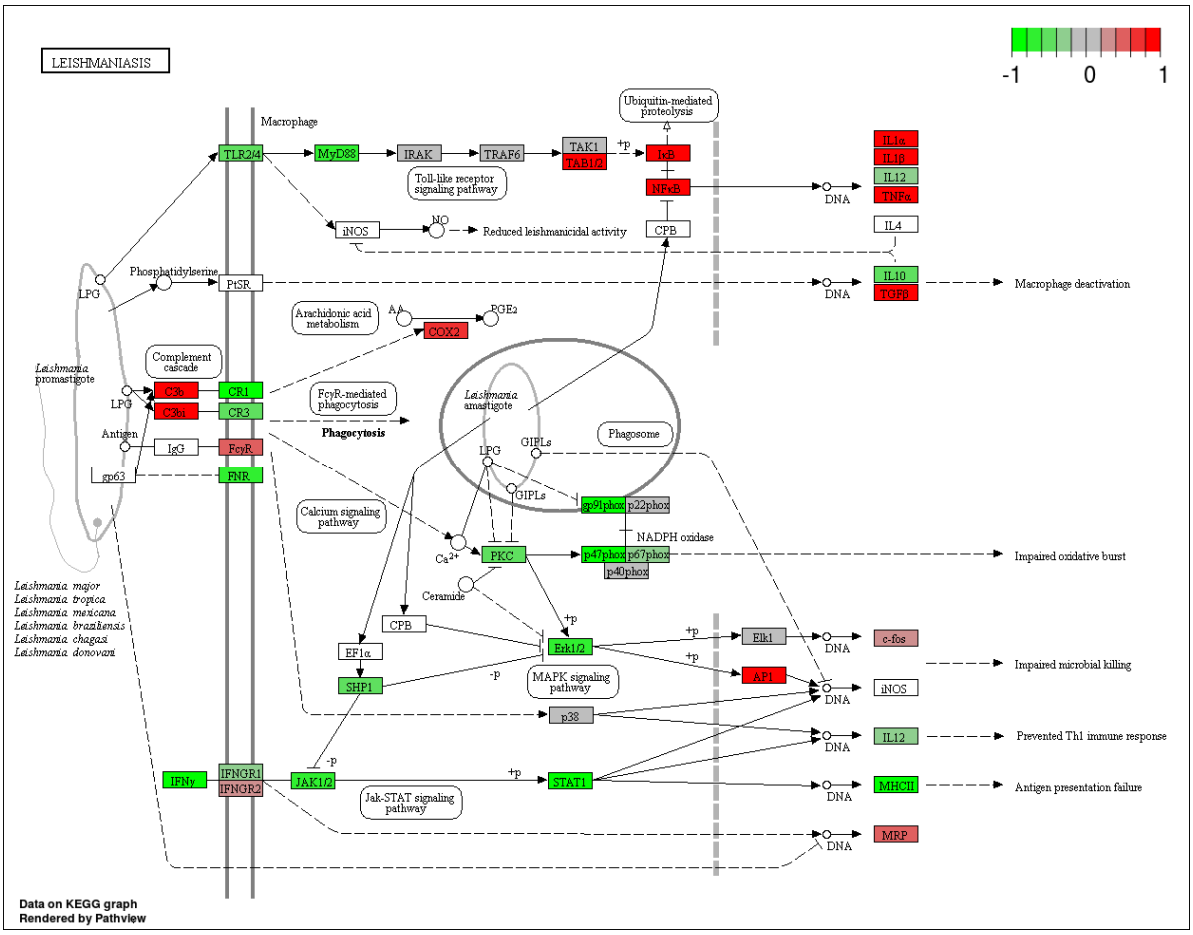

Appendix 5.42: Leishmaniasis KEGG pathway
Greater perturbed KEGG pathway from Question 2 (OA_1 v IA)

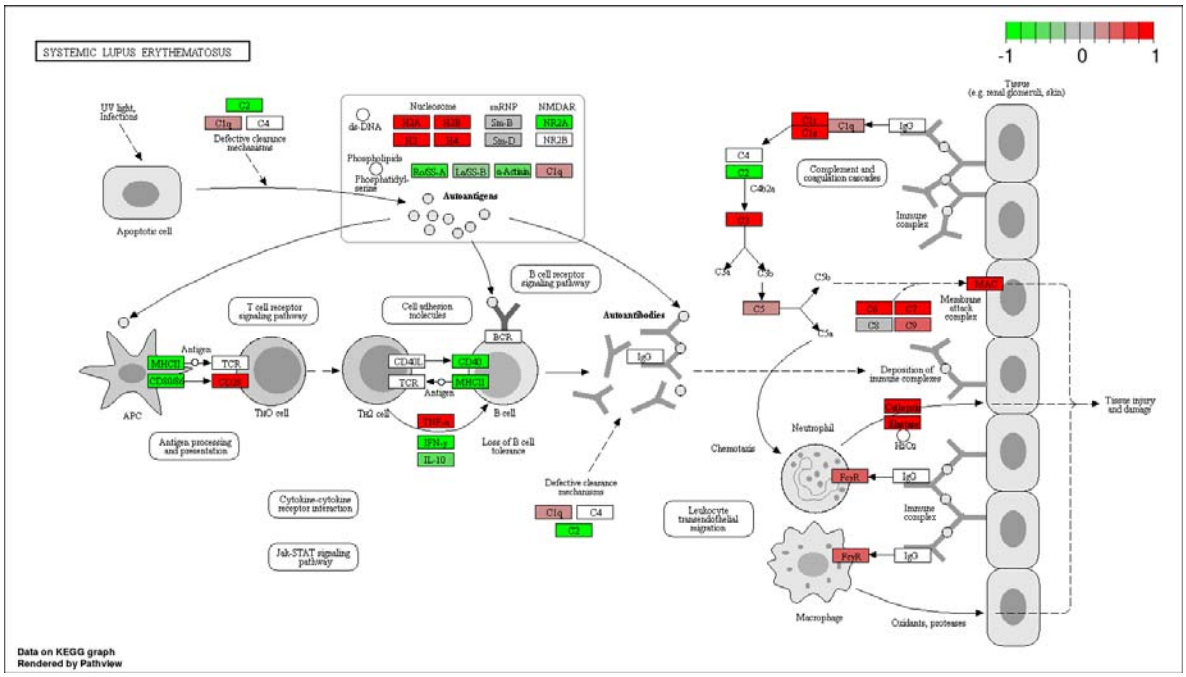

Appendix 5.43: Systemic Lupus Erythematosus KEGG pathway
Greater perturbed KEGG pathway from Question 2 (OA_1 v IA)

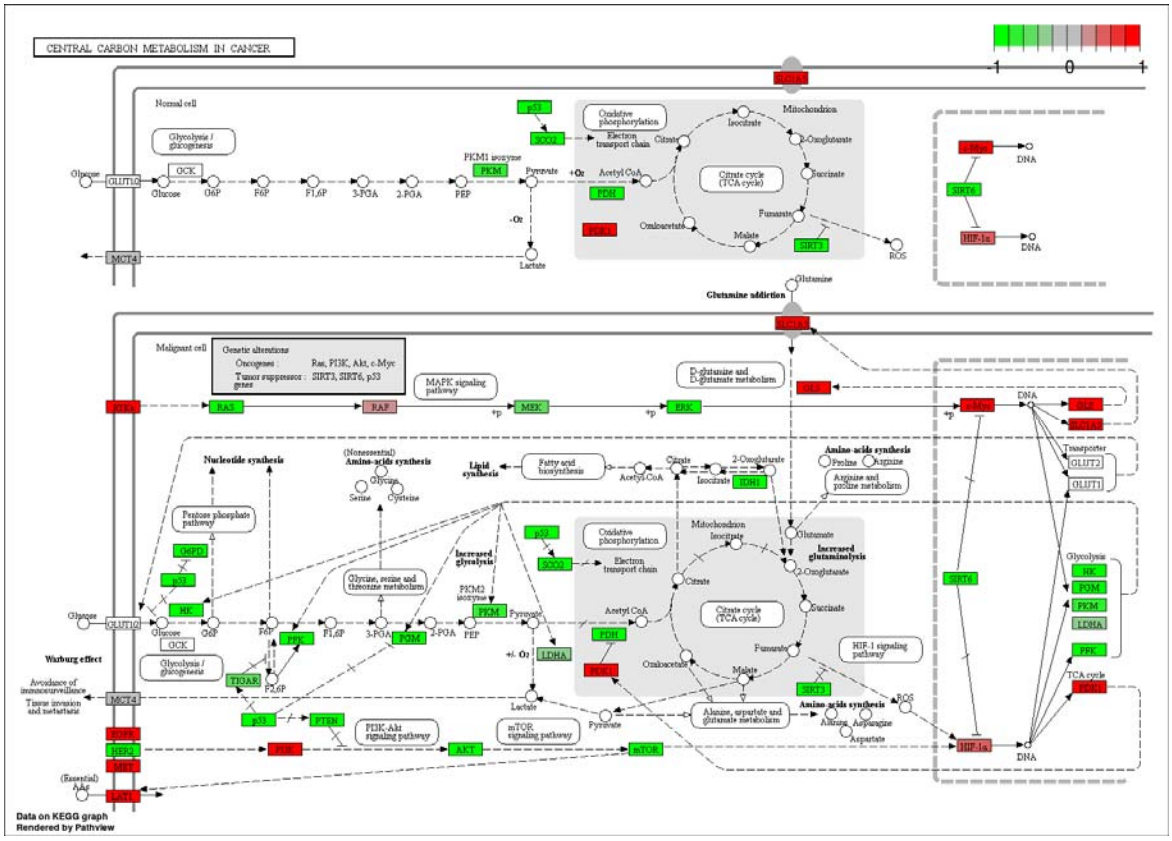

Appendix 5.44: Central Carbon Metabolism in Cancer KEGG pathway
Greater perturbed KEGG pathway from Question 3 (OA_0 v IA)

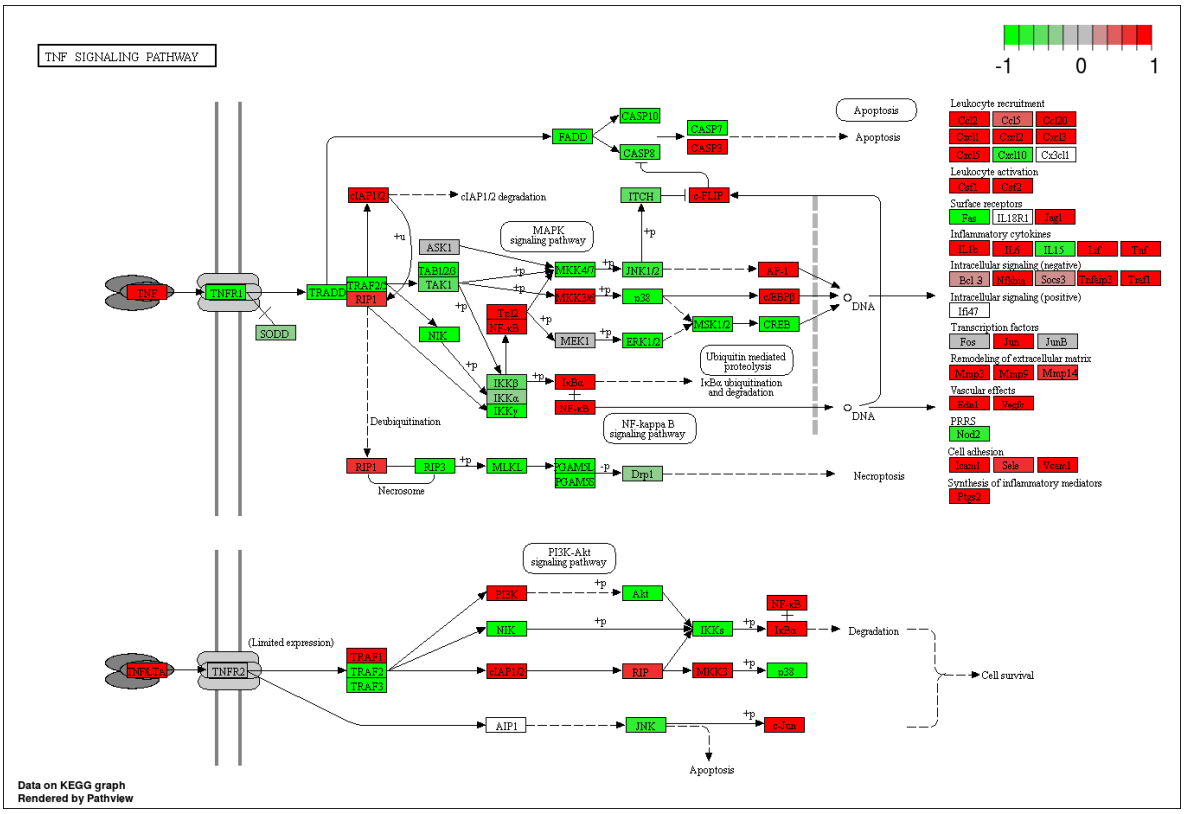

Appendix 5.45: TNF Signalling KEGG pathway
Greater perturbed KEGG pathway from Question 3 (OA_0 v IA)

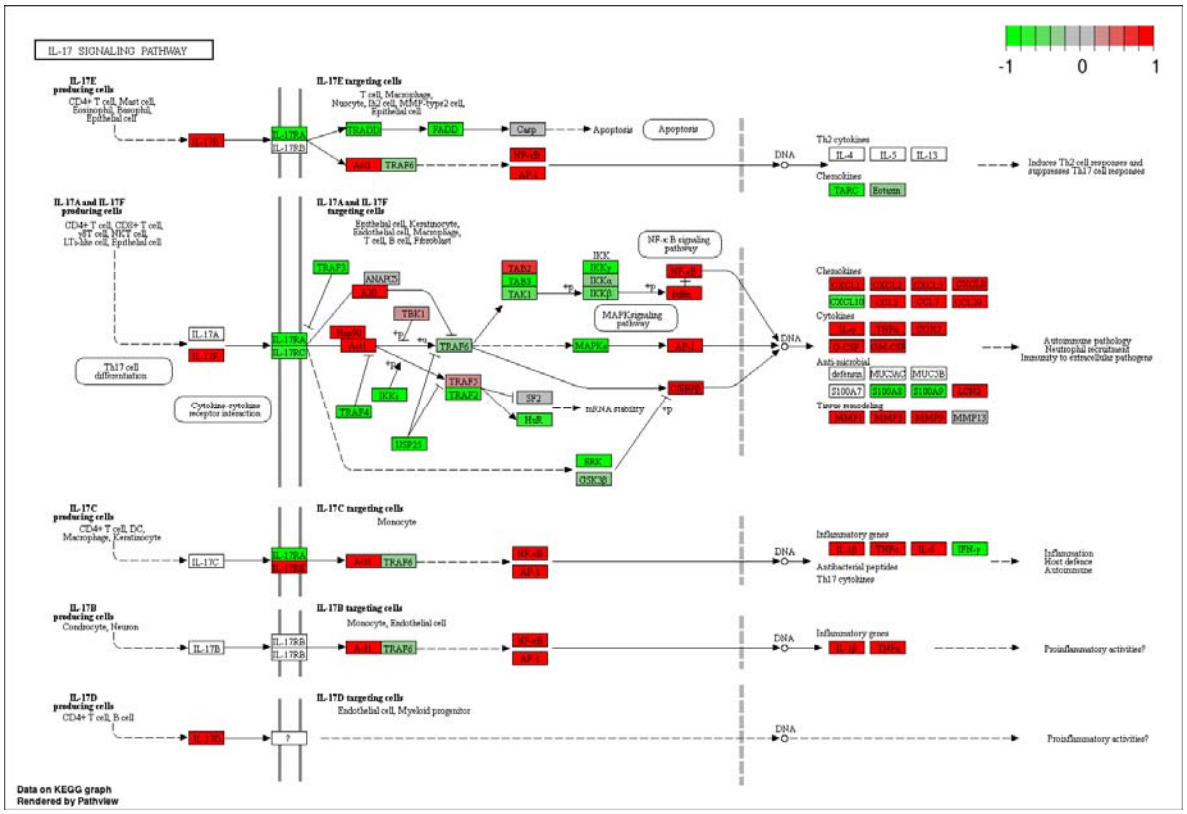

Appendix 5.46: IL-17 Signalling KEGG pathway
Greater perturbed KEGG pathway from Question 3 (OA_0 v IA)

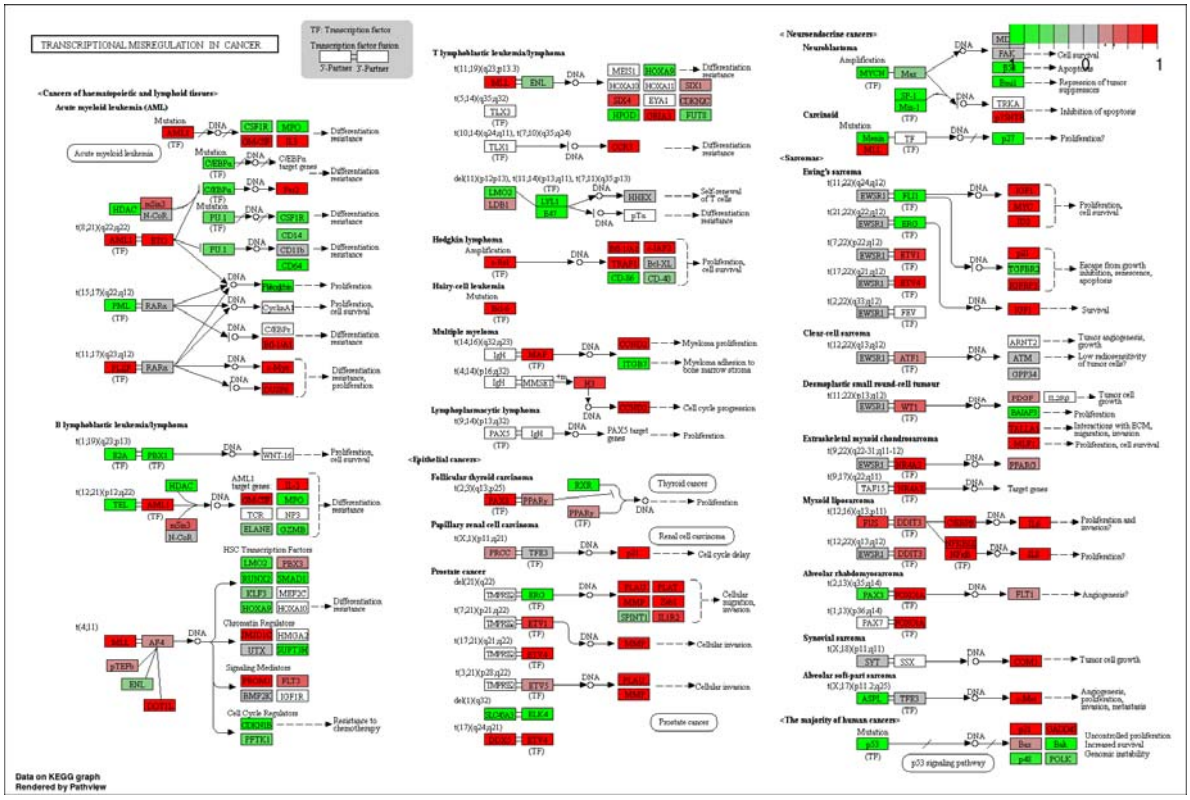

Appendix 5.47: Transcriptional Misregulation in Cancer KEGG pathway
Greater perturbed KEGG pathway from Question 3 (OA_0 v IA)

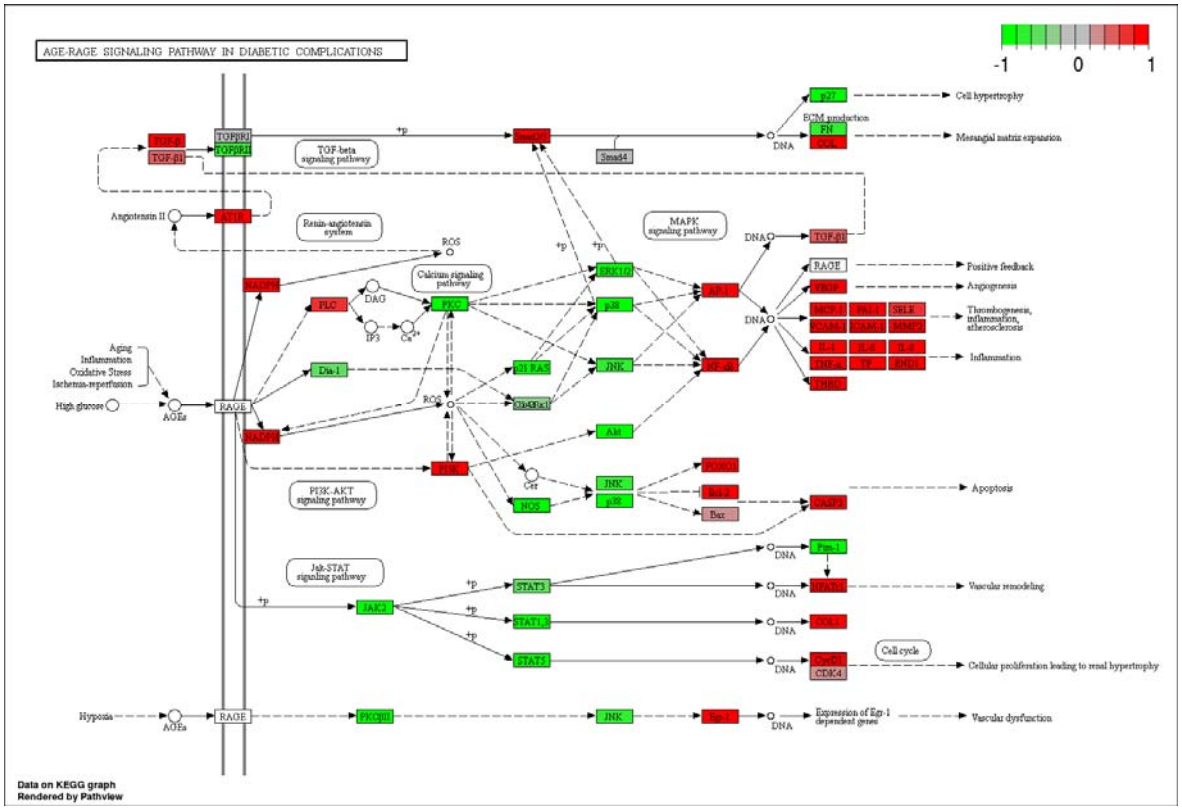

Appendix 5.48: AGE-RAGE Signalling Pathway in Diabetic Complications KEGG pathway
Greater perturbed KEGG pathway from Question 3 (OA_0 v IA)

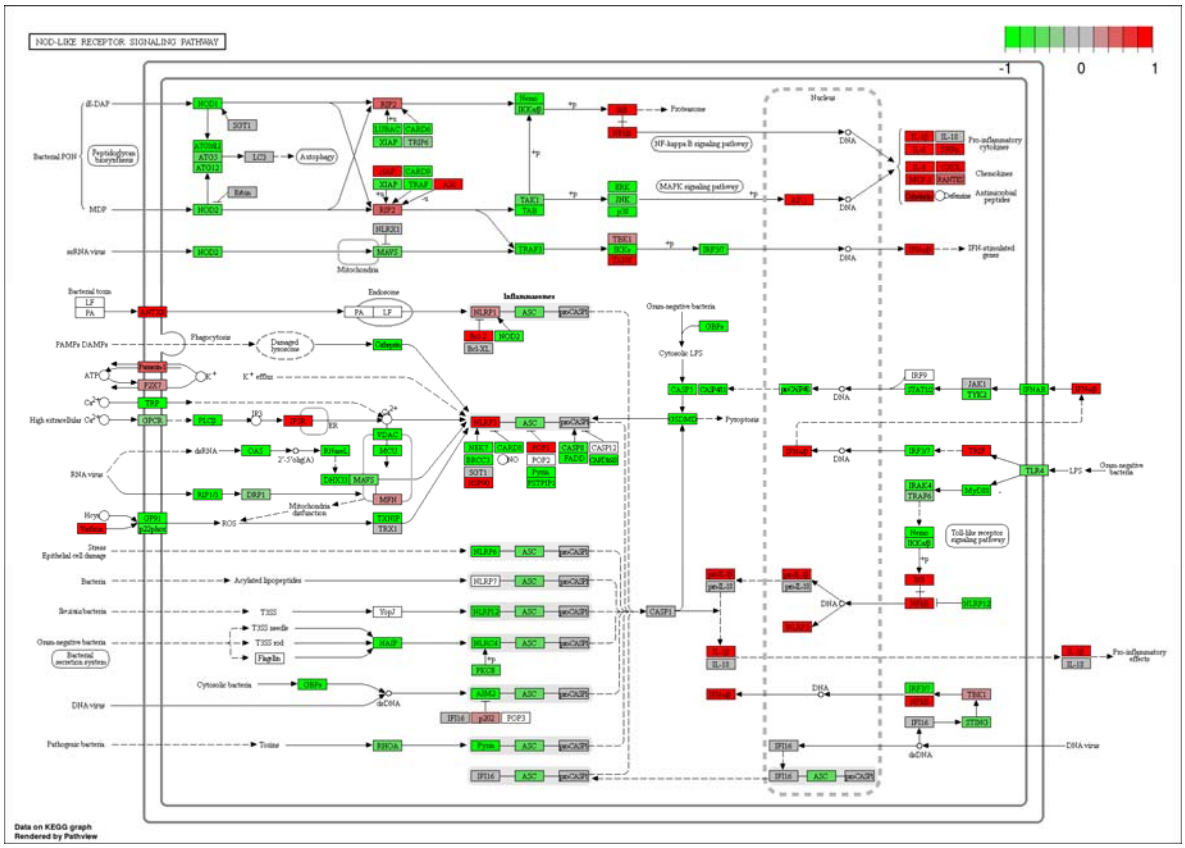

Appendix 5.49: NOD-like Receptor Signalling KEGG pathway
Greater perturbed KEGG pathway from Question 3 (OA_0 v IA)

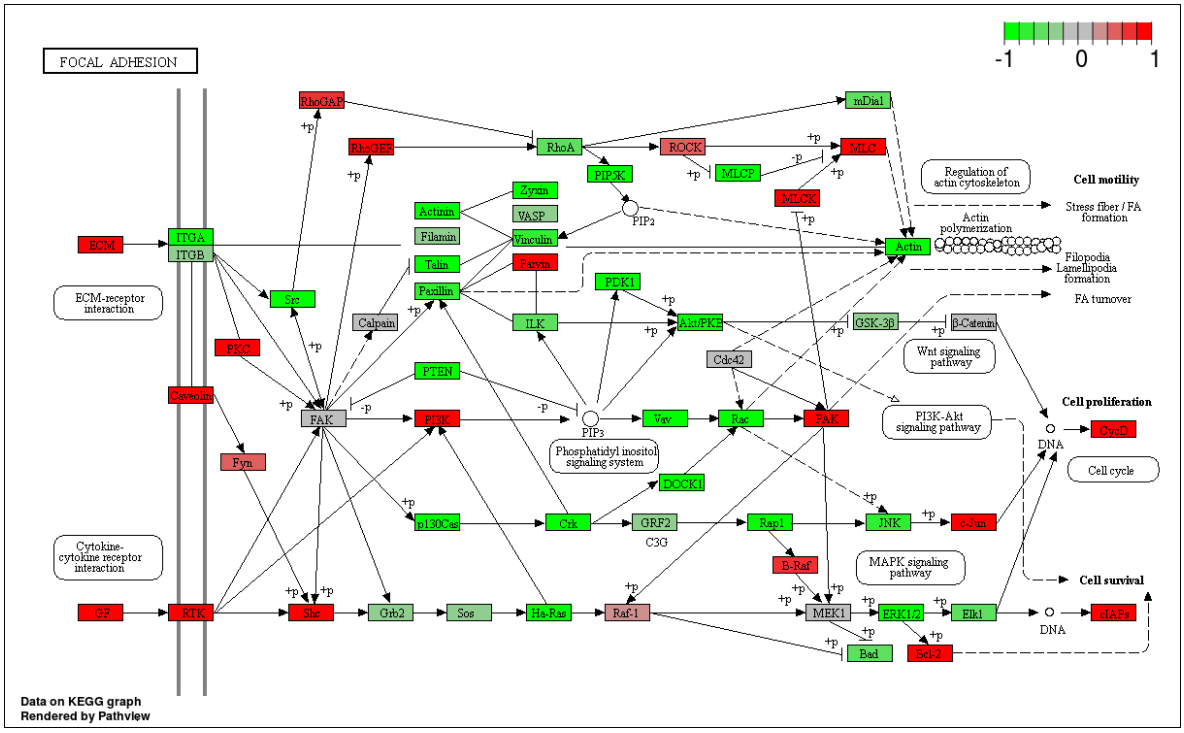

Appendix 5.50: Focal Adhesion KEGG pathway
Greater perturbed KEGG pathway from Question 3 (OA_0 v IA)

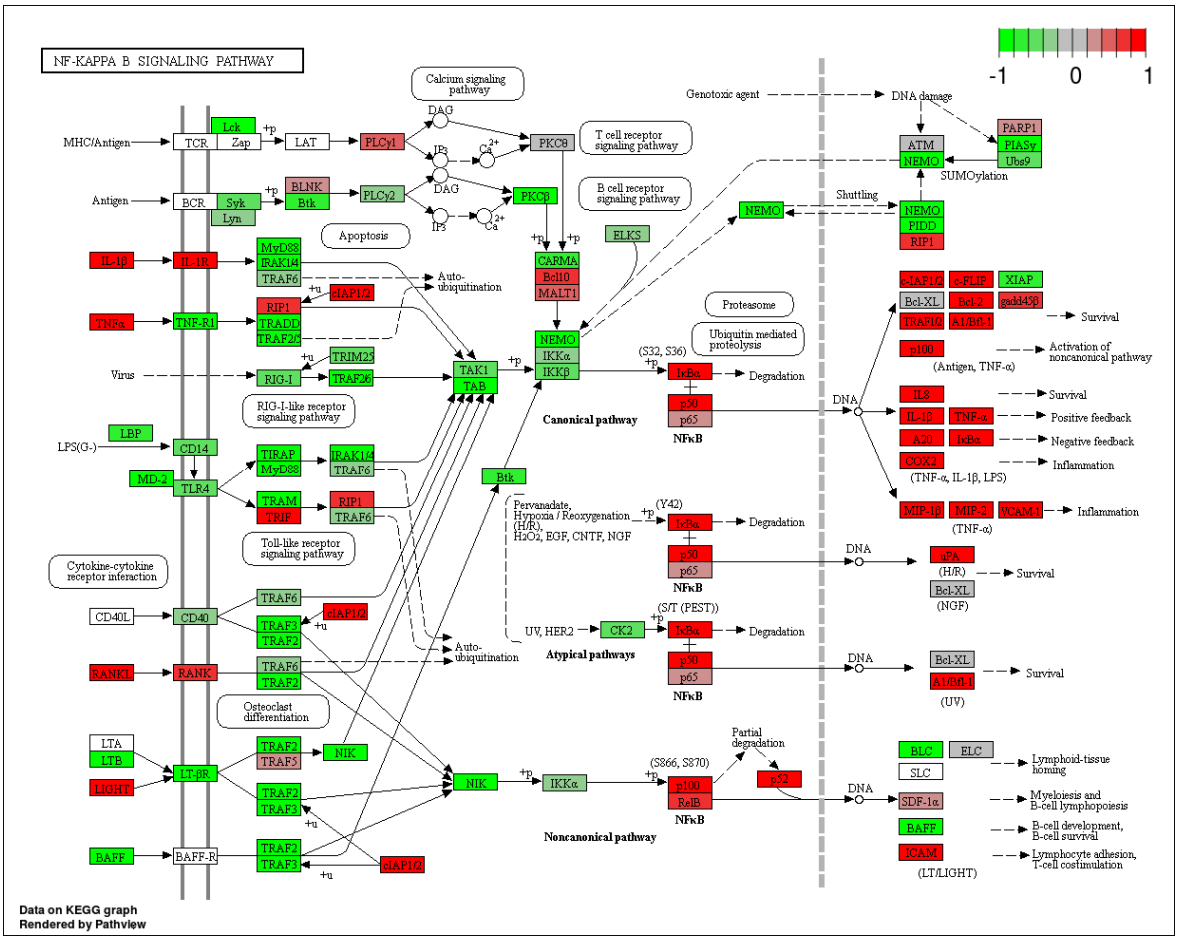

Appendix 5.51: NF-Kappa B Signalling KEGG pathway
Greater perturbed KEGG pathway from Question 3 (OA_0 v IA)

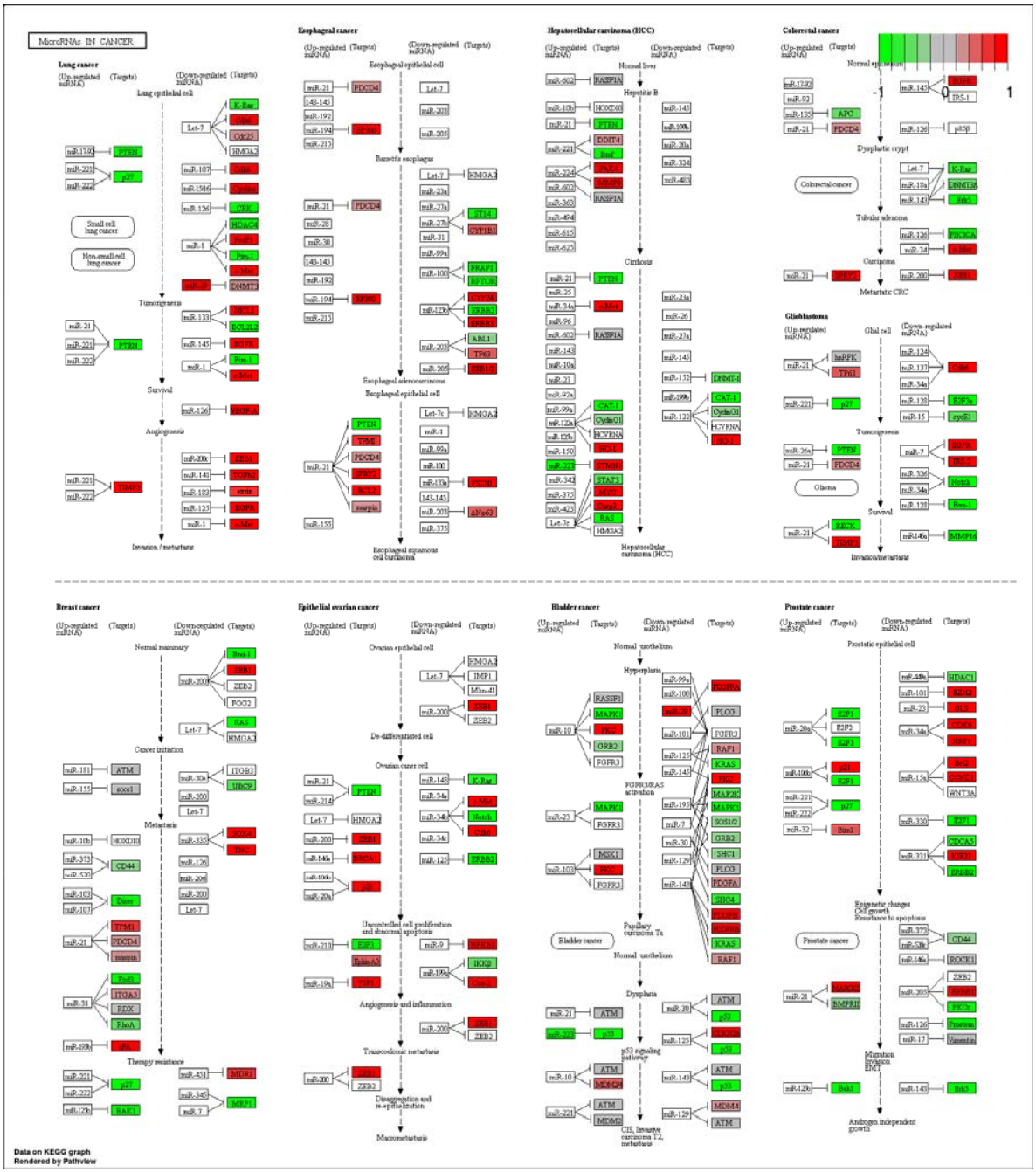

Appendix 5.52: MicroRNAs in Cancer KEGG pathway
Greater perturbed KEGG pathway from Question 3 (OA_0 v IA)

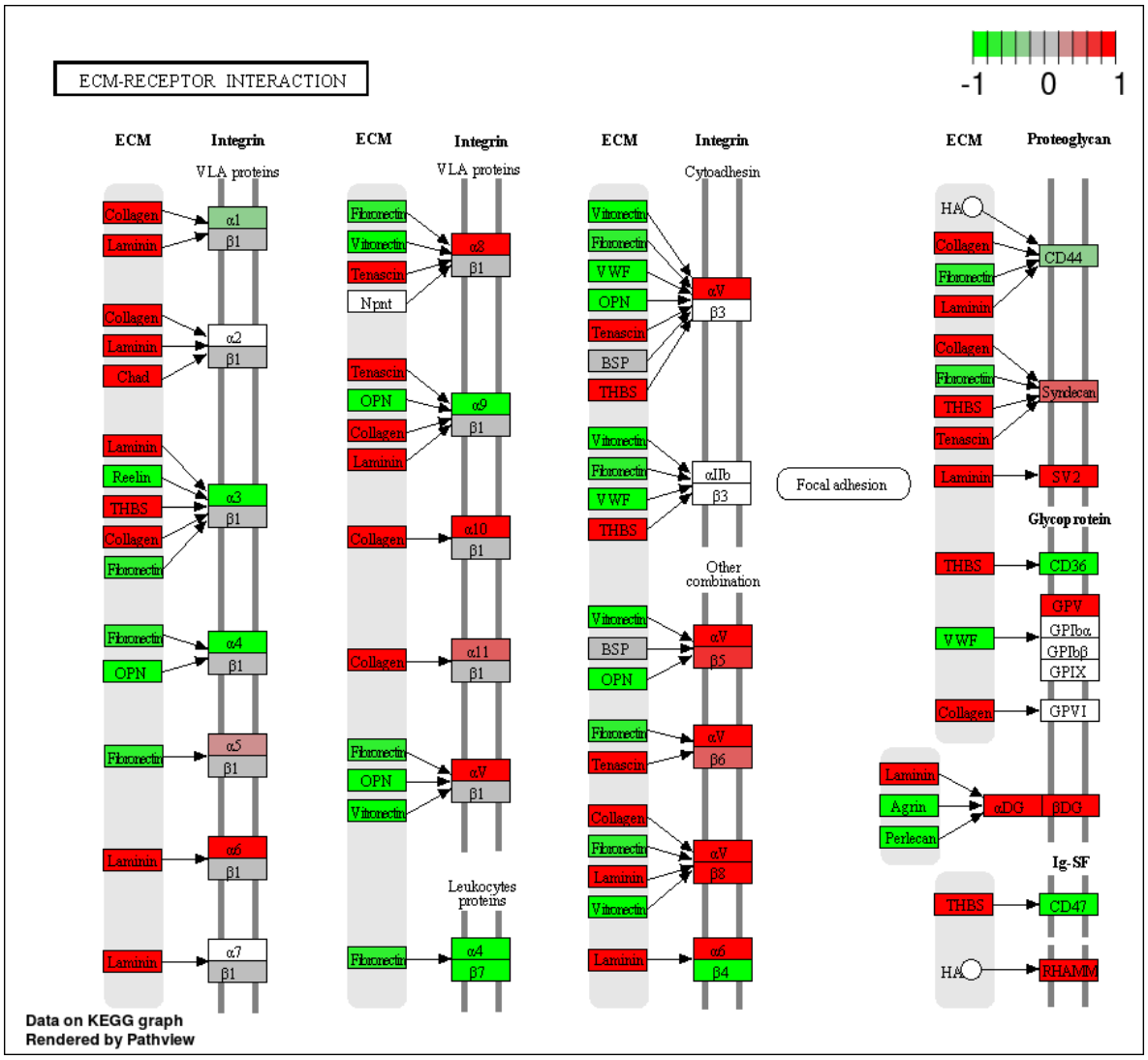

Appendix 5.53: ECM-Receptor Interaction KEGG pathway
Greater perturbed KEGG pathway from Question 3 (OA_0 v IA)

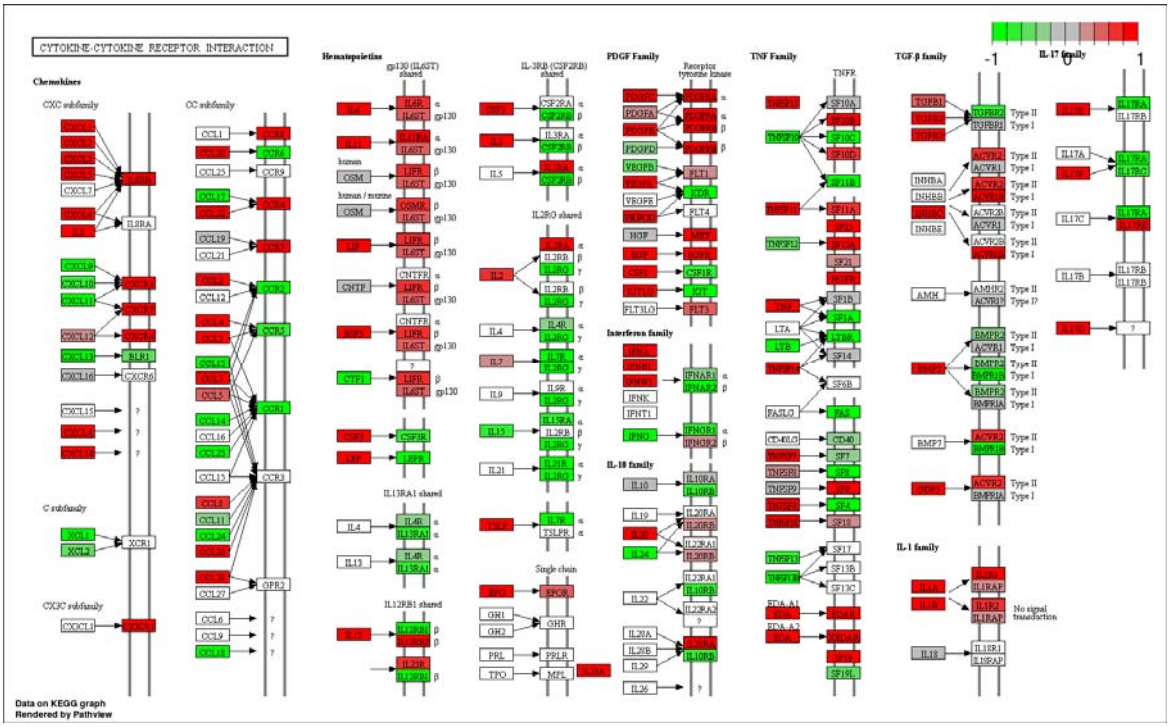

Appendix 5.54: Cytokine-Cytokine Receptor Interaction KEGG pathway
Greater perturbed KEGG pathway from Question 3 (OA_0 v IA)

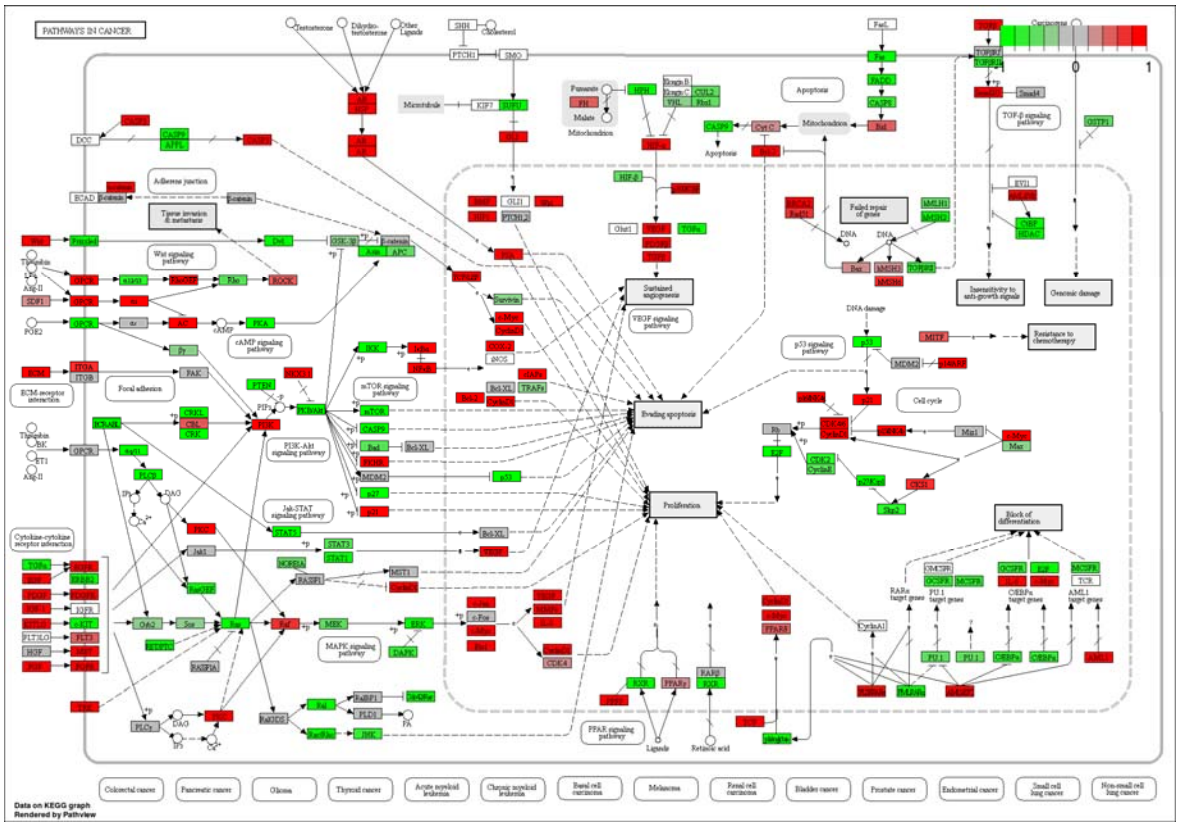

Appendix 5.55: Pathways in Cancer KEGG pathway
Greater perturbed KEGG pathway from Question 3 (OA_0 v IA)

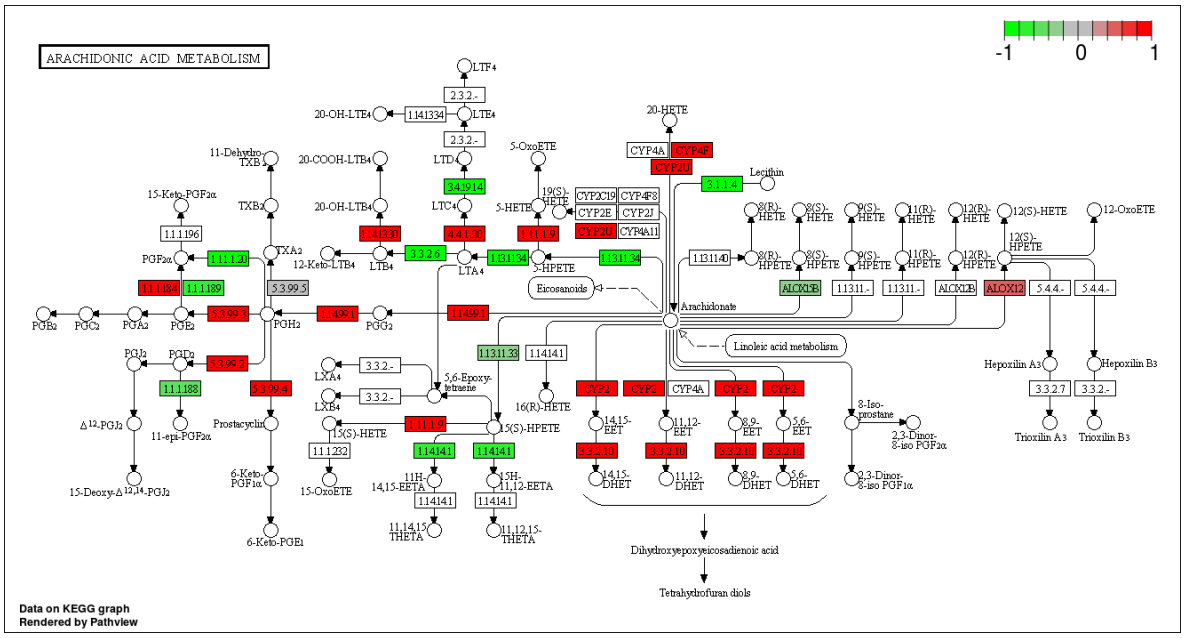

Appendix 5.56: Arachidonic Acid Metabolism KEGG pathway
Greater perturbed KEGG pathway from Question 3 (OA_0 v IA)

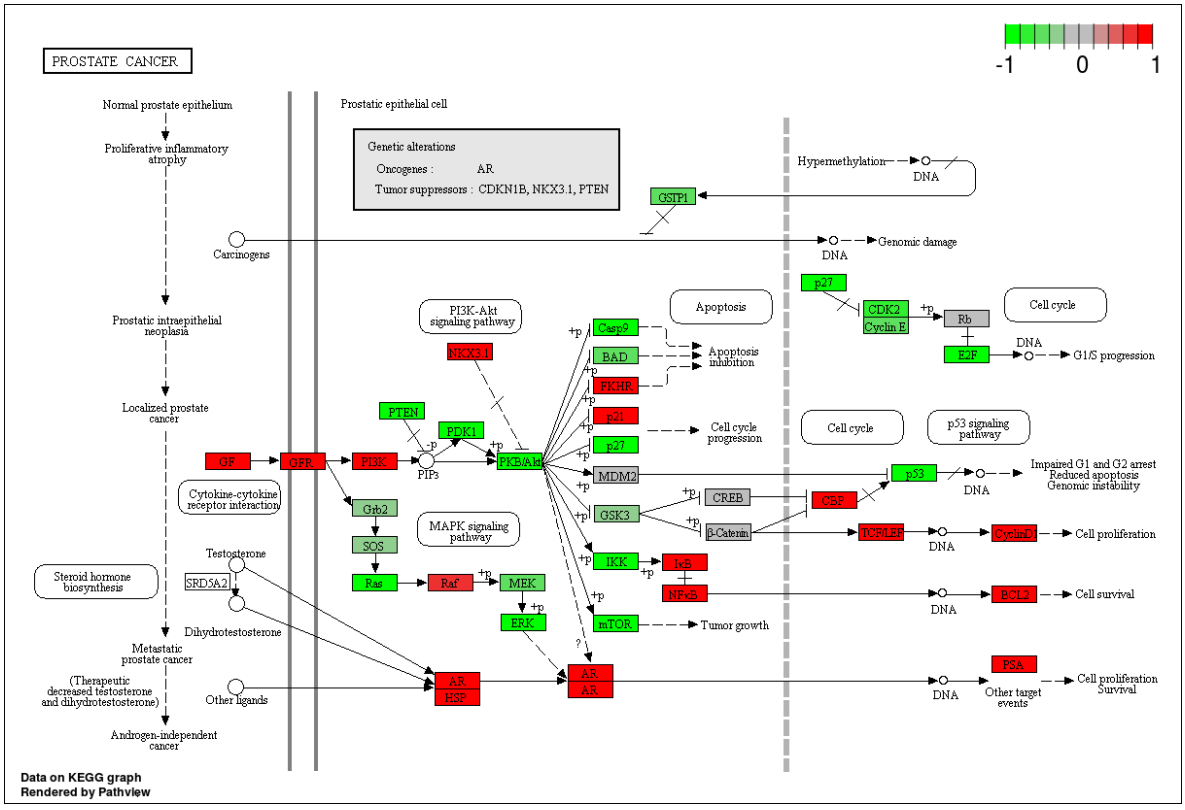

Appendix 5.57: Prostate Cancer KEGG pathway
Greater perturbed KEGG pathway from Question 3 (OA_0 v IA)

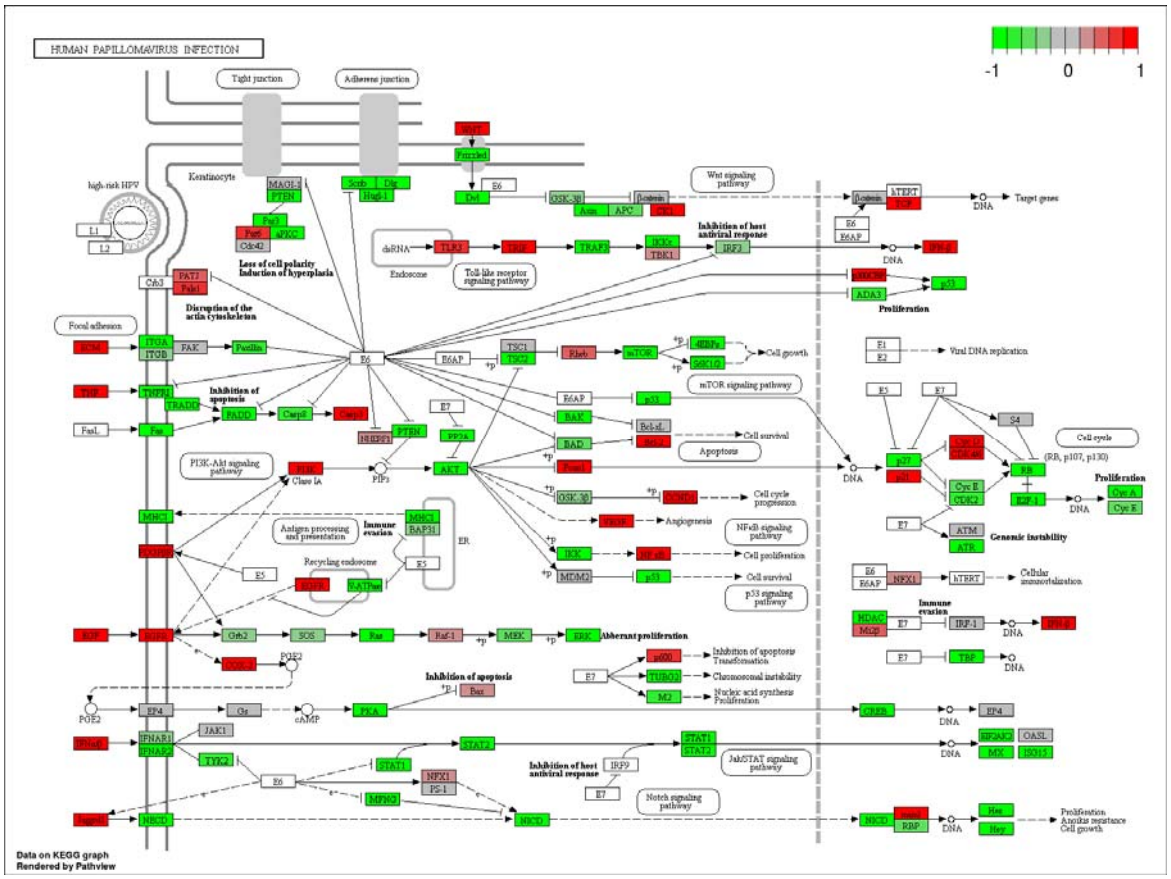

Appendix 5.58: Human Papillomavirus Infection KEGG pathway
Greater perturbed KEGG pathway from Question 3 (OA_0 v IA)

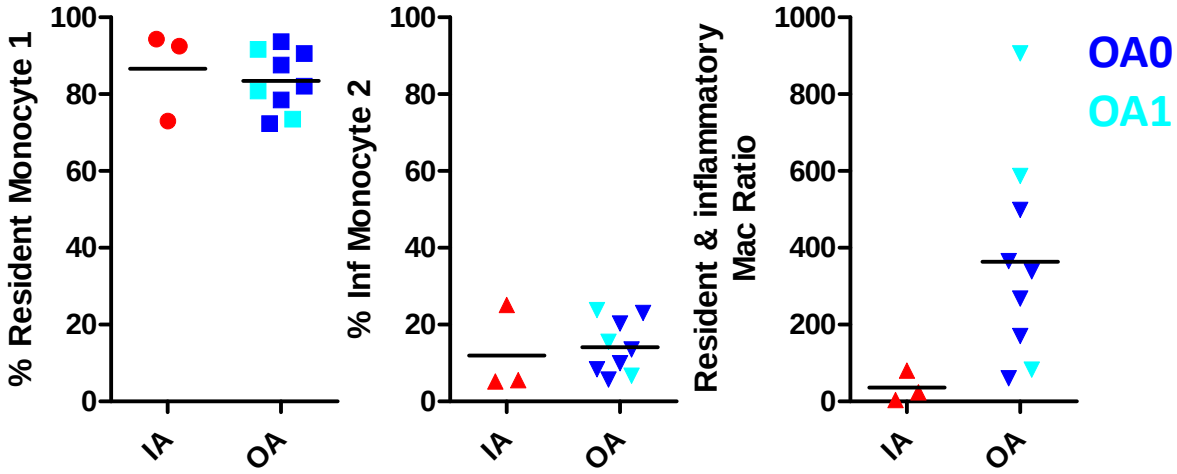

Appendix 6.1: Quantification of inflammatory monocyte and macrophage subsets in RNA-sequenced macrophage samples
Synovial tissue from OA total knee replacement and IA ultrasound guided biopsy was digested and analysed by flow cytometry using techniques described in Chapter 3. Quantification of monocytes '1' (left panel), '2' (middle panel) and resident and inflammatory macrophages (right panel)

References

Abed, E., T. F. Chan, A. Delalandre, J. Martel-Pelletier, J. P. Pelletier and D. Lajeunesse (2011). "R-spondins are newly recognized players in osteoarthritis that regulate Wnt signaling in osteoblasts." Arthritis Rheum **63**(12): 3865-3875.

Abou-Raya, A., S. Abou-Raya and T. Khadrawe (2014). "Retracted: Methotrexate in the treatment of symptomatic knee osteoarthritis: randomised placebo-controlled trial." Ann Rheum Dis.

Acuff, N. V. and J. Linden (2017). "Using Visualization of t-Distributed Stochastic Neighbor Embedding To Identify Immune Cell Subsets in Mouse Tumors." J Immunol **198**(11): 4539-4546.

Albig, A. R., J. R. Neil and W. P. Schiemann (2006). "Fibulins 3 and 5 antagonize tumor angiogenesis in vivo." Cancer Res **66**(5): 2621-2629.

Aletaha, D., T. Neogi, A. J. Silman, J. Funovits, D. T. Felson, C. O. Bingham, 3rd, N. S. Birnbaum, G. R. Burmester, V. P. Bykerk, M. D. Cohen, B. Combe, K. H. Costenbader, M. Dougados, P. Emery, G. Ferraccioli, J. M. Hazes, K. Hobbs, T. W. Huizinga, A. Kavanaugh, J. Kay, T. K. Kvien, T. Laing, P. Mease, H. A. Menard, L. W. Moreland, R. L. Naden, T. Pincus, J. S. Smolen, E. Stanislawska-Biernat, D. Symmons, P. P. Tak, K. S. Upchurch, J. Vencovsky, F. Wolfe and G. Hawker (2010). "2010 Rheumatoid arthritis classification criteria: an American College of Rheumatology/European League Against Rheumatism collaborative initiative." Arthritis Rheum **62**(9): 2569-2581.

Alshenibr, W., M. M. Tashkandi, S. F. Alsaqer, Y. Alkheriji, A. Wise, S. Fulzele, P. Mehra, M. B. Goldring, L. C. Gerstenfeld and M. V. Bais (2017). "Anabolic role of lysyl oxidase like-2 in cartilage of knee and temporomandibular joints with osteoarthritis." Arthritis Res Ther **19**(1): 179.

Amir el, A. D., K. L. Davis, M. D. Tadmor, E. F. Simonds, J. H. Levine, S. C. Bendall, D. K. Shenfeld, S. Krishnaswamy, G. P. Nolan and D. Pe'er (2013). "viSNE enables visualization of high dimensional single-cell data and reveals phenotypic heterogeneity of leukemia." Nat Biotechnol **31**(6): 545-552.

Ancuta, P., K. Y. Liu, V. Misra, V. S. Wacleche, A. Gosselin, X. Zhou and D. Gabuzda (2009). "Transcriptional profiling reveals developmental relationship and distinct biological functions of CD16+ and CD16- monocyte subsets." BMC Genomics **10**: 403.

Anderson, A. E., A. G. Pratt, M. A. Sedhom, J. P. Doran, C. Routledge, B. Hargreaves, P. M. Brown, K. A. Le Cao, J. D. Isaacs and R. Thomas (2016). "IL-6-driven STAT signalling in circulating CD4+ lymphocytes is a marker for early anticitrullinated peptide antibody-negative rheumatoid arthritis." Ann Rheum Dis **75**(2): 466-473.

Aref-Eshghi, E., Y. Zhang, D. Hart, A. M. Valdes, A. Furey, G. Martin, G. Sun, P. Rahman, N. Arden, T. D. Spector and G. Zhai (2014). "SMAD3 is associated with the total burden of radiographic osteoarthritis: the Chingford study." PLoS One **9**(5): e97786.

Attur, M., J. Samuels, S. Krasnokutsky and S. B. Abramson (2010). "Targeting the synovial tissue for treating osteoarthritis (OA): where is the evidence?" Best Pract Res Clin Rheumatol **24**(1): 71-79.

Ayral, X., E. H. Pickering, T. G. Woodworth, N. Mackillop and M. Dougados (2005). "Synovitis: a potential predictive factor of structural progression of medial tibiofemoral knee osteoarthritis -- results of a 1 year longitudinal arthroscopic study in 422 patients." Osteoarthritis Cartilage **13**(5): 361-367.

Badlani, N., Y. Oshima, R. Healey, R. Coutts and D. Amiel (2009). "Use of bone morphogenic protein-7 as a treatment for osteoarthritis." Clin Orthop Relat Res **467**(12): 3221-3229.
Bai, Y. and Q. Sun (2015). "Macrophage recruitment in obese adipose tissue." Obesity Reviews **16**(2): 127-136.

Bain, C. C., A. Bravo-Blas, C. L. Scott, E. Gomez Perdiguero, F. Geissmann, S. Henri, B. Malissen, L. C. Osborne, D. Artis and A. M. Mowat (2014). "Constant replenishment from circulating monocytes maintains the macrophage pool in the intestine of adult mice." Nat Immunol **15**(10): 929-937.

Baker, K., A. Grainger, J. Niu, M. Clancy, A. Guermazi, M. Crema, L. Hughes, J. Buckwalter, A. Wooley, M. Nevitt and D. T. Felson (2010). "Relation of synovitis to knee pain using contrast-enhanced MRIs." Ann Rheum Dis **69**(10): 1779-1783.

Banchereau, J. and R. M. Steinman (1998). "Dendritic cells and the control of immunity." Nature **392**(6673): 245-252.

Barros, M. H., F. Hauck, J. H. Dreyer, B. Kempkes and G. Niedobitek (2013). "Macrophage polarisation: an immunohistochemical approach for identifying M1 and M2 macrophages." PLoS One **8**(11): e80908.

Benito, M. J., D. J. Veale, O. FitzGerald, W. B. van den Berg and B. Bresnihan (2005). "Synovial tissue inflammation in early and late osteoarthritis." Ann Rheum Dis **64**(9): 1263-1267.

Bernardo, D., L. Durant, E. R. Mann, E. Bassity, E. Montalvillo, R. Man, R. Vora, D. Reddi, F. Bayiroglu, L. Fernandez-Salazar, N. R. English, S. T. Peake, J. Landy, G. H. Lee, G. Malietzis, Y. H. Siaw, A. U. Murugananthan, P. Hendy, E. Sanchez-Recio, R. K. Phillips, J. A. Garrote, P. Scott, J. Parkhill, M. Paulsen, A. L. Hart, H. O. Al-Hassi, E. Arranz, A. W. Walker, S. R. Carding and S. C. Knight (2016). "Chemokine (C-C Motif) Receptor 2 Mediates Dendritic Cell Recruitment to the Human Colon but Is Not Responsible for Differences Observed in Dendritic Cell Subsets, Phenotype, and Function Between the Proximal and Distal Colon." Cell Mol Gastroenterol Hepatol **2**(1): 22-39 e25.

Bertola, A., T. Ciucci, D. Rousseau, V. Bourlier, C. Duffaut, S. Bonnafous, C. Blin-Wakkach, R. Anty, A. Iannelli, J. Gugenheim, A. Tran, A. Bouloumie, P. Gual and A. Wakkach (2012). "Identification of adipose tissue dendritic cells correlated with obesity-associated insulin-resistance and inducing Th17 responses in mice and patients." Diabetes **61**(9): 2238-2247.

Beyer, M., M. R. Mallmann, J. Xue, A. Staratschek-Jox, D. Vorholt, W. Krebs, D. Sommer, J. Sander, C. Mertens, A. Nino-Castro, S. V. Schmidt and J. L. Schultze (2012). "High-resolution transcriptome of human macrophages." PLoS One **7**(9): e45466.

Bian, Z., L. Shi, Y. L. Guo, Z. Lv, C. Tang, S. Niu, A. Tremblay, M. Venkataramani, C. Culpepper, L. Li, Z. Zhou, A. Mansour, Y. Zhang, A. Gewirtz, K. Kidder, K. Zen and Y. Liu (2016). "Cd47-Sirpalpha interaction and IL-10 constrain inflammation-induced macrophage phagocytosis of healthy self-cells." Proc Natl Acad Sci U S A **113**(37): E5434-5443.

Biswas, S. K., L. Gangi, S. Paul, T. Schioppa, A. Saccani, M. Sironi, B. Bottazzi, A. Doni, B. Vincenzo, F. Pasqualini, L. Vago, M. Nebuloni, A. Mantovani and A. Sica (2006). "A distinct and unique transcriptional program expressed by tumor-associated macrophages (defective NF-kappaB and enhanced IRF-3/STAT1 activation)." Blood **107**(5): 2112-2122.

Blom, A. B., P. L. van Lent, A. E. Holthuysen, P. M. van der Kraan, J. Roth, N. van Rooijen and W. B. van den Berg (2004). "Synovial lining macrophages mediate osteophyte formation during experimental osteoarthritis." Osteoarthritis Cartilage **12**(8): 627-635.

Bondeson, J., A. B. Blom, S. Wainwright, C. Hughes, B. Caterson and W. B. van den Berg (2010). "The role of synovial macrophages and macrophage-produced mediators in driving inflammatory and destructive responses in osteoarthritis." Arthritis Rheum **62**(3): 647-657.

Bondeson, J., S. D. Wainwright, S. Lauder, N. Amos and C. E. Hughes (2006). "The role of synovial macrophages and macrophage-produced cytokines in driving aggrecanases, matrix metalloproteinases, and other destructive and inflammatory responses in osteoarthritis." Arthritis Res Ther **8**(6): R187.

Boyle, D. L., S. Rosengren, W. Bugbee, A. Kavanaugh and G. S. Firestein (2003). "Quantitative biomarker analysis of synovial gene expression by real-time PCR." Arthritis Res Ther **5**(6): R352-360.

Boyle, W. J., W. S. Simonet and D. L. Lacey (2003). "Osteoclast differentiation and activation." Nature **423**(6937): 337-342.

Braun, H. J. and G. E. Gold (2012). "Diagnosis of osteoarthritis: imaging." Bone **51**(2): 278-288.

Brown, B. N., B. M. Sicari and S. F. Badylak (2014). "Rethinking regenerative medicine: a macrophage-centered approach." Front Immunol **5**: 510.

Bruggner, R. V., B. Bodenmiller, D. L. Dill, R. J. Tibshirani and G. P. Nolan (2014). "Automated identification of stratifying signatures in cellular subpopulations." Proc Natl Acad Sci U S A **111**(26): E2770-2777.

Bujko, A., N. Atlasy, O. J. B. Landsverk, L. Richter, S. Yaqub, R. Horneland, O. Øyen, E. M. Aandahl, L. Aabakken, H. G. Stunnenberg, E. S. Bækkevold and F. L. Jahnsen (2017). "Transcriptional and functional profiling defines human small intestinal macrophage subsets." The Journal of Experimental Medicine.

Burmester, G. R., B. Stuhlmuller, G. Keyszer and R. W. Kinne (1997). "Mononuclear phagocytes and rheumatoid synovitis. Mastermind or workhorse in arthritis?" Arthritis Rheum **40**(1): 5-18.

Burska, A. N., L. Hunt, M. Boissinot, R. Strollo, B. J. Ryan, E. Vital, A. Nissim, P. G. Winyard, P. Emery and F. Ponchel (2014). "Autoantibodies to posttranslational modifications in rheumatoid arthritis." Mediators Inflamm **2014**: 492873.

Busby, W. H., Jr., S. A. Yocum, M. Rowland, D. Kellner, S. Lazerwith, F. Sverdrup, M. Yates, M. Radabaugh and D. R. Clemmons (2009). "Complement 1s is the serine protease that cleaves IGFBP-5 in human osteoarthritic joint fluid." Osteoarthritis Cartilage **17**(4): 547-555.

Carames, B., A. Hasegawa, N. Taniguchi, S. Miyaki, F. J. Blanco and M. Lotz (2012). "Autophagy activation by rapamycin reduces severity of experimental osteoarthritis." Ann Rheum Dis **71**(4): 575-581.

Carames, B., N. Taniguchi, S. Otsuki, F. J. Blanco and M. Lotz (2010). "Autophagy is a protective mechanism in normal cartilage, and its aging-related loss is linked with cell death and osteoarthritis." Arthritis Rheum **62**(3): 791-801.

Cejka, D., S. Hayer, B. Niederreiter, W. Sieghart, T. Fuereder, J. Zwerina and G. Schett (2010). "Mammalian target of rapamycin signaling is crucial for joint destruction in experimental arthritis and is activated in osteoclasts from patients with rheumatoid arthritis." Arthritis Rheum **62**(8): 2294-2302.

Cerovic, V., C. C. Bain, A. M. Mowat and S. W. Milling (2014). "Intestinal macrophages and dendritic cells: what's the difference?" Trends Immunol **35**(6): 270-277.

Chen, M., Y. H. Wang, Y. Wang, L. Huang, H. Sandoval, Y. J. Liu and J. Wang (2006). "Dendritic cell apoptosis in the maintenance of immune tolerance." Science **311**(5764): 1160-1164.

Chen, P., A. Denniston, S. Hannes, W. Tucker, L. Wei, B. Liu, T. Xiao, S. Hirani, Z. Li, S. Jawad, H. Si, R. W. Lee, H. N. Sen and R. B. Nussenblatt (2015). "Increased CD1c+ mDC1 with mature phenotype regulated by TNFalpha-p38 MAPK in autoimmune ocular inflammatory disease." Clin Immunol **158**(1): 35-46.

Clemmons, D. R., W. H. Busby, Jr., A. Garmong, D. R. Schultz, D. S. Howell, R. D. Altman and R. Karr (2002). "Inhibition of insulin-like growth factor binding protein 5 proteolysis in articular cartilage and joint fluid results in enhanced concentrations of insulin-like growth factor 1 and is associated with improved osteoarthritis." Arthritis Rheum **46**(3): 694-703.

Clockaerts, S., Y. M. Bastiaansen-Jenniskens, J. Runhaar, G. J. Van Osch, J. F. Van Offel, J. A. Verhaar, L. S. De Clerck and J. Somville (2010). "The infrapatellar fat pad should be considered as an active osteoarthritic joint tissue: a narrative review." Osteoarthritis Cartilage **18**(7): 876-882.

Collin, M., N. McGovern and M. Haniffa (2013). "Human dendritic cell subsets." Immunology **140**(1): 22-30.

Conaghan, P. G., M. A. D'Agostino, M. Le Bars, G. Baron, N. Schmidely, R. Wakefield, P. Ravaud, W. Grassi, E. Martin-Mola, A. So, M. Backhaus, M. Malaise, P. Emery and M. Dougados (2010). "Clinical and ultrasonographic predictors of joint replacement for knee osteoarthritis: results from a large, 3-year, prospective EULAR study." Ann Rheum Dis **69**(4): 644-647.

Conde, P., M. Rodriguez, W. van der Touw, A. Jimenez, M. Burns, J. Miller, M. Brahmachary, H. M. Chen, P. Boros, F. Rausell-Palamos, T. J. Yun, P. Riquelme, A. Rastrojo, B. Aguado, J. Stein-Streilein, M. Tanaka, L. Zhou, J. Zhang, T. L. Lowary, F. Ginhoux, C. G. Park, C. Cheong, J. Brody, S. J. Turley, S. A. Lira, V. Bronte, S. Gordon, P. S. Heeger, M. Merad, J. Hutchinson, S. H. Chen and J. Ochando (2015). "DC-SIGN(+) Macrophages Control the Induction of Transplantation Tolerance." Immunity **42**(6): 1143-1158.

Connolly, M., A. Marrelli, M. Blades, J. McCormick, P. Maderna, C. Godson, R. Mullan, O. FitzGerald, B. Bresnihan, C. Pitzalis, D. J. Veale and U. Fearon (2010). "Acute serum amyloid A induces migration, angiogenesis, and inflammation in synovial cells in vitro and in a human rheumatoid arthritis/SCID mouse chimera model." J Immunol **184**(11): 6427-6437.

Cooper, C., S. Snow, T. E. McAlindon, S. Kellingray, B. Stuart, D. Coggon and P. A. Dieppe (2000). "Risk factors for the incidence and progression of radiographic knee osteoarthritis." Arthritis Rheum **43**(5): 995-1000.

Corthay, A. (2006). "A three-cell model for activation of naive T helper cells." Scand J Immunol **64**(2): 93-96.

Cros, J., N. Cagnard, K. Woollard, N. Patey, S. Y. Zhang, B. Senechal, A. Puel, S. K. Biswas, D. Moshous, C. Picard, J. P. Jais, D. D'Cruz, J. L. Casanova, C. Trouillet and F. Geissmann (2010). "Human CD14dim monocytes patrol and sense nucleic acids and viruses via TLR7 and TLR8 receptors." Immunity **33**(3): 375-386.

Daigneault, M., J. A. Preston, H. M. Marriott, M. K. Whyte and D. H. Dockrell (2010). "The identification of markers of macrophage differentiation in PMA-stimulated THP-1 cells and monocyte-derived macrophages." PLoS One **5**(1): e8668.

Davis, M. A., W. H. Ettinger, J. M. Neuhaus and W. W. Hauck (1988). "Sex differences in osteoarthritis of the knee. The role of obesity." Am J Epidemiol **127**(5): 1019-1030.

Deng, Q., Q. Wang, W. Y. Zong, D. L. Zheng, Y. X. Wen, K. S. Wang, X. M. Teng, X. Zhang, J. Huang and Z. G. Han (2010). "E2F8 contributes to human hepatocellular carcinoma via regulating cell proliferation." Cancer Res **70**(2): 782-791.

Dennis, G., Jr., C. T. Holweg, S. K. Kummerfeld, D. F. Choy, A. F. Setiadi, J. A. Hackney, P. M. Haverty, H. Gilbert, W. Y. Lin, L. Diehl, S. Fischer, A. Song, D. Musselman, M. Klearman, C. Gabay, A. Kavanaugh, J. Endres, D. A. Fox, F. Martin and M. J. Townsend (2014). "Synovial phenotypes in rheumatoid arthritis correlate with response to biologic therapeutics." Arthritis Res Ther **16**(2): R90.

Dolhain, R. J., N. T. Ter Haar, R. De Kuiper, I. G. Nieuwenhuis, A. H. Zwinderman, F. C. Breedveld and A. M. Miltenburg (1998). "Distribution of T cells and signs of T-cell activation in the rheumatoid joint: implications for semiquantitative comparative histology." Br J Rheumatol **37**(3): 324-330.

Donlin, L. T., A. Jayatilleke, E. G. Giannopoulou, G. D. Kalliolias and L. B. Ivashkiv (2014). "Modulation of TNF-induced macrophage polarization by synovial fibroblasts." J Immunol **193**(5): 2373-2383.

Dzionek, A., A. Fuchs, P. Schmidt, S. Cremer, M. Zysk, S. Miltenyi, D. W. Buck and J. Schmitz (2000). "BDCA-2, BDCA-3, and BDCA-4: three markers for distinct subsets of dendritic cells in human peripheral blood." J Immunol **165**(11): 6037-6046.

Eichenfield, D. Z., T. D. Troutman, V. M. Link, M. T. Lam, H. Cho, D. Gosselin, N. J. Spann, H. P. Lesch, J. Tao, J. Muto, R. L. Gallo, R. M. Evans and C. K. Glass (2016). "Tissue damage drives co-localization of NF-kappaB, Smad3, and Nrf2 to direct Rev-erb sensitive wound repair in mouse macrophages." Elife **5**.

Ene, R., R. D. Sinescu, P. Ene, M. M. Cirstoiu and F. C. Cirstoiu (2015). "Synovial inflammation in patients with different stages of knee osteoarthritis." Rom J Morphol Embryol **56**(1): 169-173.

Fearon, U., R. Mullan, T. Markham, M. Connolly, S. Sullivan, A. R. Poole, O. FitzGerald, B. Bresnihan and D. J. Veale (2006). "Oncostatin M induces angiogenesis and cartilage degradation in rheumatoid arthritis synovial tissue and human cartilage cocultures." Arthritis Rheum **54**(10): 3152-3162.

Feldmann, M., F. M. Brennan and R. N. Maini (1996). "Role of cytokines in rheumatoid arthritis." Annu Rev Immunol **14**: 397-440.

Felson, D. T., R. C. Lawrence, P. A. Dieppe, R. Hirsch, C. G. Helmick, J. M. Jordan, R. S. Kington, N. E. Lane, M. C. Nevitt, Y. Zhang, M. Sowers, T. McAlindon, T. D. Spector, A. R. Poole, S. Z. Yanovski, G. Ateshian, L. Sharma, J. A. Buckwalter, K. D. Brandt and J. F. Fries (2000). "Osteoarthritis: new insights. Part 1: the disease and its risk factors." Ann Intern Med **133**(8): 635-646.

Fernandes, L., K. B. Hagen, J. W. Bijlsma, O. Andreassen, P. Christensen, P. G. Conaghan, M. Doherty, R. Geenen, A. Hammond, I. Kjeken, L. S. Lohmander, H. Lund, C. D. Mallen, T. Nava, S. Oliver, K. Pavelka, I. Pitsillidou, J. A. da Silva, J. de la Torre, G. Zanoli, T. P. Vliet Vlieland and R. European League Against (2013). "EULAR recommendations for the non-pharmacological core management of hip and knee osteoarthritis." Ann Rheum Dis **72**(7): 1125-1135.

Field, A. E., E. H. Coakley, A. Must, J. L. Spadano, N. Laird, W. H. Dietz, E. Rimm and G. A. Colditz (2001). "Impact of overweight on the risk of developing common chronic diseases during a 10-year period." Arch Intern Med **161**(13): 1581-1586.

Frank-Bertoncelj, M., M. Trenkmann, K. Klein, E. Karouzakis, H. Rehrauer, A. Bratus, C. Kolling, M. Armaka, A. Filer, B. A. Michel, R. E. Gay, C. D. Buckley, G. Kollias, S. Gay and C. Ospelt (2017). "Epigenetically-driven anatomical diversity of synovial fibroblasts guides joint-specific fibroblast functions." Nat Commun **8**: 14852.

Fransen, J. and P. L. van Riel (2005). "The Disease Activity Score and the EULAR response criteria." Clin Exp Rheumatol **23**(5 Suppl 39): S93-99.

Frisbie, D. D., S. C. Ghivizzani, P. D. Robbins, C. H. Evans and C. W. McIlwraith (2002). "Treatment of experimental equine osteoarthritis by in vivo delivery of the equine interleukin-1 receptor antagonist gene." Gene Ther **9**(1): 12-20.

Fu, W., Y. Cheng, Y. Zhang, X. Mo, T. Li, Y. Liu, P. Wang, W. Pan, Y. Chen, Y. Xue, D. Ma, Y. Zhang and W. Han (2015). "The Secreted Form of Transmembrane Protein 98 Promotes the Differentiation of T Helper 1 Cells." J Interferon Cytokine Res **35**(9): 720-733.

Ganguly, D., S. Haak, V. Sisirak and B. Reizis (2013). "The role of dendritic cells in autoimmunity." Nat Rev Immunol **13**(8): 566-577.

Garcia-Vallejo, J. J. and Y. van Kooyk (2013). "The physiological role of DC-SIGN: a tale of mice and men." Trends Immunol **34**(10): 482-486.

Gautier, E. L., T. Shay, J. Miller, M. Greter, C. Jakubzick, S. Ivanov, J. Helft, A. Chow, K. G. Elpek, S. Gordonov, A. R. Mazloom, A. Ma'ayan, W. J. Chua, T. H. Hansen, S. J. Turley, M. Merad, G. J. Randolph and C. Immunological Genome (2012). "Gene-expression profiles and transcriptional regulatory pathways that underlie the identity and diversity of mouse tissue macrophages." Nat Immunol **13**(11): 1118-1128.

Geissmann, F., S. Jung and D. R. Littman (2003). "Blood monocytes consist of two principal subsets with distinct migratory properties." Immunity **19**(1): 71-82.

Gensel, J. C., T. J. Kopper, B. Zhang, M. B. Orr and W. M. Bailey (2017). "Predictive screening of M1 and M2 macrophages reveals the immunomodulatory effectiveness of post spinal cord injury azithromycin treatment." Sci Rep **7**: 40144.

Gerlag, D. M., J. J. Haringman, T. J. Smeets, A. H. Zwinderman, M. C. Kraan, P. J. Laud, S. Morgan, A. F. Nash and P. P. Tak (2004). "Effects of oral prednisolone on biomarkers in synovial tissue and clinical improvement in rheumatoid arthritis." Arthritis Rheum **50**(12): 3783-3791.

Goldring, M. B. and S. R. Goldring (2010). "Articular cartilage and subchondral bone in the pathogenesis of osteoarthritis." Ann N Y Acad Sci **1192**: 230-237.

Gomez Perdiguero, E., K. Klapproth, C. Schulz, K. Busch, E. Azzoni, L. Crozet, H. Garner, C. Trouillet, M. F. de Bruijn, F. Geissmann and H. R. Rodewald (2015). "Tissue-resident macrophages originate from yolk-sac-derived erythro-myeloid progenitors." Nature **518**(7540): 547-551.

Gong, D., W. Shi, S. J. Yi, H. Chen, J. Groffen and N. Heisterkamp (2012). "TGFbeta signaling plays a critical role in promoting alternative macrophage activation." BMC Immunol **13**: 31.

Gordon, S. (2008). "Elie Metchnikoff: father of natural immunity." Eur J Immunol **38**(12): 3257-3264.

Gordon, S. and A. Pluddemann (2017). "Tissue macrophages: heterogeneity and functions." BMC Biol **15**(1): 53.

Gottfried, E., L. A. Kunz-Schughart, A. Weber, M. Rehli, A. Peuker, A. Muller, M. Kastenberger, G. Brockhoff, R. Andreesen and M. Kreutz (2008). "Expression of CD68 in non-myeloid cell types." Scand J Immunol **67**(5): 453-463.

Gracie, J. A., R. J. Forsey, W. L. Chan, A. Gilmour, B. P. Leung, M. R. Greer, K. Kennedy, R. Carter, X. Q. Wei, D. Xu, M. Field, A. Foulis, F. Y. Liew and I. B. McInnes (1999). "A proinflammatory role for IL-18 in rheumatoid arthritis." J Clin Invest **104**(10): 1393-1401.

Grau, S., P. J. Richards, B. Kerr, C. Hughes, B. Caterson, A. S. Williams, U. Junker, S. A. Jones, T. Clausen and M. Ehrmann (2006). "The role of human HtrA1 in arthritic disease." J Biol Chem **281**(10): 6124-6129.

Guerra, M. L., P. J. Singh and N. F. Taylor (2015). "Early mobilization of patients who have had a hip or knee joint replacement reduces length of stay in hospital: a systematic review." Clin Rehabil **29**(9): 844-854.

Guilliams, M., C. A. Dutertre, C. L. Scott, N. McGovern, D. Sichien, S. Chakarov, S. Van Gassen, J. Chen, M. Poidinger, S. De Prijck, S. J. Tavernier, I. Low, S. E. Irac, C. N. Mattar, H. R. Sumatoh, G. H. Low, T. J. Chung, D. K. Chan, K. K. Tan, T. L. Hon, E. Fossum, B. Bogen, M. Choolani, J. K. Chan, A. Larbi, H. Luche, S. Henri, Y. Saeys, E. W. Newell, B. N. Lambrecht, B. Malissen and F. Ginhoux (2016). "Unsupervised High-Dimensional Analysis Aligns Dendritic Cells across Tissues and Species." Immunity **45**(3): 669-684.

Guilliams, M., F. Ginhoux, C. Jakubzick, S. H. Naik, N. Onai, B. U. Schraml, E. Segura, R. Tussiwand and S. Yona (2014). "Dendritic cells, monocytes and macrophages: a unified nomenclature based on ontogeny." Nat Rev Immunol **14**(8): 571-578.

Hanada, M., M. Takahashi, H. Furuhashi, H. Koyama and Y. Matsuyama (2016). "Elevated erythrocyte sedimentation rate and high-sensitivity C-reactive protein in osteoarthritis of the knee: relationship with clinical findings and radiographic severity." Ann Clin Biochem **53**(Pt 5): 548-553.

Haniffa, M., M. Gunawan and L. Jardine (2015). "Human skin dendritic cells in health and disease." J Dermatol Sci **77**(2): 85-92.

Haniffa, M., A. Shin, V. Bigley, N. McGovern, P. Teo, P. See, P. S. Wasan, X. N. Wang, F. Malinarich, B. Malleret, A. Larbi, P. Tan, H. Zhao, M. Poidinger, S. Pagan, S. Cookson, R. Dickinson, I. Dimmick, R. F. Jarrett, L. Renia, J. Tam, C. Song, J. Connolly, J. K. Chan, A. Gehring, A. Bertoletti, M. Collin and F. Ginhoux (2012). "Human tissues contain CD141hi cross-presenting dendritic cells with functional homology to mouse CD103+ nonlymphoid dendritic cells." Immunity **37**(1): 60-73.

Hansson, M., A. Lundgren, K. Elgbratt, M. Quiding-Jarbrink, A. M. Svennerholm and E. L. Johansson (2006). "Dendritic cells express CCR7 and migrate in response to CCL19 (MIP-3beta) after exposure to Helicobacter pylori." Microbes Infect **8**(3): 841-850.

Haringman, J. J., D. M. Gerlag, A. H. Zwinderman, T. J. Smeets, M. C. Kraan, D. Baeten, I. B. McInnes, B. Bresnihan and P. P. Tak (2005). "Synovial tissue macrophages: a sensitive biomarker for response to treatment in patients with rheumatoid arthritis." Ann Rheum Dis **64**(6): 834-838.

Hashimoto, D., A. Chow, C. Noizat, P. Teo, M. B. Beasley, M. Leboeuf, C. D. Becker, P. See, J. Price, D. Lucas, M. Greter, A. Mortha, S. W. Boyer, E. C. Forsberg, M. Tanaka, N. van Rooijen, A. Garcia-Sastre, E. R. Stanley, F. Ginhoux, P. S. Frenette and M. Merad (2013). "Tissue-resident macrophages self-maintain locally throughout adult life with minimal contribution from circulating monocytes." Immunity **38**(4): 792-804.

Haugen, I. K. and P. Boyesen (2011). "Imaging modalities in hand osteoarthritis--and perspectives of conventional radiography, magnetic resonance imaging, and ultrasonography." Arthritis Res Ther **13**(6): 248.

Haywood, L., D. F. McWilliams, C. I. Pearson, S. E. Gill, A. Ganesan, D. Wilson and D. A. Walsh (2003). "Inflammation and angiogenesis in osteoarthritis." Arthritis Rheum **48**(8): 2173-2177.

Henrotin, Y., M. Gharbi, G. Mazzucchelli, J. E. Dubuc, E. De Pauw and M. Deberg (2012). "Fibulin 3 peptides Fib3-1 and Fib3-2 are potential biomarkers of osteoarthritis." Arthritis Rheum **64**(7): 2260-2267.

Heruth, D. P., M. Gibson, D. N. Grigoryev, L. Q. Zhang and S. Q. Ye (2012). "RNA-seq analysis of synovial fibroblasts brings new insights into rheumatoid arthritis." Cell Biosci **2**(1): 43.

Hong, B. K., S. You, S. A. Yoo, D. Park, D. Hwang, C. S. Cho and W. U. Kim (2017). "MicroRNA-143 and -145 modulate the phenotype of synovial fibroblasts in rheumatoid arthritis." Exp Mol Med **49**(8): e363.

Hunter, D. J. (2008). "Are there promising biologic therapies for osteoarthritis?" Curr Rheumatol Rep **10**(1): 19-25.

Isaacs, J. D. and G. Ferraccioli (2011). "The need for personalised medicine for rheumatoid arthritis." Ann Rheum Dis **70**(1): 4-7.

Italiani, P. and D. Boraschi (2014). "From Monocytes to M1/M2 Macrophages: Phenotypical vs. Functional Differentiation." Front Immunol **5**: 514.

Jakubzick, C., E. L. Gautier, S. L. Gibbings, D. K. Sojka, A. Schlitzer, T. E. Johnson, S. Ivanov, Q. Duan, S. Bala, T. Condon, N. van Rooijen, J. R. Grainger, Y. Belkaid, A. Ma'ayan, D. W. Riches, W. M. Yokoyama, F. Ginhoux, P. M. Henson and G. J. Randolph (2013). "Minimal differentiation of classical monocytes as they survey steady-state tissues and transport antigen to lymph nodes." Immunity **39**(3): 599-610.

Jameel, A., K. G. Ooi, N. R. Jeffs, G. Galatowicz, S. L. Lightman and V. L. Calder (2013). "Statin Modulation of Human T-Cell Proliferation, IL-1beta and IL-17 Production, and IFN-gamma T Cell Expression: Synergy with Conventional Immunosuppressive Agents." Int J Inflam **2013**: 434586.

Jenkins, S. J., D. Ruckerl, P. C. Cook, L. H. Jones, F. D. Finkelman, N. van Rooijen, A. S. MacDonald and J. E. Allen (2011). "Local macrophage proliferation, rather than recruitment from the blood, is a signature of TH2 inflammation." Science **332**(6035): 1284-1288.

Jetten, N., N. Roumans, M. J. Gijbels, A. Romano, M. J. Post, M. P. de Winther, R. R. van der Hulst and S. Xanthoulea (2014). "Wound administration of M2-polarized macrophages does not improve murine cutaneous healing responses." PLoS One **9**(7): e102994.

Jin, Y. R. and J. K. Yoon (2012). "The R-spondin family of proteins: emerging regulators of WNT signaling." Int J Biochem Cell Biol **44**(12): 2278-2287.

Jinnin, M., H. Ihn and K. Tamaki (2006). "Characterization of SIS3, a novel specific inhibitor of Smad3, and its effect on transforming growth factor-beta1-induced extracellular matrix expression." Mol Pharmacol **69**(2): 597-607.

Jongbloed, S. L., A. J. Kassianos, K. J. McDonald, G. J. Clark, X. Ju, C. E. Angel, C. J. Chen, P. R. Dunbar, R. B. Wadley, V. Jeet, A. J. Vulink, D. N. Hart and K. J. Radford (2010). "Human CD141+ (BDCA-3)+ dendritic cells (DCs) represent a unique myeloid DC subset that cross-presents necrotic cell antigens." J Exp Med **207**(6): 1247-1260.

Jongbloed, S. L., M. C. Lebre, A. R. Fraser, J. A. Gracie, R. D. Sturrock, P. P. Tak and I. B. McInnes (2006). "Enumeration and phenotypical analysis of distinct dendritic cell subsets in psoriatic arthritis and rheumatoid arthritis." Arthritis Res Ther **8**(1): R15.

Kalinina, N., A. Agrotis, Y. Antropova, O. Ilyinskaya, V. Smirnov, E. Tararak and A. Bobik (2004). "Smad expression in human atherosclerotic lesions: evidence for impaired TGF-beta/Smad signaling in smooth muscle cells of fibrofatty lesions." Arterioscler Thromb Vasc Biol **24**(8): 1391-1396.

Kapoor, M., J. Martel-Pelletier, D. Lajeunesse, J. P. Pelletier and H. Fahmi (2011). "Role of proinflammatory cytokines in the pathophysiology of osteoarthritis." Nat Rev Rheumatol **7**(1): 33-42.

Kawanaka, N., M. Yamamura, T. Aita, Y. Morita, A. Okamoto, M. Kawashima, M. Iwahashi, A. Ueno, Y. Ohmoto and H. Makino (2002). "CD14+,CD16+ blood monocytes and joint inflammation in rheumatoid arthritis." Arthritis Rheum **46**(10): 2578-2586.

Keenan, R. T., C. J. Swearingen and Y. Yazici (2008). "Erythrocyte sedimentation rate and C-reactive protein levels are poorly correlated with clinical measures of disease activity in rheumatoid arthritis, systemic lupus erythematosus and osteoarthritis patients." Clin Exp Rheumatol **26**(5): 814-819.

Kennedy, A., U. Fearon, D. J. Veale and C. Godson (2011). "Macrophages in synovial inflammation." Front Immunol **2**: 52.

Kettenmann, H., F. Kirchhoff and A. Verkhratsky (2013). "Microglia: new roles for the synaptic stripper." Neuron **77**(1): 10-18.

Khazen, W., P. M'Bika J, C. Tomkiewicz, C. Benelli, C. Chany, A. Achour and C. Forest (2005). "Expression of macrophage-selective markers in human and rodent adipocytes." FEBS Lett **579**(25): 5631-5634.

Kierdorf, K., D. Erny, T. Goldmann, V. Sander, C. Schulz, E. G. Perdiguero, P. Wieghofer, A. Heinrich, P. Riemke, C. Holscher, D. N. Muller, B. Luckow, T. Brocker, K. Debowski, G. Fritz, G. Opdenakker, A. Diefenbach, K. Biber, M. Heikenwalder, F. Geissmann, F. Rosenbauer and M. Prinz (2013). "Microglia emerge from erythromyeloid precursors via Pu.1- and Irf8-dependent pathways." Nat Neurosci **16**(3): 273-280.

Kim, J. H. and N. Kim (2014). "Regulation of NFATc1 in Osteoclast Differentiation." J Bone Metab **21**(4): 233-241.

King, W., A. Bendele, T. Marohl and J. Woodell-May (2017). "Human blood-based anti-inflammatory solution inhibits osteoarthritis progression in a meniscal-tear rat study." J Orthop Res.

Kinne, R. W., R. Brauer, B. Stuhlmuller, E. Palombo-Kinne and G. R. Burmester (2000). "Macrophages in rheumatoid arthritis." Arthritis Res **2**(3): 189-202.

Kohem, C. L., R. I. Brezinschek, H. Wisbey, C. Tortorella, P. E. Lipsky and N. Oppenheimer-Marks (1996). "Enrichment of differentiated CD45RBdim,CD27- memory T cells in the peripheral blood, synovial fluid, and synovial tissue of patients with rheumatoid arthritis." Arthritis Rheum **39**(5): 844-854.

Kohyama, M., W. Ise, B. T. Edelson, P. R. Wilker, K. Hildner, C. Mejia, W. A. Frazier, T. L. Murphy and K. M. Murphy (2009). "Role for Spi-C in the development of red pulp macrophages and splenic iron homeostasis." Nature **457**(7227): 318-321.

Koller, U., W. Waldstein, V. Krenn, R. Windhager and F. Boettner (2017). "Varus knee osteoarthritis: Elevated synovial CD15 counts correlate with inferior biomechanical properties of lateral-compartment cartilage." J Orthop Res.

Komatsu, N., K. Okamoto, S. Sawa, T. Nakashima, M. Oh-hora, T. Kodama, S. Tanaka, J. A. Bluestone and H. Takayanagi (2014). "Pathogenic conversion of Foxp3+ T cells into TH17 cells in autoimmune arthritis." Nat Med **20**(1): 62-68.

Koo, J., S. Kim, W. J. Jung, Y. E. Lee, G. G. Song, K. S. Kim and M. Y. Kim (2013). "Increased Lymphocyte Infiltration in Rheumatoid Arthritis Is Correlated with an Increase in LTi-like Cells in Synovial Fluid." Immune Netw **13**(6): 240-248.

Kraan, M. C., R. J. Reece, E. C. Barg, T. J. Smeets, J. Farnell, R. Rosenburg, D. J. Veale, F. C. Breedveld, P. Emery and P. P. Tak (2000). "Modulation of inflammation and metalloproteinase expression in synovial tissue by leflunomide and methotrexate in patients with active rheumatoid arthritis. Findings in a prospective, randomized, double-blind, parallel-design clinical trial in thirty-nine patients at two centers." Arthritis Rheum **43**(8): 1820-1830.

Kraan, M. C., R. J. Reece, T. J. Smeets, D. J. Veale, P. Emery and P. P. Tak (2002). "Comparison of synovial tissues from the knee joints and the small joints of rheumatoid arthritis patients: Implications for pathogenesis and evaluation of treatment." Arthritis Rheum **46**(8): 2034-2038.

Kraus, V. B., G. McDaniel, J. L. Huebner, T. V. Stabler, C. F. Pieper, S. W. Shipes, N. A. Petry, P. S. Low, J. Shen, T. A. McNearney and P. Mitchell (2016). "Direct in vivo evidence of activated macrophages in human osteoarthritis." Osteoarthritis Cartilage **24**(9): 1613-1621.

Krausgruber, T., K. Blazek, T. Smallie, S. Alzabin, H. Lockstone, N. Sahgal, T. Hussell, M. Feldmann and I. A. Udalova (2011). "IRF5 promotes inflammatory macrophage polarization and TH1-TH17 responses." Nat Immunol **12**(3): 231-238.

Kunz-Schughart, L. A., A. Weber, M. Rehli, E. Gottfried, G. Brockhoff, S. W. Krause, R. Andreesen and M. Kreutz (2003). "[The "classical" macrophage marker CD68 is strongly expressed in primary human fibroblasts]." Verh Dtsch Ges Pathol **87**: 215-223.

Lang, C. H., B. J. Krawiec, D. Huber, J. M. McCoy and R. A. Frost (2006). "Sepsis and inflammatory insults downregulate IGFBP-5, but not IGFBP-4, in skeletal muscle via a TNF-dependent mechanism." Am J Physiol Regul Integr Comp Physiol **290**(4): R963-972.

Larkin, D. J., J. Z. Kartchner, A. S. Doxey, W. R. Hollis, J. L. Rees, S. K. Wilhelm, C. S. Draper, D. M. Peterson, G. G. Jackson, C. Ingersoll, S. S. Haynie, E. Chavez, P. R. Reynolds and D. L. Kooyman (2013). "Inflammatory markers associated with osteoarthritis after destabilization surgery in young mice with and without Receptor for Advanced Glycation End-products (RAGE)." Front Physiol **4**: 121.

Lebre, M. C., S. L. Jongbloed, S. W. Tas, T. J. Smeets, I. B. McInnes and P. P. Tak (2008). "Rheumatoid arthritis synovium contains two subsets of CD83-DC-LAMP- dendritic cells with distinct cytokine profiles." Am J Pathol **172**(4): 940-950.

Leipe, J., M. A. Schramm, I. Prots, H. Schulze-Koops and A. Skapenko (2014). "Increased Th17 cell frequency and poor clinical outcome in rheumatoid arthritis are associated with a genetic variant in the IL4R gene, rs1805010." Arthritis Rheumatol **66**(5): 1165-1175.

Li, Y. S., F. J. Zhang, C. Zeng, W. Luo, W. F. Xiao, S. G. Gao and G. H. Lei (2016). "Autophagy in osteoarthritis." Joint Bone Spine **83**(2): 143-148.

Liew, F. Y., X. Q. Wei and I. B. McInnes (2003). "Role of interleukin 18 in rheumatoid arthritis." Ann Rheum Dis **62 Suppl 2**: ii48-50.

Liu, D., Y. Wang, Z. Jia, L. Wang, J. Wang, D. Yang, J. Song, S. Wang and Z. Fan (2015). "Demethylation of IGFBP5 by Histone Demethylase KDM6B Promotes Mesenchymal Stem Cell-Mediated Periodontal Tissue Regeneration by Enhancing Osteogenic Differentiation and Anti-Inflammation Potentials." Stem Cells **33**(8): 2523-2536.

Liu, Y., X. Gao, E. Masuda, P. B. Redecha, M. C. Blank and L. Pricop (2006). "Regulated expression of FcgammaR in human dendritic cells controls cross-presentation of antigen-antibody complexes." J Immunol **177**(12): 8440-8447.

Lo, S. Z., J. H. Steer and D. A. Joyce (2011). "Tumor necrosis factor-alpha promotes survival in methotrexate-exposed macrophages by an NF-kappaB-dependent pathway." Arthritis Res Ther **13**(1): R24.

Loboda, A., M. Sobczak, A. Jozkowicz and J. Dulak (2016). "TGF-beta1/Smads and miR-21 in Renal Fibrosis and Inflammation." Mediators Inflamm **2016**: 8319283.

Loewi, G., E. M. Lance and J. Reynolds (1975). "Study of lymphoid cells from inflamed synovial membranes." Ann Rheum Dis **34**(6): 524-528.

Long, E. O. (2011). "ICAM-1: getting a grip on leukocyte adhesion." J Immunol **186**(9): 5021-5023.

Lurati, A., A. Laria, A. Gatti, B. Brando and M. Scarpellini (2015). "Different T cells' distribution and activation degree of Th17 CD4+ cells in peripheral blood in patients with osteoarthritis, rheumatoid arthritis, and healthy donors: preliminary results of the MAGENTA CLICAO study." Open Access Rheumatol **7**: 63-68.

Maa, M. C., M. Y. Chang, Y. J. Chen, C. H. Lin, C. J. Yu, Y. L. Yang, J. Li, P. R. Chen, C. H. Tang, H. Y. Lei and T. H. Leu (2008). "Requirement of inducible nitric-oxide synthase in lipopolysaccharide-mediated Src induction and macrophage migration." J Biol Chem **283**(46): 31408-31416.

MacDonald, K. P., D. J. Munster, G. J. Clark, A. Dzionek, J. Schmitz and D. N. Hart (2002). "Characterization of human blood dendritic cell subsets." Blood **100**(13): 4512-4520.

MacGregor, A. J., H. Snieder, A. S. Rigby, M. Koskenvuo, J. Kaprio, K. Aho and A. J. Silman (2000). "Characterizing the quantitative genetic contribution to rheumatoid arthritis using data from twins." Arthritis Rheum **43**(1): 30-37.

Manferdini, C., F. Paolella, E. Gabusi, Y. Silvestri, L. Gambari, L. Cattini, G. Filardo, S. Fleury-Cappellesso and G. Lisignoli (2016). "From osteoarthritic synovium to synovial-derived cells characterization: synovial macrophages are key effector cells." Arthritis Res Ther **18**: 83.

Mantovani, A., A. Sica, S. Sozzani, P. Allavena, A. Vecchi and M. Locati (2004). "The chemokine system in diverse forms of macrophage activation and polarization." Trends Immunol **25**(12): 677-686.

Mao, M., J. Chen, X. Li and Z. Wu (2015). "siRNA-TMEM98 inhibits the invasion and migration of lung cancer cells." Int J Clin Exp Pathol **8**(12): 15661-15669.

Martinez, F. O. and S. Gordon (2014). "The M1 and M2 paradigm of macrophage activation: time for reassessment." F1000Prime Rep **6**: 13.

Martinez, F. O., S. Gordon, M. Locati and A. Mantovani (2006). "Transcriptional profiling of the human monocyte-to-macrophage differentiation and polarization: new molecules and patterns of gene expression." J Immunol **177**(10): 7303-7311.

McGovern, N., A. Schlitzer, M. Gunawan, L. Jardine, A. Shin, E. Poyner, K. Green, R. Dickinson, X. N. Wang, D. Low, K. Best, S. Covins, P. Milne, S. Pagan, K. Aljefri, M. Windebank, D. Miranda-Saavedra, A. Larbi, P. S. Wasan, K. Duan, M. Poidinger, V. Bigley, F. Ginhoux, M. Collin and M. Haniffa (2014). "Human dermal CD14(+) cells are a transient population of monocyte-derived macrophages." Immunity **41**(3): 465-477.

McInnes, I. B. and J. R. O'Dell (2010). "State-of-the-art: rheumatoid arthritis." Ann Rheum Dis **69**(11): 1898-1906.

McInnes, I. B. and G. Schett (2011). "The pathogenesis of rheumatoid arthritis." N Engl J Med **365**(23): 2205-2219.

Meixlsperger, S., C. S. Leung, P. C. Ramer, M. Pack, L. D. Vanoaica, G. Breton, S. Pascolo, A. M. Salazar, A. Dzionek, J. Schmitz, R. M. Steinman and C. Munz (2013). "CD141+ dendritic cells produce prominent amounts of IFN-alpha after dsRNA recognition and can be targeted via DEC-205 in humanized mice." Blood **121**(25): 5034-5044.

Milano, A., S. A. Pendergrass, J. L. Sargent, L. K. George, T. H. McCalmont, M. K. Connolly and M. L. Whitfield (2008). "Molecular subsets in the gene expression signatures of scleroderma skin." PLoS One **3**(7): e2696.

Miller, M. C., H. B. Manning, A. Jain, L. Troeberg, J. Dudhia, D. Essex, A. Sandison, M. Seiki, J. Nanchahal, H. Nagase and Y. Itoh (2009). "Membrane type 1 matrix metalloproteinase is a crucial promoter of synovial invasion in human rheumatoid arthritis." Arthritis Rheum **60**(3): 686-697.

Minaur, N. J., C. Jefferiss, A. K. Bhalla and J. N. Beresford (2002). "Methotrexate in the treatment of rheumatoid arthritis. I. In vitro effects on cells of the osteoblast lineage." Rheumatology (Oxford) **41**(7): 735-740.

Mizoguchi, F., K. Slowikowski, J. L. Marshall, K. Wei, D. A. Rao, S. K. Chang, H. N. Nguyen, E. H. Noss, J. D. Turner, B. E. Earp, P. E. Blazar, J. Wright, B. P. Simmons, L. T. Donlin, G. D. Kalliolias, S. M. Goodman, V. P. Bykerk, L. B. Ivashkiv, J. A. Lederer, N. Hacohen, P. A. Nigrovic, A. Filer, C. D. Buckley, S. Raychaudhuri and M. B. Brenner (2017). "Single Cell Transcriptomics And Flow Cytometry Reveal Disease-Associated Fibroblast Subsets In Rheumatoid Arthritis." bioRxiv.

Moradi, B., N. Rosshirt, E. Tripel, J. Kirsch, A. Barie, F. Zeifang, T. Gotterbarm and S. Hagmann (2015). "Unicompartmental and bicompartmental knee osteoarthritis show different patterns of mononuclear cell infiltration and cytokine release in the affected joints." Clin Exp Immunol **180**(1): 143-154.

Mosser, D. M. and J. P. Edwards (2008). "Exploring the full spectrum of macrophage activation." Nat Rev Immunol **8**(12): 958-969.

Muller, P. A., B. Koscso, G. M. Rajani, K. Stevanovic, M. L. Berres, D. Hashimoto, A. Mortha, M. Leboeuf, X. M. Li, D. Mucida, E. R. Stanley, S. Dahan, K. G. Margolis, M. D. Gershon, M. Merad and M. Bogunovic (2014). "Crosstalk between muscularis macrophages and enteric neurons regulates gastrointestinal motility." Cell **158**(2): 300-313.

Murray, P. J. and T. A. Wynn (2011). "Protective and pathogenic functions of macrophage subsets." Nat Rev Immunol **11**(11): 723-737.

Nagai, H., Y. Miyamoto, A. Nakata, S. Hatakeyama, Y. Iwanami and M. Fukuda (2006). "Isolation and characterization of synovial cells from the human temporomandibular joint." J Oral Pathol Med **35**(2): 104-110.

Nakajima, M., I. Kou, H. Ohashi, L. Genetic Study Group of the Investigation Committee on the Ossification of Spinal and S. Ikegawa (2016). "Identification and Functional Characterization of RSPO2 as a Susceptibility Gene for Ossification of the Posterior Longitudinal Ligament of the Spine." Am J Hum Genet **99**(1): 202-207.

Nakamura, K., J. J. Fuster and K. Walsh (2014). "Adipokines: A link between obesity and cardiovascular disease." Journal of Cardiology **63**(3-4): 250-259.

Netea, M. G., G. D. Brown, B. J. Kullberg and N. A. Gow (2008). "An integrated model of the recognition of Candida albicans by the innate immune system." Nat Rev Microbiol **6**(1): 67-78.

Neurath, M. F., K. Hildner, C. Becker, J. F. Schlaak, K. Barbulescu, T. Germann, E. Schmitt, P. Schirmacher, S. Haralambous, M. Pasparakis, K. H. Meyer Zum Buschenfelde, G. Kollias and E. Marker-Hermann (1999). "Methotrexate specifically modulates cytokine production by T cells and macrophages in murine collagen-induced arthritis (CIA): a mechanism for methotrexate-mediated immunosuppression." Clin Exp Immunol **115**(1): 42-55.

Ng, C. T., M. Biniecka, A. Kennedy, J. McCormick, O. Fitzgerald, B. Bresnihan, D. Buggy, C. T. Taylor, J. O'Sullivan, U. Fearon and D. J. Veale (2010). "Synovial tissue hypoxia and inflammation in vivo." Ann Rheum Dis **69**(7): 1389-1395.

Nizzoli, G., J. Krietsch, A. Weick, S. Steinfelder, F. Facciotti, P. Gruarin, A. Bianco, B. Steckel, M. Moro, M. Crosti, C. Romagnani, K. Stolzel, S. Torretta, L. Pignataro, C. Scheibenbogen, P. Neddermann, R. De Francesco, S. Abrignani and J. Geginat (2013). "Human CD1c+ dendritic cells secrete high levels of IL-12 and potently prime cytotoxic T-cell responses." Blood **122**(6): 932-942.

Novak, M. L. and T. J. Koh (2013). "Phenotypic transitions of macrophages orchestrate tissue repair." Am J Pathol **183**(5): 1352-1363.

Okabe, Y. and R. Medzhitov (2014). "Tissue-specific signals control reversible program of localization and functional polarization of macrophages." Cell **157**(4): 832-844.

Olney, R. C., K. Tsuchiya, D. M. Wilson, M. Mohtai, W. J. Maloney, D. J. Schurman and R. L. Smith (1996). "Chondrocytes from osteoarthritic cartilage have increased expression of insulin-like growth factor I (IGF-I) and IGF-binding protein-3 (IGFBP-3) and -5, but not IGF-II or IGFBP-4." J Clin Endocrinol Metab **81**(3): 1096-1103.

Passlick, B., D. Flieger and H. W. Ziegler-Heitbrock (1989). "Identification and characterization of a novel monocyte subpopulation in human peripheral blood." Blood **74**(7): 2527-2534.

Pearle, A. D., C. R. Scanzello, S. George, L. A. Mandl, E. F. DiCarlo, M. Peterson, T. P. Sculco and M. K. Crow (2007). "Elevated high-sensitivity C-reactive protein levels are associated with local inflammatory findings in patients with osteoarthritis." Osteoarthritis Cartilage **15**(5): 516-523.

Peat, G., E. Thomas, R. Duncan, L. Wood, E. Hay and P. Croft (2006). "Clinical classification criteria for knee osteoarthritis: performance in the general population and primary care." Ann Rheum Dis **65**(10): 1363-1367.

Petersson, I. F., L. Sandqvist, B. Svensson and T. Saxne (1997). "Cartilage markers in synovial fluid in symptomatic knee osteoarthritis." Ann Rheum Dis **56**(1): 64-67.

Philp, A. M., E. T. Davis and S. W. Jones (2017). "Developing anti-inflammatory therapeutics for patients with osteoarthritis." Rheumatology (Oxford) **56**(6): 869-881.

Pieringer, H. and M. Pichler (2011). "Cardiovascular morbidity and mortality in patients with rheumatoid arthritis: vascular alterations and possible clinical implications." QJM **104**(1): 13-26.

Pilling, D., T. Fan, D. Huang, B. Kaul and R. H. Gomer (2009). "Identification of markers that distinguish monocyte-derived fibrocytes from monocytes, macrophages, and fibroblasts." PLoS One **4**(10): e7475.

Porta, C., M. Rimoldi, G. Raes, L. Brys, P. Ghezzi, D. Di Liberto, F. Dieli, S. Ghisletti, G. Natoli, P. De Baetselier, A. Mantovani and A. Sica (2009). "Tolerance and M2 (alternative) macrophage polarization are related processes orchestrated by p50 nuclear factor kappaB." Proc Natl Acad Sci U S A **106**(35): 14978-14983.

Pozo, P. N. and J. G. Cook (2016). "Regulation and Function of Cdt1; A Key Factor in Cell Proliferation and Genome Stability." Genes (Basel) **8**(1).

Pratt, A. G., D. C. Swan, S. Richardson, G. Wilson, C. M. Hilkens, D. A. Young and J. D. Isaacs (2012). "A CD4 T cell gene signature for early rheumatoid arthritis implicates interleukin 6-mediated STAT3 signalling, particularly in anti-citrullinated peptide antibody-negative disease." Ann Rheum Dis **71**(8): 1374-1381.

Qu, C., N. S. Brinck-Jensen, M. Zang and K. Chen (2014). "Monocyte-derived dendritic cells: targets as potent antigen-presenting cells for the design of vaccines against infectious diseases." Int J Infect Dis **19**: 1-5.

Radwan, M., D. J. Wilkinson, W. Hui, A. P. Destrument, S. H. Charlton, M. J. Barter, B. Gibson, J. Coulombe, D. A. Gray, A. D. Rowan and D. A. Young (2015). "Protection against murine osteoarthritis by inhibition of the 26S proteasome and lysine-48 linked ubiquitination." Ann Rheum Dis **74**(8): 1580-1587.

Raine, E. V., L. N. Reynard, I. M. van de Laar, A. M. Bertoli-Avella and J. Loughlin (2014). "Identification and analysis of a SMAD3 cis-acting eQTL operating in primary osteoarthritis and in the aneurysms and osteoarthritis syndrome." Osteoarthritis Cartilage **22**(5): 698-705.

Reece, R. J., J. D. Canete, W. J. Parsons, P. Emery and D. J. Veale (1999). "Distinct vascular patterns of early synovitis in psoriatic, reactive, and rheumatoid arthritis." Arthritis Rheum **42**(7): 1481-1484.

Reis, J., X. Q. Guan, A. F. Kisselev, C. J. Papasian, A. A. Qureshi, D. C. Morrison, C. W. Van Way, 3rd, S. N. Vogel and N. Qureshi (2011). "LPS-induced formation of immunoproteasomes: TNF-alpha and nitric oxide production are regulated by altered composition of proteasome-active sites." Cell Biochem Biophys **60**(1-2): 77-88.

Reizis, B., A. Bunin, H. S. Ghosh, K. L. Lewis and V. Sisirak (2011). "Plasmacytoid dendritic cells: recent progress and open questions." Annu Rev Immunol **29**: 163-183.

Remst, D. F., E. N. Blaney Davidson and P. M. van der Kraan (2015). "Unravelling osteoarthritis-related synovial fibrosis: a step closer to solving joint stiffness." Rheumatology (Oxford) **54**(11): 1954-1963.

Rocher, C. and D. K. Singla (2013). "SMAD-PI3K-Akt-mTOR pathway mediates BMP-7 polarization of monocytes into M2 macrophages." PLoS One **8**(12): e84009.

Roemer, F. W., M. D. Crema, S. Trattnig and A. Guermazi (2011). "Advances in imaging of osteoarthritis and cartilage." Radiology **260**(2): 332-354.

Rollin, R., F. Marco, J. A. Jover, J. A. Garcia-Asenjo, L. Rodriguez, L. Lopez-Duran and B. Fernandez-Gutierrez (2008). "Early lymphocyte activation in the synovial microenvironment in patients with osteoarthritis: comparison with rheumatoid arthritis patients and healthy controls." Rheumatol Int **28**(8): 757-764.

Rooney, M., A. Whelan, C. Feighery and B. Bresnihan (1989). "Changes in lymphocyte infiltration of the synovial membrane and the clinical course of rheumatoid arthritis." Arthritis Rheum **32**(4): 361-369.

Roszer, T. (2015). "Understanding the Mysterious M2 Macrophage through Activation Markers and Effector Mechanisms." Mediators Inflamm **2015**: 816460.

Runhaar, J., C. Sanchez, S. Taralla, Y. Henrotin and S. M. Bierma-Zeinstra (2016). "Fibulin-3 fragments are prognostic biomarkers of osteoarthritis incidence in overweight and obese women." Osteoarthritis Cartilage **24**(4): 672-678.

Saeys, Y., S. V. Gassen and B. N. Lambrecht (2016). "Computational flow cytometry: helping to make sense of high-dimensional immunology data." Nat Rev Immunol **16**(7): 449-462.

Saito, I., T. Koshino, K. Nakashima, M. Uesugi and T. Saito (2002). "Increased cellular infiltrate in inflammatory synovia of osteoarthritic knees." Osteoarthritis Cartilage **10**(2): 156-162.

Sakuraba, K., K. Fujimura, Y. Nakashima, K. Okazaki, J. Fukushi, M. Ohishi, A. Oyamada, Y. Esaki, H. Miyahara, Y. Iwamoto, Y. Yoshikai and H. Yamada (2015). "Brief report: successful in vitro culture of rheumatoid arthritis synovial tissue explants at the air-liquid interface." Arthritis Rheumatol **67**(4): 887-892.

Saliba, A. E., L. Li, A. J. Westermann, S. Appenzeller, D. A. Stapels, L. N. Schulte, S. Helaine and J. Vogel (2016). "Single-cell RNA-seq ties macrophage polarization to growth rate of intracellular Salmonella." Nat Microbiol **2**: 16206.

Salih, D. A., G. Tripathi, C. Holding, T. A. Szestak, M. I. Gonzalez, E. J. Carter, L. J. Cobb, J. E. Eisemann and J. M. Pell (2004). "Insulin-like growth factor-binding protein 5 (Igfbp5) compromises survival, growth, muscle development, and fertility in mice." Proc Natl Acad Sci U S A **101**(12): 4314-4319.

Satoh, T., O. Takeuchi, A. Vandenbon, K. Yasuda, Y. Tanaka, Y. Kumagai, T. Miyake, K. Matsushita, T. Okazaki, T. Saitoh, K. Honma, T. Matsuyama, K. Yui, T. Tsujimura, D. M. Standley, K. Nakanishi, K. Nakai and S. Akira (2010). "The Jmjd3-Irf4 axis regulates M2 macrophage polarization and host responses against helminth infection." Nat Immunol **11**(10): 936-944.

Scanzello, C. R. and S. R. Goldring (2012). "The role of synovitis in osteoarthritis pathogenesis." Bone **51**(2): 249-257.

Scanzello, C. R., B. McKeon, B. H. Swaim, E. DiCarlo, E. U. Asomugha, V. Kanda, A. Nair, D. M. Lee, J. C. Richmond, J. N. Katz, M. K. Crow and S. R. Goldring (2011). "Synovial inflammation in patients undergoing arthroscopic meniscectomy: molecular characterization and relationship to symptoms." Arthritis Rheum **63**(2): 391-400.

Schelbergen, R. F., E. J. Geven, M. H. van den Bosch, H. Eriksson, T. Leanderson, T. Vogl, J. Roth, F. A. van de Loo, M. I. Koenders, P. M. van der Kraan, W. B. van den Berg, A. B. Blom and P. L. van Lent (2015). "Prophylactic treatment with S100A9 inhibitor paquinimod reduces pathology in experimental collagenase-induced osteoarthritis." Ann Rheum Dis **74**(12): 2254-2258.

Schlitzer, A., N. McGovern, P. Teo, T. Zelante, K. Atarashi, D. Low, A. W. Ho, P. See, A. Shin, P. S. Wasan, G. Hoeffel, B. Malleret, A. Heiseke, S. Chew, L. Jardine, H. A. Purvis, C. M. Hilkens, J. Tam, M. Poidinger, E. R. Stanley, A. B. Krug, L. Renia, B. Sivasankar, L. G. Ng, M. Collin, P. Ricciardi-Castagnoli, K. Honda, M. Haniffa and F. Ginhoux (2013). "IRF4 transcription factor-dependent CD11b+ dendritic cells in human and mouse control mucosal IL-17 cytokine responses." Immunity **38**(5): 970-983.

Segura, E., M. Touzot, A. Bohineust, A. Cappuccio, G. Chiocchia, A. Hosmalin, M. Dalod, V. Soumelis and S. Amigorena (2013). "Human inflammatory dendritic cells induce Th17 cell differentiation." Immunity **38**(2): 336-348.

Sellam, J. and F. Berenbaum (2010). "The role of synovitis in pathophysiology and clinical symptoms of osteoarthritis." Nat Rev Rheumatol **6**(11): 625-635.

Shepherd, C., A. J. Skelton, M. D. Rushton, L. N. Reynard and J. Loughlin (2015). "Expression analysis of the osteoarthritis genetic susceptibility locus mapping to an intron of the MCF2L gene and marked by the polymorphism rs11842874." BMC Med Genet **16**: 108.

Sindrilaru, A., T. Peters, S. Wieschalka, C. Baican, A. Baican, H. Peter, A. Hainzl, S. Schatz, Y. Qi, A. Schlecht, J. M. Weiss, M. Wlaschek, C. Sunderkotter and K. Scharffetter-Kochanek (2011). "An unrestrained proinflammatory M1 macrophage population induced by iron impairs wound healing in humans and mice." J Clin Invest **121**(3): 985-997.

Smeets, T. J., M. C. Kraan, M. E. van Loon and P. P. Tak (2003). "Tumor necrosis factor alpha blockade reduces the synovial cell infiltrate early after initiation of treatment, but apparently not by induction of apoptosis in synovial tissue." Arthritis Rheum **48**(8): 2155-2162.

Smith, M. D. (2011). "The normal synovium." Open Rheumatol J **5**: 100-106.

Smith, M. D., E. Barg, H. Weedon, V. Papengelis, T. Smeets, P. P. Tak, M. Kraan, M. Coleman and M. J. Ahern (2003). "Microarchitecture and protective mechanisms in synovial tissue from clinically and arthroscopically normal knee joints." Annals of the Rheumatic Diseases **62**(4): 303-307.

Smith, M. D., M. C. Kraan, J. Slavotinek, V. Au, H. Weedon, A. Parker, M. Coleman, P. J. Roberts-Thomson and M. J. Ahern (2001). "Treatment-induced remission in rheumatoid arthritis patients is characterized by a reduction in macrophage content of synovial biopsies." Rheumatology (Oxford) **40**(4): 367-374.

Soilleux, E. J., L. S. Morris, G. Leslie, J. Chehimi, Q. Luo, E. Levroney, J. Trowsdale, L. J. Montaner, R. W. Doms, D. Weissman, N. Coleman and B. Lee (2002). "Constitutive and induced expression of DC-SIGN on dendritic cell and macrophage subpopulations in situ and in vitro." J Leukoc Biol **71**(3): 445-457.

Sokolove, J. and C. M. Lepus (2013). "Role of inflammation in the pathogenesis of osteoarthritis: latest findings and interpretations." Ther Adv Musculoskelet Dis **5**(2): 77-94.

Sokolovic, A., P. S. Montenegro-Miranda, D. R. de Waart, R. M. Cappai, S. Duijst, M. Sokolovic and P. J. Bosma (2012). "Overexpression of insulin like growth factor binding protein 5 reduces liver fibrosis in chronic cholangiopathy." Biochim Biophys Acta **1822**(6): 996-1003.

Staunton, D. E., M. L. Dustin and T. A. Springer (1989). "Functional cloning of ICAM-2, a cell adhesion ligand for LFA-1 homologous to ICAM-1." Nature **339**(6219): 61-64.

Stefanovic-Racic, M., X. Yang, M. S. Turner, B. S. Mantell, D. B. Stolz, T. L. Sumpter, I. J. Sipula, N. Dedousis, D. K. Scott, P. A. Morel, A. W. Thomson and R. M. O'Doherty (2012). "Dendritic cells promote macrophage infiltration and comprise a substantial proportion of obesity-associated increases in CD11c+ cells in adipose tissue and liver." Diabetes **61**(9): 2330-2339.

Steinman, R. M. (1991). "The dendritic cell system and its role in immunogenicity." Annu Rev Immunol **9**: 271-296.

Steinman, R. M. and Z. A. Cohn (1973). "Identification of a novel cell type in peripheral lymphoid organs of mice. I. Morphology, quantitation, tissue distribution." J Exp Med **137**(5): 1142-1162.

Steinman, R. M. and J. Idoyaga (2010). "Features of the dendritic cell lineage." Immunol Rev **234**(1): 5-17.

Struglics, A., S. Larsson, M. A. Pratta, S. Kumar, M. W. Lark and L. S. Lohmander (2006). "Human osteoarthritis synovial fluid and joint cartilage contain both aggrecanase- and matrix metalloproteinase-generated aggrecan fragments." Osteoarthritis Cartilage **14**(2): 101-113.

Su, S. L., H. Y. Yang, H. S. Lee, G. S. Huang, C. H. Lee, W. S. Liu, C. C. Wang, Y. J. Peng, C. H. Lai, C. Y. Chen, C. Lin, Y. T. Pan, D. M. Salter and H. C. Chen (2015). "Gene-gene interactions between TGF-beta/Smad3 signalling pathway polymorphisms affect susceptibility to knee osteoarthritis." BMJ Open **5**(6): e007931.

Sureshbabu, A., H. Okajima, D. Yamanaka, E. Tonner, S. Shastri, J. Maycock, M. Szymanowska, J. Shand, S. Takahashi, J. Beattie, G. Allan and D. Flint (2012). "IGFBP5 induces cell adhesion, increases cell survival and inhibits cell migration in MCF-7 human breast cancer cells." J Cell Sci **125**(Pt 7): 1693-1705.

Surmi, B. K. and A. H. Hasty (2008). "Macrophage infiltration into adipose tissue: initiation, propagation and remodeling." Future Lipidol **3**(5): 545-556.

Tak, P. P., T. J. Smeets, M. R. Daha, P. M. Kluin, K. A. Meijers, R. Brand, A. E. Meinders and F. C. Breedveld (1997). "Analysis of the synovial cell infiltrate in early rheumatoid synovial tissue in relation to local disease activity." Arthritis Rheum **40**(2): 217-225.

Tak, P. P., P. C. Taylor, F. C. Breedveld, T. J. Smeets, M. R. Daha, P. M. Kluin, A. E. Meinders and R. N. Maini (1996). "Decrease in cellularity and expression of adhesion molecules by anti-tumor necrosis factor alpha monoclonal antibody treatment in patients with rheumatoid arthritis." Arthritis Rheum **39**(7): 1077-1081.

Takayama, K., Y. Kawakami, M. Kobayashi, N. Greco, J. H. Cummins, T. Matsushita, R. Kuroda, M. Kurosaka, F. H. Fu and J. Huard (2014). "Local intra-articular injection of rapamycin delays articular cartilage degeneration in a murine model of osteoarthritis." Arthritis Res Ther **16**(6): 482.

Tchetina, E. V., N. V. Demidova, G. A. Markova, E. A. Taskina, S. I. Glukhova and D. E. Karateev (2017). "Increased baseline RUNX2, caspase 3 and p21 gene expressions in the peripheral blood of disease-modifying anti-rheumatic drug-naive rheumatoid arthritis patients are associated with improved clinical response to methotrexate therapy." Int J Rheum Dis.

Tchetina, E. V., A. N. Pivanova, G. A. Markova, G. V. Lukina, E. N. Aleksandrova, A. P. Aleksankin, S. A. Makarov and A. N. Kuzin (2016). "Rituximab Downregulates Gene Expression Associated with Cell Proliferation, Survival, and Proteolysis in the Peripheral Blood from Rheumatoid Arthritis Patients: A Link between High Baseline Autophagy-Related ULK1 Expression and Improved Pain Control." Arthritis **2016**: 4963950.

Thurlings, R. M., K. Vos, C. A. Wijbrandts, A. H. Zwinderman, D. M. Gerlag and P. P. Tak (2008). "Synovial tissue response to rituximab: mechanism of action and identification of biomarkers of response." Ann Rheum Dis **67**(7): 917-925.

Torres, L., D. D. Dunlop, C. Peterfy, A. Guermazi, P. Prasad, K. W. Hayes, J. Song, S. Cahue, A. Chang, M. Marshall and L. Sharma (2006). "The relationship between specific tissue lesions and pain severity in persons with knee osteoarthritis." Osteoarthritis Cartilage **14**(10): 1033-1040.

Tsuchiya, A., M. Yano, J. Tocharus, H. Kojima, M. Fukumoto, M. Kawaichi and C. Oka (2005). "Expression of mouse HtrA1 serine protease in normal bone and cartilage and its upregulation in joint cartilage damaged by experimental arthritis." Bone **37**(3): 323-336.

Tuomisto, T. T., H. Lumivuori, E. Kansanen, S. K. Hakkinen, M. P. Turunen, J. V. van Thienen, A. J. Horrevoets, A. L. Levonen and S. Yla-Herttuala (2008). "Simvastatin has an anti-inflammatory effect on macrophages via upregulation of an atheroprotective transcription factor, Kruppel-like factor 2." Cardiovasc Res **78**(1): 175-184.

van der Helm-van Mil, A. H., K. N. Verpoort, F. C. Breedveld, R. E. Toes and T. W. Huizinga (2005). "Antibodies to citrullinated proteins and differences in clinical progression of rheumatoid arthritis." Arthritis Res Ther **7**(5): R949-958.

van der Kraan, P. M., E. N. Blaney Davidson, A. Blom and W. B. van den Berg (2009). "TGF-beta signaling in chondrocyte terminal differentiation and osteoarthritis: modulation and integration of signaling pathways through receptor-Smads." Osteoarthritis Cartilage **17**(12): 1539-1545.

van Furth, R. and Z. A. Cohn (1968). "The origin and kinetics of mononuclear phagocytes." J Exp Med **128**(3): 415-435.

Van Landuyt, K. B., E. A. Jones, D. McGonagle, F. P. Luyten and R. J. Lories (2010). "Flow cytometric characterization of freshly isolated and culture expanded human synovial cell populations in patients with chronic arthritis." Arthritis Res Ther **12**(1): R15.

van Lent, P. L., A. B. Blom, P. van der Kraan, A. E. Holthuysen, E. Vitters, N. van Rooijen, R. L. Smeets, K. C. Nabbe and W. B. van den Berg (2004). "Crucial role of synovial lining macrophages in the promotion of transforming growth factor beta-mediated osteophyte formation." Arthritis Rheum **50**(1): 103-111.

Varol, C., L. Landsman, D. K. Fogg, L. Greenshtein, B. Gildor, R. Margalit, V. Kalchenko, F. Geissmann and S. Jung (2007). "Monocytes give rise to mucosal, but not splenic, conventional dendritic cells." J Exp Med **204**(1): 171-180.

Veale, D. J. and U. Fearon (2015). "What makes psoriatic and rheumatoid arthritis so different?" RMD Open **1**(1): e000025.

Villani, A. C., R. Satija, G. Reynolds, S. Sarkizova, K. Shekhar, J. Fletcher, M. Griesbeck, A. Butler, S. Zheng, S. Lazo, L. Jardine, D. Dixon, E. Stephenson, E. Nilsson, I. Grundberg, D. McDonald, A. Filby, W. Li, P. L. De Jager, O. Rozenblatt-Rosen, A. A. Lane, M. Haniffa, A. Regev and N. Hacohen (2017). "Single-cell RNA-seq reveals new types of human blood dendritic cells, monocytes, and progenitors." Science **356**(6335).

Wakabayashi, T., A. Matsumine, S. Nakazora, M. Hasegawa, T. Iino, H. Ota, H. Sonoda, A. Sudo and A. Uchida (2010). "Fibulin-3 negatively regulates chondrocyte differentiation." Biochem Biophys Res Commun **391**(1): 1116-1121.

Wallet, M. A., S. M. Wallet, G. Guiulfo, J. W. Sleasman and M. M. Goodenow (2010). "IFNgamma primes macrophages for inflammatory activation by high molecular weight hyaluronan." Cell Immunol **262**(2): 84-88.

Wang, X., S. Xia and B. Fu (2014). "RNAseq analysis of synovial fibroblasts in human rheumatoid arthritis." Mol Med Rep **10**(1): 241-247.

Wang, X. N., N. McGovern, M. Gunawan, C. Richardson, M. Windebank, T. W. Siah, H. Y. Lim, K. Fink, J. L. Li, L. G. Ng, F. Ginhoux, V. Angeli, M. Collin and M. Haniffa (2014). "A three-dimensional atlas of human dermal leukocytes, lymphatics, and blood vessels." J Invest Dermatol **134**(4): 965-974.

Weisberg, S. P., D. McCann, M. Desai, M. Rosenbaum, R. L. Leibel and A. W. Ferrante, Jr. (2003). "Obesity is associated with macrophage accumulation in adipose tissue." J Clin Invest **112**(12): 1796-1808.

Wenham, C. Y., A. J. Grainger, E. M. Hensor, A. R. Caperon, Z. R. Ash and P. G. Conaghan (2013). "Methotrexate for pain relief in knee osteoarthritis: an open-label study." Rheumatology (Oxford) **52**(5): 888-892.

Willekens, F. L., J. M. Werre, J. K. Kruijt, B. Roerdinkholder-Stoelwinder, Y. A. Groenen-Dopp, A. G. van den Bos, G. J. Bosman and T. J. van Berkel (2005). "Liver Kupffer cells rapidly remove red blood cell-derived vesicles from the circulation by scavenger receptors." Blood **105**(5): 2141-2145.

Wong, K. L., J. J. Tai, W. C. Wong, H. Han, X. Sem, W. H. Yeap, P. Kourilsky and S. C. Wong (2011). "Gene expression profiling reveals the defining features of the classical, intermediate, and nonclassical human monocyte subsets." Blood **118**(5): e16-31.

Wong, K. L., W. H. Yeap, J. J. Tai, S. M. Ong, T. M. Dang and S. C. Wong (2012). "The three human monocyte subsets: implications for health and disease." Immunol Res **53**(1-3): 41-57.

Wu, C. L., J. McNeill, K. Goon, D. Little, K. Kimmerling, J. Huebner, V. Kraus and F. Guilak (2017). "Conditional Macrophage Depletion Increases Inflammation and Does Not Inhibit the

Development of Osteoarthritis in Obese Macrophage Fas-Induced Apoptosis-Transgenic Mice." Arthritis Rheumatol **69**(9): 1772-1783.

Wu, H., X. D. Perrard, Q. Wang, J. L. Perrard, V. R. Polsani, P. H. Jones, C. W. Smith and C. M. Ballantyne (2010). "CD11c expression in adipose tissue and blood and its role in diet-induced obesity." Arterioscler Thromb Vasc Biol **30**(2): 186-192.

Wynn, T. A. and T. R. Ramalingam (2012). "Mechanisms of fibrosis: therapeutic translation for fibrotic disease." Nat Med **18**(7): 1028-1040.

Xue, J., S. V. Schmidt, J. Sander, A. Draffehn, W. Krebs, I. Quester, D. De Nardo, T. D. Gohel, M. Emde, L. Schmidleithner, H. Ganesan, A. Nino-Castro, M. R. Mallmann, L. Labzin, H. Theis, M. Kraut, M. Beyer, E. Latz, T. C. Freeman, T. Ulas and J. L. Schultze (2014). "Transcriptome-based network analysis reveals a spectrum model of human macrophage activation." Immunity **40**(2): 274-288.

Yang, J., L. Zhang, C. Yu, X. F. Yang and H. Wang (2014). "Monocyte and macrophage differentiation: circulation inflammatory monocyte as biomarker for inflammatory diseases." Biomark Res **2**(1): 1.

Yanni, G., M. Nabil, M. R. Farahat, R. N. Poston and G. S. Panayi (1994). "Intramuscular gold decreases cytokine expression and macrophage numbers in the rheumatoid synovial membrane." Ann Rheum Dis **53**(5): 315-322.

Yao, J. Y., Y. Wang, J. An, C. M. Mao, N. Hou, Y. X. Lv, Y. L. Wang, F. Cui, M. Huang and X. Yang (2003). "Mutation analysis of the Smad3 gene in human osteoarthritis." Eur J Hum Genet **11**(9): 714-717.

Ye, L., L. Guo, Z. He, X. Wang, C. Lin, X. Zhang, S. Wu, Y. Bao, Q. Yang, L. Song and H. Lin (2016). "Upregulation of E2F8 promotes cell proliferation and tumorigenicity in breast cancer by modulating G1/S phase transition." Oncotarget **7**(17): 23757-23771.

Yeo, L., N. Adlard, M. Biehl, M. Juarez, T. Smallie, M. Snow, C. D. Buckley, K. Raza, A. Filer and D. Scheel-Toellner (2016). "Expression of chemokines CXCL4 and CXCL7 by synovial macrophages defines an early stage of rheumatoid arthritis." Ann Rheum Dis **75**(4): 763-771.

Yeo, L., H. Lom, M. Juarez, M. Snow, C. D. Buckley, A. Filer, K. Raza and D. Scheel-Toellner (2015). "Expression of FcRL4 defines a pro-inflammatory, RANKL-producing B cell subset in rheumatoid arthritis." Ann Rheum Dis **74**(5): 928-935.

Yilmaz, A., C. Reiss, A. Weng, I. Cicha, C. Stumpf, A. Steinkasserer, W. G. Daniel and C. D. Garlichs (2006). "Differential effects of statins on relevant functions of human monocyte-derived dendritic cells." J Leukoc Biol **79**(3): 529-538.

Yu, W., J. Chen, Y. Xiong, F. J. Pixley, Y. G. Yeung and E. R. Stanley (2012). "Macrophage proliferation is regulated through CSF-1 receptor tyrosines 544, 559, and 807." J Biol Chem **287**(17): 13694-13704.

Zawada, A. M., K. S. Rogacev, B. Rotter, P. Winter, R. R. Marell, D. Fliser and G. H. Heine (2011). "SuperSAGE evidence for CD14++CD16+ monocytes as a third monocyte subset." Blood **118**(12): e50-61.

Zhang, L., Y. G. Li, Y. H. Li, L. Qi, X. G. Liu, C. Z. Yuan, N. W. Hu, D. X. Ma, Z. F. Li, Q. Yang, W. Li and J. M. Li (2012). "Increased frequencies of Th22 cells as well as Th17 cells in the peripheral blood of patients with ankylosing spondylitis and rheumatoid arthritis." PLoS One **7**(4): e31000.

Zhang, L., Y. Wang, F. Xiao, S. Wang, G. Xing, Y. Li, X. Yin, K. Lu, R. Wei, J. Fan, Y. Chen, T. Li, P. Xie, L. Yuan, L. Song, L. Ma, L. Ding, F. He and L. Zhang (2014). "CKIP-1 regulates macrophage proliferation by inhibiting TRAF6-mediated Akt activation." Cell Res **24**(6): 742-761.

Zhang, Y., F. Vasheghani, Y. H. Li, M. Blati, K. Simeone, H. Fahmi, B. Lussier, P. Roughley, D. Lagares, J. P. Pelletier, J. Martel-Pelletier and M. Kapoor (2015). "Cartilage-specific deletion of mTOR upregulates autophagy and protects mice from osteoarthritis." Ann Rheum Dis **74**(7): 1432-1440.

Zhang, Y., Y. Xing, L. Zhang, Y. Mei, K. Yamamoto, T. W. Mak and H. You (2012). "Regulation of cell cycle progression by forkhead transcription factor FOXO3 through its binding partner DNA replication factor Cdt1." Proc Natl Acad Sci U S A **109**(15): 5717-5722.

Ziegler-Heitbrock, H. W., M. Strobel, D. Kieper, G. Fingerle, T. Schlunck, I. Petersmann, J. Ellwart, M. Blumenstein and J. G. Haas (1992). "Differential expression of cytokines in human blood monocyte subpopulations." Blood **79**(2): 503-511.

Ziegler-Heitbrock, L., P. Ancuta, S. Crowe, M. Dalod, V. Grau, D. N. Hart, P. J. Leenen, Y. J. Liu, G. MacPherson, G. J. Randolph, J. Scherberich, J. Schmitz, K. Shortman, S. Sozzani, H. Strobl, M. Zembala, J. M. Austyn and M. B. Lutz (2010). "Nomenclature of monocytes and dendritic cells in blood." Blood **116**(16): e74-80.